Design Optimisation and Analysis of Heat Sinks for Electronic Cooling

Amer Jameel Shareef Al-damook

Submitted in accordance with the requirements for the degree of Doctor of Philosophy

The University of Leeds

School of Mechanical Engineering

Institute of ThermoFluids (iTF)

April, 2016

Work Formed from Jointly Authored Publications

1- Chapters 2, 3, 4, 5, and section 7.2 of this thesis are journal paper jointly authored by: Amer Al-damook, Kapur N., Summers J.L., Thompson H.M., An experimental and computational investigation of thermal airflows through perforated pin heat sinks, Applied Thermal Engineering Journal, 2015. 89: p.365-376.

2- Chapters 4, 6, and 7 of this thesis are journal paper jointly authored by: Amer Al-damook, Kapur N., Summers J.L., Thompson H.M., Computational design and optimisation of pin fin heat sinks with rectangular perforations, Applied Thermal Engineering Journal, 2016, has been accepted.

3- Chapter 4 and sections 5.7 and 5.8 of this thesis are journal paper jointly authored by: Amer Al-damook, Kapur N., Summers J.L., Thompson H.M., Effect different perforations shapes on the thermal-hydraulic performances of perforated pinned heat sinks. Journal of Multidisciplinary Engineering Science and Technology, 2016. 3(4): p. 4475–4480.

The following papers are in preparation:

1- Amer Al-damook, Kapur N., Summers J.L., Thompson H.M., Effect of the variable air properties on the thermal airflow pinned heat sinks. In preparation to be submitted for publication in International Communication in Heat and Mass Transfer Journal.

The candidate has conducted the majority of the work that appears in the published papers, such as developing the model, presenting and analysing the results. The co-authors provided valuable review and guidance to the candidate.

Acknowledgements

I would like to express my extreme gratefulness to my supervisors, Prof. Harvey Thompson, Prof. Nikil Kapur, and Dr. Jonathan Summers for their advice, supportive guidance, encouragement, and assistance throughout the entire research.

Furthermore, I would like to thank the Higher Committee for Education Development in Iraq (HCED) for financial support of this work, as well as Iraqi Ministry of Higher Education and Scientific Research (MOHE), and Mechanical Engineering Department University of Anbar, Iraq.

Above all else, I thank my family, my parents especially for my late father, my sister, and my brother so much for their support and prayers. They gave me a lot, but most especially, they gave me the strength to go on. Thank you very much.

Abstract

Since industrial devices create power dissipation in the form of heat created as a by-product, which can have a negative effect on their performance, certain temperature limit constraints are required for almost all these applications to work within suitable conditions. That is, these engineering devices might fail in some way if these limitations are surpassed by overheating. In all the related industries, inexorable increases in power densities are driving innovation in heat exchange techniques. Furthermore, electronic devices are becoming smaller at the same time as their thermal power generation increases. Thus, heat sinks can be applied for cooling critical components in many important applications ranging from aero-engines and nuclear reactors to computers, data centre server racks and other microelectronic devices.

The most common cooling technique for heat dissipation for thermal control of electronics is air cooling. Reduced cost, simplicity of design, the easy availability of air, and increased reliability are the main benefits of this cooling method. Heat sinks with a fan/blower are commonly used for air-cooled devices as a forced convection heat transfer. An amount of heat is dissipated from the heat source to environmental air utilising a heat sink as a heat exchanger, which is a vital practice employed in air-cooling systems. This transfer mechanism is easy, simple and leads to reduced cost and increased reliability, and pinned heat sinks are more beneficial than plate fin heat sinks.

The main interest of this study is to investigate the benefits of using perforated, slotted, and notched pinned heat sinks with different configurations to reduce CPU temperature and fan power consumption to overcome the pressure drop and maximise a heat transfer rate through the heat sink. An experimental heat sink with multiple perforations is designed and fabricated, and parameter studies of the effect of this perforated pin fin design on heat transfer and pressure drops across the heat sinks are undertaken, to compare it to solid pinned heat sinks without perforations. Experimental data is found to agree well with predictions from a CFD model for the conjugate heat transfer and turbulent airflow model into the cooling air stream. The validated CFD model is used to carry out a parametric study of the influence of the number and positioning of circular perforations, and slotted/notched pinned heat sinks. Then, the multi-objective optimum pinned heat sink designs are tested to obtain CPU temperature and fan power consumption as lowest as possible through the heat sink. In addition, the limitations in application of pinned heat sinks based on the pin density and applied heat flux are reported for active air-cooling electronic systems.

An overview of the findings indicates that the CPU temperature, the fan power consumption, and the heat transfer rate in terms of Nusselt number are enhanced with the number of pin perforations and slotted/notched pinned heat sinks, while the locations of the pin perforations are much less influential. These benefits arise due to not only the increased surface area but also to the heat transfer enhancement near the perforations through the formation of localised air jets. Finally, the perforated heat sinks will be lighter in weight compared with solid pinned heat sinks.

Table of Contents

List of Tables

List of Figures

Nomenclature

A_c	Cross-sectional area of the flow passage of the heat sink (m^2)
A_P	Projected heat transfer surface area (m^2)
A_T	Total heat transfer surface area (m^2)
C_p	Specific heat constant at constant pressure (kJ/kg.K)
d	Diameter of perforations (m)
D	Diameter of pin fins (m)
D_h	Hydraulic diameter (m)
F	The view factor
h	Height of slot or notch (m)
h_P	Projected heat transfer coefficient based on the total surface area ($W/m^2.^oC$)
h_T	Average heat transfer coefficient based on the total surface area ($W/m^2.^oC$)
H	Height of duct (m)
J	Profit factor
k	Turbulent kinetic energy (m^2/s^2)
k_{air}	Air thermal conductivity ($W/m.^oK$)
k_{ins}	Insulation thermal conductivity ($W/m.^oK$)
L	Length of heat sinks (m)
n	Number of perforations
N	Number of pins
Nu	Nusselt number
p	Perimeter of cross duct (m)
P_d	Pressure drag coefficient

P_{fan}	Fan power (W)
$P_{in,\ out}$	Inlet and outlet pressure of heat sink, respectively (Pa)
Pr	Prandtl number
Pr_t	Turbulent Prandtl number
Q	Applied heating power (W)
$Q_{conv.}$	Convective heat rate (W)
$Q_{elec.}$	The total heat applied on the base of heat sink (W)
Q_{loss}	Conductive heat losses (W)
$Q_{rad.}$	Radiative heat losses (W)
R_{th}	Thermal resistance (K/W)
Re	Reynolds number
S_x, S_z	Streamwise and Spanwise distance or longitudinal and transverse distance, respectively (m)
T_{air}	Ambient air temperature (K)
T_{case}	CPU temperature or the base temperature of heat sinks (K)
T_{in}, T_{out}	Inlet and outlet air temperature (K)
T_m	Average bulk mean temperature (K)
T_0	Absolute bulk fluid temperature (K)
T_w	Bottom surface of heat sink temperature (K)
U	Inlet air velocity (m/s)
Un	Uncertainty range of experimental test
U_x,U_v,U_z	Velocities in x, y and z directions, respectively (m/s)
V	Solid pin volume (m^3)
V_{hole}	Perforation volume (m^3)
(x,y,z)	Cartesian coordinates (m)

w	Width of slot or notch (m)
W	Width of duct (m)
ΔP	Pressure drop (Pa)
ΔX	Insulation thickness (m)

Greek Symbols

μ	Dynamic viscosity (N.s/m^2)
μ_t	Turbulent eddy viscosity (N.s/m^2)
υ	Kinematic viscosity (m^2/s)
υ_t	Turbulent kinematic viscosity (m^2/s)
ε	Turbulent dissipation rate (m^2/s^3)
ρ	Density (kg/m^3)
ϕ	Porosity
ω	Specific dissipation rate (1/s)

Abbreviations

CFD	Computational Fluid Dynamics
CHS	Compact Heat Sink
CPU	Central Processing Unit
DoE	Design of Experiments
FVM	Finite Volume Method
HSs	Heat Sinks
ICT	Information and Communication Technology
MLS	Moving Least Squares
PC	Personal Computer
PCPFHS	Plate-Circular Pin Fin Heat Sink
PEPFHS	Plate-Elliptic Pin Fin Heat Sink

PFHSs	Plate Fins Heat Sinks
PHSs	Pinned Heat Sinks
PPHSs	Perforated Pinned Heat Sinks
PSPFHS	Plate-Square Pin Fin Heat Sink
NPHSs	Notched Pinned Heat Sinks
RANS	Reynolds-Averaged Navier-Stokes
SPHSs	Slotted Pinned Heat Sinks
SIMPLE	Semi-Implicit Method for Pressure-Linked Equations
SST	Shear-Stress Transport
0P	Solid Pinned Heat Sink Model
3P	Pinned Heat Sink with Three Perforations Model
5P	Pinned Heat Sink with Five Perforations Model
3CP	Triple Circular Perforated Pinned Heat Sink Model
3SP	Triple Square Perforated Pinned Heat Sink Model
3EP	Triple Elliptic Perforated Pinned Heat Sink Model

Chapter One: Introduction

1.1 Motivation

Education, business, transportation, social media and the sectors economic have become very dependent on Information and Communication Technology (ICT), to which end, ICT has become the most important source of information and data in our society (Zeadally et al., 2012). Thus, data centres, which are essentially digital factories, have become a vital part of ICT processing, management, storage and exchange of data and information (Pan et al., 2008). A data centre consists of four main parts: power equipment such as power distribution units and batteries, cooling equipment (chillers and computer room air-conditioning (CRAC) units), IT equipment (servers, storage and network), and miscellaneous component loads (lighting and fire protection systems) (Dai et al., 2014). Electronic component systems that arrange processing, storing and transmission of data is the main part of the data centre, according to Shah et al. (2008) and Greenberg et al. (2006), all of which and create a large amount of heat, which must be removed from the ICT components at a rate sufficient to avoid serious overheating problems and system failures (Sahin et al., 2005). More than 30% of the heat removal costs of a typical data centre is used in IT equipment and cooling equipment. Thus, an important part of a server is the heat sink that is set over the CPU (Dai et al., 2014), as shown in Figure 1.1.

The thermal effect can cause failure of mechanisms in electronic component devices, due to metal migration, void formation, and inter-metallic growth. Actually, one of the common factors that control the reliability of electronic products is the maximum temperature limitation of these devices. For each 10^{o}C increase above the critical operating temperature (~85°C) of high-power electronics, the rate of these failures almost doubles (Gurrum et al., 2004). Therefore, electronics thermal management is of crucial significance, as is reflected in the market (Mostafavi, 2012). Another important factor is the cost increase of thermal management products, which went from nearly $7.5 billion in 2010 to $8 billion in 2011, and is predicted reach $10.9 billion by 2016; the annual rate of increase is 6.4%. Fans and

heat sinks (HSs) as thermal management hardware components take an 84% share of the total market. However, software, interface materials, and substrates as the other main cooling products account for between 4% and 6% of the market (BCC Research, 2014).

Many researchers have therefore been studying the thermal and fluid flow through heat sinks, but there is still a lack of information about heat sinks, especially for perforated heat sinks. This fact has motivated the exploring of the design optimisation and analysis of thermal airflow through perforated pinned heat sinks (PPHSs) for electronics cooling systems.

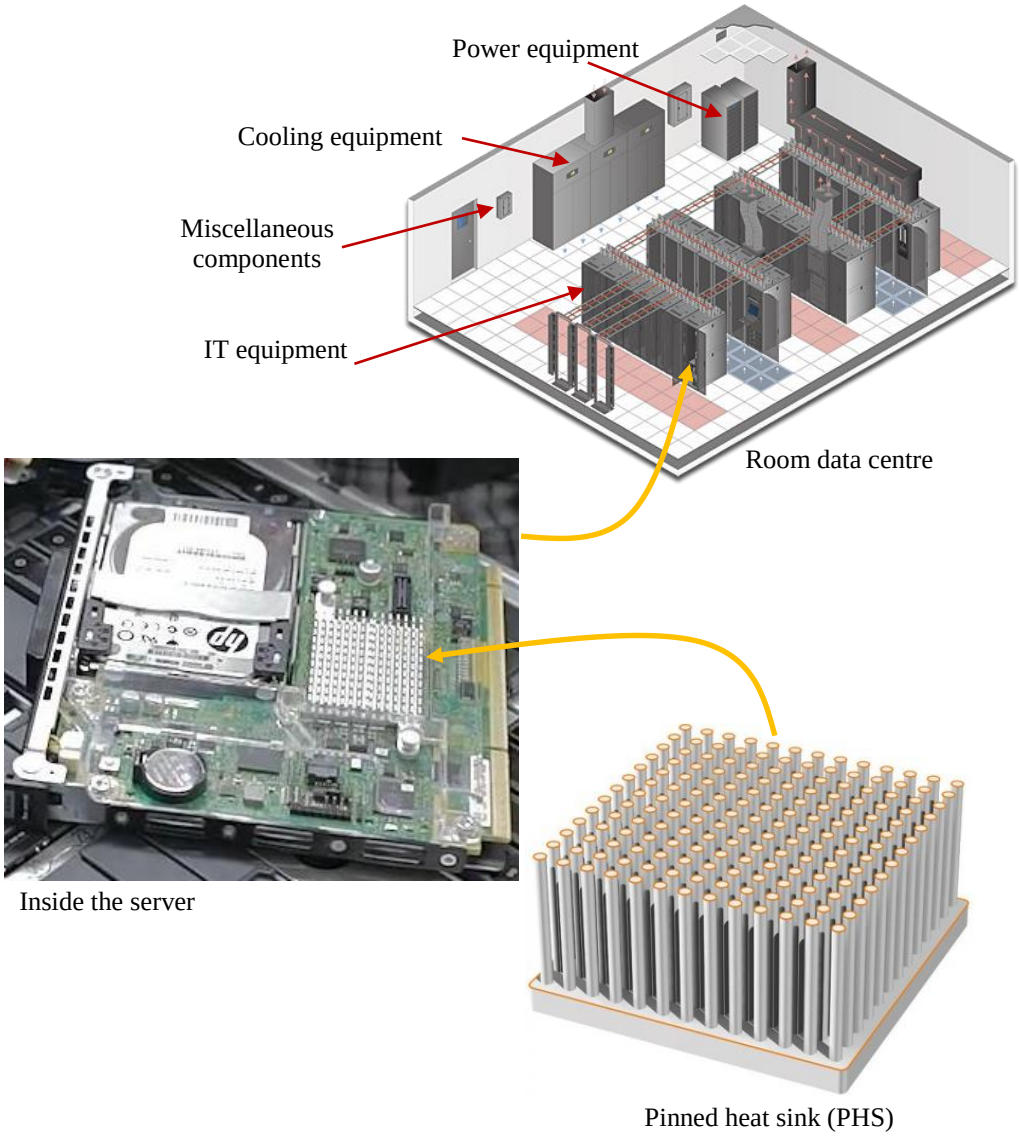

Figure 1.1: Data centre infrastructure (Tripplite, 2012), server (DeepInIt, 2013), and pinned heat sink (Alutronic, 2015)

1.2 Introduction to Heat Sink Technology

Finned heat sinks are classified into two main types: plate fin heat sinks (PFHSs) and pin heat sinks or pinned heat sinks (PHSs), as shown in Figure 1.2. Such heat sinks are manufactured and produced by several companies, both large and small, such as Airedale in the UK, Raypak in the USA, to name of few. A set of base tube materials that have high thermal conductivity, such as copper and aluminium, can be employed to manufacture heat sinks depending on their cost and ease of manufacturing. In recent years, the technology relating to heat sinks designed for cooling electronics has become widespread and familiar, since their initial cost is low, and they are simple to install, and have a reliable manufacturing process (Chingulpitak, 2015).

Fin morphology has an important function in manufacturing and heat transfer characteristics. Cylindrical, rectangular, square, elliptic, and conical or semi-conical are the widespread uniform pin fins geometries. In addition, pins offer a practical means of achieving a large heat transfer area without excessive primary surface area and act as turbulence promoters, thus further enhancing heat transfer rates by breaking up the thermal boundary layer for many applications, such as cooling electronic devices, including processes that use gas or liquid coolants (Denpong, 2001; Zhou & Catton, 2011; Naphon et al., 2009; Brigham & Van Fossen, 1984). Therefore, it seems that it is a suitable time to employ this technology in traditional heat sinks and in industrial applications as well.

In general, pin fin layouts are made up of a network of solid pins mounted directly on the heat sink surface. Either a staggered or an in-line arrangement is usually configured for arrays of pins with the working fluid flowing parallel or perpendicular to the pin axes.

1.3 Importance of Electronics Cooling

In many engineering applications, the power dissipation creates heat as a by-product, which may cause system failures in these devices due to serious overheating. This is mainly due to the certain temperature limits that are required for almost all applications to work within suitable conditions. Currently, as electronic devices decrease in size, their thermal power losses increase (Mostafavi, 2012).

Additionally, the forced convection of heat sinks covers a wide range of industrial applications in order to overcome the damaging effects of overheating or burning. Hence, it is very important to consider the cooling system for electronic components.

The main industrial applications of heat sinks are cooling of tiny electronic components, electronic boards and components, the central processing unit (CPU) of personal computers and data centres, internal combustion (IC) engine cooling (fins in a car radiator), gas turbine blade coolant path, sophisticated electronic chips, electrical appliances (computer power supplies, substation transformers, etc.), the aerospace industry, and cooling of fuel elements in nuclear reactors (Prashanta, 1998; Sahin & Demir, 2008a; Sahin & Demir, 2008b; Amol & Farkade, 2013; Sara et al., 2000; Sara et al., 2001).

Plate and pin fins are commonly used for cooling the CPUs of a personal computer and electronic components devices (Dempong, 2001; Kim & Kim, 2009; Yakut et al., 2006a; Zhang et al., 2005; Yakut et al., 2006b; Naphon & Knonseur, 2009); Naphon & Wiriyasart, 2009; Naphon & Wonwises, 2010; Naphon, 2011; Konsue, 2012; Diani et al. (2013), integrated circuit chips in electronic equipment, compact heat exchangers, and cooling of advanced gas turbine blades (Jonsson & Moshfegh, 2001; Yang et al., 2007; Jeng & Tzeng, 2007; Sahin et al., 2005).

According to the author's knowledge, the fin perforations might play an important role in the thermal airflow through heat sinks; in other words, the cooling performance will enhance and the pressure drop will reduce. It is possible those heat sinks are useful for cooling electronic applications and for IC engine cooling such as substation transformers, computer power supply, and fins in a car radiator (Prashanta, 1998, Sahin & Demir, 2008a; Sahin & Demir, 2008b; Amol & Farkade, 2013; Sara et al., 2000; & Sara et al., 2001).

1.4 Liquid and Air Cooling of Data Centres

Generally, electronic systems in data centres are cooled by liquid or air (Anandan & Ramaligam, 2008).

Liquid cooling such as water, nanofluids, polymers, and dielectric liquid (Hydrofluoroethers, HFE) can be used to cool the heat sinks and servers of racks in data centres. Direct contact liquid cooling techniques, such as immersing servers into

dielectric liquid (Tuma, 2010; Almaneea, 2014) may be used. Ramifications of immersion on data centre cooling and energy performance can be found in Chi et al (2014). Another technique to cool data centres is indirect contact liquid cooling via bringing the cooled liquid to heat sinks on the top of the chips or alternatively to the rack or into the server as a heat exchanger on the front or rear of the rack (Villa, 2006). The main advantages of this method are the heat transfer rate enhancement is greater than that of the air-cooling method since the thermal conductivity and thermal capacity of liquids are superior to those of air. In addition, dielectric liquids act as electrical insulators without any electrical discharge (Naidu & Kamaraju, 2009; Alkasmoul, 2015). However, the main disadvantages of the pressure drop and pumping power of liquids is higher compared with that of air because the viscosity and density of liquids are larger than those of air. Furthermore, liquid cooling are risk of the liquid leaking, which may damage the server's electronic components, resulting in data centre loss; the risk of condensation forming, which may lead to a failure in the system; the high cost of maintenance and installation; and an increase in infrastructure such as pipe work, leak detection, and installation of insulation (Villa, 2006; Naidu & Kamaraju, 2009).

Due to all the above disadvantages of liquid cooling, the most common method of heat dissipation for thermal control of electronics is air cooling. Reduced cost, the availability of air, and the simplicity of design are the main benefits of this cooling method. As an example of an active air-cooled device, heat sinks with a fan or blower are commonly employed. An amount of heat is dissipated from the heat source to environmental air utilising a heat sink as a heat exchanger, which is a vital practice employed in air-cooling systems. This transfer mechanism is easy, simple and leads to reduced cost (McMillin, 2007). However, the heat transfer rate of the air-cooling method is lower than that of the liquid cooling, as indicated previously.

In this technique, the heat transfer rate of the heat sink can be augmented, either by increasing the fan speed or the surface temperature of the heat sink. As the fan speed increases, however, the fan's reliability reduces and it consumes a lot more power and the noise level increases to undesirable levels, particularly for the office or home consumer. Increasing the temperature is also unacceptable because it reduces the reliability of the central processing units (CPUs) and that leads to earlier

chip short circuit (McMillin, 2007). Hence, increasing fan speed and increasing the temperature are not a favoured approach.

Therefore, these challenges need to be addressed by inventing an effective air cooling solution that has direct influences on the reliability, power, and performance of electronic devices. In this study, active air-cooling of perforated pinned heat sinks (PPHSs) is investigated as a new technique (see sections 6.3 & 6.4.1) to cool central processing units (CPUs), enhance heat transfer rate, and reduce fan power consumption.

Due to the importance of the fin heat sink applications, which impact on the forced heat transfer and fluid flow enhancement (and they have many serious applications, especially to cool electronic devices such as large scale datacom equipment and PC desktops), it is important to conduct a literature review that relates to this interesting subject. In this chapter, many previous studies, both numerical and experimental works, are reported, split into six groups based on the type of fins: solid plate fins (A), solid pins (B), compact plate-pins (C), perforated plate (D), perforated pins (E), and perforated folded fins (F) heat sinks, as shown in Figure 1.2.

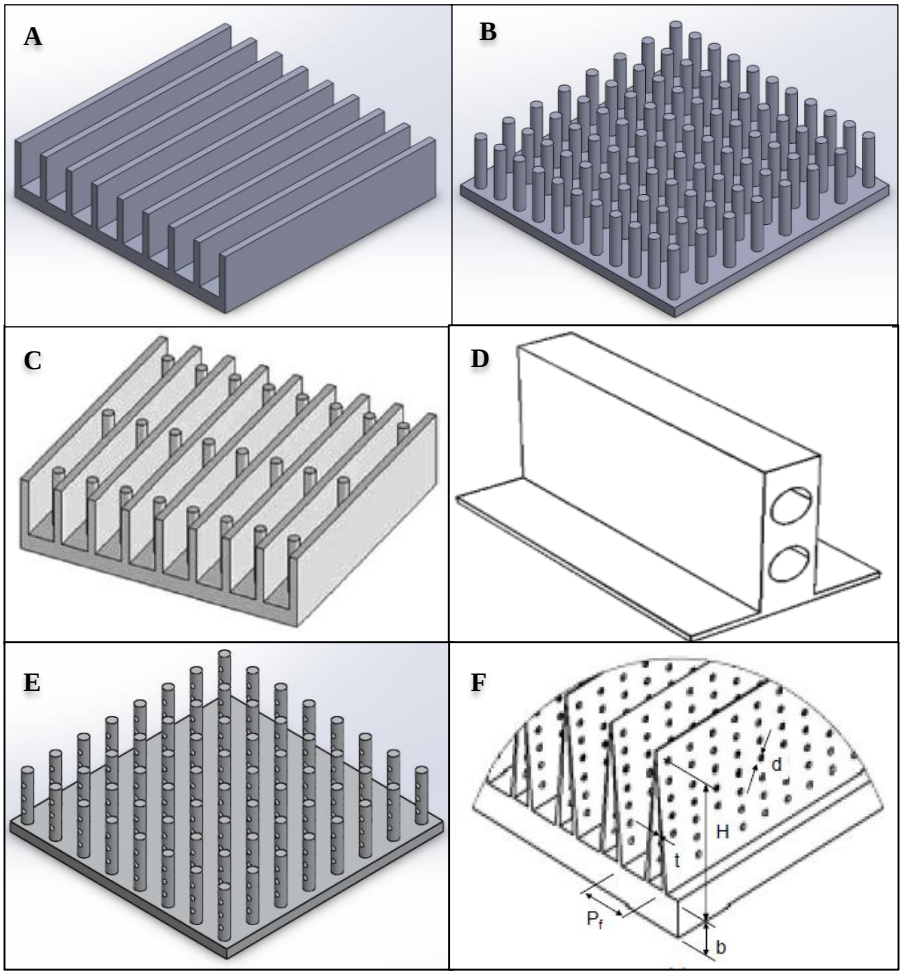

Figure 1.2: Different types of fins: (A) solid plate fins, (B) solid pins, (C) compact plate-pins, (D) perforated plate, (E) perforated pins, and (F) perforated folded fin heat sinks

1.5 Solid Plate Fin Heat Sinks (SPFHSs)

The most widely used heat sink designs in industrial applications are those based on rectangular plate fin heat sinks (PFHSs), Figure 1.2A, due to their simple structure and ease of manufacture. These have been widely studied, and several researchers have used experimental and numerical methods to remove the intrinsic limitation that the air flow through parallel heat sink channels is smooth, thus limiting the achievable heat transfer rate.

In this section, the reviewed literature can be categorised into two types of work: experimental and numerical studies on solid plate fin heat sinks.

1.5.1 Experimental Studies

Plate fins as a flat plate, based on the literature reviews, single and multiple cross-cut plate fins (strip fins) have been investigated by many experimental works to study the effects of several parameters on the heat transfer and turbulent flow of solid fin heat sinks. Such parameters are the height, width, number of fins, the streamwise and spanwise distance between fins, and the type of material used in the fin heat sink. Air and water are both used as a coolant in these studies.

It is indicated that the thermal resistance (see section 2.5.6) of single cross-cut fin heat sinks is lower than that of the multiple cross-cut fins, plate fins, and square pin fin heat sinks. This may be because the total wetted surface of the cross-cut fins (see section 2.5.5) is larger than that of other types of fins, in addition to the spacing between fins being suitable for airflow to pass through easily that leads to demolish the growth of the boundary layer over the heat sink. Thus, it would be beneficial to study the optimum thermal and airflow performance of cross-cut fins.

Air Cooling

Air is used as a coolant in the next three studies: Kim & Kim (2009), Didarul et al. (2007), and Naphon & Khonseur (2009). The effects of cross-cut fins are used for cooling electronic device applications are examined by Kim & Kim (2009). The findings show that the thermal resistance of single cross-cut heat sinks outperforms on the multiple cross-cut heat sinks. In addition, the comparison of the thermal resistance of these heat sinks with pin and plate fin heat sinks indicates that the

cross-cut heat sinks offer less thermal resistance than plate fin HSs and square pin HSs by 5–18% and 14–16%, respectively.

Generally, if the dimensionless fan power (x-axis of Figure 1.3) is tiny and the dimensionless heat sink size (y-axis of Figure 1.3) is large, an optimized plate fin heat sink is recommended. However, the optimum pinned heat sink is suggested as the dimensionless fan power is large and the dimensionless size of the heat sink is tiny. The area in between the optimized plate fin and optimized pinned heat sinks is represented the optimized cross-cut heat sinks.

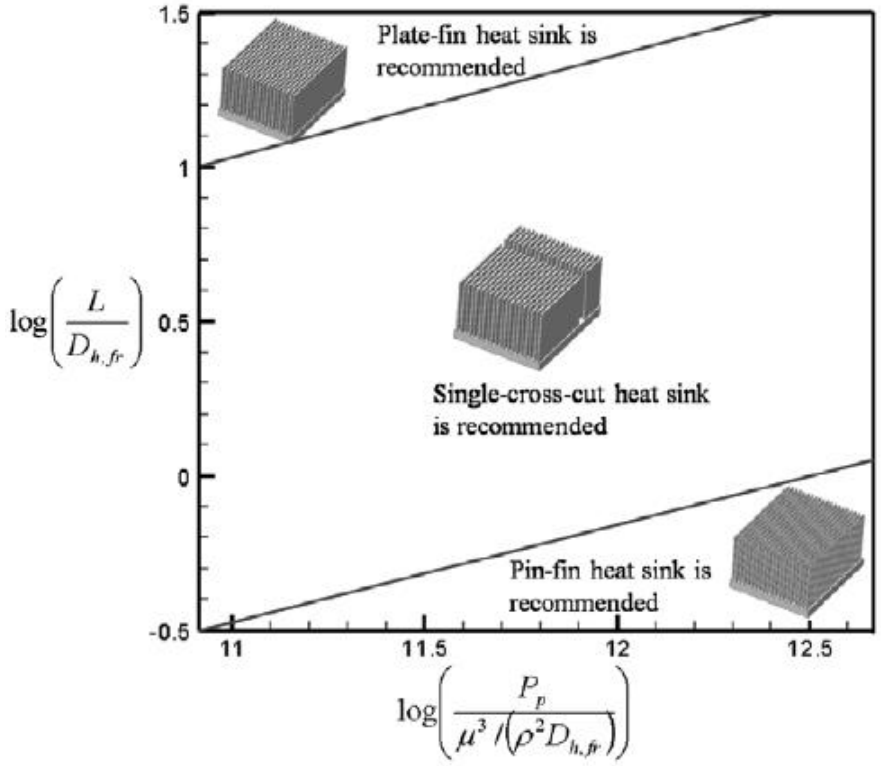

Figure 1.3: Contour map of the thermal ratio for optimised plate, pin, and cross-cut FHSs (Kim & Kim, 2009)

Didarul et al. (2007) indicated the effects of the direction of the short rectangular plate fin, Figure 1.4, on the heat transfer rate and flow inside a duct for turbulent airflow. The characteristic considered in this study was that the directions of the fins were co-angular and zigzag, Figure 1.5. They observed that the optimum improvement of local heat transfer coefficient (h_x) is at 20^o angle. In addition, the average heat transfer coefficient (h_{ave}) is largest for the zigzag fin model and it is four times more than that without fins. However, the friction factor of the zigzag model is larger than that for the co-angular pattern. These fins are utilised to cool the trailing edge region and the internal passage of turbine blades.

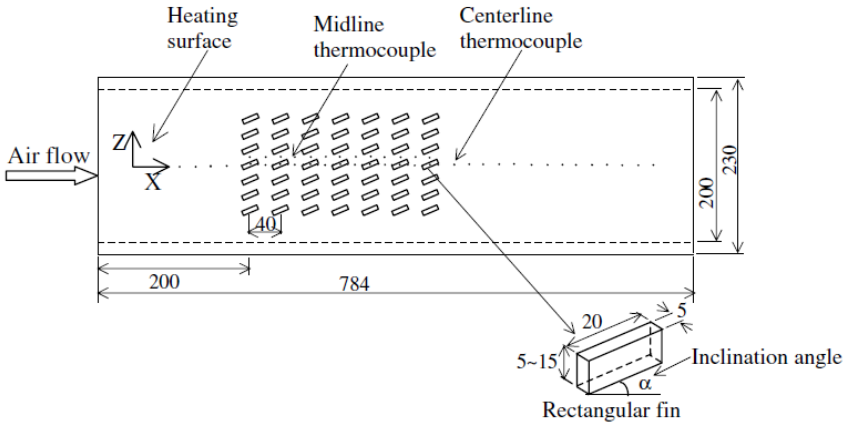

Figure 1.4: Test section and direction of short rectangular plate fins (Didarul et al., 2007)

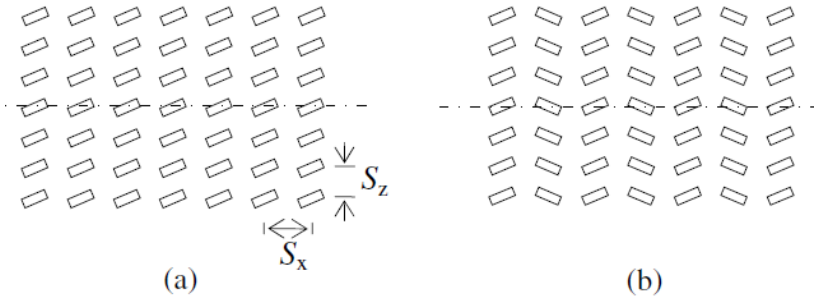

Figure 1.5: Short rectangular fins: (a) co-angular pattern, (b) zigzag pattern (Didarul et al., 2007)

The effect of the channel height and the width of the microchannel were investigated by Naphon & Khonseur (2009) with laminar airflow. They found that the heat sink temperature decreases and Nusselt number (see section 2.5.5) increases with increasing the channel height decreasing channel width. In addition, the shape and the size of rough irregularities on the microchannel surface will influence the pressure drop.

Liquid Cooling

Zhang et al (2005) reported that liquids can be utilised to cool electronic system packages for two sizes of chip at 12×12mm and 10×10mm using micro-rectangular plate fins with de-ionised water as a coolant. In general, the experimental data indicates that pressure drop increases while chip temperature and thermal resistance decreases with increasing flow rate for both chip sizes. For the 10×10mm chip, however, the overall thermal resistance is higher than that of the 12×12mm chip.

1.5.2 Numerical Studies

Heat sinks that are used in the cooling of electronic devices, microchips, and other systems consider the optimum design for fin array geometry. Heat transfer and turbulent fluid flow have been presented numerically using solid plate fin heat sinks. The governing equations Navier-Stokes and energy equations with k-ε turbulence models are chosen by most of the researchers via employing the finite volume method. The next papers in this section deal with this topic. The numerical and experimental data are consistent in that the strip fins have achieved the smallest thermal resistance.

The optimum design of parallel flat plate fin HSs was studied by Arularasan and Velraj (2008) with a turbulent airflow. The findings indicate that the optimum plate fin heat sink design based on the base temperature, thermal resistance, and pressure drop is found at the specific parameters of the fin height, fin thickness, pitch of the fin and the base height.

The Taguchi method is used to predict the optimum cooling design of parallel plate fin HSs used in desktop PC CPUs by Ko-Ta (2005). It is indicated that two design parameters have an important effects on the cooling performance of this heat sink: the air speed and the fin flake gap. The lowest value of the base temperature is decreased by 8^{o}C and the temperature reduction is nearly 15%.

Velayati & Yaghoubi (2005) studied the effect of different fin blockage ratios (D/W= fins thickness/fins spacing) and Reynolds numbers on the turbulent flow and heat transfer characteristics of plate fin heat sinks. They found that the D/W and Reynolds highly influence the separation flow, reattachment over the plate surface, and the recirculation downstream of the plate. Thus, the Nu increases and the friction factor decreases when both these parameters, D/W and Re, are increased. In addition, fin efficiency ($q_{with\ fins}/q_{without\ fins}$) enhances when D/W and Re are decreased.

The optimum design of different fin heat sinks was theoretically investigated by Ndao et al. (2009) by using water and the dielectric liquid, HFE-7000. The heat sink models are micro-plate channel, in-line and staggered circular pin HS, strip fin HS, single and multiple impinging jet, shown in Figure 1.6. These heat sinks are applied in electronic devices and chips. This optimisation is carried out in two steps: simultaneous minimisation of the total thermal resistance ($R_{th,T}$, based on the total

wetted surface area) and the pumping power consumption for each of these heat sinks. The data indicates that the strip fins HS has the lowest thermal resistance of the cooling devices, followed by the staggered and in-line circular pin HSs. Furthermore, the micro-plate HS offers the lowest thermal resistance at relatively very low pumping power.

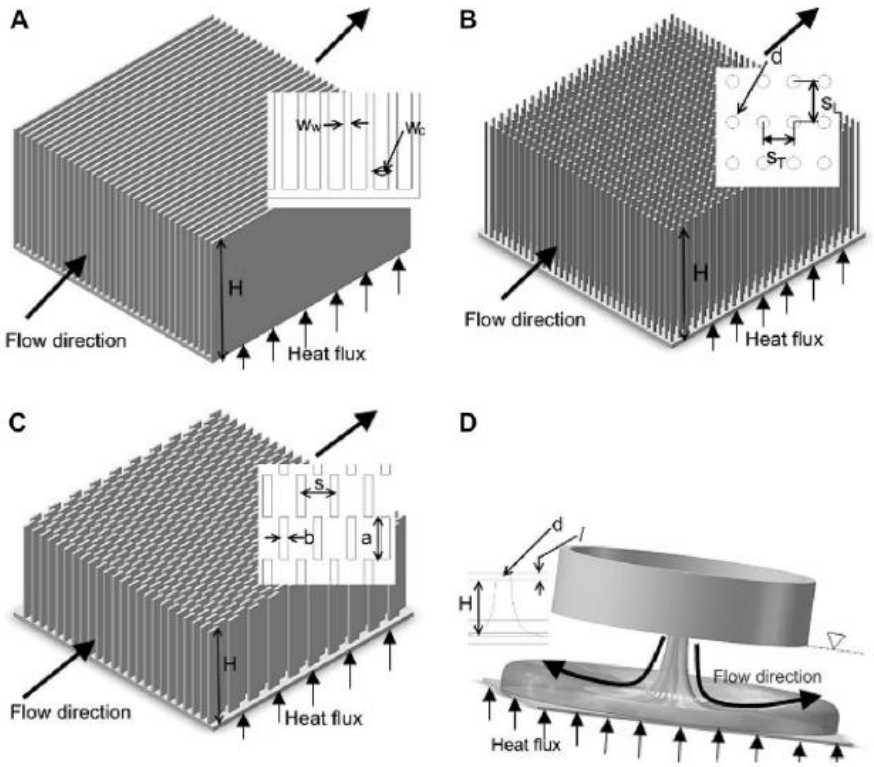

Figure 1.6: Different heat sink models: (A) micro-plate channel (B) circular pins (C) offset strip fins (D) jet impingement cooling (Ndao et al., 2009)

1.6 Solid Pinned Heat Sinks (SPHSs)

Although many optimisation reports have investigated plate fin heat sinks, see e.g. Chiang (2005) and other previous studies such as Velayati & Yaghoubi (2005), Arularasan and Velraj (2008), they cannot remove the intrinsic limitation that stops air flowing through the heat sink channels is smooth, due to the parallel plate arrangement, leading to the development of a boundary layer and limiting the achievable heat transfer rates. Pinned heat sinks (PHSs), as shown in Figure 1.2B, can be an effective alternative to plate fin HSs since they have the advantage of hindering the development of the thermal boundary layer on smooth surfaces that is responsible for limiting the heat transfer rates in plate fin designs (Zhou & Catton,

2011). Pinned heat sinks play important role as turbulence promoters lead to enhance heat transfer rates by disrupting boundary layer with greater pressure drop compared with plated fin heat sinks (Jonsson & Moshfegh, 2001)

The major difference between plate fins and pin heat sinks is that the pressure drop and heat transfer rate of pinned HSs are higher than those of plate fin HSs. In addition, the thermal resistance and the average temperature of pinned HSs are lower compared to plate fin HSs. In the next studies, by Jonsson & Moshfegh (2001) and Yang et al. (2007), various cross-sections of pins, such as square, circular, hexagonal, diamond and elliptic, are investigated with air and water coolants.

1.6.1 Experimental Studies

It can be observed that several parameters are considered in these studies in order to report the effects of a parameter studies on the heat transfer and turbulent flow through solid pinned heat sinks. These parameters are: cross-section of pin fin shape, which can be circular; square; elliptic; diamond; hexagonal pin in in-line and staggered arrangements; the height, width and number of fins; pin heat sink material; and the streamwise and spanwise distance between pins. Air, water, and nanofluids (coolants seeded with nano sized particles) are utilised as a coolant in these experimental works.

Air Cooling

Vanfossen & Brigham (1984), Tanda (2001), Jeng & Tzeng (2007), Jonsson & Moshfegh (2001), Yang et al. (2007), and Sahin et al. (2005) have all studied air cooling. The important outcomes illustrate that the circular and elliptic pin shapes have the higher heat transfer rate enhancement and lower thermal resistance. Additionally, the pin density, which means the increasing number of pin fins, leads to improvement the heat transfer rate while the pressure drop through solid pinned heat sinks increases. Commonly, the staggered pin array achieves a higher heat transfer rate and pressure drop compared with the in-line array.

To explain the effect of the in-line and staggered pin arrangements on the heat transfer rate and pressure drop through PHSs, Tanda (2001) and Jeng & Tzeng (2007) investigated this subject. Tanda (2001) studied diamond-shaped element pins, which are useful for engineering applications such as electronic devices, compact heat exchangers, and in cooling of advanced gas turbine blades, whilst Jeng & Tzeng

(2007) examined square PHSs. Both studies indicated that the Nusselt number and pressure drop of PHSs in the staggered array is the largest. Furthermore, Jeng & Tzeng (2007) compared square pins with open article of circular pin fins and explain that the pressure drop and Nusselt number of square pins and circular pins for both in-line and staggered arrays depend on the spacing pins values and Reynolds number. Generally, the staggered square pin arrangements have larger pressure drops than the circular and square pins with in-line array arrangements.

In the next two articles, Jonsson & Moshfegh (2001) and Yang et al. (2007), pin heat sinks are used for turbine blade and electronic device cooling. The pins' shapes affect the heat transfer and pressure drop in in-line and staggered arrays, as explained below.

Jonsson & Moshfegh (2001) investigated the different configurations of fins: plate fins, strip fins, square pin, and circular pin, in in-line and staggered arrays, all of which influence the Nusselt number and pressure drop. It is identified that Nusselt number and pressure drop depend on the height and thickness (diameter) of the pins and the distance between them, as well as the height and width of the wind tunnel. In addition, the lowest pressure drop is observed at the plate fins due to their fin length. Furthermore, the circular PHSs have a lower pressure drop than that of the square PHSs.

The effects of the shape and density of PHSs with in-line and staggered arrangements on heat transfer and pressure drop are reported by Yang et al. (2007). The cross-section pins are circular, elliptic, square, and flat plate rectangular fins. The experimental data imply that the highest average heat transfer coefficient occurs at the staggered arrangement of the circular PHS. Furthermore, the thermal resistance based on the projected area is smallest at the circular pins in-line, Figure 1.7. For staggered arrays, however, the lowest pressure drop is at the elliptic pin, and this pin has a slightly higher performance than that of the circular pin. In general, the average heat transfer coefficient and pressure drop increase with increasing pin density.

Sahin et al. (2005) investigated the effects of geometric parameters of the HS fins, as shown in Figure 1.8, on Nusselt number and friction factor. This kind of heat sink is utilised for electronic cooling equipment. They explained that the optimum design for the slices fin is obtained at 15mm fin width; 15^{o} angle of attack; 100mm

fin height; 20mm spanwise distance between fins; 15mm streamwise separation between fins; 20mm streamwise separation between slices; 20mm spanwise distance between slices; and 4m/s fluid velocity.

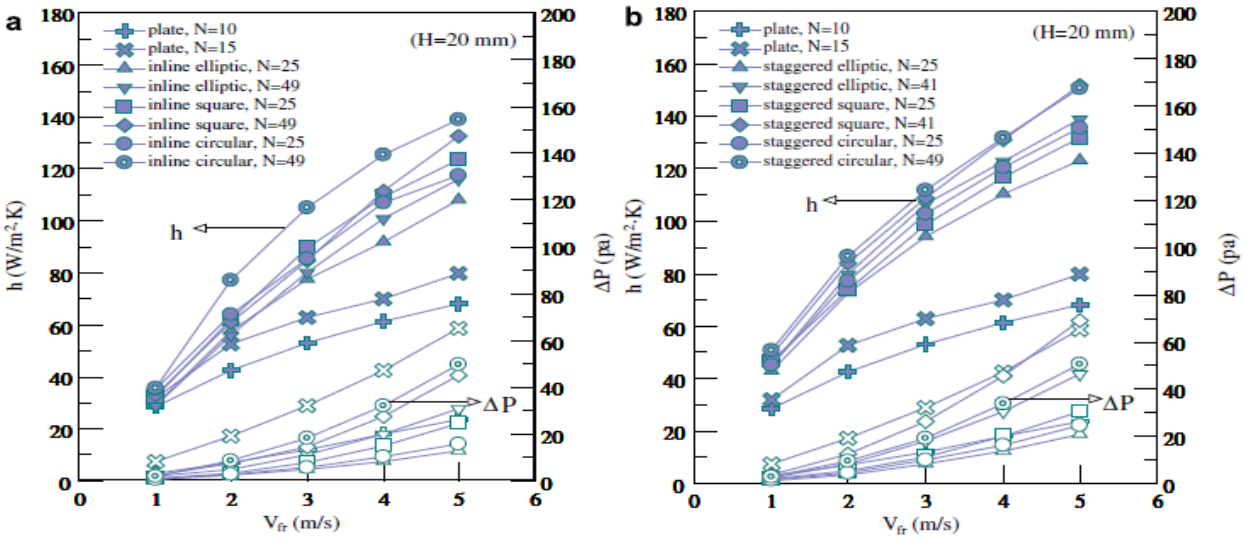

Figure 1.7: Heat transfer coefficient and pressure drop with inlet velocity for plate fin and pin fin in (a) in-line array and (b) staggered array (Yang et al., 2007)

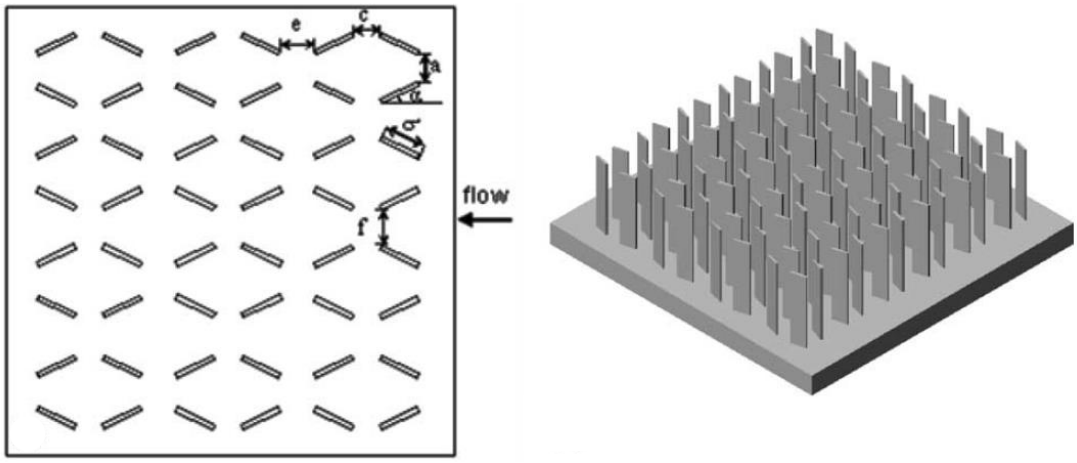

Figure 1.8: Fin heat sink slices: (a) spanwise (c) streamwise distance between the fins, (e) spanwise (f) streamwise distance between slices (Sahin et al., 2005)

In the following two studies, Yakut et al. (2006a, 2006b), the results of using hexagonal pin fins for cooling the CPU of a personal computer and electronic component devices are reported. They have used the Taguchi optimisation design method to explain the influence of the height, width of the hexagonal fins, and spacing between fins on the thermal resistance and pressure drop (Yakut et al., 2006a) and on the Nusselt number and friction factor (Yakut et al., 2006b). Commonly, it can be observed that the pin height is the most effective parameter on

Nu and thermal resistance while pin width is the most effective parameter on ΔP and friction factor.

Liquid Cooling

Liquids such as water and Nanofluids can also be utilised to cool electronic system packages. The heat transfer rates increase and the thermal resistances decrease once TiO_2 nanofluid coolant is used, in comparison with water-cooling for the same heat sink and under the same boundary conditions such as same applied heat flux, concentration of nanofluid, and inlet mass flow rate and temperature (Naphon & Nakharintr, 2013). In this literature, it is possible to utilise the jet cooling method to cool the CPU of a personal computer (PC) and enhance the CPU temperature. Heat transfer rate and CPU temperature enhance with increasing mass flow rate and when decreasing both nozzle diameter and channel width.

Naphon & colleagues (2010, 2011, and 2013) have produced three important papers relating to mini-pin heat sinks using laminar water and nanofluid flow as a coolant to cool the CPU of a PC. In the first two papers (2010 and 2011) employed a jet flow techniques (parallel flow method) while their other one Naphon & Wongwises (2013) used the traditional cross-flow method. Generally, the authors found that the nanofluid achieve a significant enhancement in heat transfer rate and Nusselt number while the pressure drop is higher compared with air- and water-cooling.

Naphon & Wongwises (2010) investigated the jet impingement heat transfer by utilising mini-rectangular pin heat sinks, which are constructed from copper, to cool the CPU of a PC. This study used de-ionised water as a coolant and the PC was examined with no load and with full load operating conditions. They indicated that CPU temperature reduces when the channel width and the nozzle diameter decrease. Furthermore, the largest CPU temperature drops and energy consumption increases take place when the CPU is working under full load conditions. Naphon & Wongwises (2011) reported the jet nanofluid effect on cooling the CPU by utilising mini-channel HSs, Figure 1.9. TiO_2 particles were used as nanofluid coolant. Using the jet nanofluid lowered the average temperatures of the CPU by nearly 3% and 6.25% than those of the jet water and the conventional cooling system, respectively. As a result, the Nusselt number for the jet nanofluid is higher than that for the two other techniques, jet water and conventional water cooling system, Figure 1.10.

Maybe the nanofluid can capture and transfer more heat since their thermal conductivity and thermal capacity are higher.

Naphon & Nakharintr (2013) studied the effect of the channel height on the heat transfer rate of mini-rectangular fin heat sinks with nanofluid (TiO_2) as a laminar flow. In this study, heat transfer rate and Nusselt number enhance with increasing channel height. Comparing the results with water indicate that the heat transfer rate and Nusselt number of the nanofluid are higher than those of the water. In addition, the thermal resistance of the heat sink with the nanofluid is lower than that of the water. However, the pressure drop of both nanofluid and water is approximately the same in this study.

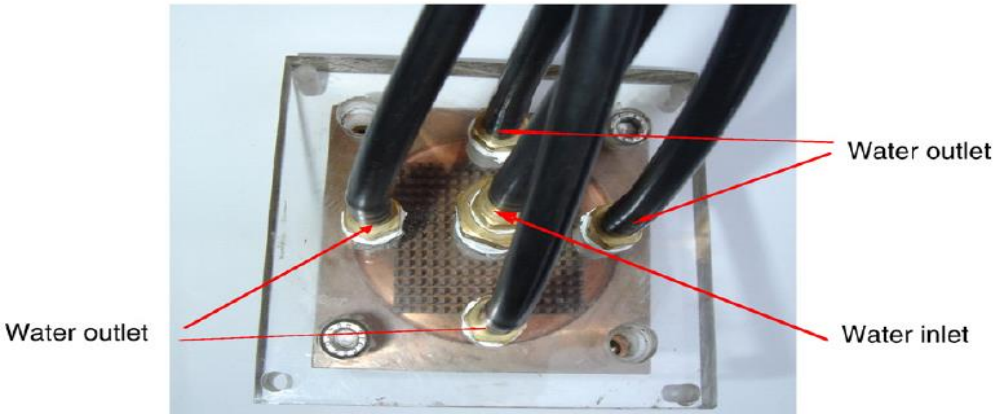

Figure 1.9: Jet impingement heat sink unit for cooling the CPU of a PC (Naphon & Wongwises, 2010)

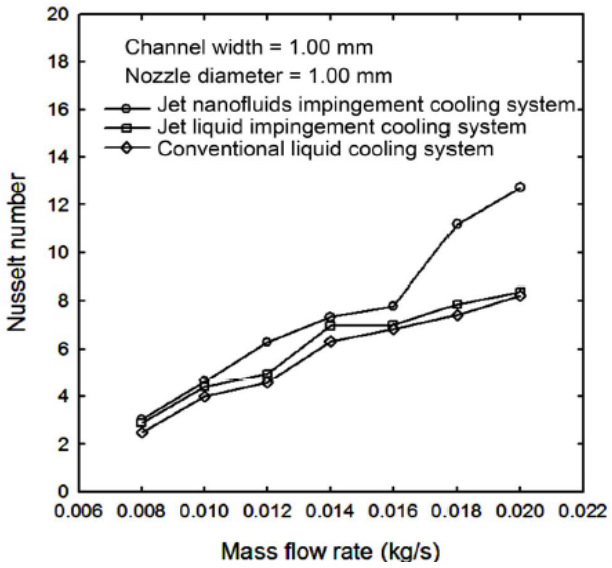

Figure 1.10: Variation of the Nusselt number with mass flow rate for different cooling methods (Naphon & Wongwises, 2011)

1.6.2 Numerical Studies

In this part, the literature review discusses the enhancement of heat transfer with laminar and turbulent fluid flow for solid fin heat sinks numerically by using different fin shapes. Turbulent flow is in common use while laminar flow is specifically utilised according to the application's requirements. Several kinds of commercial CFD software program are utilised to solve the governing equations, Navier-Stokes and energy equations with k-ε and k-ω turbulence models, which are chosen by most researchers via employing the finite volume and the finite elements methods.

The main conclusions indicate that the circular pinned heat sinks have a larger Nusselt number and lower friction factor than most other types of fin heat sinks such as plate fins, strip plate fins, elliptic pins, and square pins in in-line and staggered arrays under laminar airflow. The elliptic and circular pins, however, have the lowest pressure drop therefore requiring lower pumping power values under laminar flow conditions.

Air Cooling

In the next two works, by Ramesha & Madhusudan (2012) and Soodphakdee et al. (2001), laminar airflow and heat transfer characteristics are numerically reported.

Ramesha & Madhusudan (2012) investigated the effect of pin heat sink profile on the laminar forced convection heat transfer. These pin fins, which are useful for electronic cooling applications, are square twisted with various attack angles of airflow direction, as shown in Figure 1.11. The outcomes indicate that the twisted pins enhance the heat transfer rate of the heat sink especially at 30^o, 45^o, and 60^o twisted angles by comparing the performance of a straight pin fin heat sink at 0^o twisted. In addition, the pressure drop of the twisted pins at 30^o and 45^o improves and is nearly similar to the straight pins.

The effect of cross-section fins on laminar forced convection heat transfer and pressure drop has been investigated by Soodphakdee et al. (2001). The shapes of these cross sections are plate fins, circular, elliptic, and square pins in in-line and staggered arrays, as shown in Figure 1.12, and these fins can be applied in integrated circuit chips. The findings explain that elliptic fins have the highest heat transfer

coefficient at lower pressure drop and pumping power values. At larger pressure drop and pumping power values, however, the circular pin fins possess the highest heat transfer coefficient, as shown in Figure 1.13.

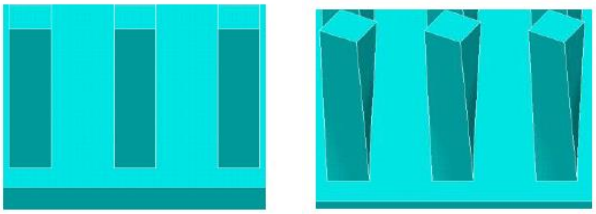

Figure 1.11: Straight and twisted pin heat sinks (Ramesha & Madhusudan, 2012)

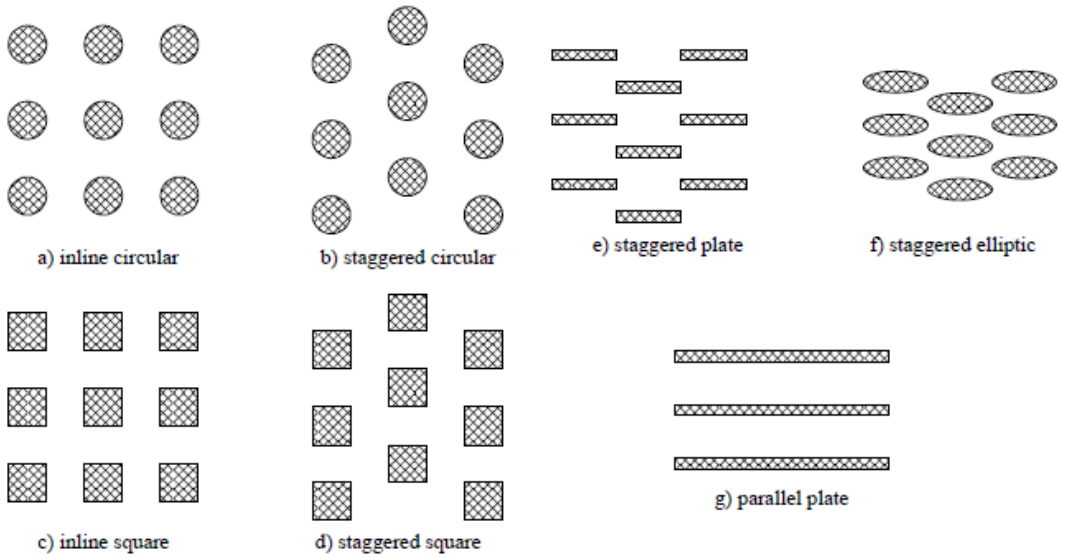

Figure 1.12: Different types of fin heat sinks (Soodphakdee et al., 2001)

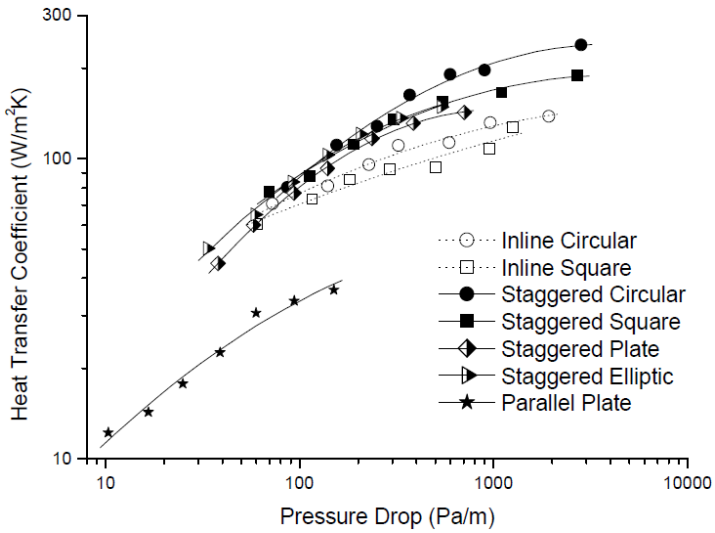

Figure 1.13: Heat transfer coefficient versus pressure drop of various fin geometries (Soodphakdee et al., 2001)

Mohan & Govindarajan (2010) reported the optimum forced convection heat transfer and temperature distribution through two kinds of heat sink: plate fins and pins HSs, which are adequate for the CPUs of desktop computers. They found that the CPU temperature of the heat sink decreases when the base plate thickness and thickness of the fin increase. If copper is selected as the base plate material rather than aluminium, the thermal resistance of the heat sink reduces as expected, while the heat sink will be more expensive and heavier compared with when using aluminium. Thus, this study demonstrated the practical compromise that has to be struck between a low thermal resistance when using copper as the base plate material, which is costlier and heavier, and a higher thermal resistance for aluminium, which is cheaper and lighter.

Liquid Cooling

The following researchers, Naphon et al. (2009 and 2011) and Mohan & Govindarajan (2010) have used numerical methods to study turbulent flow and heat transfer in heat sinks.

Naphon et al. (2009 and 2011) report on two experiments using forced heat transfer and turbulent fluid flow for mini-square PHS. The first one studied variable channel width, which is used for the CPU of a PC, and a de-ionised water coolant was used to explain the flow structure and behaviour of the working fluid. The findings explain that the flow pattern, pressure and temperature distribution are not uniform over the mini-heat sink. That is because all these results depend on liquid velocity, which is non-uniform through heat sinks. In addition, the direction and distribution of velocity at the entrance region of the mini-heat sink is dependent on the liquid flow pattern at the inlet plenum (Naphon et al., 2009). The second work studied the effect of the outlet port position on jet impingement heat transfer and fluid flow of two models, A and B, which have four different outlet port positions (Naphon et al., 2011), Figure 1.14, for the same mini-square fin heat sink as in the last report. The numerical results showed that the flow velocity and the temperature distribution of coolant fluid through the second design (B) are uniformly better than in the first model (A). This means that both heat transfer rate and the overall performance of the second model (B) are higher than that in the first model (A). Thus, the uniformity of temperature distribution has an important effect on the thermal performance of the mini-heat sink.

Based on the previous literature review, the main advantages and disadvantages of the plate fin heat sinks and pinned heat sinks are shown in Table 1.1

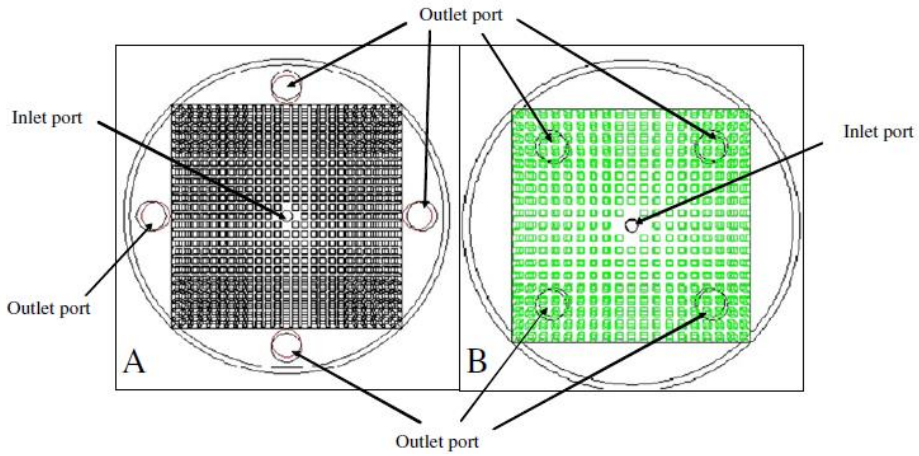

Figure 1.14: Schematic diagram of the different cross sections of model A and model B (Naphon et al., 2009)

Table 1.1: The comparison between the plate fin heat sinks and pinned heat sinks

Plate fin heat sinks (PFHSs)	Pinned heat sinks (PHSs)
The most widely used in industrial applications	
Air, water and Nanofluids are used to cool different engineering devices	
Simple structure and ease of manufacture	Relatively complex structure and manufacture
Parallel plate fins only	Different type of pin configurations: circular, square, elliptic, strip in in-line and staggered arrays
The intrinsic limitation that the air flow through parallel heat sink channels that is smooth	Act as turbulence promoters lead to break up a boundary layer
The development of a boundary layer easily	Hindering the development of a boundary layer
Limiting the achievable heat transfer rate	Enhancement heat transfer rates
Lower pressure drop and fan power	Greater pressure drop and fan power
Higher the base average temperature	Lower the base average temperature
Higher thermal resistance to some extent	Lower thermal resistance to some extent

1.7 Plate-Pin Fin Heat Sinks (PPFHSs) or Compact Heat Sinks (CHSs)

Plate-pin fin heat sinks are a kind of compact heat sinks (CHSs), as shown in Figure 1.15B and C, and have been reported on only in relation to turbulent airflow. Compact heat sinks (CHSs) consist of some pins among plate fins in in-line and staggered arrangements. As more pins are present among the plate fins, the boundary layer growth through the heat sink is inhibited because the pins act as obstructions. The benefits of compact heat sinks are reduction of the CPU temperature and thermal resistance and enhancement of the Nusselt number, compared with plate fins and pin HSs. However, these pins will impede airflow, which leads to a pressure drop, and fan power for compact heat sinks is huge in comparison with other plate fins and pin HSs.

In the next literature surveys, all types of compact heat sinks (CHSs) are applied to cool electronic components under a turbulent airflow.

Yu et al. (2003, 2004, and 2005) conducted numerical and experimental investigations into the thermal airflow through plate-circular pin fin heat sinks (PCPFHSs), which consist of some circular pin fins among plate fins. The results indicate that the thermal resistance of the PCPFHS is nearly 30% smaller than that of the plate fin heat sink (PFHS). However, the pressure drop of the PCPFHS is much higher than that of the PFHS. The performance profit factor (Q/P_{fan}) of the PCPFHS is about 20% higher than that of the PFHS.

Yang & Peng (2009a and 2009b) produced two papers relating to the compact heat sink. Thermal characteristics and pressure drop of the plate-circular pin fin heat sink (PCPFHS) in in-line and staggered arrangements are considered with a mixed-height design of pins, as shown in Table 1.2. The results indicate that the Nusselt number enhancement of the PCPFHS is over 30% superior to that of the plate fin heat sink (PFHS). However, the pressure drop of the PCPFHS is nearly 110% higher than that of the PFHS. For the in-line arrays design, the profit factor is higher than for the staggered arrays model. The profit factor of Type-3 is the highest while the largest *Nu* is for Type-4 (Yang & Peng, 2009a). Yang & Peng's (2009b) second report deals with the effects of pin shape and arrangement on the thermal and hydraulic characteristics of compact heat sinks utilising circular and square pin fins

between plate fins. These compact heat sinks are called the plate-circular pin fin heat sink (PCPFHS) and the plate-square pin fin heat sink (PSPFHS), as shown in Figure 1.15. The findings show that the profit factor of the PCPFHS outperforms the PSPFHS by approximately 7%. In addition, the thermal resistance and pressure drop of the PCPFHS are about 10% and 90% respectively smaller than those of the PSPFHS.

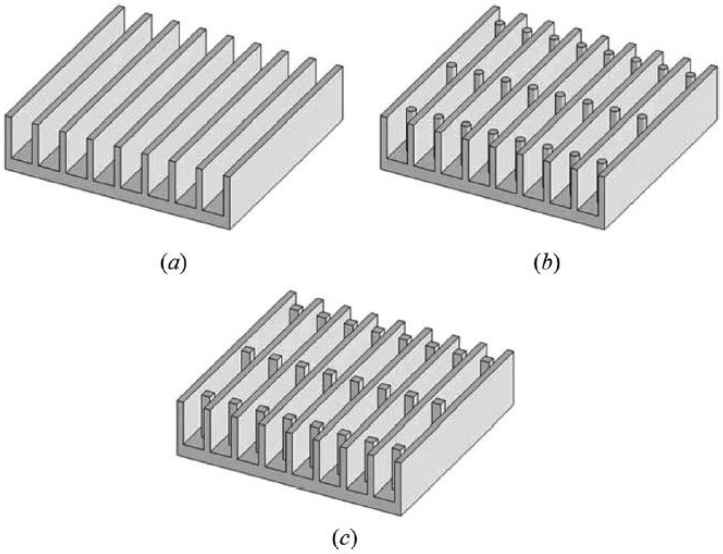

Figure 1.15: Compact heat sinks: (a) plate-fin heat sink, (b) plate-circular pin heat sink, and (c) plate-square heat sink (Yang and Peng, 2009)

Table 1.2: The practical examples of the heat sinks dimensions (Yang and Peng, 2009)

Type	The height of pin fins (mm)		
	Pin-1	Pin-2	Pin-3
Type-1	5	5	5
Type-2	5	5	10
Type-3	5	10	10
Type-4	10	10	10

L = 51 mm, H = 10 mm, N = 9, t = 1.5 mm, and D = 2 mm.

Kumar & Bartaria (2013) assessed the thermal characteristics and pressure drop of the plate-elliptic pin fin heat sink (PEPFHS), which means some elliptic pins distribute between plate fins in an in-line arrangement with three different minor radiuses of elliptic pins. The results indicate that the thermal resistance and the Nusselt number of the PEPFHS enhance as the minor radiuses of the elliptic pins increase. Furthermore, the Nusselt number of the PEPFHS is higher than that of the plate pin (PFHS) while the pressure drop of the PFHS is lower than that of the PEPFHS.

The results of using more different plate-pin fin heat sink models with various cross-section types of pin-fin, square, circular, elliptic, NACA 0050 profile, and dropform are by reported Zhou & Catton (2011) to enhance thermal and hydraulic characteristics of this kind of heat sink. The numerical data, which are obtained from the *k-ω* turbulent model as provided in ANSYS CFX-12.1 program, illustrated that PPFHSs improve the Nusselt number by up to 85% while a maximum pressure drop of 525% is reached in comparison with plate fin heat sinks (PFHSs), as shown in Figures 1.16 and 1.17.

Yuan et al. (2012) investigated the thermal hydraulic characteristics of the compact plate-circular pin fin heat sink (PCPFHS) in in-line and staggered arrangements to find its potential application in the CPU of a PC. Heat sink dimensions and boundary conditions are similar to the previous papers (Yang & Peng, 2009a and 2009b) with mixed pins; the diameter design of the PPFHS is shown in Table 1.3. They proposed that all these PCPFHS models achieve the cooling requirement of a desktop PC CPU at less than 60W as a heating power and with a maximum temperature of 85^{o}C. The pressure drop over PPFHSs increases while the thermal resistance and the profit factor will significantly decrease as pin diameter and air velocity increase. However, the effects of pin distance and pin array of this compact HS were less remarkable.

Table 1.3: Different pin diameter combinations for four types of PPFHS (Yuan et al., 2012)

Four types of PPFHS.

Type	Diameter of pin fins (mm)		
	Pin-1	Pin-2	Pin-3
Type-1	1	1	1
Type-2	1	1	2
Type-3	1	2	2
Type-4	2	2	2

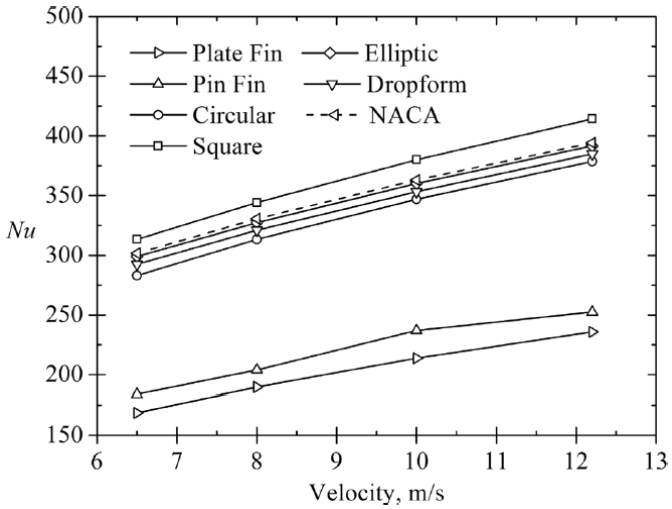

Figure 1.16: Nusselt numbers of compact heat sinks with variation in air velocity (Zhou & Catton, 2011)

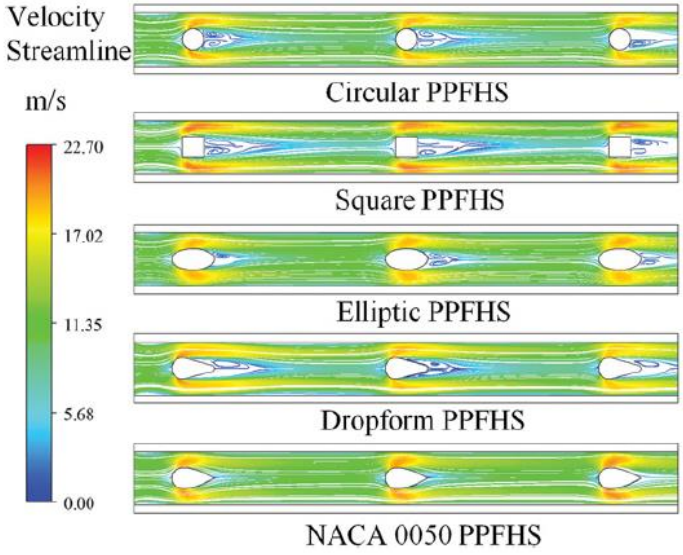

Figure 1.17: Streamlined patterns at Uc=10m/s, in the plane z=8 mm (Zhou & Catton, 2011)

1.8 Perforated Fin Heat Sinks (PFHSs)

The main reason for interest in this subject is that forced convection fins have various applications, from cooling of tiny electronic components to cooling of fuel elements in nuclear reactors. Furthermore, according to the author's knowledge and the next literature reviews in this section, the fin perforations play an important role by way of improving the thermal and flow characteristics of heat sinks and vanishing the vortexes and boundary layers behind solid plate fins and pin heat sinks. In addition, devices with these perforated fins will be lighter in weight and material will

also be saved in their design (Yaghoubi et al., 2009). Only air is used as a coolant in the following works.

The numerical studies calculated Nu_T based on total wetted surface area of the perforated fins is lower than that of solid fins heat sink. Hence, we recommend determining the projected Nusselt number (Nu_P), based on surface area of only the heat sink base, $L \times W$: where L, and W are length and width of the heat sink, respectively, as this may be a more effective measure of cooling capacity for a given heat sink size. The CPU temperature should not exceed the reference critical temperature of 85^{o}C (Gurrum et al., 2004; Yuan et al., 2012). Furthermore, it should be considered to minimise CPU temperature and fan power consumption in order to select the optimum heat sink design.

1.9 Perforated Plate Fin Heat Sinks

Either perforation can be along the length of the plate fins as a small channel (frontal perforations) Figure 1.18A, or on the side of the plate fins as lateral perforations, Figure 1.18B. They are able to enhance thermal airflow of these heat sinks compared to the equivalent solid fin heat sinks.

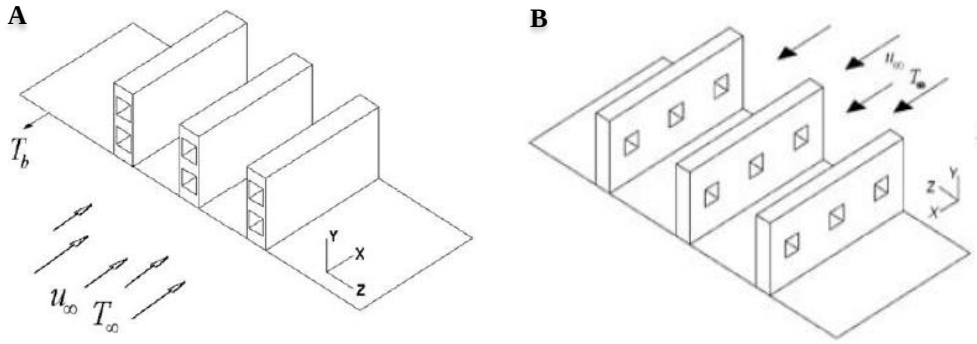

Figure 1.18: (A) Frontal and (B) lateral perforated flat plate heat sinks (Yaghoubi et al., 2009; Shaeri & Yaghoubi, 2009)

1.9.1 Plate Fins with Lateral Perforations

The first section deals with several experimental reports on lateral circular perforated plate fin heat sinks. The main conclusion is that the Nusselt number and friction factor of perforated plate fins are larger than those of the solid fins. For instance, Dhanawade et al. (2010, 2014, and 2014) have produced three studies on lateral perforation PFHSs. The first one investigates the effect of lateral circular

perforated plate fins on forced convection heat transfer (Dhanawade & Dhanawade, 2010), and found that, at low applied heat flux levels up to 14000W/m^2, the Nusselt number for the 12mm perforation diameter is larger than that for the 10mm perforation diameter. However, at high heat flux levels up to 20000W/m^2, the largest Nusselt number is for the 10mm perforation diameter.

Ganorkar & Kriplani (2012) produced another study explaining the effect of the lateral circular perforated plate fins on the heat transfer rate. This kind of HS is used to cool electronic applications and in IC engine cooling such as substation transformer, computer power supply, and fins in a car radiator. The effects of the lateral perforated plate fins' shape on forced convection heat transfer and friction factor (*f*) are investigated in another report by Dhanawade et al. (2014). Evidently, the data point out that the *Nu* and *f* of the perforated fins are higher compared to solid fins and they increase with increases in the perforations' diameter. The effectiveness of the square perforated fins, $\frac{Q_{perforated\ fins}-Q_{solid\ fins}}{Q_{solid\ fins}}$, is nearly the same as that of the circular perforated fins, while, with respect to the friction factor, the circular perforated fins have the lowest value. Dhanawade et al. (2014) have developed their previous work utilising the Taguchi design experimental method for optimum design of the thermal performance of circular lateral perforated PFHSs. They found that the most vital parameters are *Re*, perforation porosity, and then fin thickness, respectively. The highest level of effectiveness for the perforated fins is nearly 19%, noted at *Re*=87000, 0.22 porosity, and 5mm of fin thickness. The findings show agreement with the results of Ganorkar & Kriplani (2012).

According to numerical studies, several factors such as average friction factor, Nusselt number based on the total wetted surface area (Nu_T), and fin weight reduce as increasing the number of perforations. However, the percentage of heat transfer enhancement or fin effectiveness ($\varepsilon=q_{with\ fins}/q_{without\ fins}$) decreases incrementally with the number of perforations up to eight holes and then this enhancement increases as the perforations rise up to 50 holes, according to work by Yaghoubi et al. (2009) and Shaeri, et al. (2009). They investigated thermal and airflow characteristics of square lateral perforated PFHSs at variable porosity under laminar and turbulent airflow. Under the laminar flow conditions, the perforated fins effectiveness is nearly the same value as that of the solid fins, even though the perforations have increased in

number, whereas, for the turbulent flow, heat transfer rate increases when increasing the number of perforations.

1.9.2 Plate Fins with Longitudinal (Frontal) Perforations

The thermal and hydraulic characteristics of perforated plate fin HSs have only been numerically reported with laminar and turbulent airflow; there is no experimental work. Either *k*-ε standard or RNG models are utilised in the following literature to solve the governing equations. Similarly to lateral perforation plate fins, total drag (friction and pressure drag), Nusselt number based on the total wetted surface area (Nu_T) and the weight of the fins reduce as the number of these longitudinal perforations along the length of the plate fins increases. Fin effectiveness is enhanced via these perforations, which alleviate the recirculation zones that are behind the plate fins for both laminar and turbulent airflow. For example, Shaeri & colleagues (2009 and 2012) have presented work related to the perforated PFHSs in the presence of laminar and turbulent airflow.

The laminar flow and heat transfer characteristics have been numerically investigated by the following researchers.

The effects of the number of perforations with variable porosity on the heat transfer rate and laminar airflow have been investigated by Shaeri & Yaghoubi (2009). Numerical data explain that the average friction coefficient, pressure drop, average Nusselt number (Nu_T) and the weight of the fins decrease, but the effectiveness of the perforated fins increases when the number of perforations increases. Perforated plate fins reduce the shape and the size of recirculation zones (wakes) behind these fins compared with solid fins. The effects of size and number of perforations of a flat plate of the same porosity on thermal performance and laminar airflow have been studied by Shaeri & Jen (2012). The outcomes illustrate that the total drag, friction and pressure drag stay nearly constant for all kinds of perforated and solid fins because the airflow has a low velocity inside those perforations. Conversely, the thermal entrance length (the distance of thermal boundary layer inside the perforations) is smaller with a larger number of perforations than with a smaller number perforations, by which means the heat transfer rate of fins with a smaller number of perforations (larger perforation sizes) improves by approximately 80% compared with solid fins.

The following researchers report turbulent airflow and heat transfer characteristics numerically.

Shaeri & Yaghoubi (2009) have reported the influence of perforations with a variable porosity in perforated plate fins on the heat transfer rate and turbulent airflow. The results indicate that the rising number of perforations influences: the size of the wakes that form behind the fin; the length of the recirculation zone around the lateral surfaces of the fin; total drag; skin friction coefficient; and the weight of the fins decreases. Fin effectiveness of perforated fins with three perforations is almost 65% higher than that of the solid fin. On the other hand, Shaeri & Jen (2012) report the effects of size and number of perforations for the same porosity on thermal performance and level of turbulent fluid flow. The results prove that the friction drag of the perforated fins is higher but the pressure drag and the total drag of the perforated fins are smaller than those of the solid fins. Furthermore, fin effectiveness increases with increasing number of perforations; in other words, heat transfer rate enhances with decreases in perforation size at constant porosity.

1.9.3 Effect of Differently Shaped Perforations

Concerning the shape of the perforations along the plate fins, Ismail et al. (2013 and 2014) have only numerically demonstrated this with laminar and turbulent airflow.

The effects of circular and square perforations along the plate fins on the thermal and turbulent airflow performance have been considered by Ismail et al. (2013). The results show that the heat transfer rate of the perforated fins is nearly the same for both the circular and square perforations, while the pressure drop is lower for the circular perforated fins. In addition, as the number of perforations increases from two to three, fin effectiveness is almost the same but pressure drop decreases. Ismail et al. (2013 and 2014) have developed this study via considering more perforation shapes in an investigation into the effects of perforation shapes on the thermal and hydraulic performance under laminar and turbulent airflow. Circular, square, triangular, and hexagonal perforation shapes have the same surface area, as shown in Figure 1.19. Commonly, the results are the same for both laminar and turbulent airflow. The hexagonal and circular perforations have higher heat transfer performance enhancement (HTPE) and lower pressure drag coefficient than the other

perforations, Figure 1.20. In addition, the maximum Nusselt number, $Nu_{T,}$ still occurs for the solid plate fins.

According to the shapes of the fins with lateral perforations, Ismail et al. (2014) have demonstrated the effects of number and shape of lateral perforations, circular, square, triangular, and hexagonal, on the turbulent airflow and heat transfer. RANS-based modified *k-ω* turbulent flow has been considered. They indicate that the shapes of the perforations have a significant role in enhancing the cooling and hydraulic performance. Hexagonal perforated fins, however, have the largest effectiveness and heat transfer performance enhancement (HTPE) of the perforated fins. As indicated earlier, solid fins have the maximum Nusselt number, $Nu_{T,}$ and the largest friction coefficient and this decreases with increasing in the number of perforations.

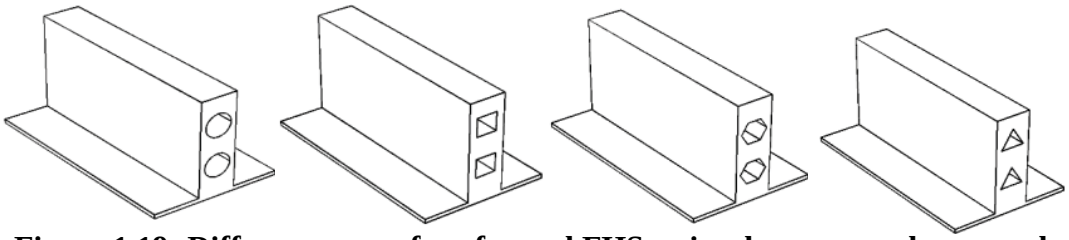

Figure 1.19: Different sorts of perforated FHSs: circular, square, hexagonal, and triangular (Ismail et al., 2013)

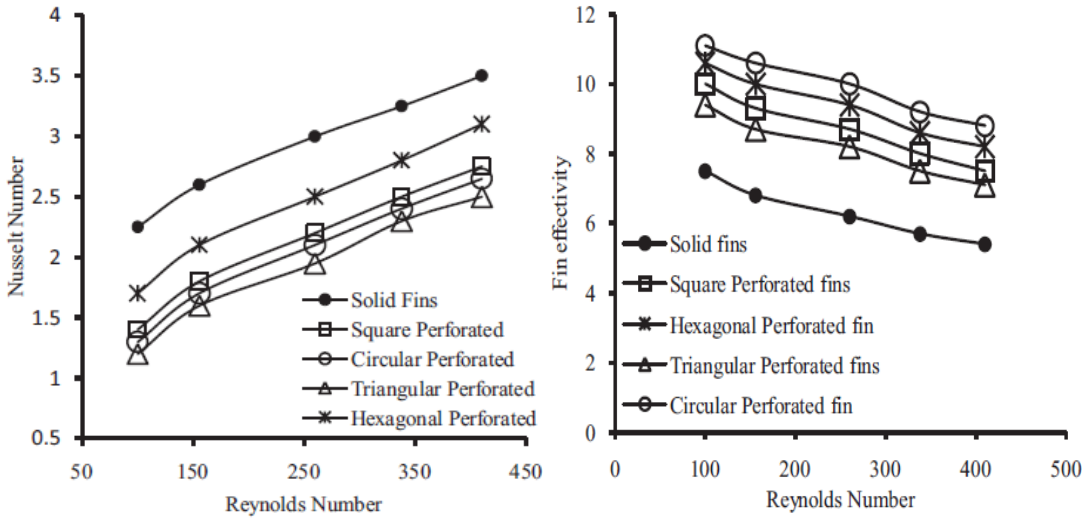

Figure 1.20: Nusselt number and fin effectivity variations for different types of fin (Ismail, 2013)

1.9.4 Perforated Ribs and Blocks as Fins

The experimental testing of the other types of perforated blocks as fin heat sinks, ribs or baffles towards the flow direction is investigated in this section. These perforations have differently shaped perforations. For instance, turbulent forced convection heat transfer and friction loss of a single baffle that has perforations in different positions, of different sizes, and with inclined orientations inside the rectangular channel have been investigated by Dutta and Dutta (1998). The results point out that both local and average Nusselt numbers increase when increasing the angle of baffle orientation and baffle size, and with a decreasing number of circular perforations. With regard to the position of the baffle, when it is located at the start from the heat source, the Nusselt number is higher than that of the baffle, which is placed far away of the heat source. Furthermore, friction factor ratio decreases as the angle of baffle decreases and circular perforation density increases.

Sara et al. (2000 and 2001) have produced two works related to solid and perforated blocks, which are used in many practical applications. These works are focused on the thermal performance efficiency ($\eta=h_a/h_s$, where h_a and h_s are the convective heat transfer coefficient with and without blocks, respectively) of these perforated block types with turbulent airflow, Figure 1.21. The results show that the performance efficiency and Nusselt number of the perforated blocks are greater than the solid blocks and they increase by nearly 30%-60% as increasing the perforation inclination angle, perforation open-area ratio, and perforation diameter. Additionally, friction factor and pressure drop of the perforated blocks are lower than those of the solid ones. Therefore, the gained energy performance of the perforated blocks compared to the solid blocks is up to nearly 77% due to the enhanced Nusselt number and the reduced pressure drop of the perforated blocks.

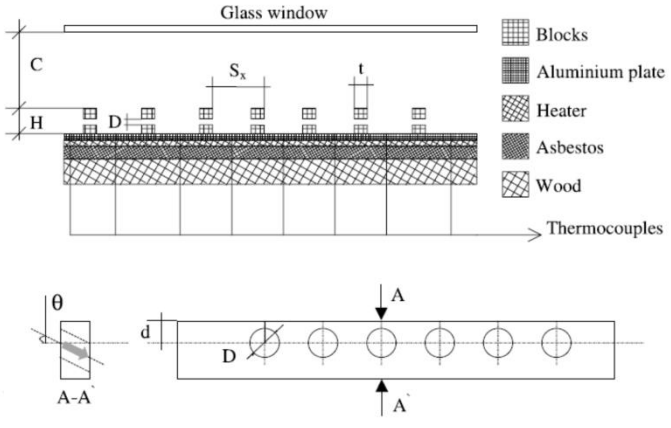

Figure 1.21: The test section of perforated blocks/ribs with different views (Sara et al., 2001)

With respect to numerical reports of perforated ribs as fins, it is indicated that the numerical data are in agreement with the previous experimental reports. For example, Khoshnevis et al. (2009a) studied the effects of circular perforated ribs with various attack angles towards the flow direction on the thermal airflow of heat sinks inside a rectangular channel. However, the effects of two kinds of perforation, circular and slotted perforated ribs shown in Figure 1.22, were reported in another study by Khoshnevis et al. (2009b). The Nusselt number enhances as the perforation inclination angles, perforation diameter and perforation open-area ratio increase. Furthermore, pressure drop reduces with increasing perforation diameter and open-area ratio, but it is not affected by perforation inclination angles. Generally, the Nusselt number and pressure drop of the perforated ribs are slightly enhanced compared to slotted ribs with the same open-area ratio.

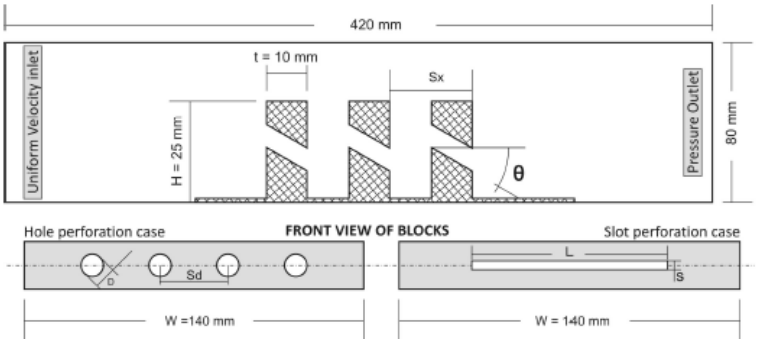

Figure 1.22: The angle of perforations and slots in rectangular blocks towards flow directions (Khoshnevis et al., 2009b)

1.10 Perforated Folded Fin Heat Sinks (PFFHSs)

The thermal resistance of several triangular folded fin heat sinks is investigated by Jia et al. (2003, 2004 and 2007). The fin types are: extruded plate fin (a model), slit folded fin (b model), perforated folded fin (c model), and perforated slit folded fin (d model), as shown in Figure 1.23, and they are tested for the same boundary conditions such as applied heat flux, inlet air velocities and inlet air temperature. The experimental results indicated that the thermal resistance of the new triangular folded fins design (b, c, and d models) is superior to that of the traditional plate fins (a model). The most effective for application in high-powered electronic devices are the slit folded fin (b model) and/or perforated slit folded fin (d model) heat sink models. The thermal resistance of the slit folded fin (b model) and the perforated slit folded

fin (d model) is nearly 18% and 20% respectively less than that of conventional plate fin heat sinks (a model) at a fixed fan power. In addition, the cooling performance of these heat sinks depends remarkably on the increasing fin height, number of slits for the perforated slit folded fin, decreasing fin pitch, and Reynolds number.

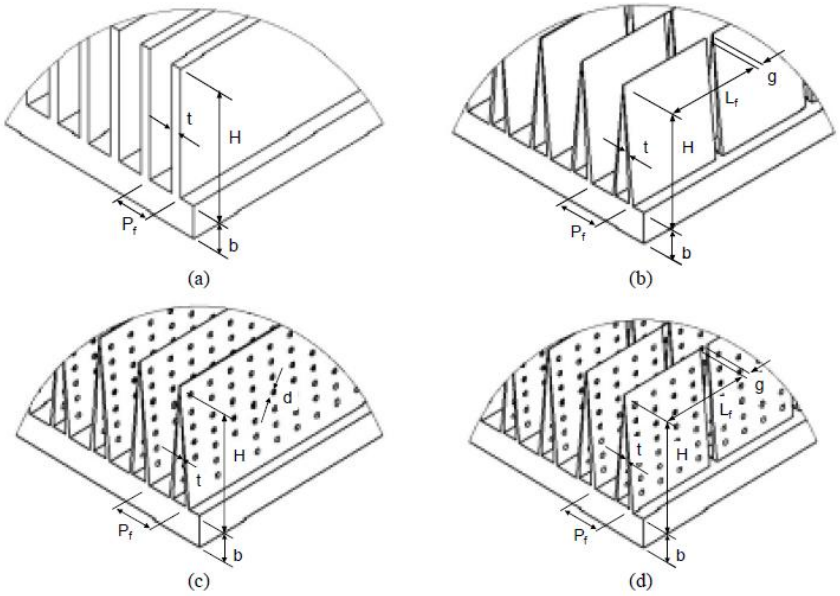

Figure 1.23: Different designs of folded fin heat sinks: a) Extruded plate fin, (b) Slit folded fin, (c) Perforated folded fin, (d) Perforated slit (Jia et al., 2003)

1.11 Perforated Pinned Heat Sinks (PPHSs)

Relatively few studies have considered the effect of perforations on the heat transfer and pressure drop of perforated pinned heat sinks (PPHSs), shown in Figure 1.24 which is investigated experimentally in the following literature survey, rather than through numerical reports. It is indicated that pin perforations offer considerable benefits by enabling the heat transfer to be improved while at the same time reducing both the pressure drop across the heat sink and the fan power required to pump the air through it. In addition, reduction in the weight of the pinned heat sink can be obtained via these perforations. These perforated PHSs can be classified into two types, single and multiple perforations.

1.11.1 Single Perforated Pinned HSs

PHSs with only one perforation are called single perforated PHSs. The effects of square and circular cross-section perforated pinned heat sinks in an in-line array have been reported by Sahin & Demir (2008a and 2008b), while Amol & Farkade (2013) considered the effect of a staggered arrangement of circular cross-section

perforated pinned heat sinks. The various parameters with Reynolds number, such as turbulent airflow, clearance ratio (*C/H*) and inter-fin spacing ratio (streamwise distance) in the flow direction, were studied in these three reports to investigate the Nusselt number and pressure drop of perforated pinned HSs where *C* is the distance from the tip of the pins to the upper surface of the wind tunnel, and *H* is the height of the pins. In addition, this perforation is just a single circular perforation located near the bottom of the fin. These studies have found consistently that a single perforation leads to an enhancement of Nusselt number and a reduction in pressure drop compared to the equivalent solid pin system, as shown in Figure 1.25. For example, Sahin & Demir (2008a) have found that the enhancement efficiencies of square cross-section perforated pinned heat sinks vary between 1.1 and 1.9, while the enhancement efficiencies of circular cross-section perforated pinned heat sinks are the highest, varying from 1.4 to 2.6 depending on the inter-fin spacing ratio and clearance ratio (Sahin & Demir, 2008b). In addition, the projected Nusselt number, $Nu_{P,}$ is enhanced and the friction factor increases when reducing both clearance ratio (*C/H*) and streamwise distance.

It can be concluded that the main outcomes of this design are that localised jet flows through the perforations increase local heat transfer by alleviating the recirculation zones that form behind solid pins, and increasing shear-induced mixing leads to enhance thermal airflow and reduce pressure drop through perforated pinned heat sinks. To select the optimum design, the Taguchi experimental design method design is used in these studies utilising the ANOVA-TM software package to evaluate the effect of each parameter on the optimisation criterion. The trade-offs among goals are considered and the optimum design occurs as pin height and pitch are 50mm and 3.417, respectively at *Re*=42000 (Sahin & Demir, 2008).

As indicated in the previous three reports, the perforated pinned heat sinks can be used for large heat exchange applications because the dimensions of the heat sink are 250×250mm, which is large, and the aspect ratio of height to diameter, *H/d*, is greater than four (Vanfossen & Brigham, 1984). However, it is difficult to apply this size of perforated PHSs for cooling electronics systems due to restrictions in the size of these systems. Thus, a mini-perforated pinned heat sink design is required to enhance heat transfer rate and at same time reduce fan power consumption to drive air through PHSs, and that leads to the desirable benefit of reducing the CPU

temperatures of the heat sink in the case of a fixed heat sink size, which is our goal in this study.

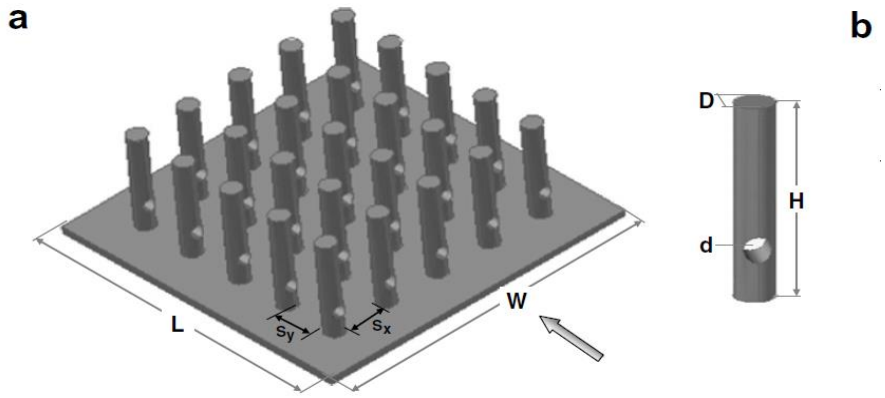

Figure 1.24: (a) Perspective view of the heat exchanger and a single perforated pin configuration (b) Sectional view of heating unit and tested model assembly (Sahin & Demir, 2008b)

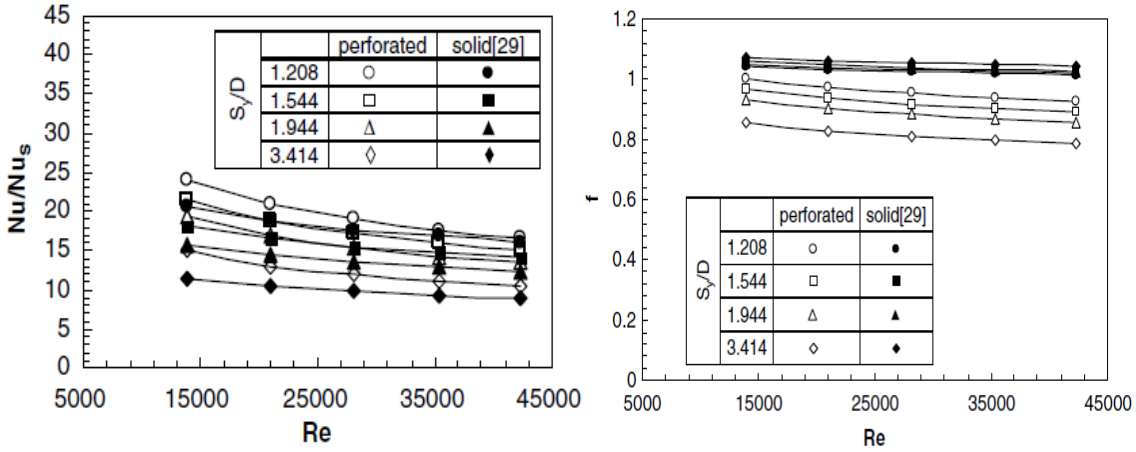

Figure 1.25: Nusselt number and friction factor variations for single perforated pin fins (Sahin & Demir, 2008b)

1.11.2 Multiple Perforated Pinned HSs

Based on the literature review and our knowledge, the combination of experimental and numerical studies relating to the benefits of single and multiple perforated pinned heat sinks for electronic cooling applications has not yet been reported. Hence, illustrating the comprehensive thermal airflow of this kind of heat sink has motivated a full study of the benefits of multiple perforated PHSs, as shown in previous Figure 1.2E and 1.27.

The expected benefits of multiple pin perforations may enhance the heat transfer rate (increasing Nu_T and Nu_P) while reducing the fan power consumption, which is required to overcome the pressure drop across the heat sink. The minimisation of CPU temperature and thermal resistance are the other important factors for thermal management of systems containing electronic components, together with minimising the fan power consumption. The additional benefit of a reduction in the weight of the pinned heat sinks is important to reduce the cost and save material.

The previous studies can be summarised by the flowchart illustrated in Figure 1.26.

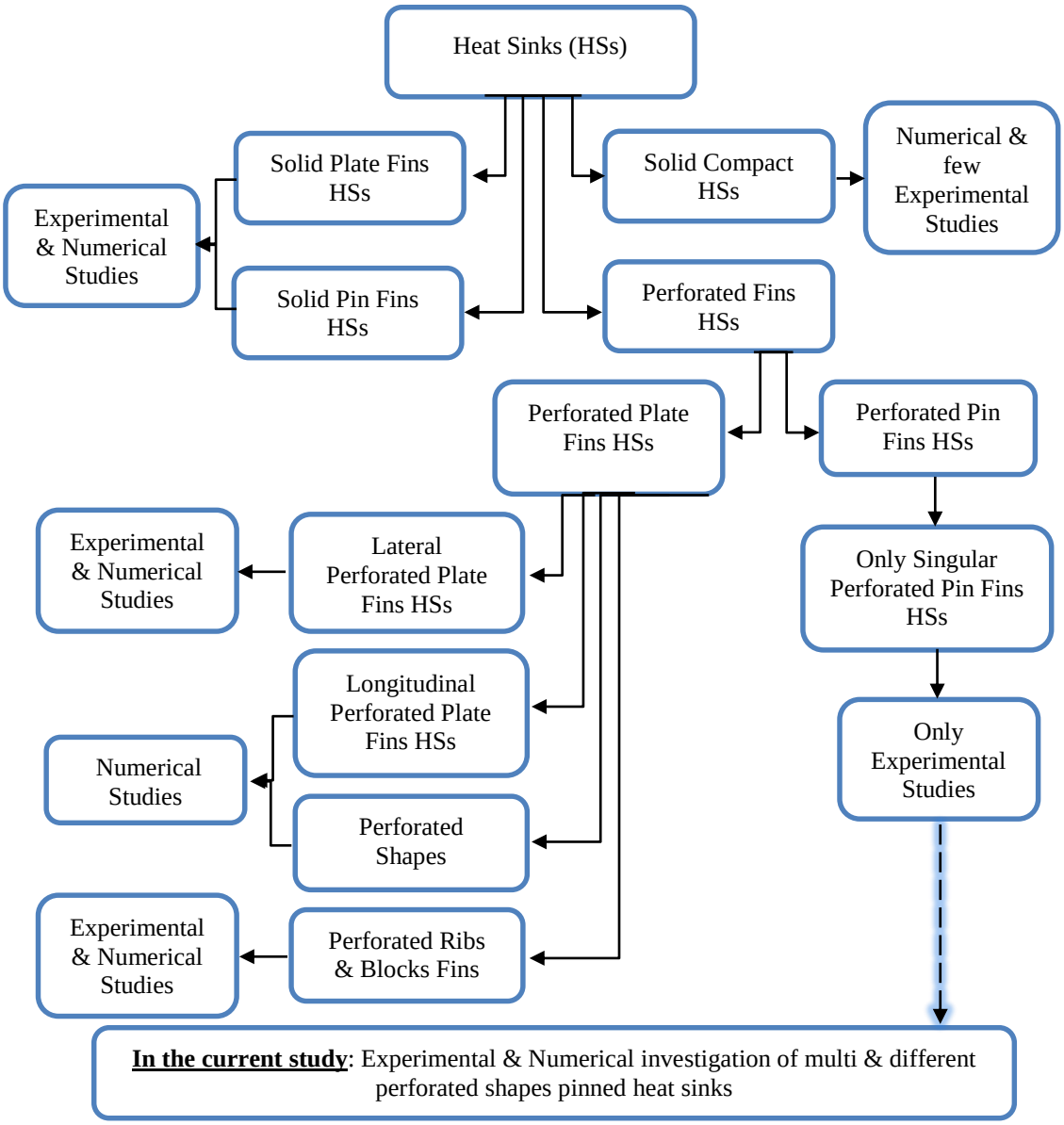

Figure 1.26: Simple flowchart of literature review of different heat sink types

1.12 The Aims and Objectives of the Current Study

According to the literature review, as indicated previously that many optimisation reports have investigated plate fin heat sinks, see e.g. Chiang (2005), but they cannot remove the intrinsic limitation that air flows, which is smooth through the heat sink channels. This is due to the parallel plate arrangement, limiting the achievable heat transfer rates. Pinned heat sinks (PHSs) can be an effective alternative to plate fin heat sinks since they have the advantage of hindering the development of the thermal boundary layer on smooth surfaces responsible for limiting the heat transfer rates in plate fin designs (Zhou & Catton, 2011). However, this the heat transfer enhancement of pinned heat sinks is always accompanied by a substantial increase in fan power losses (pressure drop). Hence, in most pinned HS applications, both the heat transfer and pressure drop characteristics should be considered.

Based on the author's knowledge, very few experimental studies have been reported; only three papers have examined the thermal airflow characteristics of a single circular perforation at the bottom of a pin fin HS (Sahin & Demir, 2008a; Sahin & Demir, 2008b; Amol & Farkade, 2013). The perforations are a useful air-cooling technique to enhance the thermal airflow characteristics of the pinned heat sink. Furthermore, there exists neither numerical data with respect to the use of perforated pin fins nor combination of experimental and numerical works relating to notched and slotted pin fins for heat sink applications.

As a result of that, the main aim of this study is a numerical and experimental investigation of different configurations of perforated, notched and slotted pinned heat sinks that are presented to enhance the heat transfer rate, reduce CPU temperature, and decrease the fan power to overcome the pressure drop through pinned HSs. Then, the optimum thermal airflow characteristics of PHSs design such as perforations dimensions are examined to obtain the lowest CPU temperature and fan power consumption through a heat sink. In addition, the application specifications of pinned heat sinks is reported for active air-cooling of electronic systems since, at a smaller scale, convective heat transfer to air as it flows over a network of fins is also the most common approach to cooling microelectronics due to its low cost, availability, relatively simple structure and easy manufacturing (Zhou &

Catton, 2001). Finally, the weight of these heat sinks will be lighter when using aluminium and perforations.

The types of pin fin heat sinks that will be studied in this thesis are, as shown in Figure 1.27:

1. Circular perforated pin fins are aligned in the direction of flow; the locations and number of holes can be changed as follows: single (1P), double (2P), triple (3P), and five perforations (5P).
2. The shape of these perforations can be changed to square (3PS), and elliptic (3PE).
3. Slotted pin fins (SPHSs) are aligned in the direction of flow, and the slot height can be 3S, 6S, and 10S with constant slot width.
4. Notched pin fins (NPHSs) are arranged in the direction of flow, and the notch height can be 2.5N, 5N, and 7.5N with constant notch width**.**

To reach the specified aims, this study is divided into five objective parts:

1. To design, fabricate, and examine experimentally the thermal airflow characteristics of perforated and solid pin fin heat sinks to be used for active air-cooling of electronic systems.
2. To investigate numerically the thermal airflow characteristics of solid and perforated pinned heat sink devices in order to validate the CFD approach against the experimental results.
3. To investigate numerically the thermal airflow characteristics of various configurations of perforated, notched and slotted pinned heat sink devices to demonstrate how the thermal airflow characteristics of these models enhance pinned heat sinks compared with solid pin fins.
4. The optimal variable design of perforated and notched pinned heat sink models are considered to achieve the multi-objective function that is represented to minimise CPU temperature and fan power consumption and select the optimum pinned heat sink design
5. Lastly, to consider the limitations in the application of pinned heat sinks based on the pin density and the supplied heat flux for investigating the capability of these pinned heat sink designs to be used in the desktop PC CPU for waste heat dissipation. Furthermore, to evaluate the allowance level of applied heating power on these pinned heat sink models.

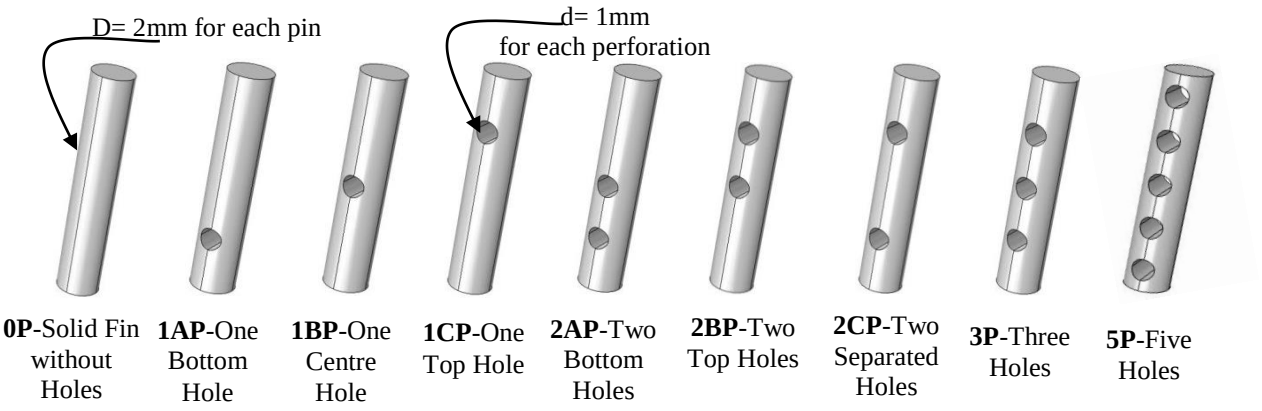

A- Circular Perforations – each holes has a diameter= 1mm and each pin diameter=2mm

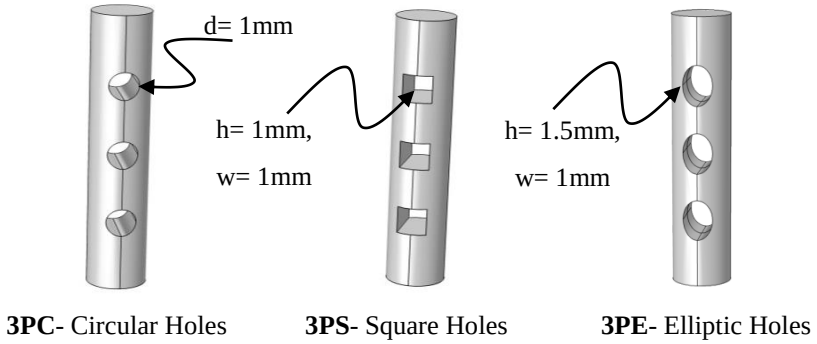

B- Circular, Square, and Elliptic Perforations

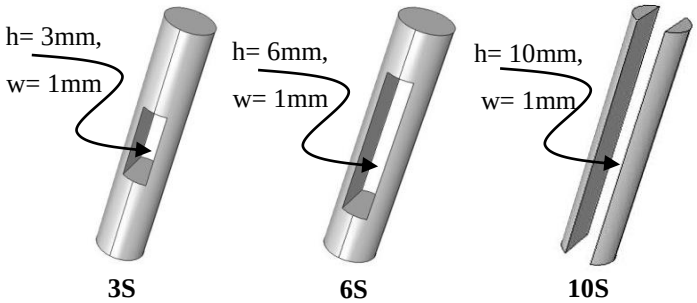

C- Slotted Pin Fins, SPHSs

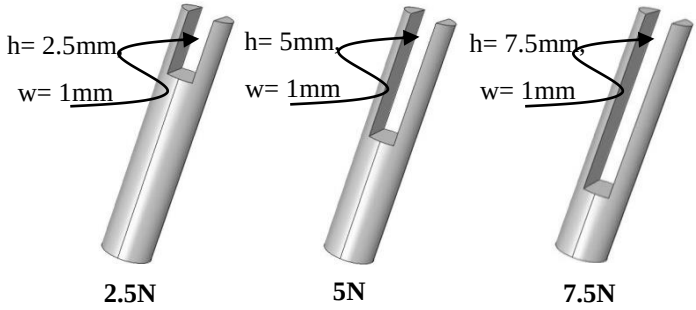

C- Notched Pin Fins, NPHSs

Figure 1.27: Different types of pin fins heat sinks

Finally, the scope of the current work can be represented as shown in Figure 1.28.

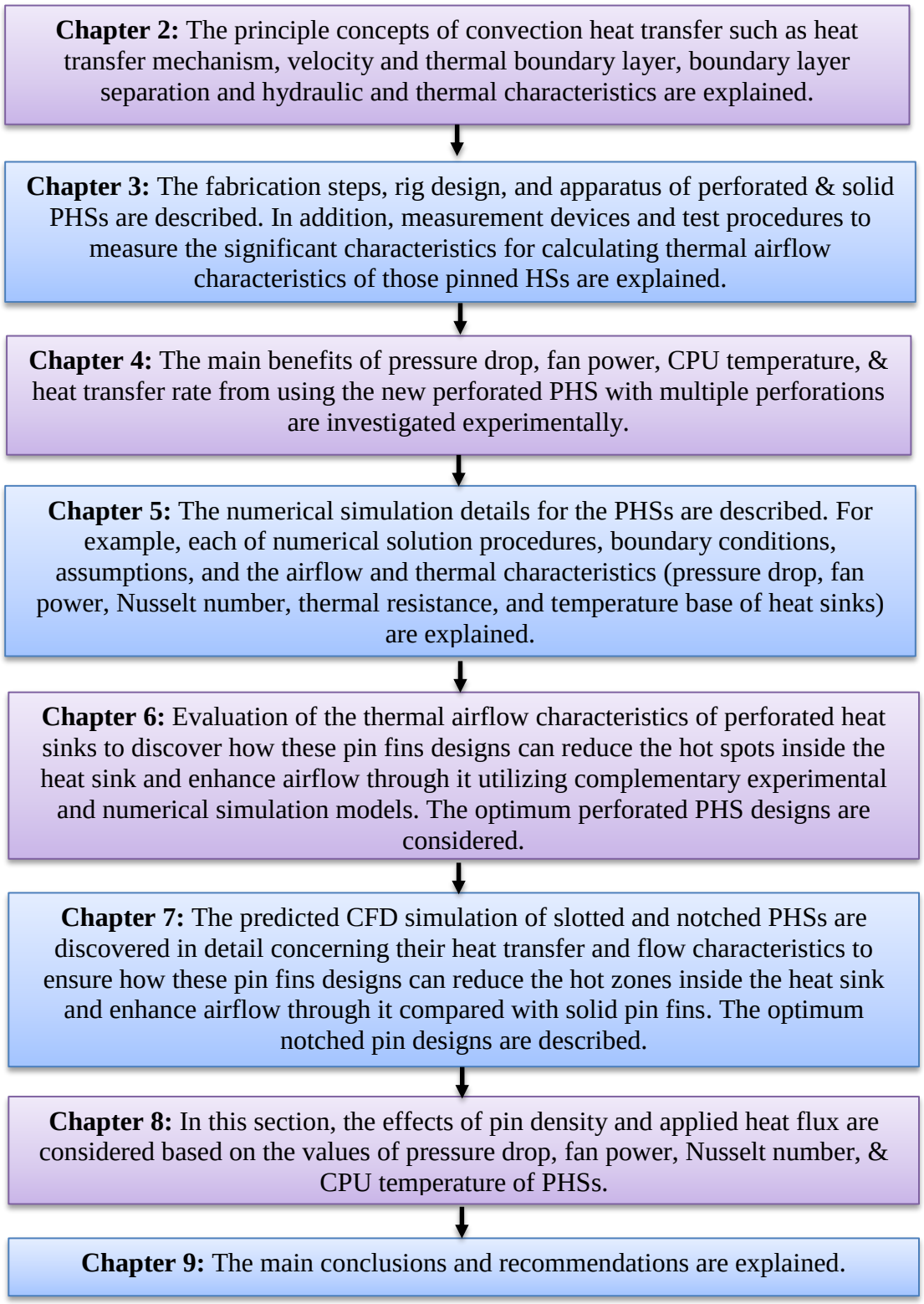

Figure 1.28: The scope of the present thesis work

Chapter Two: The Fundamental of Convection Heat Transfer

2.1 Introduction

In this chapter, the basic concepts of fluid flow and heat transfer are illustrated. The basic concepts are included the physical mechanism of convection heat transfer, the types of fluid flows, the velocity and thermal boundary layers, and the boundary layer separation. In addition, the hydraulic and the heat transfer characteristics of heat sink that are investigated in the current study.

2.2 Physical mechanism of convection heat transfer

Heat transfer through fluids (liquids or gases) can be by conduction or convection depending on the presence or absence of any bulk fluid motion. In the case of bulk fluid motion, heat transfer occurs by convection, as shown in Figure 2.1 (a) and (b), while heat transfer occurs by conduction in the absence of bulk fluid motion, Figure 2.1 (c).

In reality, convection heat transfer involves fluid motion and heat conduction. Heat moves from a hot surface to an adjacent cooler fluid layer by conduction, and then this heat transfers to the next cooler fluid layer by fluid motion, and so on. Thus, the rate of convection heat transfer is much higher than that of by conduction, (Cengel, 2006).

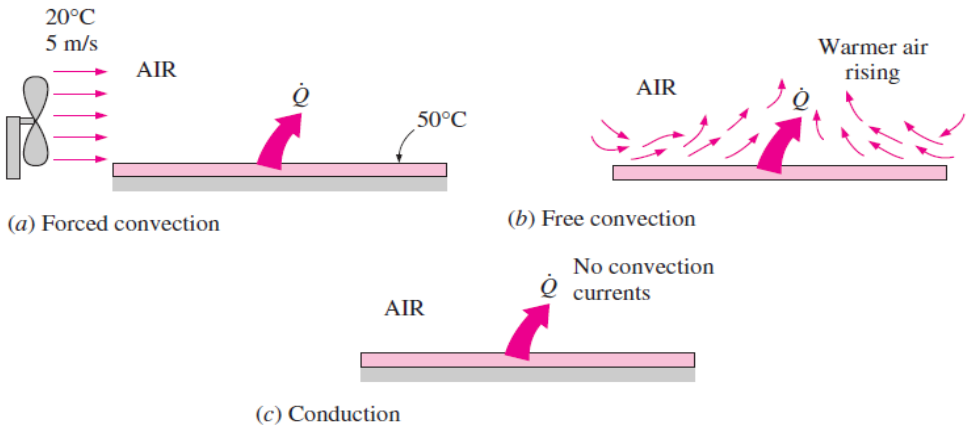

Figure 2.1: Physical mechanism of heat transfer from hot surface to cool surrounding air by convection and conduction, (Cengel, 2006).

The convection heat transfer, by experience, depends on the fluid properties such as dynamic viscosity (μ), thermal conductivity (k), thermal capacity (C_p), and density (ρ) and the fluid velocity (U). Furthermore, it depends on the geometry, solid surface roughness and the type of fluid flow. Therefore, the heat transfer by convection is a complex mechanism, (Cengel, 2006). The rate of convection heat transfer increases with increasing temperature difference between a hot surface and a cold fluid. This rate can be defined by Newton's law of cooling:

$$\dot{Q}_{conv} = hA_s(T_s - T_\infty) \tag{2.1}$$

which relates the average convective heat transfer coefficient (h), the heat transfer surface area (A_s), the surface temperature (T_s) and the ambient fluid temperature (T_∞).

2.3 The basic concept of fluid flow types

Since convection heat transfer is accompanied with fluid mechanics, the common general categories of fluid flow are explained below to understand fluid flow behaviour that effects the enhancement of convection heat transfer, (Cengel, 2006).

2.3.1 Viscous and Inviscid Flow

When the viscosity of a fluid is considered and its effects are significant due to an internal resistance of a fluid to flow, that is called viscous flow. However, inviscid flow is assumed no viscosity and its effects is very trivial in some flows and can be ignored.

2.3.2 Internal and External Flow

If a fluid is forced to flow inside a channel, duct and pipe and it is confined by a surface, this is called internal flow. However, external flow can be defined as when fluid is forced over or around an object and without restriction by adjacent surfaces of an object.

2.3.3 Compressible and Incompressible Flow

Certain gas flows involve substantial variations in the fluid density, and these are known as compressible flows. For example, high-speed aircraft, rocket motors and jet engines are relevant to compressible flow. Liquid densities are essentially

considered constant and thus classified as incompressible flow. Air flows are also commonly modelled as incompressible flow if the flow speed is sufficiently low.

2.3.4 Laminar and Turbulent Flow

If a fluid flows in parallel flow with smooth streamlines and orderly flow without interaction between the fluid flow layers, this is called laminar flow. For example, the flow with low speed and high viscosity such as oils. In contrast, turbulent flows involve chaotic fluctuations in the local fluid velocity, resulting in disruption between the fluid layers, and it is not an orderly flow. The process of a laminar fluid flow that is becoming fully turbulent flow is called transient fluid flow. Such flows occur at high speed and with low viscosity fluids such as air.

2.3.5 Natural and Forced Flow

Based on how the fluid moves, if a fluid is forced to flow inside or over a pipe by a fan or a pump that is classified as forced fluid flow or forced convection, as shown in Figure 2.1 (a). However, the buoyancy force effect is a response to a fluid motion where warmer fluid (lighter fluid) rises up and cooler fluid (denser) goes down; this is called natural convection (thermosiphon effect), as shown in Figure 2.1 (b).

2.3.6 Steady and Unsteady Fluid Flow

Steady flow is the type of fluid flow in which the fluid characteristics (velocity, pressure, etc) at a point are independent of time. While, the unsteady flow is the type of fluid flow in which the fluid characteristics (velocity, pressure, etc.) at a point change with respect to time.

2.4 The concept of boundary layers

The concept of boundary layers is important to understand the convection heat transfer between a surface and a fluid flowing over it. Velocity and thermal boundary layers are described in this section.

2.4.1 Velocity Boundary Layer (δ_u)

Figure 2.2 shows the velocity boundary layer of fluid flowing over a flat plate. The x-axis represents the fluid flow direction over the surface of a flat plate from the leading edge of the plate, and the y- axis represents the normal flow direction from

the plate surface. The velocity of fluid (V) at the leading edge of the plate in x-direction is uniform velocity. It can be imagined that the fluid consists of many adjacent fluid layers on top of each other. The velocity of the fluid particles in the first layer next to the surface plate is zero due to the no-slip condition. This layer then will affect the motion of the next adjacent fluid layer due to the friction force between the fluid particles of these two neighbouring layer at different velocities and this act to the fluid particles motion in the next layer, and so on until. The velocity reaches the free-stream velocity (u_∞) at a certain distance from the surface of the plate. This distance is known as the boundary layer thickness (δ_u) and is defined as the distance at which $u=0.99u_\infty$. The velocity boundary layer (δ_u) involves four flow regions in which the fluid viscous: the fluid flow velocity is zero at the surface of flat plate. The laminar sublayer (viscous sublayer) is a very thin layer above the flat plate surface. The buffer layer is a layer just next the laminar sublayer and a flow begins to develop to turbulent flow. The third region is the turbulent layer. The free stream region is far away from the surface, where $u=u_\infty$, (Cengel, 2006).

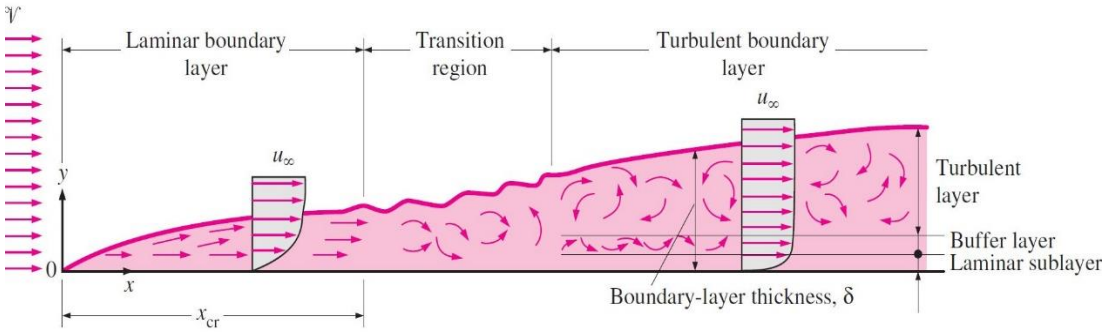

Figure 2.2: The velocity boundary layer development on a flat plate surface, (Cengel, 2006).

2.4.2 Thermal Boundary Layer (δ_{th})

Figure 2.3 shows the thermal boundary layer of cool fluid flowing at a specific uniform temperature (T_∞) over a hot flat plate (T_s). The thermal boundary layer is similar to the velocity boundary layer and the former will develop due to the temperature difference between the fluid flow and the surface plate. The hot surface of the plate will achieve thermal equilibrium with the fluid layer, adjacent to the surface. The energy of the fluid particles will be exchanged with the particles of the adjoining fluid layer, and so on. The temperature gradients of the thermal boundary layer are represented by:

$$(T_s - T) = 0.99(T_s - T_\infty) \tag{2.2}$$

The thickness of the thermal boundary layer increases with increasing distance from the leading edge in the flow direction, since the effects of heat transfer penetrate farther into the fluid flow. The relation between conditions and the convection heat transfer at any distance x from the leading edge are represented by applying Fourier's law at the interface between the solid surface plate and the fluid layer as *y=0*:

$$k_f \frac{dT_f}{dy}\Big|_{y=0} = k_s \frac{dT_s}{dy}\Big|_{y=0} \tag{2.3}$$

where k_f and k_s are the thermal conductivity of fluid and solid flat plate, respectively, (Incropera, 2011).

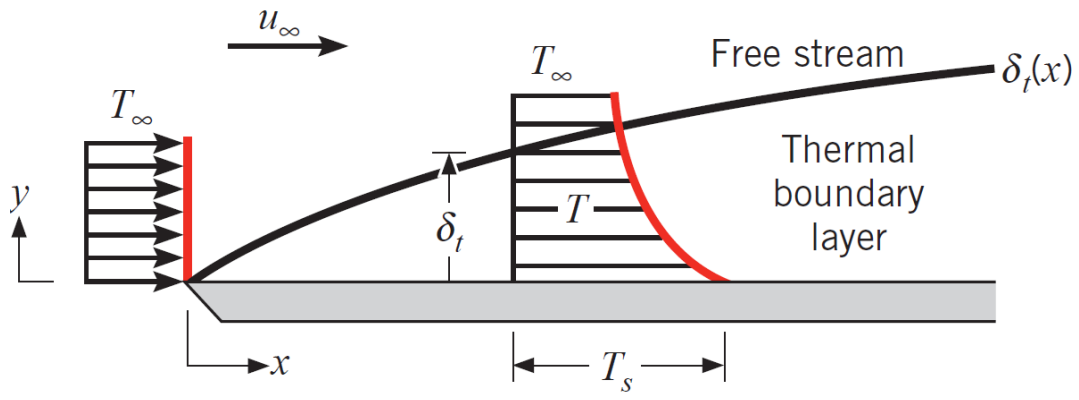

Figure 2.3: The thermal boundary layer development on an isothermal flat plate surface, (Incropera, 2011)

2.4.3 Boundary Layer Separation

To understand the phenomenon of boundary layer separation, consideration fluid flow around a cylinder is very important for engineering applications. For example, shell-and-tube heat exchangers, bundle circular tubes heat exchangers, circular pinned heat sinks, etc.

The upstream fluid velocity (V) around a cylinder and the free stream velocity (u_∞) that depends on the distance (x) from the stagnation point are considered, as shown in Figure 2.4. The fluid velocity is equal to zero at the stagnation point ($\theta=0$). As the fluid flow accelerates due to the favourable pressure gradient ($du/dx > 0$ *as* $dp/dx < 0$), the fluid flow reaches to the maximum value at $dp/dx=0$ and then it decelerates due to the adverse pressure gradient ($du/dx < 0$ *as* $dp/dx > 0$), as shown

in Figure 2.5. The fluid velocity gradient becomes zero at the surface when the fluid flow decelerates, this point is called “separation point”. At this point, the momentum of fluid is not sufficient to overcome the pressure gradient and the continued fluid movement downstream is impossible. In addition, the oncoming fluid flow prevents flow back upstream. Thus, boundary layer separation must happen. This is the main reason the boundary layer separates from the surface and reversed flow and vortices are formed just behind the cylinder at the downstream region, (Incropera, 2011).

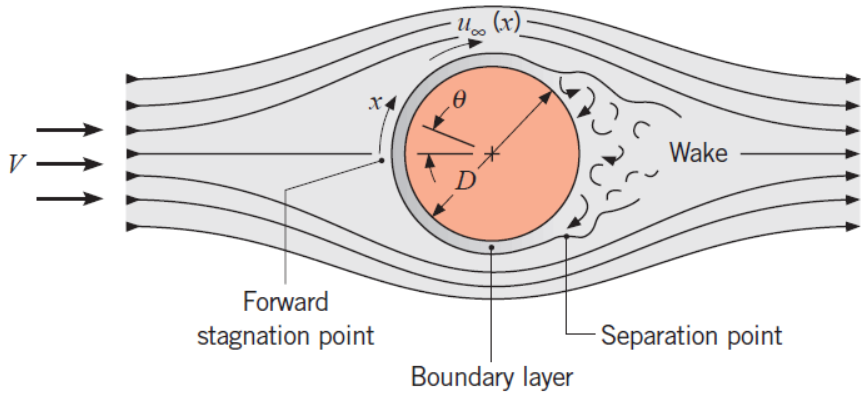

Figure 2.4: Boundary layer separation on a cylinder and formations eddies in the downstream region, (Incropera, 2011)

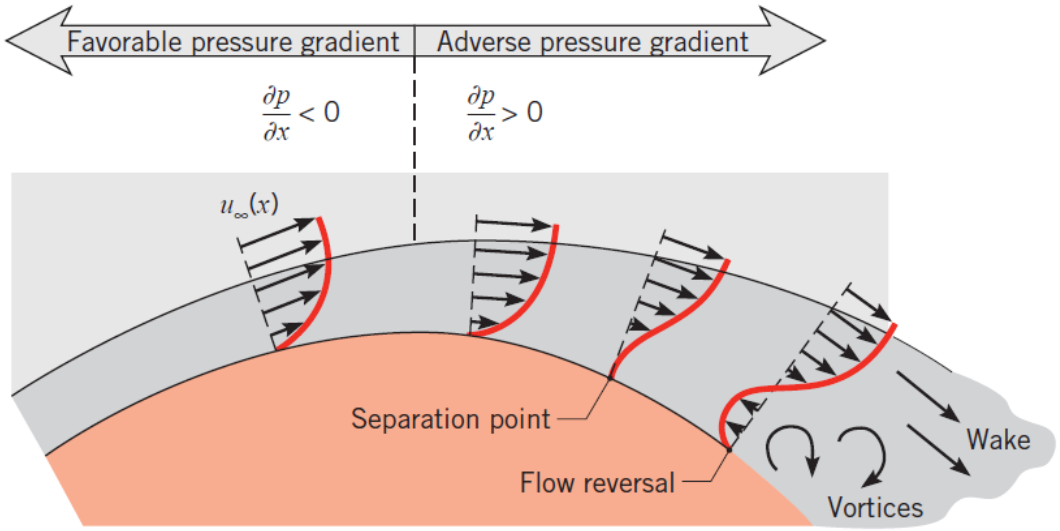

Figure 2.5: Velocity profile associated with pressure gradient and separation on a cylinder, (Incropera, 2011)

2.5 Hydraulic and Heat Transfer Characteristics

Airflow and heat transfer characteristics including Reynolds Number, pressure drop, fan power, profit power factor, pressure drag coefficient, Nusselt number, thermal resistance, average temperature base case heat sinks (CPU temperature), temperature and velocity air distribution along pin fin heat sinks, are important parameters, to evaluate pinned heat sinks designs, which can be obtained from the ANSYS FLUENT post processing options. These factors are defined below.

2.5.1 Reynolds Number (*Re*)

Reynolds number is the ratio between inertial forces and viscous forces and is defined as:

$$\mathrm{Re} = \frac{\rho U D_h}{\mu} \tag{2.4}$$

$$D_h = 4\frac{A_c}{p} = 2\frac{(H.W)}{(H+W)} \tag{2.5}$$

where U: the air inlet velocity, D_h: duct hydraulic diameter , ρ (kg/m^3),and μ (kg/m.s) are the density and viscosity of air. In the present study, the inlet velocities are varied from 6.5m/s to 12m/s and the range of Reynolds numbers is 3500-6580.

2.5.2 Pressure Drop (*ΔP*)

Pressure drop (Pa) is defined as the difference in pressure between inlet and outlet airflow of test section (heat sink).

$$\Delta \mathrm{P} = P_{outlet} - P_{inlet} \tag{2.6}$$

where ΔP is the pressure drop over the heat sink, and $P_{inlet,\ outlet}$ are inlet and outlet pressure of the airflow in the test section.

2.5.3 Fan Power (P_{fan}) and Profit Power Factor (J)

Fan power (W) is the required power to drive the air through the heat sink and can be evaluated as Sparrow et al. (1980) and Yuan et al. (2012) by:

$$P_{fan} = UA_c\Delta P \tag{2.7}$$

where A_c: cross sectional area of the flow passage of the heat sink $=h.S_z.(N-1)$ (m^2), h: pin fins height (m), S_z: spacing between pins (m), N: number of pins in a row. In this study, fan efficiency is assumed 100% (Yuan et al., 2012).

The profit factor (dimensionless) is another factor to compare between heat sink designs (Yu et al., 2005)

$$J = \frac{Q}{P_{fan}} \tag{2.8}$$

where Q: the applied heating power on the base heat sink surface (W).

2.5.4 Pressure Drag Coefficient (P_d)

It is dimensionless and used for the drag or resistance quantity of an object against fluid flow and found as:

$$P_d = \Delta P/0.5\rho U^2 \tag{2.9}$$

2.5.5 Nusselt Number (Nu)

The Nusselt number of the pin-fins array is the ratio between the heat transfer rates of convection and conduction. Previous researchers have calculated heat transfer coefficient based on either the projected, A_P, or total, A_T, surface area of the heat sink and these are related to one another via the relationship (Sara, 2003; Sahin & Demir, 2008):

$$h_P = h_T\left(\frac{A_T}{A_P}\right) \tag{2.10}$$

$$h_T = \frac{Q_{conv}}{A_T[T_s - (\frac{T_{out}+T_{in}}{2})]} \tag{2.11}$$

where Q_{conv}: power applied to the base (W), h_T: the total heat transfer coefficient ($W/K.m^2$), h_P: the projected heat transfer coefficient ($W/K.m^2$), A_T: total surface area (m^2), A_P: projected surface area (m^2)T_s: the upper surface of heat sink temperature (^oC), $T_{in,\ out}$: inlet and outlet air temperature (^oC).

The Nusselt number (Nu_T) based on the total surface area of the pin-fins is:

$$Nu_T = \frac{h_T.L}{k_{air}} \tag{2.12}$$

While the projected Nusselt number (Nu_p) based on the projected surface area of the pin fins is:

$$Nu_P = \frac{h_P . L}{k_{air}} \tag{2.13}$$

where L: length heat sink in flow direction (m), k_{air}: is the thermal conductivity of air (W/K.m).

2.5.6 Thermal Resistance (R_{th})

The thermal resistance (K/W) of the heat sinks R_{th} is an object or material resists to a heat flow through heat sink and it is defined by:

$$R_{th} = \Delta T / \dot{Q} \tag{2.14}$$

The temperature difference ΔT is defined as the difference between the average temperature on the base (T_{case}) and the inlet air temperature (T_{in}) (Jonsson & Moshfegh, 2001).

2.5.7 Porosity ($\emptyset$)

The porosity of perforated pin fins has been calculated from the void volume of perforations divided by the volume of solid pin fin:-

$$\text{Porosity}(\phi) = \frac{V_{hole}}{\text{V}} \tag{2.15}$$

where V_{hole}, is perforations, slots, and notches void volume, and V solid pin volume.

Chapter Three: Experimental Methods

3.1 Introduction

This chapter focuses on two important elements of the work:

1. The description of the fabrication procedure of the heat sinks and the integration of these heat sinks into a measurement section.
2. The equipment and test procedures to measure the significant characteristics such as the local (inlet and outlet) air temperatures; variation of the upper and lower heat sink surfaces temperatures; ambient air temperature: inlet and outlet local pressure differences (pressure drop); and inlet air velocities for calculating thermal and airflow characteristics of solid and perforated pin fins heat sinks. These heat sinks are designed, fabricated, and tested during this study.

The main goal of the experimental work is an investigation into the benefits of pin fin perforations on the heat transfer and fan power in pinned heat sinks (PHSs) for cooling electronics packaging. Experimental data is presented, for the first time, on the benefits of using multiple perforations and the data used to validate a corresponding Computational Fluid Dynamics (CFD) model of the conjugate heat transfer problem in the Chapter 4.

3.2 Experimental Objectives

The principal objectives of the experimental work are:

1. Design solid (0P) and novel perforated pinned heat sinks (3P).
2. Fabricate the aluminium heat sinks.
3. Experimentally determine the forced convection conjugate heat transfer and pressure drop for air flows over solid and perforated pin fin heat sinks.

3.3 Heat Sink and Test Section Descriptions

Two types of aluminium heat sinks have been designed and fabricated; solid and perforated pinned heat sinks (Figure 3.1) that can be supplied with a heat load of approximately 24000W/m^2 in line with Yuan et al. (2012) using a thin film heater. As follows Zhou & Catton (2011), the pin fins have a circular cross-section of 2mm and are spaced uniformly on the upper surface of an aluminium base plate of 50mmx50mmx2mm. The height of these pin fins is 10mm located on an 8x8 array with a constant spacing between the streamwise and spanwise directions of 6.5mm. The perforated pin fins have three perforations of 1mm diameter. These perforations are aligned in the direction of the airflow and distributed up the length of the pins. Pin designs were studied with both 0 and 3 perforations with corresponding different porosity ($\phi = V_{hole}/V_{pin}$) of 0, and 0.15 where V_{hole}, and V_{pin} are the perforations volume and pin volume, respectively.

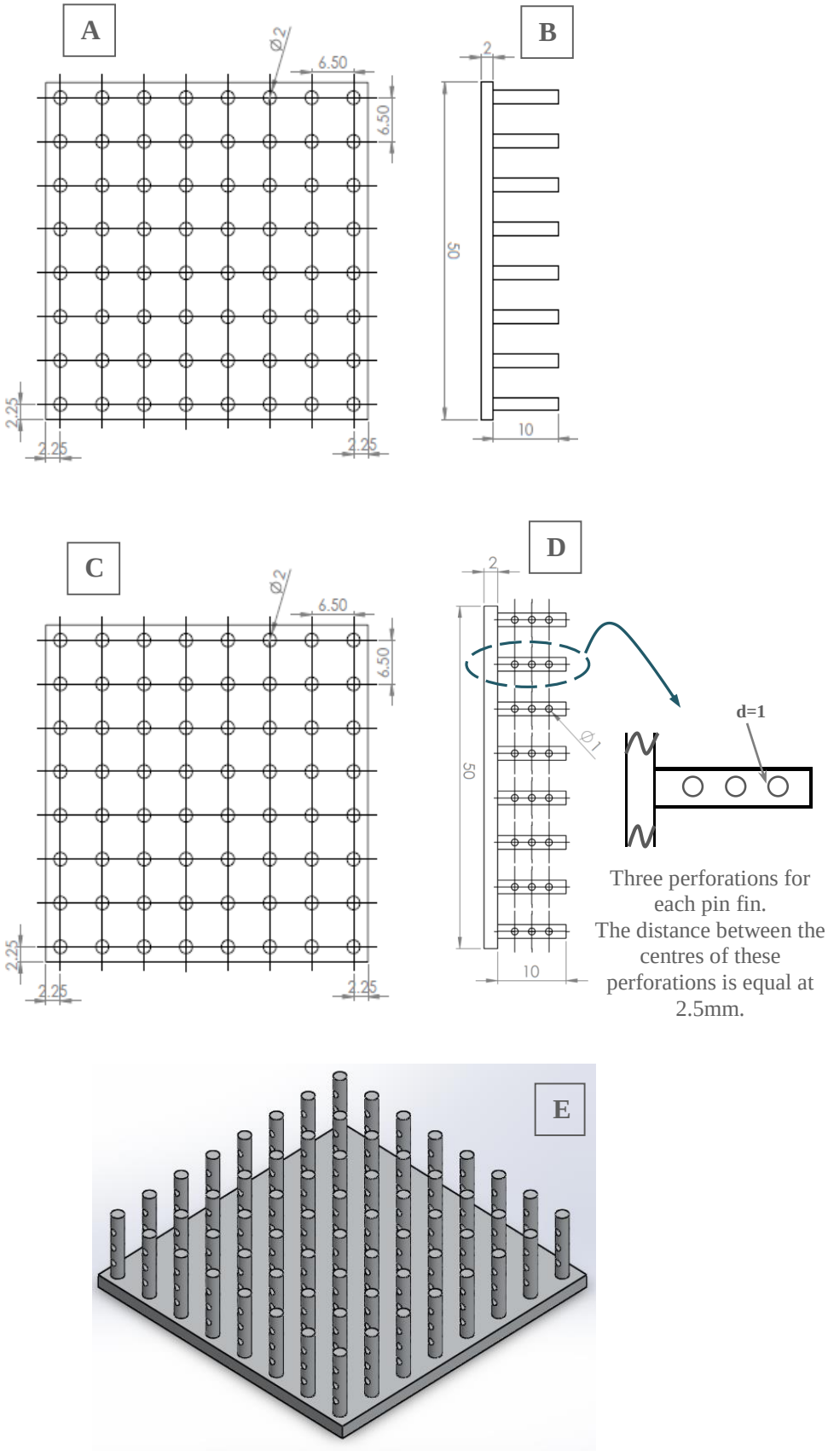

Figure 3.1: (A) Plan view, and (B) solid pin fins side view, (C) Plan view, (D) perforated pin fins side view, and (E) 3D of the perforated pin fins heat sink being analysed

3.3.1 Heat Sink Fabrication

The aluminium heat sink consists of two main parts; (I) the base plate (II) pin fins, as shown in Figure 3.2. The base plate of heat sink dimensions used in this study are 50mm x 50mm and 2mm thickness for both types of pin fins; under study. Each pin was cut from 2mm aluminium bar using a rivet cutter to a length of 12mm.

Two heat sinks have been designed and fabricated from aluminium, the first one with solid pins (0P) and the second with perforated pins (3P). The fabrication of heat sinks formed from 64 pin fins in 8x8 in-line arrangement with a constant spacing between the pins in two directions; streamwise and spanwise of 6.5mm is two stages. The first description is about the production of perforated pin fins and the second stage describes the assembly into solid and perforated heat sinks.

Manufacture of perforated pins: Sixty-four solid pins have been drilled with three perforations each of 1mm diameter with a constant centre to centre spacing between these perforations of 2.5mm in a vertical direction of a pin to produce the perforated pin fins (3P). To aid in the manufacture, a steel drilling guide was first constructed with 3×1mm guide holes, Figure 3.3. To manufacture a single pin, the aluminium bar was inserted until the end was flush with the guide outlet. Three holes were then drilled using the guide to ensure the spacing and alignment of these holes. Finally, the pins were cut to length using a rivet cutter.

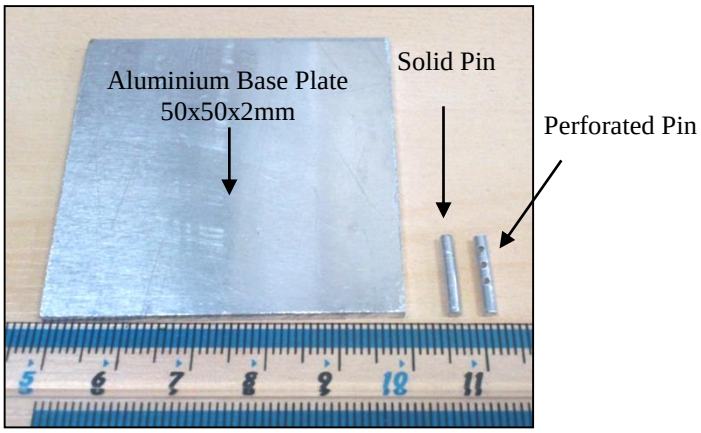

Figure 3.2: Aluminium base plate with solid and perforated pin fins

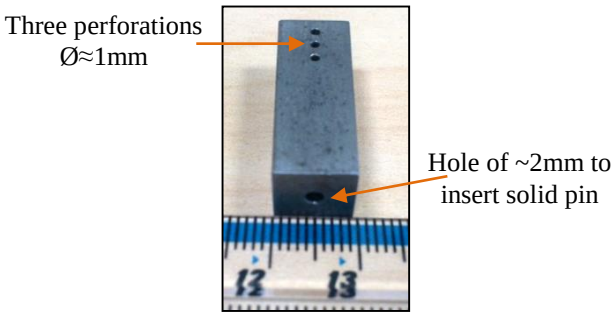

Figure 3.3: Drilling jig for producing perforated pin fins

Forming the heat sinks: The second fabrication part is a manufacturing of solid and perforated heat sinks. Two base plates were prepared by drilling 64 holes of 1.9mm diameter in which a pin fin can be inserted for each one through these holes. The holes at the bottom of the base plate are countersunk to a depth of 1.5mm with the widest diameter of 6mm, Figure 3.4. The main purpose of this is allowing the brazing alloy to flow more easily around the pin fins inside those holes. Besides, enlarging the soldering area gives a greater interaction between pin fins and the base plate of the heat sink from a thermal perspective, as shown in Figure 3.5. This minimises any resistance to heat transfer from the bottom of heat sink passes through pin fins to the surrounding air. The individual pins were brazed onto a square (50mm) base plate that was predrilled with a regular array of holes spaced on 6.5mm centres. During the brazing process, a Fibre based heat resistant mat, Figure 3.6, is used to hold and avoid any movement of the pin fins. After the brazing has been completed, the bottom surface of the heat sink is smoothed and polished with emery paper to avoid any extra material on the lower surface of the heat sink from the soldering process.

With respect to the perforated pin fins, copper wires of 0.8mm diameter are passed through the holes of perforated pins prior to assembly to ensure all these perforations are aligned in the same direction of airflow as much as possible, as illustrated in Figure 3.6. These wires were removed before testing.

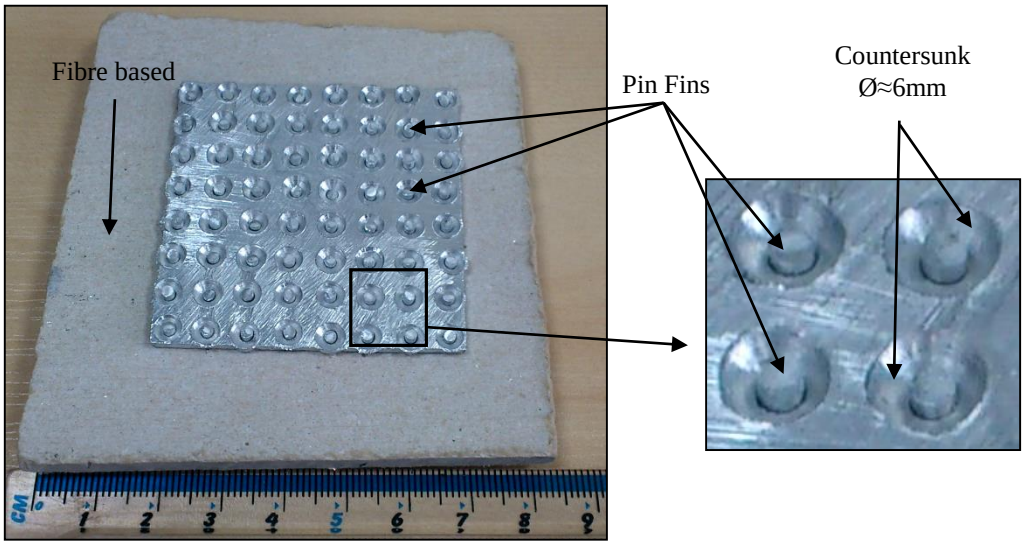

Figure 3.4: Inserting pin fins through holes of base plate with countersunk at the bottom of the heat sink

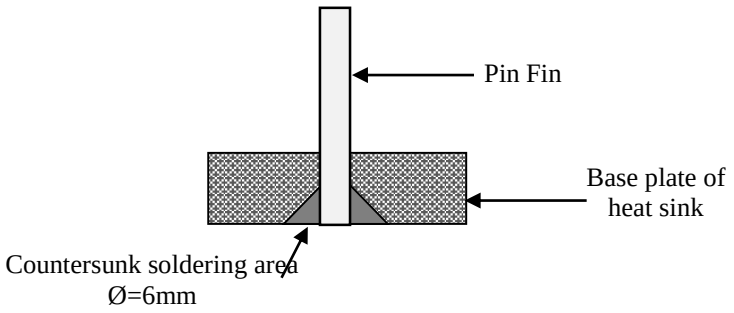

Figure 3.5: Schematic drawing of soldering area at the base plate of heat sink

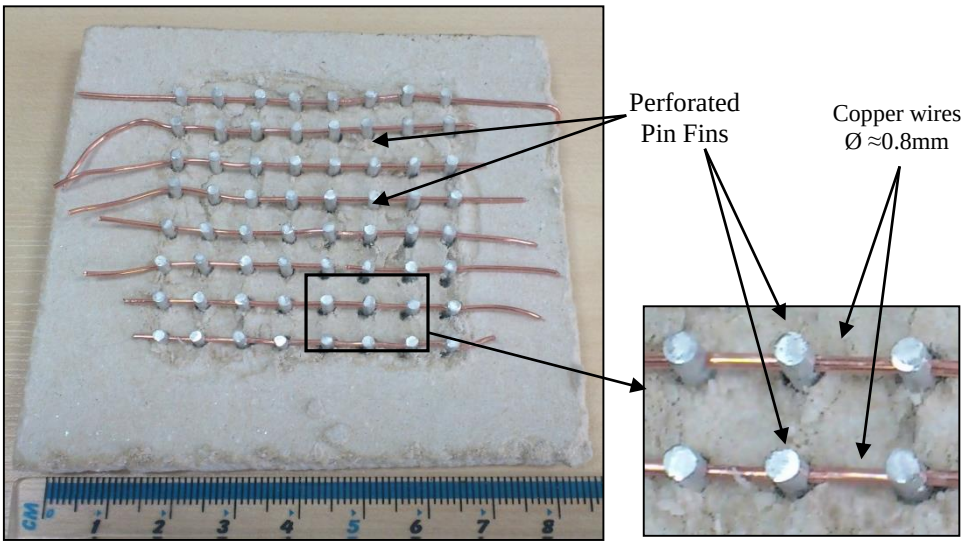

Figure 3.6: Preparing aligned perforations of perforated pins in flow direction

The result of this work was two types of heat sink; solid and perforated pin fins heat sinks each pin having 2mm diameter and 10mm height with 64 pins in-line array (8x8) with a constant spacing between the streamwise and spanwise directions of 6.5mm, as shown in Figure 3.7. The new perforated pin fins have 3 circular perforations of 1mm diameter, distributed along each pin. This allows the effect of 0 and 3 perforations to be studied. To assess the quality of the brazing process, a cross section was taken and imaged with a camera, as shown in Figure 3.8. In general, the brazing produced a strong joint, although some occlusions were seen as indicated on the Figure 3.8.

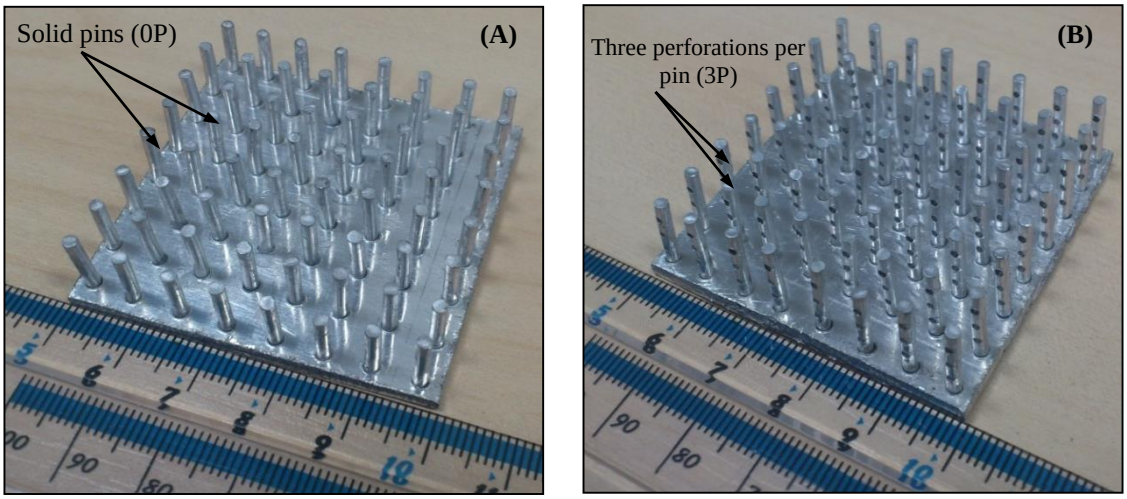

Figure 3.7: Final design of (A) solid pin fins and (B) perforated pin fins heat sinks

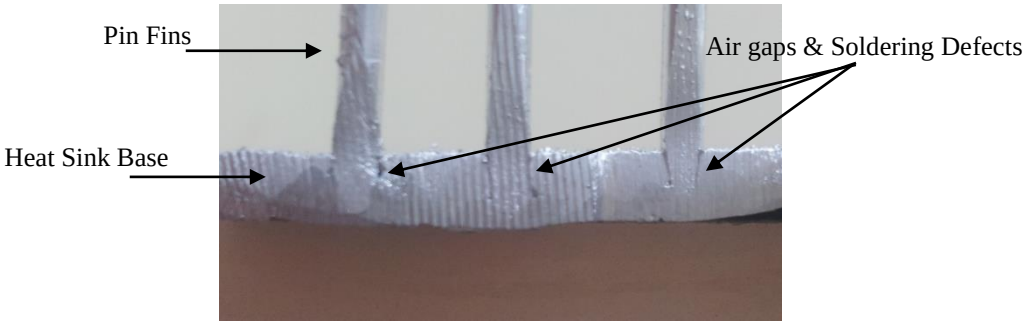

Figure 3.8: Detection of pin fin soldering zones at the base of heat sinks

3.4 Rig Description

The test rig is designed and manufactured to fulfil the requirements of the pin heat sink test system as summarised below. The experimental apparatus is shown in Figure 3.9 and consists of:

1. Airflow channel (channel section).
2. Heat sinks and test section descriptions.
3. Heating and control sections.
4. Measuring devices and traversing system.

These parts are designed and manufactured with care and fastened using adhesive and some screws between composite parts of the test rig to prevent any air leakage between the connected sections during operation.

3.4.1 Airflow Channel

An experimental rig that is designed and fabricated consists of a closed rectangular channel with removable test section (heat sink). The heat sink sits tightly within the channel ensuring no flow over the top of the pins or around the side of the heat sink. This channel is constructed of clear Perspex of 8mm thickness and has a rectangular internal cross-section of 50mm width, 10mm height, and 370mm total length, as shown in Figure 3.10. The test section (heat sink) is located at the centre of the straight airflow channel, a distance of 110mm from the upstream entrance to the channel. This heat sink section is heated using an electrical thin film heater that is attached immediately below the heat sink. The important elements of the experimental approach include a miniature fan, a power supply, an anemometer with a hot wire, a digital manometer, digital thermometers and several thermocouples as explained below.

The ambient air is driven over the heat sink at different velocities by an axial-flow fan. The dimensions of the miniature fan (model San Ace 36: 9GV3612P3J03) are 36x36x28mm with the rate voltage at 12VDC and the turbulent airflow can be obtained easily by rotating this fan with maximum volumetric airflow 0.00708m^3/s. The fan curve is shown in Figure 3.11. The fan is located at the inlet of the test section and the air motion created by the fan flows into the converging test section. The channel is equipped with tappings allowing the pressure drop across the heat sink to be measured using a digital manometer and insertion points allowing the

change in temperature of the air to be recorded via a digital thermometer. Metal meshes are positioned at a distance of 50mm on either side of the heat sink to minimise flow maldistribution and create uniform airflow profile over the heat sink. Air is discharged by the miniature fan into the mini airflow channel and passes through a flow straightener (metal meshes), test section and then discharged to the atmosphere. Figure 3.12 shows the final assembly rig design test with three views.

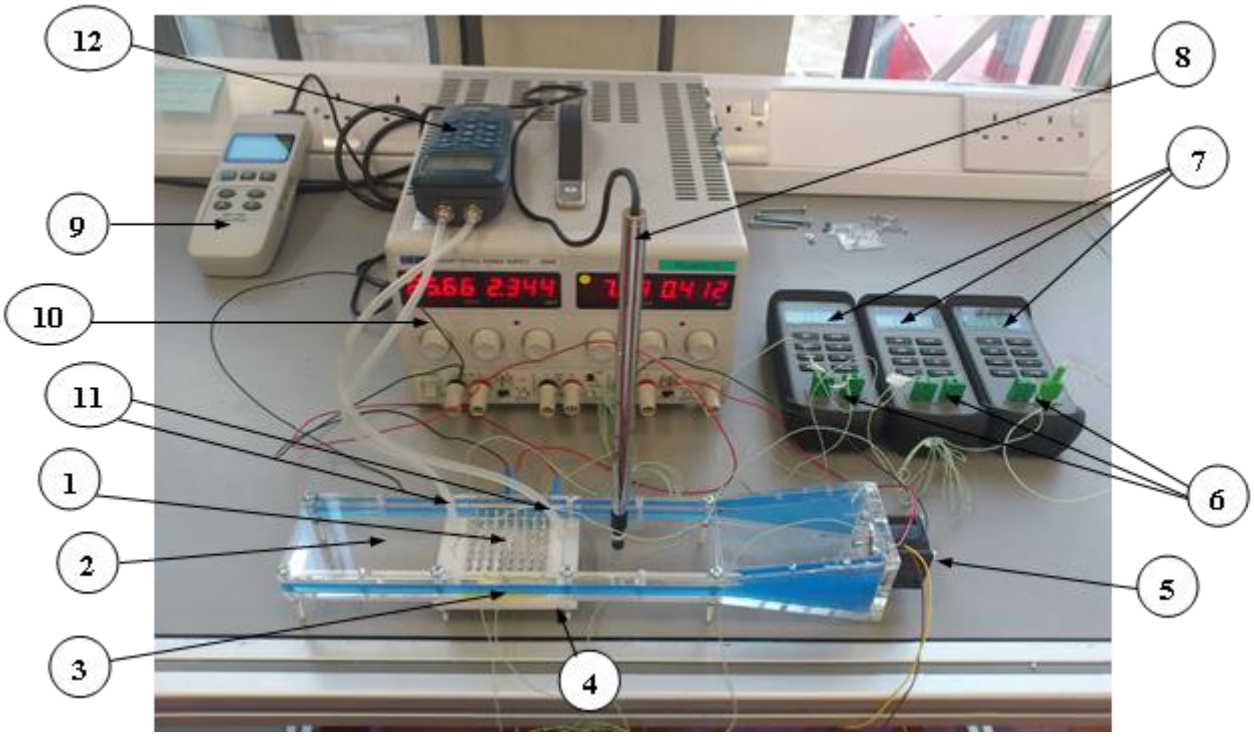

1: Heat Sink	2: Mini Channel	3: Film Heater Resistance	4: Teflon Insulation
5: Miniature Fan	6: Thermocouples	7: Digital Thermometers	8: Hot Wire
9: Anemometer	10: Power Supplied	11: Pressure Taps	12: Digital Manometer

Figure 3.9: Overall rig design and experimental measurements system

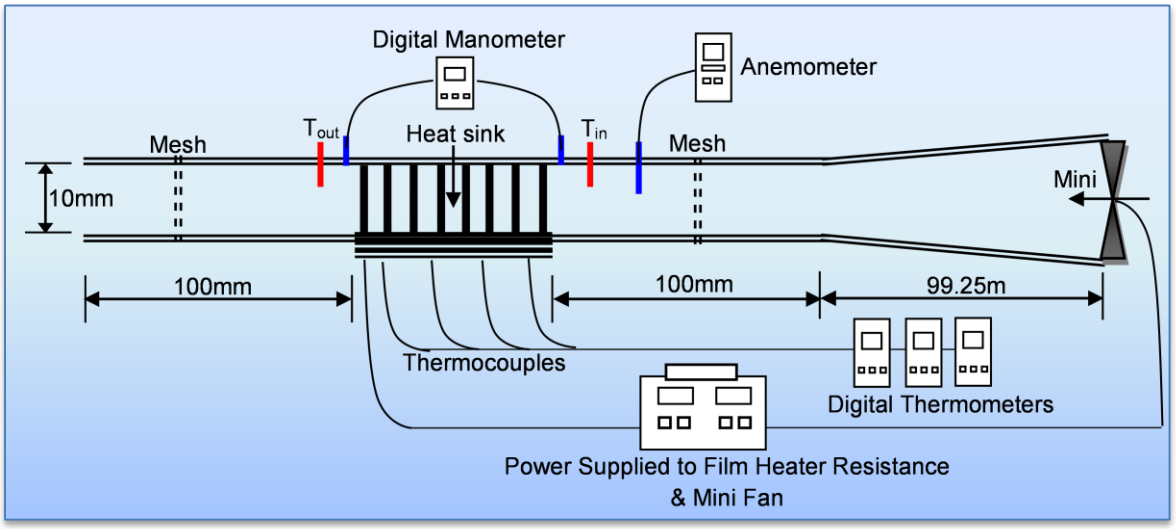

Figure 3.10: Schematic Drawing of Overall Experimental System

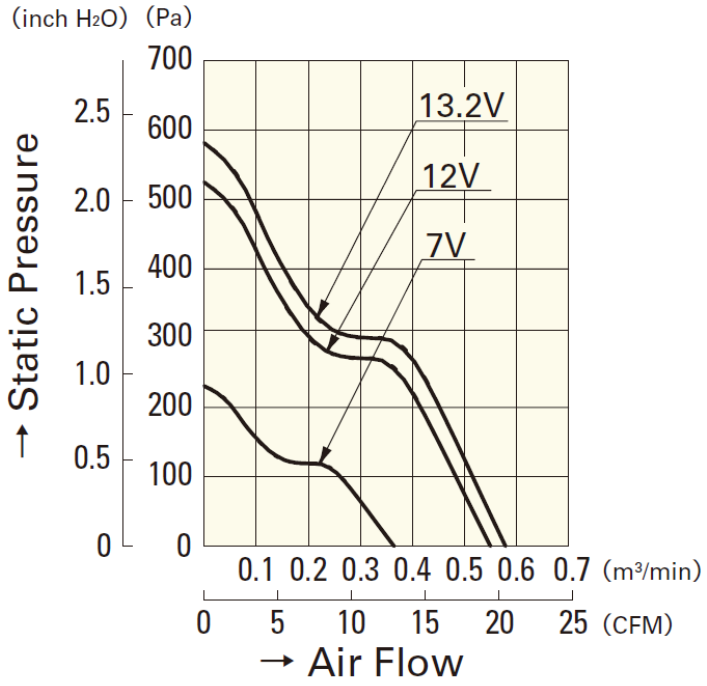

Figure 3.11: Typical performance fan curve (model San Ace 36: 9GV3612P3J03)

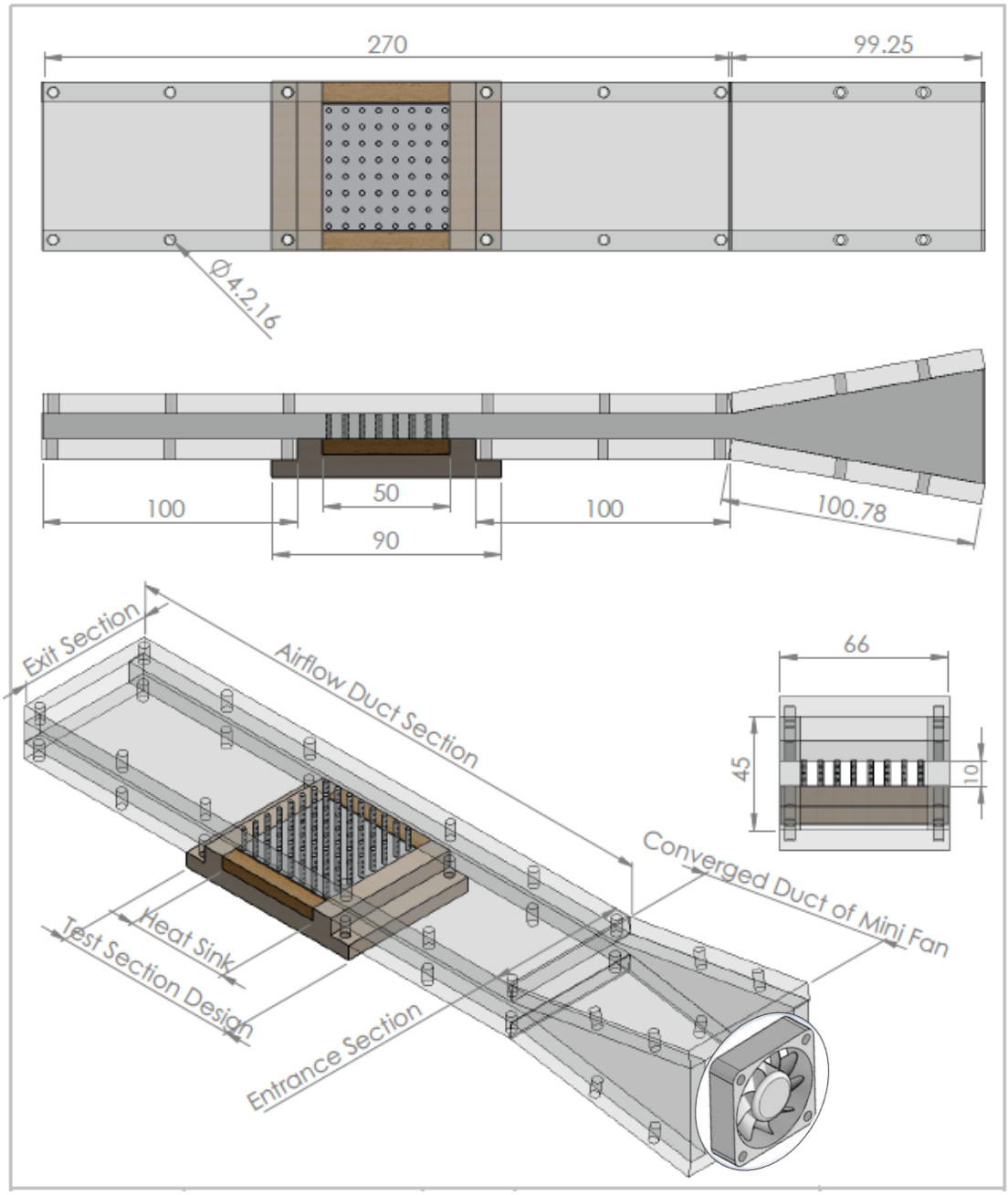

Figure 3.12: Final assembly of rig design with three views

3.4.2 Heating and Control Sections

The heat sink is heated using an electrical heater (50x50x0.2mm) uniformly along at the lower surface of the heat sink to provide a uniform heat flux, Figure 3.13. The electrical heater mimics the heat generation a CPU of a personal computer. A maximum allowed heat flux in this sort of CPU is 24000W/m^2, Yuan et al. (2012) via the electrical power supplied (Aim-TTi EX354RD, EX-R Series).

This electrical heater has been fabricated from two lengths of wire Nickel-Chrome of 0.2mm that has been coiled around a mica sheet for obtaining uniform constant heat flux along the heater. The heater dimensions have the same base heat sink dimensions of 50mmx50mm with 0.2mm thickness to give a uniform heat flux. Thermally conductive Epoxy was used between the heat sink and the thin heater to avoid any electrical contact with thin heater resistance. The bottom and side surfaces of the heater are insulated with Fibreglass and Teflon as isolator layers to minimise the heat loss through these sides.

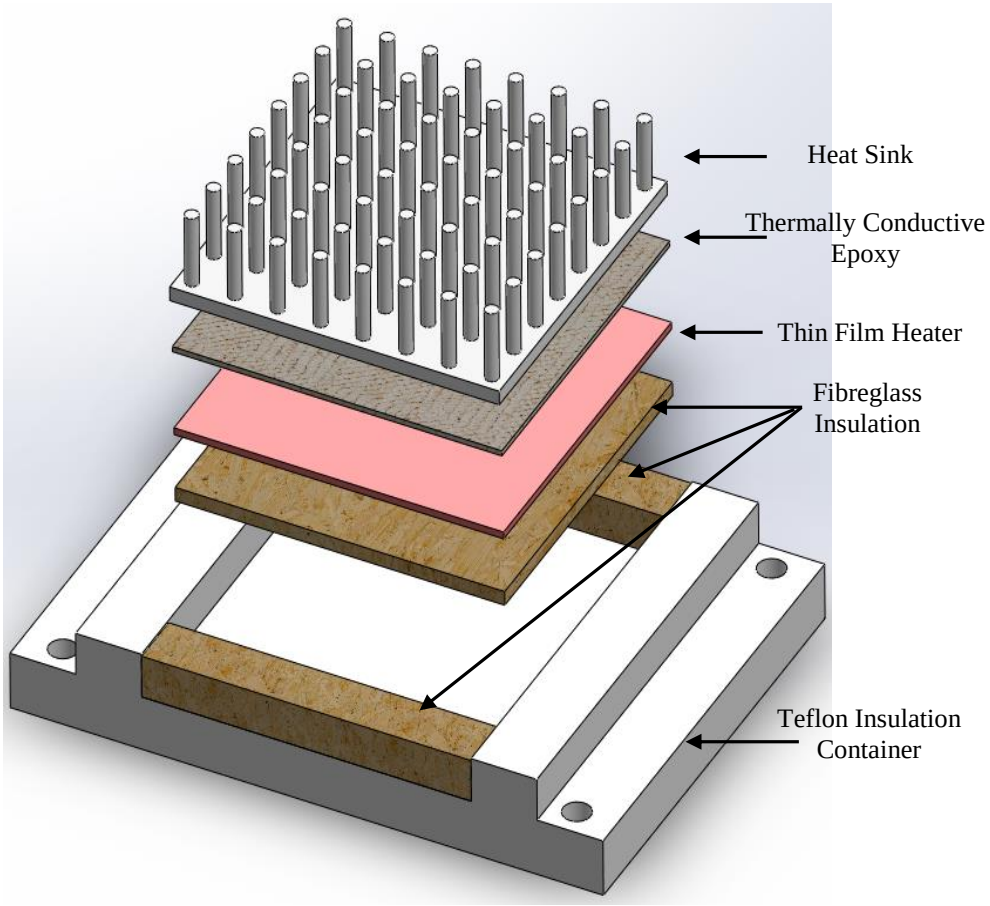

Figure 3.13: Installation of the heat sink with film heater into insulation container

3.4.3 Measurement Devices

A Hot wire, thermocouples, and digital manometer are utilized in the present experiments to measure the local (inlet and outlet) air temperatures; variation of the upper and lower heat sink surfaces temperatures; ambient air temperature: inlet and outlet local pressure differences (pressure drop); and inlet air velocities.

3.5 Experimental Measurements

3.5.1 Hot Wire Anemometer

The hot wire anemometer (HHF2005HW) is located at the inlet of the channel to measure inlet air velocity, Figure 3.9. The head of this device consist of a very thin wire that is connected between two supports for local air velocity (hot wire) and a second sensor is for the local air temperature. The resolution of device is 0.1m/s for 0.2 to 20m/s inlet airflow velocity.

3.5.2 Thermocouples

Type K thermocouples of 0.2mm diameter are used to measure the top and bottom surface of the heat sink. The operating range of this type of sensor is from -75^{o}C to 250^{o}C with very fast thermal response measurements.

The thermocouple at the back surface of the heat sink is fixed by an adhesive material and used to measure the temperature of the heat sink. In a real world application that is equivalent to CPU temperature (T_{case}). The thermal resistance (R_{th}) of solid and perforated pin fin heat sinks is also calculated. The thermocouple at the upper surface of the heat sink is used to measure the mean temperature of the upper wall to determine the heat transfer coefficient, the heat transfer rate, and the Nusselt number. At the same time, other thermocouples are placed at the inlet and outlet of the mini channel to measure the local air inlet and outlet temperature to find the average bulk mean temperature (T_m). At this temperature (T_m), the values of the thermo-physical properties of the air are known from tabulated data of Cengel (2006).

3.1.1 Digital Manometer

A digital manometer (2083P Digitron) is used in the experiments to measure pressure at a specific point or a differential pressure of airflow through the test section, heat sinks (Figure 3.9). Fan power and pressure drag coefficient are based on pressure drop that is measured via the digital manometer. Two pressure taps are located in front of and behind the test section to measure the airflow pressure drop (ΔP) with 0.1% as full-scale accuracy reading.

3.6 Experimental Procedure and Measurements

Several experimental parameters are measured such as the temperature, velocity, and pressure drop to study the heat transfer and flow characteristics of solid and perforated pin fins heat sinks. For each heat sink, four ranges of inlet air velocity flow (6.5, 8, 10, and 12) m/s and constant heat flux (20000W/m^2) are used. Furthermore, repeatability tests are conducted to detect the influence of any noise sources on the heat transfer and pressure drop. Thus, each experiment is repeated three times under the same conditions for both solid and perforated pin heat sinks. Figure 3.14 shows the repeatability tests of pressure drop and the CPU temperature with varying inlet air velocity. It is observed that the deviation of these measured values is less than 2% for both heat sinks models. Generally, 24 experimental runs (four different velocities for two types of heat sinks, each repeated three times) are carried out to ensure repeatability.

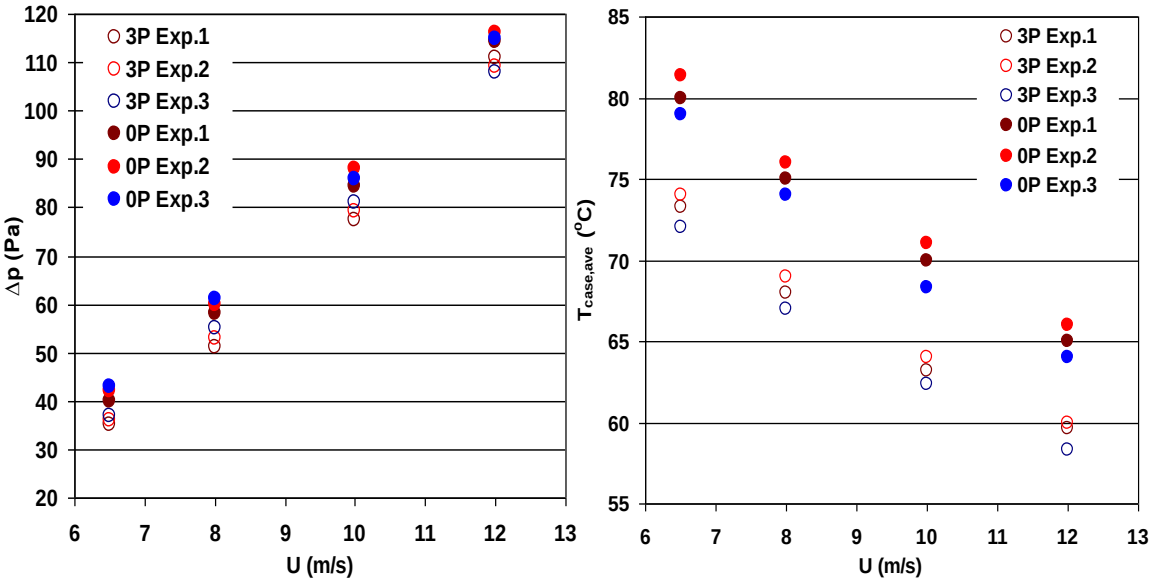

Figure 3.14: Repeatability of pressure drop and CPU temperature with variation inlet air velocity for solid (0P) and perforated (3P) pin models

3.6.1 Experimental Procedure

For a specified type of heat sink, the following procedure is applied for conducting the experiments,

1. Check digital Manometer for the two taps and hot-wire anemometer at entrance test section have zero readings before an operation.
2. Switch on the fan to pump the air through the mini test section.
3. The power supplied (Voltage and Amp) is adjusted for the required input power to the film heater resistance and fan.
4. To achieve a steady state condition, the temperature difference between the previous and the new reading is approximately zero. Thus, the system is left for 20mins, as shown in Figure 3.15.
5. Finally, record the pressure drop, upper and lower surfaces temperature of the heat sink and supplied power after the test reaches a steady state condition.

To check the repeatability, a set of tests were represented three times to ensure that the variation in the experimental measurements recorded for the same parameter and under the same conditions is small.

During each experimental run, the following measurement readings are recorded:

1. The local upper surface temperatures of heat sinks (T_s) are recorded via the outputs of thermocouples type K.
2. The local lower surface temperatures of heat sinks (T_{case}) are recorded via the outputs of thermocouples type K.
3. The inlet and outlet air bulk temperatures (T_{in}, T_{out}) are the readings of two thermocouples at the entrance and the exit of the mini heat sink.
4. The surrounding air temperature (T_{air}).
5. The thermocouples readings are recorded after 20mins via the digital electronic thermometer the final set of steady state readings are then recorded.
6. The pressure drop of the test section (ΔP) is recorded using the digital manometer.
7. The inlet air velocity (U) through the mini test channel is measured using a hot-wire anemometer.
8. The inlet air velocity is confirmed every 5mins to be sure that this is constant during testing.

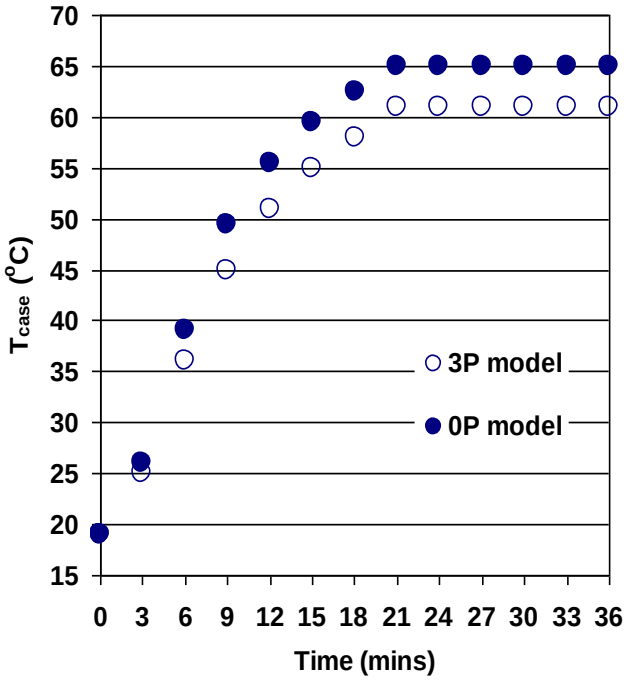

Figure 3.15: Time evaluation of T_{case} for 0P and 3P heat sinks models at Re= 5393. Steady state is reached after 20mins

3.7 Experimental Data Analysis and Calculations

The experimental data recorded for the temperature, pressure, current, and voltage are used for the following heat and fluid flow analyses and the experimental uncertainty analysis is considered, as shown in Appendix B.

3.8 Hydraulic Characteristics Analysis

An important quantity in the flow analysis of pin fins heat sinks is the pressure drop (ΔP) along the test heating section in the direction of flow. The pressure drop is directly related to the power requirements of the pump to maintain the flow, (Cengel 2006; and Incropera 2011) and the pressure drag coefficient. The pressure drop is measured to calculate the fan power, P_{fan} and pressure drag coefficient, P_d these parameters define the consumed energy for solid and perforated pin fin heat sinks and allow the assessment of designs from an energy consumption perspective, see section 2.5.2. The mechanical fan power (P_{fan}) and pressure drag coefficient (P_d) are defined in sections 2.5.3 and 2.5.4.

3.9 Heat Transfer Analyses

Heat transfer rate, Nusselt number, the average temperature of the base heat sinks, and the thermal resistance of heat sink are measured experimentally. These are defined below.

3.1.2 Heat Transfer Rate

The steady-state rate of heat transfer can be expressed as follows:

$$\dot{Q}_{conv} = \dot{Q}_{elec} - \dot{Q}_{rad} - \dot{Q}_{losses} \tag{3.1}$$

where $\dot{Q}_{elec}$ refers to the total heat applied on the base of the heat sink and is calculated from the electrical potential (V) and electrical current (I):

$$\dot{Q}_{elec} = IV \tag{3.2}$$

$\dot{Q}_{rad}, \dot{Q}_{losses}$ are the heat transfer rate from the heat sink by radiation and thermal losses, respectively.

The total steady-state rate of radiative heat transfer loss ($\dot{Q}_{rad}$) from the test section is evaluated from Naik et al. (1987):

$$\dot{Q}_{rad} = \varepsilon\sigma F A_T \left(T_s^4 - T_a^4\right) \tag{3.3}$$

For the typical condition of the view factor (F) that can be found for the effect of fins array geometry and emissivities between the fin material and the bounding environmental surfaces, the Stefan-Boltzmann constant (σ=5.67×10^{-8}W/m^2.k^4), the total wetted surface area of pinned heat sin (A_T), the upper surface temperature of the heat sink (T_s), and the surrounding air temperature (T_a) (Naik et al. 1987). The pin fins and base plate of the heat sink are made of highly polished aluminium to reduce their emissivities (ε=0.05) and the experimental data of the present work showed that $\dot{Q}_{rad}/\dot{Q}_{elec} \approx 0.002$. Therefore, $\dot{Q}_{rad}$ is neglected in the results presented in the next chapter.

The thermal losses ($\dot{Q}_{losses}$) include the conductive and convective heat losses through the insulations and channel walls are given by:

$$\dot{Q}_{losses} = U_{overall}.A.(T_w - T_a) \tag{3.4}$$

where A is the heat sink base area, $U_{overall}$ is the heat transfer coefficient losses, ΔT is the temperature difference between the bottom surface of heat sink temperature (T_w) and the surrounding air temperature (T_a). These losses are minimised by ensuring that all the outer walls of the heat sink are well-insulated and thermocouple readings of the heat sink outer wall temperatures are close to the ambient temperatures that caused the thermal losses, which are estimated to be $\dot{Q}_{losses}/\dot{Q}_{elec} \approx 0.02$ and can therefore be neglected.

Therefore, it can be assumed with some confidence that the last two terms of Eq. (3.1) may be ignored.

The heat transfer rate from the heat sink by convection ($\dot{Q}_{conv.}$) can be deduced as, Sara (2003):

$$\dot{Q}_{conv} = h_T.A_T\left[T_s - \left(\frac{T_{out} + T_{in}}{2}\right)\right] \tag{3.5}$$

Hence, the average convective heat-transfer coefficient (h_T) based on the total wetted surface area (A_T) can also be expressed via:

$$h_T = \frac{\dot{Q}_{conv}}{A_T[T_s - (\frac{T_{out} + T_{in}}{2})]} \tag{3.6}$$

where T_s is the upper surface of heat sink temperature, T_{in} and T_{out} are the average inlet and outlet air temperatures, respectively, and A_T is the total surface area of the heat sink.

According to previous researchers, the average heat transfer rate (h_{ave}) has been calculated based on either the projected, A_P, or total, A_T, total wetted surface area of the heat sink and these are related to one another via the relationship $h_P=h_T(A_T/A_P)$. Thus, these two areas can be related to each other by:

Total wetted area = Projected area + Total surface area contribution from the pin fins

For solid pin fins:

$$A_T = W.L + N.(\pi.D.H) \tag{3.7}$$

For perforated pin fins

$$A_T = W.L + N[(\pi.D.H) - (2\pi.n.(\frac{d}{2})^2) + (\pi.n.D.d)]$$
$$A_T = W.L + \pi.N[(H.D) - (\frac{1}{2}n.d^2) + (n.d.D)] \tag{3.8}$$

where *(W, L)* are the width length of the base plate heat sink, *(N)* the total number of fins, *(H)* the height and *(D)* the diameter of the fins and *(d)* the diameter of the fin holes, and *(n)* the number of perforations, respectively.

The Nusselt number (Nu) and thermal resistance (R_{th}) are determined as per sections 2.5.5 and 2.5.6.

In all the experimental calculations, the values of the thermo-physical properties of the air are specified from Cengel (2006) using the average bulk mean temperature (T_m), which is:

$$T_m = (T_{in} + T_{out})/2 \tag{3.9}$$

3.10 Summary

In this chapter, the design and fabrication of two types of aluminium heat sinks, solid (0P) and perforated (3P) pinned heat sinks and the integration of these heat sinks into a test section are described. The measurement devices and test procedures to measure the significant characteristics for calculating the crucial thermal and airflow characteristics for solid and perforated pin fins heat sinks such as heat transfer rate, Nusselt number, CPU temperature, and thermal resistance are also described. The experimental uncertainty analysis is considered, as shown in Appendix B.

Chapter Four: Experimental Results

4.1 Introduction

In this chapter, the main characteristics of using new perforated pin heat sinks with multiple perforations for cooling electronic components system are considered. Two experimental heat sinks were designed and fabricated, one with solid pins (0P) without perforations and another one with triple perforated (3P) pin heat sinks (Chapter 3), to appraise the effect of perforated pin fin design on the thermal airflow characteristics of those heat sinks, such as pressure drop, fan power, pressure drag coefficient, CPU temperature, thermal resistance, and the total and projected Nusselt number to be determined. The inlet velocities from 6.5m/s to 12m/s for the range of Reynolds numbers are 3500-6580 and the mini-duct hydraulic diameter with 8x8 in-line pin array at constant longitudinal and transverse distance is 6.5mm.

4.2 Hydraulic Characteristics

The effect of the perforated pinned heat sink design (3P) on the airflow characteristics are compared with the solid pin fins (0P) in this section. The main characteristics of airflow are measured pressure drop (ΔP), calculated fan power (P_{fan}), and pressure drag coefficient (P_d).

Figures 4.1A and 4.1B show experimental measurements from the effect of perforations on the pressure drop, ΔP, across pinned heat sinks (PHSs) and the power required to overcome the pressure drop.

Data are presented for the two models, the solid pin fins and the 3P once with three perforations. The pressure drop and fan power consumption data in Figures 4.1A and 4.1B show that the perforations reduce ΔP and P_{fan} throughout the velocity range. The main reason for that is the dead thermal-flow regions created just behind the solid pin fins. In other words, those regions mean a hotter area and lower air movement relative to other regions for the same test section. This leads to the pressure drop and the fan power of the solid pin fin heat sinks increasing due to flow separation and air recirculation; evidence for this will be provided in Chapter 5,

where the numerical prediction will be presented. The perforations reduce the pressure drop and fan power of the heat sinks. This is because a part of the frontal area of the pins is removed, which allows an amount of airflow to pass through these perforations (Alam et al., 2014a).

In the experimental data, the pressure drop and fan power consumption seen with three perforations is typically around 7% smaller than that of the solid pin fins.

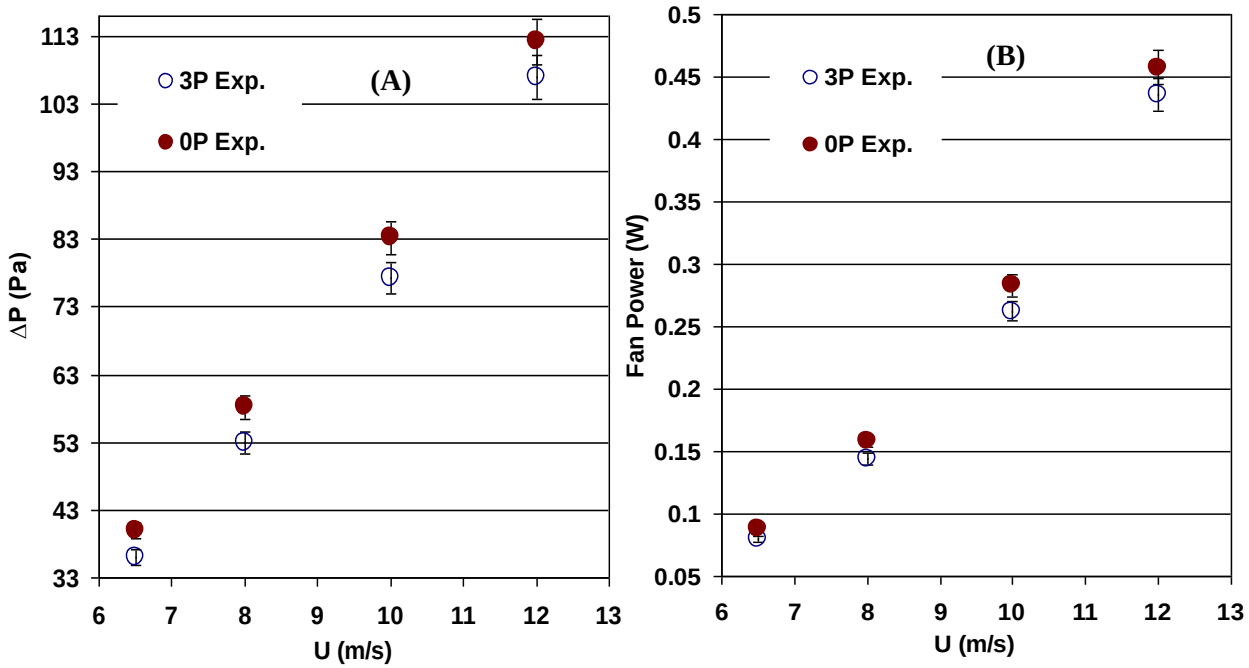

Figure 4.1: Effect of pin perforations on (A) pressure drop and (B) fan power as a function of airflow speed

Figure 4.2 shows the effect of the perforated pinned heat sink model (3P) on the pressure drag coefficient, $P_{d,}$ for a range of inlet velocities from 6.5m/s to 12m/s at Re=3500-6580 and 8×8 in-line pins with longitudinal and transverse distance of 6.5mm.

Following previous authors, e.g. Ismail (2013) and Ismail et al. (2013), the drag force on the air due to heat sinks can be expressed in terms of a pressure drag coefficient. The pressure drag coefficient associated with the perforated pins is lower than that of the sold pins. For example, the P_d of the solid PHS is 1.33 while it is reduced to 1.27 when using the perforated PHS at 10m/s. Overall, the P_d of the perforated PHS is 7% lower than that of the solid pin fins model. The major reason for this is that the frontal area of the perforated pins (3P) is smaller than that of the

solid pins (0P) and so some airflow can easily pass through these perforations. Generally, these benefits increase with increasing air velocity.

As a result of airflow parameter studies in this section, the amount of energy spent to achieve a certain flow is reduced due to perforations. Thus, the perforations are a useful technique for reducing fan power consumption. The second characteristic (fan power) that also must be met is the ability to remove heat; this is studied in the next section.

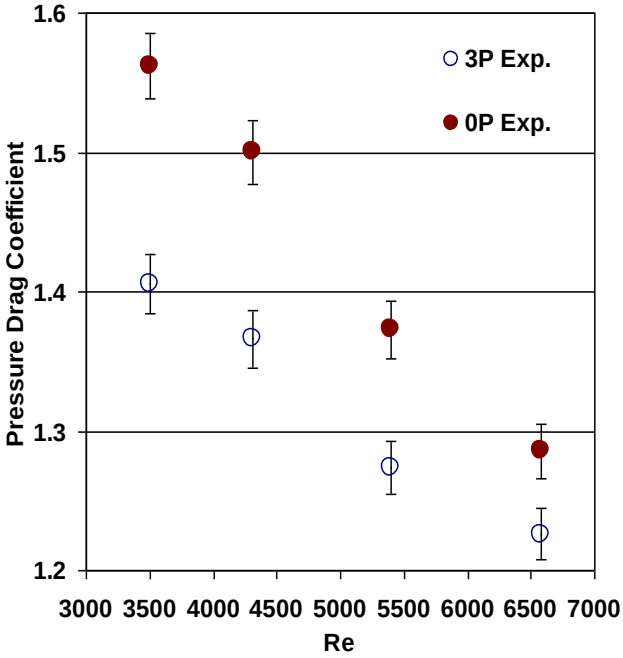

Figure 4.2: Effect of pin design and inlet air velocity on the pressure drag coefficient

4.3 Heat Transfer Characteristics

The heat transfer characteristics such as the total and projected Nusselt number, Nu_T, Nu_P, the CPU temperature (T_{case}), and thermal resistance (R_{th}) of the 3P pinned heat sink design (3P) are described and compared with those of the solid pin (0P) fins.

4.3.1 Average Nusselt Number

Since the overall design goal for PHSs is to achieve a high heat transfer rate at the minimum energy cost, Figure 4.3 presents the corresponding experimental measurements of the Nusselt number, based either on the total wetted surface area of PHS (Nu_T) or on the projected surface area (Nu_P), the base surface area of HS. The latter is perhaps a more effective measure of cooling capacity for a given PHS size.

The data show that both Nu_T and Nu_P increase approximately linearly with the inlet air velocity and that the 3P pin fins design achieves a significant enhancement in heat transfer, with Nu_T and Nu_P typically 5% and 11% larger than that of the solid pin fins for experimental data, respectively.

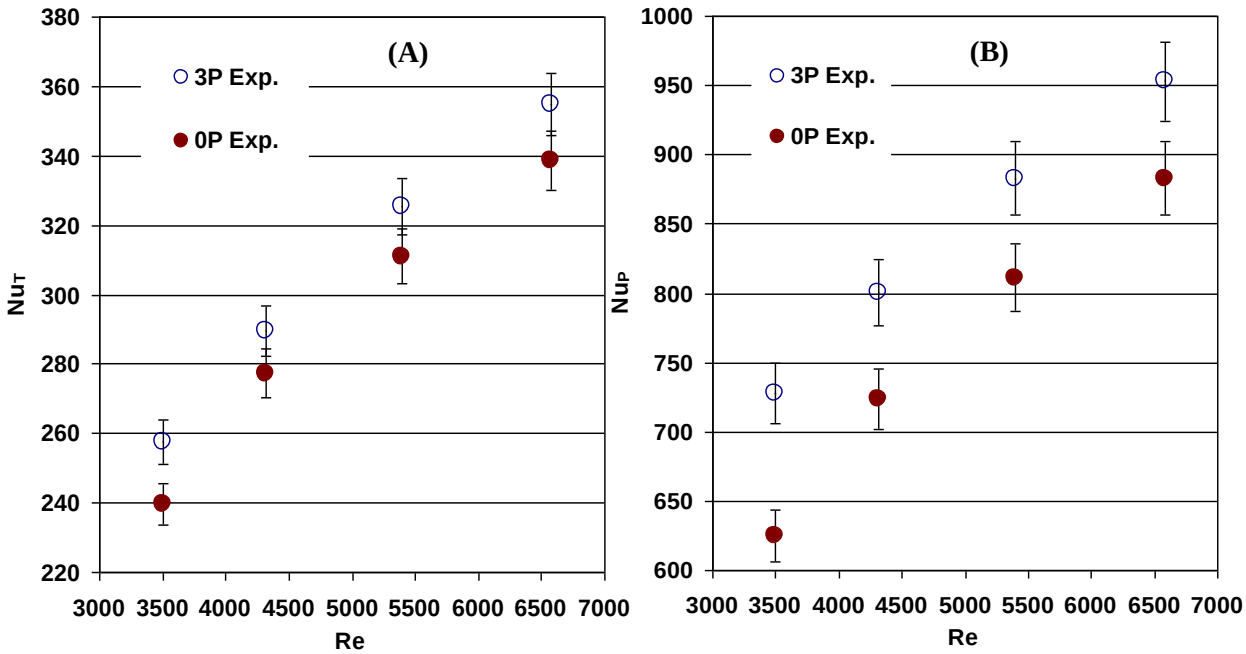

Figure 4.3: Effect of inlet velocity on Nusselt number based on (A) total and (B) projected surface area

4.3.2 Thermal Management of PHSs

A key issue in the thermal management of electronics packaging is to ensure that the CPU temperature, $T_{case,}$ for typical desktop computers is kept below the critical temperature of approximately 85^{o}C (Gurrum et al., 2004; Yuan et al., 2012) at the minimum energy cost. The major aim of thermal management is to illustrate the benefits and thermal reliability of the perforated pinned heat sink design on the thermal management of a typical CPU. Figures 4.4 and 4.5 show the following experimental measurements: the average base plate temperature, $T_{case,}$ and thermal resistance, $R_{th,}$ with fan power for 6.5m/s$\leq U\leq$12m/s, through a system of 8x8 pins, a pin pitch of 6.5mm.

These figures confirm that the improved heat transfer with perforated pins leads to a desirable effect of reducing base plate temperatures and thermal resistance. For example, T_{case} of the 3P model with three perforations reduces from 72^{o}C to 58^{o}C while it only reduces from 77^{o}C to 61^{o}C for the solid pins (0P) with increasing fan power. This improved heat transfer from the perforated pins (3P) leads to significantly lower CPU temperatures for the same fan power input compared with the solid pins (0P). In the experimental data, the T_{case} with three perforations is typically around 6% (nearly 5^{o}C) smaller than for the solid pin fins. The potential sources of experimental errors are attributed to some practical considerations. One of the possible areas where errors could arise is around the additional thermal resistance as a result of the brazing process, see section 3.3.1.

As a result of thermal and airflow parameter studies, the amount of energy that is spent by a fan which is used to cool the perforated pin fin heat sink (3P) with three perforations is less than that required for the solid pins model. Thus, the perforations are a useful technique for reducing fan power consumption and CPU temperature.

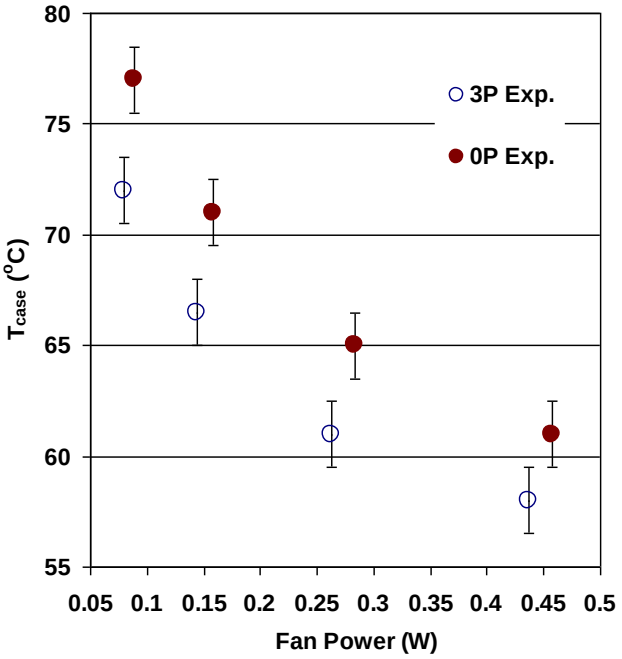

Figure 4.4: CPU temperature variation with fan power for 0P and 3P heat sinks

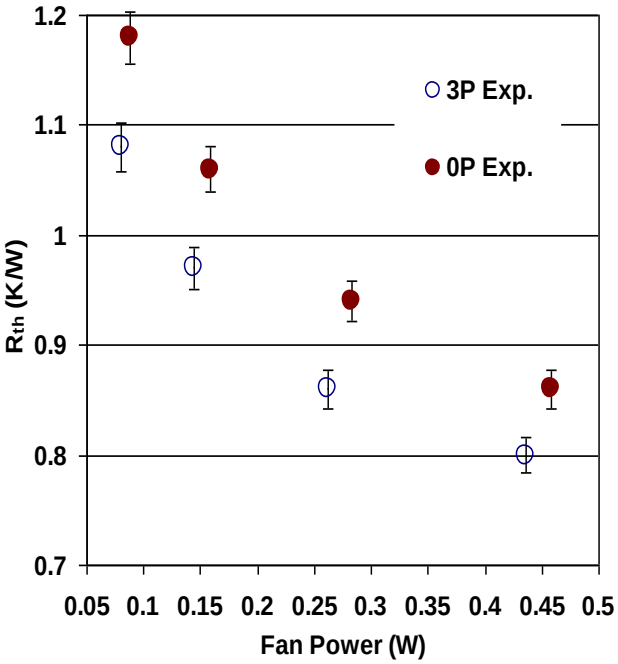

Figure 4.5: Experimental results of influence of fan power on R_{th}

The pin fin design can be optimised by maximising the heat transfer rate for a given fin weight or by minimising the weight for a specified heat transfer rate has been considered by Shaeri & Yagoubi (2009). For example, each perforation reduces the weight of the pin by 5%. Accordingly, the CPU temperature, heat transfer, pressure drop and fan power benefits of the pin with three perforations are achieved with the additional benefit of a 4% the total reduction in pinned heat sink weight.

4.4 Conclusion

Heat transfer of the solid pinned heat sink (0P) is lower compared with that of the perforated pins (3P) because hot or dead regions are created behind those solid pin fins as a result of the flow separation and poor air recirculation at these hot zones. Thus, to avoid this problem, perforations could be added to accelerate flow and reduce the dead zones. These perforations substantially improve the heat transfer rate at the hot zones while at the same time reducing the pressure drop through the pinned heat sink and the fan power needed to pump the air through it as well, as detailed in Table 4.1. The perforations allow some of the airflow to pass through them and mix well with the primary flow to create a larger amount of mixing and turbulence, in addition to reducing PHS weight considerably. Furthermore, the enhanced heat transfer due to perforations leads to considerably reduced processor temperatures, a key goal of the thermal management of electronics.

Table 4.1: The experimental enhancement of Nusselt number (*Nu*), fan power (P_{fan}), and CPU temperature (T_{case}) of the 3P heat sink compared to the solid pinned heat sink

Parametric Studies / Heat Sink Design	$\uparrow A_T$	Nusselt Number		$\downarrow P_{fan}$ (W)	$\downarrow T_{case}$ (°C)
		$\uparrow Nu_T$	$\uparrow Nu_P$		
Experimental Perforated Pins with Three Perforations (3P)	15%	5%	11%	7%	6%

Chapter Five: Numerical Methods

5.1 Introduction

In this chapter, the numerical methods for simulating thermal airflows through pinned heat sinks (PHSs) are described. The conjugate heat transfer model with turbulent airflow is used to simulate this kind of heat sinks via commercial ANSYS FLUENT 14.5 CFD code. Furthermore, each component of the numerical solutions, boundary conditions, assumptions, and airflow and thermal characteristics of pinned heat sinks calculations such as pressure drop, fan power, Nusselt number, thermal resistance, and temperature base of heat sinks are explained. Finally, the test numerical approaches such as domain verification and code validation of pinned HSs are investigated.

5.2 Numerical Modelling Overview

During recent decades, both in-house and commercial CFD codes have become ever more powerful. In addition, complex heat transfer and fluid flow problems can be solved using these method. CFD analyses consist of three important processes:

1. Pre-processing: this is the first step where the geometry and grid mesh are generated, and the boundary conditions are set.
2. Processing or Solver: in this step, the governing equations are solved.
3. Post-processing: the final step includes a presentation the results, graphics, animations, plots, analyses and full reports that are created.

5.3 Numerical Simulation

CFD is now used to study the effect of pin perforations on the enhancement of heat transfer rate and reduction in pressure drop (Shaeri & Yaghoubi, 2009; Shaeri & Jen, 2012) the latter having a direct benefit on the associated power required to drive the cooling air through perforated plate heat sinks, which is given by the product of the flow rate and the pressure drop. ANSYS FLUENT-CFD software program is selected to investigate numerical analysis of the heat sink models.

This program uses the finite volume method (FVM) to solve the governing equations. The Navier-Stokes equations combined with the continuity equation and the energy equation in three dimensions are solved by FVM to show the dynamic airflow and heat transfer around the pinned heat sinks (PHSs). The continuity equation is satisfied using the Semi-Implicit Method for Pressure Linked Equations (SIMPLE). Second order upwind discrimination schemes are used in the calculations to reduce the numerical errors for the Navier-Stokes equations and the energy equation (Versteeg & Malalasekera, 2007).

As mentioned earlier, each model consists of three parts: the entrance section is a first part as a smooth duct, which has enough length to provide a fully turbulent flow condition. The pinned heat sink (test section) that has 8 symmetric Aluminium pins follows the first region, as the second part. The final section is the exit one that comes after the test section and is long enough to prevent any feedback of boundary condition into the test section. Each those parts have the same cross-section at (6.5x10)mm. The air passes through all these three regions for different Reynolds number range.

In the current numerical study, many heat sinks configurations are investigated and the optimum model giving the lowest pressure loss and the highest heat transfer (lowest CPU temperature) can be determined. These configurations are: circular perforated pin fins; slotted pin fins; notched pin fins heat sinks; as well as different types of perforations shape such as square, and elliptic perforations, Figure 1.27.

5.4 Pre-processing (Mesh Generation)

The set mesh volume elements are Tetrahedron Hyper cells and the type is Hex Core T-grid to generate grids for all the heat sink models, including the complex geometry of pinned heat sinks and the entrance and exit regions set as a Hexahedral mesh type due to a straight and simple shape of those regions (Seyf & Layeghi, 2010; Nabati, 2008), as show in Figure 5.1. Both those types of mesh generation are suitable for pinned heat sinks to reduce the time to reach a converged solution, and save the memory of a computer (Chaube et al., 2006). After that, refining meshing step is important for some critical area such as no-slip walls condition, the spaces between the pins, perforations, slots, and notches zones that are included in those

pinned heat sinks to ensure appropriate convergent solution because of the high velocity and temperature supposed to be for heat sinks. Besides, the change of the temperature, the velocity, and the pressure drop through pin fins heat sink are very important in this study. Therefore, a large number of nodes are focused around curved pin surfaces, perforations, slots, notches that are created in the test section. Thus, the y_+, which is the distance from a wall to the cell centres of the first grid layer nearest to the wall, has a value approximately equal to 1 or less than 1 for cells adjacent to these surfaces for SST k-ω turbulent model, as shown in Figure 5.2. Furthermore, this grid independence is always verified that will be discussed hereafter.

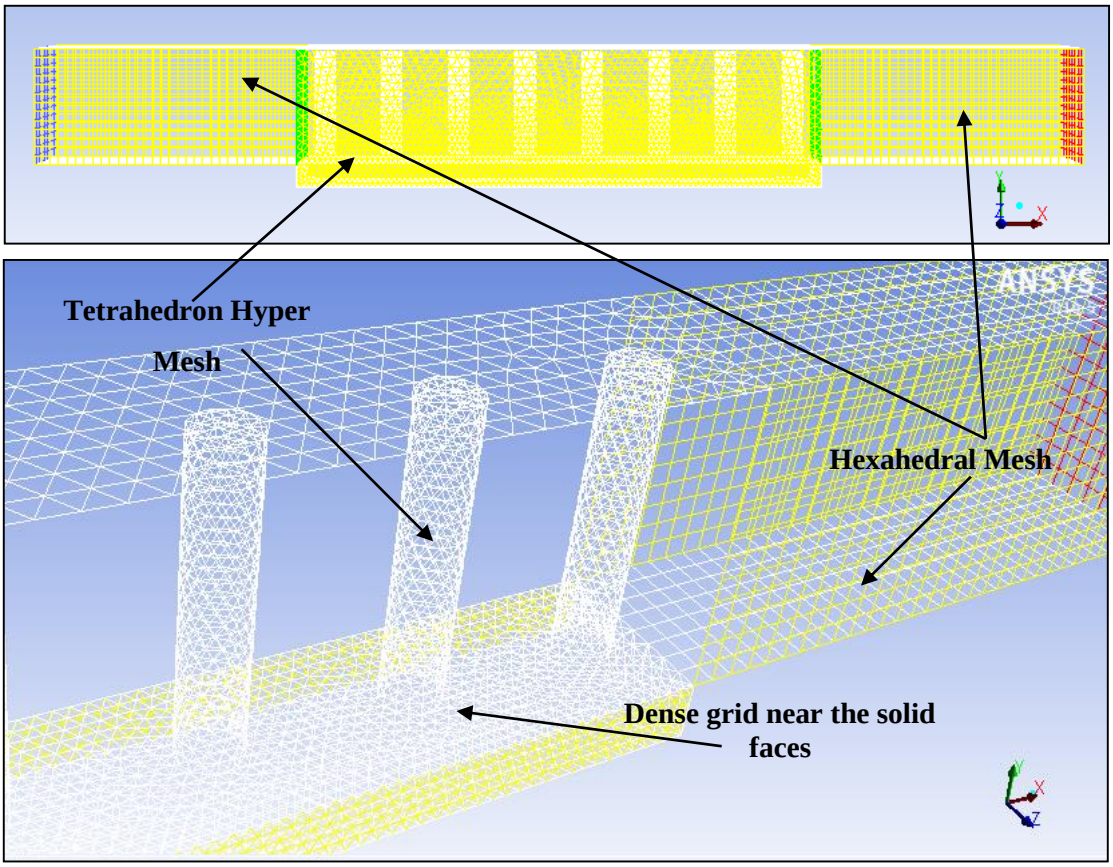

Figure 5.1: Mesh generation for pinned heat sink

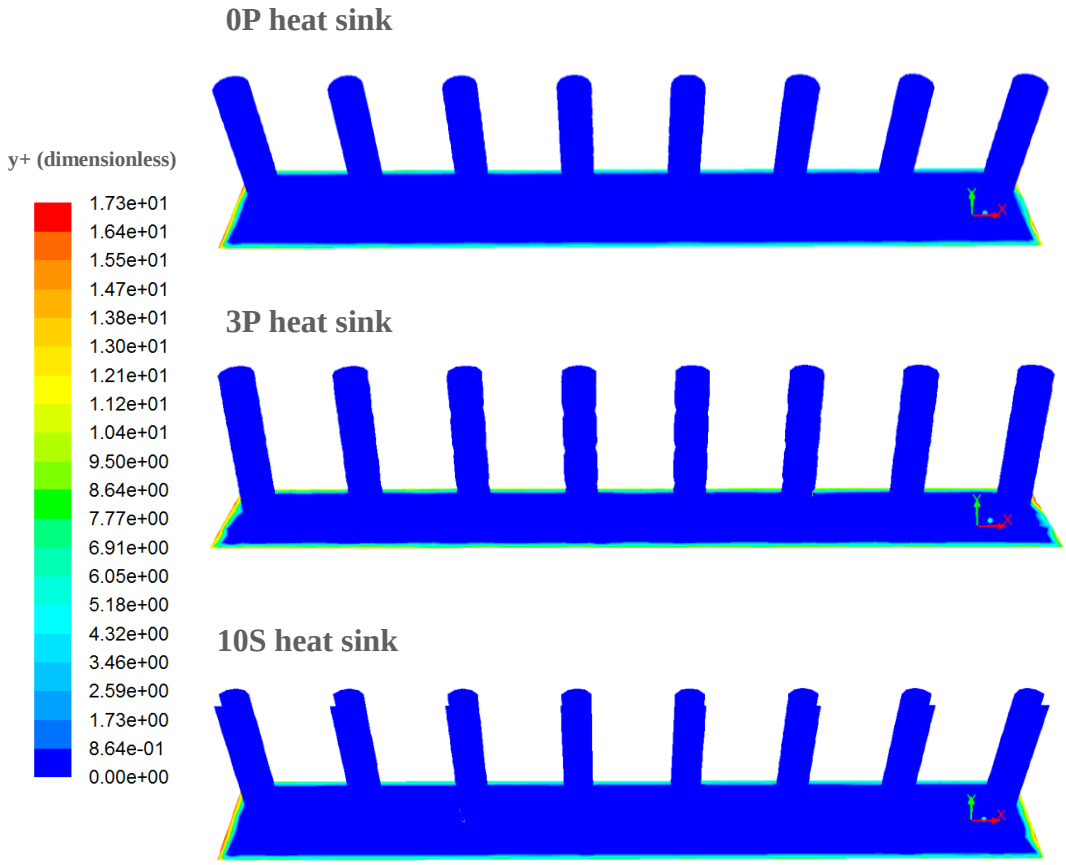

Figure 5.2: y+ contour values for solid (0P), perforated (3P) and slotted (10S) pinned heat sinks

5.5 Numerical Solution (Processing)

The thermal air flows are modelled as three-dimensional, steady state, turbulent airflow, with constant heat flux at the bottom of heat sinks and a *k-ω* SST model, following Zhou & Catton's (2011) CFD study of solid pin fins, and is used to investigate airflow, pressure drop, and heat transfer through all PHSs models.

5.5.1 Turbulent Airflow Model

Several previous studies have used the Reynolds-Averaged Navier-Stokes (RANS) equations to model turbulent flow through heat sinks successfully (Anandan & Ramaligam, 2008; Naphon & Klangchart, 2011). RANS models consider the turbulence fluctuation by splitting the velocity into a mean value plus fluctuation, then time averaging the terms of the Navier –Stokes equations. Thus, this method can be solved for the turbulent flow in the CFD methods and it is the most commonly used in practical application (Versteeg & Malalasekera, 2007). Time-averaging the continuity, momentum and energy equations with variables decomposed into mean and fluctuating components leads to the Reynolds-Averaged Navier-Stokes (RANS) equations, namely:

$$\frac{\partial \rho}{\partial t} + \nabla . \rho \underline{U} = 0 \tag{5.1}$$

$$\frac{\partial (\rho \underline{U})}{\partial t} + \nabla . (\rho \underline{U}) \underline{U} = \nabla . \left(\underline{\underline{\sigma}} - \rho \overline{\underline{U}}' \overline{\underline{U}}' \right) \tag{5.2}$$

where $\underline{\underline{\sigma}} = -p\underline{\underline{I}} + \mu\left(\nabla \underline{U} + [\nabla \underline{U}]^T\right)$ and $-\rho \overline{\underline{U}}' \overline{\underline{U}}' = \mu_t \left(\nabla \underline{U} + [\nabla \underline{U}]^T\right) - 2/3(\rho k \underline{\underline{I}})$ are the Newtonian and Reynolds Stress tensors respectively, μ is the air viscosity, ρ its density, $\underline{U}$ and $\overline{\underline{U}}'$ the average and turbulent fluctuation velocity vectors respectively, *P* is the pressure, *k* turbulent kinetic energy and $\underline{\underline{I}}$ the unit tensor. The RANS equations are solved with the energy equation for the temperature field, *T*, with a power source $\dot{Q}$ Watts, as is illustrated previously, using the following equation

$$\rho \frac{\partial C_p T_f}{\partial t} + \rho \underline{U} . \nabla (C_p T_f) = \nabla \left(k + \frac{C_p \mu_t}{\mathrm{Pr}_t} \right) \nabla T_f + \dot{Q} \tag{5.3}$$

where *Cp* is the specific heat capacity of the air, *Pr* and *v* are the Prandtl number and

kinematic viscosity of the air, respectively and the subscript *t* indicates their turbulent counterparts.

Following Zhou & Catton (2011) and Leung & Probert (1989), the thermal airflow through the PHS is modelled using the *k-ω* SST model with automatic wall function treatment. The radiation heat transfer rate is neglected as explained previously in the experimental method Chapter 3. This model combines the accurate formulation of the *k-ω* model in the near-wall region with the free-stream independence of the *k-ε* one in the far field, and has been shown to predict highly separated flows accurately in a number of previous validation studies, see e.g. Zhou & Catton (2011), Anandan & Ramaligam (2008), Ndao et al. (2009), Shaeri & Yaghoubi (2009b), Chaube et al. (2006).

The equations for the SST model are:

$$\frac{\partial(\rho k)}{\partial t}+\nabla.(\rho k\underline{U})=\widetilde{P}_k-\beta^*\rho k\omega+\nabla.\left[(\mu+\sigma_k\mu_t)\nabla k\right] \tag{5.4}$$

$$\frac{\partial(\rho\omega)}{\partial t}+\nabla.(\rho\omega\underline{U})=\alpha\rho S^2-\beta\rho\omega^2+\nabla.\left[(\mu+\sigma_\omega\mu_t)\nabla\omega\right]+2(1-F_1)\rho\sigma_{\omega_2}\frac{1}{\omega}\nabla k.\nabla\omega \tag{5.5}$$

where the blending function F1 is defined by

$$F_1=\tanh\left(\left\{\min\left[\max\left(\frac{\sqrt{k}}{\beta^*\omega y},\frac{500\nu}{y^2\omega}\right),\frac{4\rho\sigma_{\omega_2}k}{CD_{k\omega}y^2}\right]\right\}^4\right) \tag{5.6}$$

in which $$CD_{k\omega}=\max\left(2\rho\sigma_{\omega_2}\frac{1}{\omega}\nabla k.\nabla\omega,10^{-10}\right) \tag{5.7}$$

the turbulent eddy viscosity is computed from

$$\nu_t=\frac{a_1k}{\max(a_1\omega,SF_2)} \tag{5.8}$$

where *S* is the invariant measure of the strain rate and F_2 is a second blending function defined by

$$F_2=\tanh\left(\left[\max\left\{2\frac{\sqrt{k}}{\beta^*\omega y},\frac{500\nu}{y^2\omega}\right\}\right]^2\right) \tag{5.9}$$

To limit the build-up of turbulence in stagnation regions, a production limiter is used in the SST model.

$$P_k = \mu_t \frac{\partial u_i}{\partial x_j}\left(\frac{\partial u_i}{\partial x_j} + \frac{\partial u_j}{\partial x_i}\right) \rightarrow \tilde{P}_k = \min\left(P_k, 10\beta^* \rho k \omega\right) \tag{5.10}$$

The empirical constants turbulent model for this model are, Zhou & Catton (2011):

$$\beta^* = 0.09,\ \alpha_1 = \frac{5}{9},\ \beta_1 = \frac{3}{40},\ \sigma_{k1} = 0.85,\ \sigma_{\omega_1} = 0.5,\ \alpha_2 = 0.44,\ \sigma_{k2} = 1,\ \sigma_{\omega 2} = 0.856$$

5.5.2 Conjugate Heat Transfer Model

Heat sinks are simulated using a conjugate heat transfer model. The rate of heat conduction passes through solid material of pin fins heat sink is balanced with convection heat transfer from material of heat sink into moving air stream through a coupled boundary condition at the solid/fluid interface, (Kraus, 2002) as illustrated in Figure 5.3.

The energy equations in the fluid and solid domains are given by:

$$\rho \underline{U} \nabla (C_p T_f) = \nabla\left(k_f + \frac{C_p \mu_t}{\mathrm{Pr}_t}\right)\nabla T_f \quad \text{For the fluid domain} \tag{5.11}$$

$$\nabla (k_s \nabla T_s) = 0 \quad \text{For the solid domain} \tag{5.12}$$

where $\underline{U}$ is fluid (air) velocity; T_f and T_s are fluid and solid temperature, respectively; μ_T, Pr_T, k_f and k_s are the turbulent viscosity, the turbulent Prandtl number, the thermal conductivity of the fluid and solid, respectively.

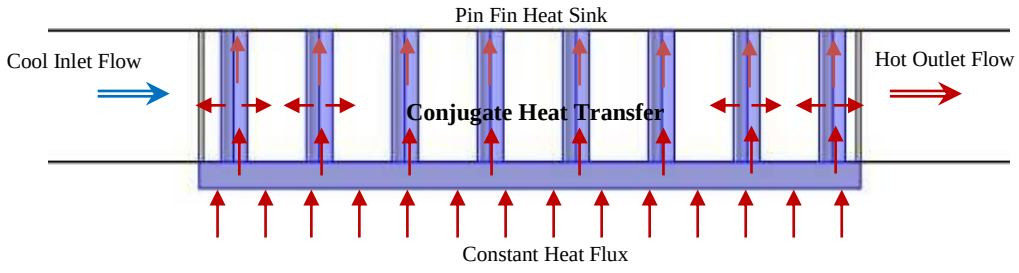

Figure 5.3: Conjugate heat transfer model of pin fin heat sink

5.5.3 Solver Settings

A commercial finite volume method (FVM) based code is used which employs the SIMPLE method for the continuity equation in which the velocity components are first calculated from the Navier–Stokes equations using a guessed pressure field. The fully coupled momentum and energy equations are solved, using second order upwinding to reduce the numerical errors for the Navier-Stokes equations and the energy equation. Computation is started first by solving the continuity, momentum, k and ω equations to determine the airflow field and then the energy equation to find the thermal field in the computational domain. Following previous studies such as Zhou & Catton (2011) and Yuan et al (2012), the procedure continues until the sum of the residuals of continuity and momentum equations is less than 10^{-4} and for energy equation is taken smaller than 10^{-6} in each cell.

The numerical data is considered at constant and variable thermodynamic air properties. For constant thermodynamic air properties, they are equal to those at the inlet temperature of 25ºC. However, for variable air properties such as viscosity, density, thermal conductivity and specific heat capacity vary with temperature through the test section, as shown in Table 5.1. Thus, the air temperature variation inside the heat sink is significant to highlight the effect of air properties on thermal and airflow characteristics of pinned heat sinks when comparing with experimental results and it cannot be disregarded when temperature changes through heat sink. It can be chosen among different methods to compute the corrected air properties. A piecewise-linear interpolation method is selected to define the properties values (Yuan et al., 2012) that are considered in this study at several air temperatures based on the following function of temperature:

$$\phi(T) = \phi_m + \left(\frac{\phi_{m+1} - \phi_m}{T_{m+1} - T_m} \right) (T - T_m) \tag{5.13}$$

where $1 \leq m \leq M$ and M is the number of segments. ANSYS FLUENT-CFD code will calculate the property values by linearly interpolating among the values defined.

Table 5.1: The variation of air properties with increasing air temperature, Cengel (2006)

Air temperature (^oC)	Dynamic Viscosity (kg/m.s)	Density (kg/m^3)	Thermal Conductivity (W/m.K)	Specific Heat (J/kg.K)
15	1.802×10^5	1.225	0.02476	1007
25	1.849×10^5	1.184	0.02551	1007
45	1.941×10^5	1.109	0.02699	1007
60	2.008×10^5	1.059	0.02808	1007
80	2.096×10^5	0.9994	0.02953	1008
100	2.181×10^5	0.9458	0.03095	1009
120	2.264×10^5	0.8977	0.03235	1011

5.6 Boundary Conditions

Fluid flow and heat transfer for problems require suitable boundary conditions (BCs). Therefore, in this study, the boundary conditions for the present problem are assumed below, as shown in Table 5.2 and Figure 5.4.

5.6.1 On the Pins

The rejected heat conduction rate through the aluminium pins heat sink is balanced with the gained heat transfer convection into the moving air stream through a coupled boundary condition at the solid/fluid interface. In other words, each pin fin has two BCs: the one is a fluid surface that represents fluid flow and another one is a solid surface as a material of pin fin heat sink itself that is known as conjugate heat transfer.

5.6.2 At the Bottom Wall of the Heat Sink

A constant heat flux is applied at the bottom wall of the heat sink. No slip condition is applied so the velocity of fluid (air) is zero in all directions, $Ux=Uy=Uz=0$ due to a rigidity wall heat sink.

5.6.3 At the Inlet Side

The inlet air velocity is set to a series of values as Ux=6.5, 8, 10, and 12m/s and $Uy=Uz=0$, such as Yang & Peng (2009a), Yang & Peng (2009b), Kumar & Bartaria (2013), Zhou & Catton (2011). In addition, the inlet fluid temperature (T_{in}) is constant at 25^{o}C. The turbulence intensity of the flow entering through the inlet

boundary is set to 5% (Zhou & Catton, 2011). The range of Reynolds number for heat sinks in the most industrial electronic applications cooling varies from 1300 to 50000 (Ventola et al., 2014). Thus, *Re* is varied from 3500 to 6580 as a turbulent airflow in this study to reduce consumption fan power and the noise level to desirable levels, particularly in the office or home.

5.6.4 At the Outlet Side

The outlet boundary condition is set to pressure outflow to avoid the backflow and diverged solution. The gauge pressure is zero at this condition, Dewan et al. (2010), Zhou & Catton (2011), Ramesha & Madhusudan (2012), and Yuan et al. (2012). The turbulence intensity of the flow exiting through the outlet boundary is set to 5% as well, Zhou & Catton (2011).

5.6.5 Right and Left Sides

The right and left sides of the channel are a symmetric boundary condition result from the uniform airflow and symmetry in the fin arrays, Zhou & Catton (2011). Computations, therefore, are applied just for eight pin fins instead of the total array of pin fins to shrink the model domain and the number of nodes. This reduces the time to reach a converged solution, and saves computer memory.

5.6.6 The Other Surface Walls

All the other surfaces walls of computation domain are imposed as adiabatic surfaces with zero heat flux resulting in no heat transfer passed through those walls. A no slip condition is applied due to a rigidity of those wall that leads to a zero fluid velocity in all directions (Zhou & Catton, 2011): $U_x=U_y=U_z=0$ are set.

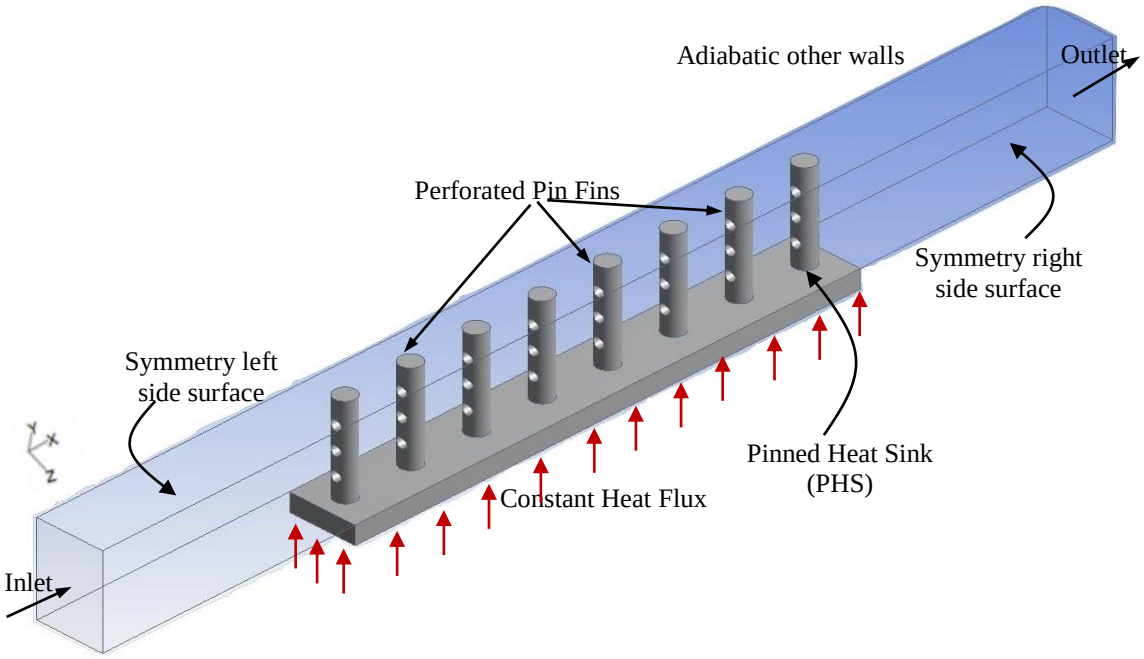

Figure 5.4: Schematic diagram of the flow domain used in the CFD analyses, showing eight perforated pin fins.

Table 5.2: The boundary conditions of the conjugate heat transfer model

Locations	Fluid Conditions	Thermal Conditions	Locations	Fluid Conditions	Thermal Conditions
Inlet	U= (6.5-12) m/s	T=25°C	Bottom wall of heat sink	U=0	Q=constant
Right and left sides (symmetry)	$\frac{du}{dy}=0$	$\frac{dT}{dy}=0$	outlet	P_{gage}=0	$\frac{dT}{dx}=0$
Top wall and other walls	U=0	$\frac{dT}{dz}=0$	Pin heat sink	U=0	$k_{air}.\frac{dT_{air}}{dn}=k_S.\frac{dT_S}{dn}$

5.7 Numerical Data Analysis (Post Processing)

The main important characteristics of airflow and heat transfer are explained, to evaluate the hydraulic and thermal parameters of pinned heat sinks designs, which can be obtained from the ANSYS FLUENT post processing options. These factors are defined in section 2.5.

5.8 Methods of Validation

In order to validate the numerical results, mesh verification and other validation with the previous literature must be carried out. Therefore, the verification of the computational domain, grid independence test (GIT) and the previous validation studies of solid pins and single perforated pin fins heat sinks are investigated and explained in this section.

5.8.1 Domain Verification

The verification of the computational domain that is used in this study must also consider the entrance and exit regions. These regions should be sufficiently far from the pinned heat sink to ensure that the numerical results are independent of the boundary positions. For this reason, some tests have been carried out to determine a sufficient distances away from the test section.

In this study, the Nusselt number (Nu_T), pressure drop (ΔP), and the CPU temperature (T_{case}) are determined in a range of cases for inlet air velocities between 6.5m/s and 12m/s. The distances of the entrance and exit zones to the heat sinks are as shown in Table 5.3 where L=50mm refers to the length of the heat sink (test section) in the flow direction. It can be noticed that the numerical solution is converged for those domains except in domain 1 since the backflow (reversed flow) will clearly happen at the outlet boundary of the heat sink due to its zero the exit length.

Table 5.3 indicates that increasing in the length of entrance and exit regions beyond domain 3 (0.5L), the errors in the numerical data is less than 2% for each of the Nu_T, ΔP, and T_{case} for 0P and 3P models for different inlet air velocities values (6.5m/s and 12m/s). Thus, the computational domains used from now on have 0.5L entrance and exit length (Domain 3) as a standard domain to save computer memory and computational time.

Table 5.3: The entrance and exit regions length of pin fins heat sinks

			Domain 1	Domain 2	Domain 3	Domain 4	Domain 5	Domain 6
Entrance Length			*0L*	*0L*	*0.5L*	*1L*	*1.5L*	*2L*
Exit Length			*0L*	*0.5L*	*0.5L*	*1L*	*1.5L*	*2L*
Solid Pins (0P)	*U= 6.5m/s*	*Nu*	Solution is not converged	279.95	276.28	277.28	277.69	277.39
		ΔP (Pa)		38.59	36.36	38.66	38.77	38.55
		T_{case} *(°C)*		88.69	89.58	89.16	89.07	89.14
	U= 12m/s	*Nu*		384.34	380	382.2	380.38	381.66
		ΔP (Pa)		106	106.59	108	108.7	109
		T_{case} *(°C)*		72.57	73.17	72.77	72.96	72.83
Perforated Pins (3P)	*U= 6.5m/s*	*Nu*		305.16	299.4	300.39	300.63	300.79
		ΔP (Pa)		39.78	35.61	36	36.43	37.84
		T_{case} *(°C)*		79.72	80.62	80.43	80.4	80.37
	U= 12m/s	*Nu*		423.3	415.63	416.46	416.65	416.93
		ΔP (Pa)		111.85	97.68	98.45	100.12	101.81
		T_{case} *(°C)*		66.13	66.75	66.68	66.67	66.65

The effect of turbulence intensity boundary conditions is now investigated, as shown in Figure 5.5. Thus, the turbulence intensity for both inlet and outlet are set to 2.5%, 5%, and 7.5% (Almoli, 2013). The pressure drop and temperature of the solid base with solid (0P) and perforated (3P) pinned heat sinks for different inlet air velocity are obtained. It is shown that the turbulent intensity at the inlet and outlet do not have any substantial effect on the results in these specific cases. Hence, the turbulence intensity is used from now on has 5% as a standard value (Zhou & Catton, 2011).

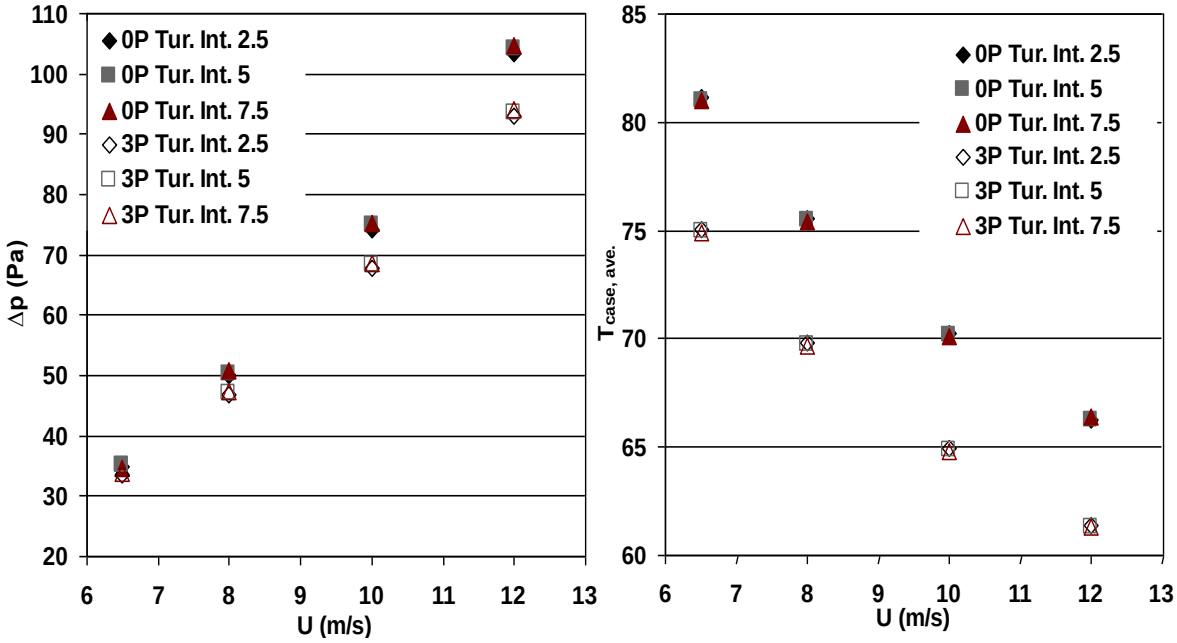

Figure 5.5: Inlet air velocity versus the pressure drop and temperature case of HSs for different turbulence intensities

5.8.2 Grid Independent Tests (GIT) (Mesh Verification)

Tetrahedron Hyper cells (Hex Core T-grid) are utilized for several various grid distributions to ensure that mesh independence is achieved and the numerical data is reliable and independent of grid density. Consequently, the CFD methodology is firstly verified by comparing predictions of Nusselt number, pressure drop, and the CPU temperature for the present solid pin (0P), and perforated pin fins 1A, 2A, 3P, and 5P heat sink models with the number of cells with air velocity at 6.5m/s and 12m/s. Cases studies should be refined near the solid faces and near perforations to predict the accurately fluid flow and temperature distributions.

In the case of solid pin fins (0P), the number of cells is from 98,104 to 171,059 in various steps. It is determined that after 124,00 cells, increasing the number of cells leads to less than 3% of the average Nusselt number, pressure drop, and the CPU temperature as shown in Table 5.4. Thus, the number of cells 124,000 is taken as a standard for mesh independence.

With respect to the perforated pin fins 1A, 2A, 3P, and 5P designs, the number of cells is varied from 102,000 to 233,000 with different levels, Table 5.4. Increasing the number of cells beyond 147,000 has typically a 3% change in all outlet parameters. Therefore, all results presented in this study have been obtained from 147,000 cells.

For the present slotted pin 3S, 6S, and 10S, and notched pin 2.5N, 5N, and 7.5N fin heat sink models. The grid points should be densely distributed near the solid faces, slotted, and notched surfaces to predict accurately the fluid flow and temperature distribution.

According to three slotted 3S, 6S, and 10S designs and three notched pins 2.5N, 5N, and 7.5N models, the number of cells is from 93,000 to 180,000 in various steps. It is indicated that increasing the number of cells beyond 115,000 results in typically a 2% change in all outlet parameters. Thus, the number of grid points 115,000 is chosen as a standard for mesh independence for slotted pins and 115,000 is selected for notched pins as grid independence.

Table 5.4: Mesh validation of Solid and Perforated pinned heat sink designs

Parametric Studies	Solid Pins (0P)			Triple Perforated Pins (3P)			Notched pins (5N)		
	No. Cells	6.5m/s	12m/s	No. Cells	6.5m/s	12m/s	No. Cells	6.5m/s	12m/s
Nu	98104	253.15	348.23	113000	273.98	373.59	95008	253.83	336.7
	124092	262.1	360.1	123689	275.95	379.7	115100	262.21	348.71
	134035	263.49	362.31	161916	282.62	395.17	134112	267.34	358.78
	171059	268.13	367	202678	287.71	400	171112	271.15	365.72
ΔP (Pa)	98104	35.28	107.18	113000	32.93	92.72	95008	26.47	78.8
	124092	35.22	104.09	123689	32.76	94	115100	26.15	77.4
	134035	35	103.8	161916	33.65	93.55	134112	26.03	77.72
	171059	35.74	103.67	202678	34.79	95.16	171112	26.71	77.36
T_{case} (ºC)	98104	82.66	67.43	113000	75.9	63	95008	80.47	67.4
	124092	81.06	66.22	123689	75.58	62.39	115100	78.76	65.84
	134035	81.18	66.31	161916	74.97	61.34	134112	78.34	65.16
	171059	80.24	65.6	202678	74.53	61.66	171112	77.55	64.2

5.8.3 Validation with Previous Studies

In this study, to ensure the CFD approach is accurate and reliable, validations against four previous experimental and numerical studies are carried out at constant air properties because the most previous numerical works such as Zhou & Catton (2011) and Yuan et al (2012) have assumed that air properties is constant.

Solid Pin Fins Heat Sinks

The first validation of the numerical solutions is for the predicted Nusselt number and pressure drop across the solid pin fins heat sinks and compared with those of the numerical study of Zhou & Catton (2011). Figure 5.6 compares predictions of Nusselt number (Nu_T) and pressure drop (ΔP) across the pin fins with various inlet air velocities from 6.5m/s to 12.2m/s. These both agree well with the prediction of Zhou & Catton (2011) with typical discrepancies in the predictions of Nu_T and ΔP of 3% and 4%, respectively.

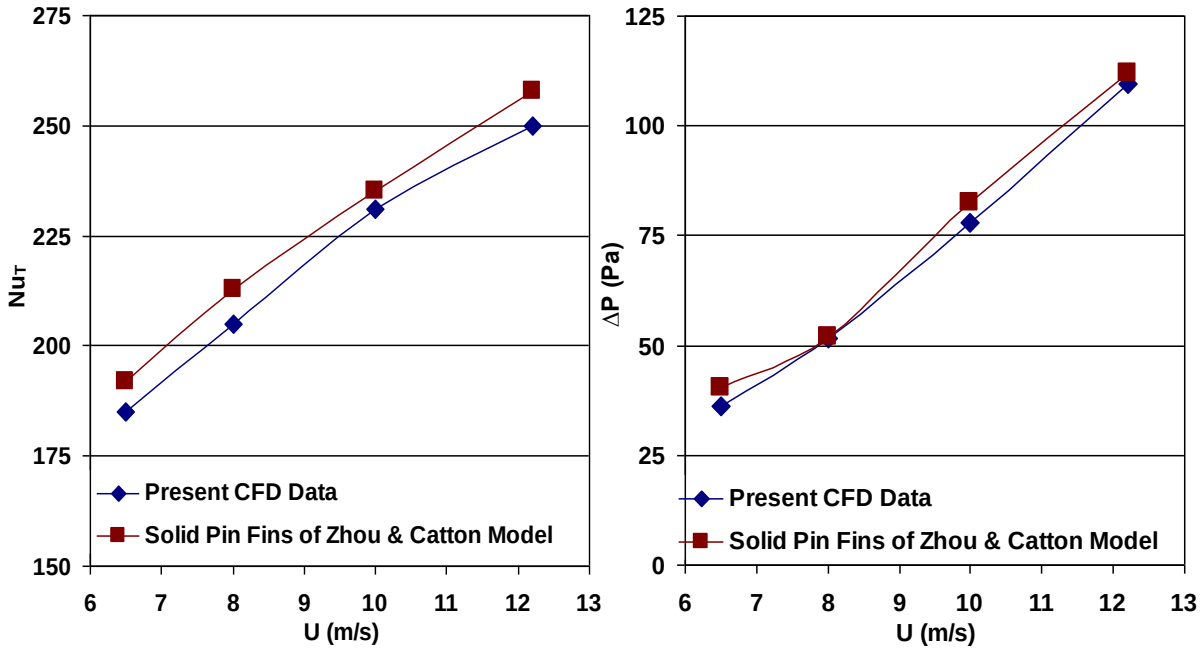

Figure 5.6: Validation of Nusselt number (Nu_T) and pressure drop (ΔP) predictions with those of Zhou & Catton (2011)

The comparison of thermal resistance, R_{th} of solid pin fins heat sink between the present CFD study data with the experimental results of Jonsson & Moshfegh (2001) and the numerical data of Zhou & Catton (2011) are shown in Figure 5.7 for 6.5m/s≤ U_{in} ≤10m/s. It found that the maximum deviation of thermal resistance of predicted CFD was less than 3% for both previous studies.

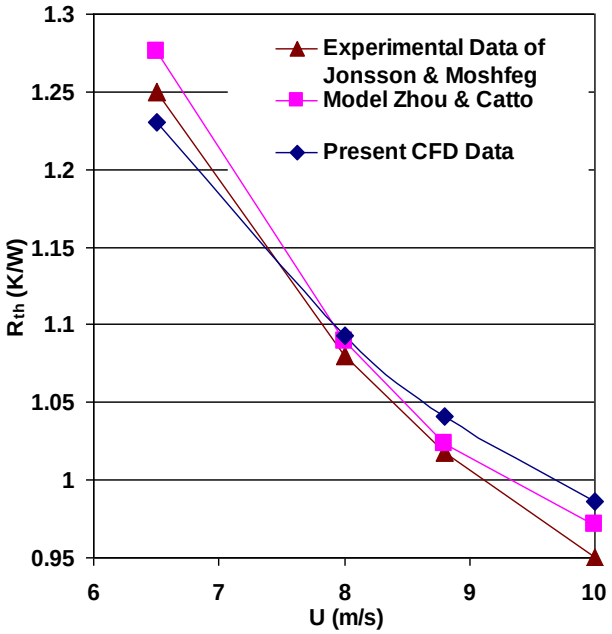

Figure 5.7: Comparison of thermal resistance predictions with those CFD results of Zhou & Catton (2011), and experimental data of Jonsson & Moshfeg (2001)

A further validation case is the pressure drop (ΔP) over the solid pin fins heat sink for experimental data of Yang et al (2007) and the current numerical results. Figure 5.8 indicates that the error percentage between predicted numerical results and the literature's data with various inlet air velocities is less than 2%. It is clear that pressure drop measurement from the previous experimental study is in good agreement with those predicted by the CFD.

An alternative approach of comparing the present simulation data with experimental results in terms of heat transfer is to compare the heat transfer coefficient (h_T). The variation of heat transfer coefficient with inlet airflow for the present CFD model and experiment are given in Figure 5.8. The results of this figure show that the agreement is acceptable, with a typical error percentage of 5%.

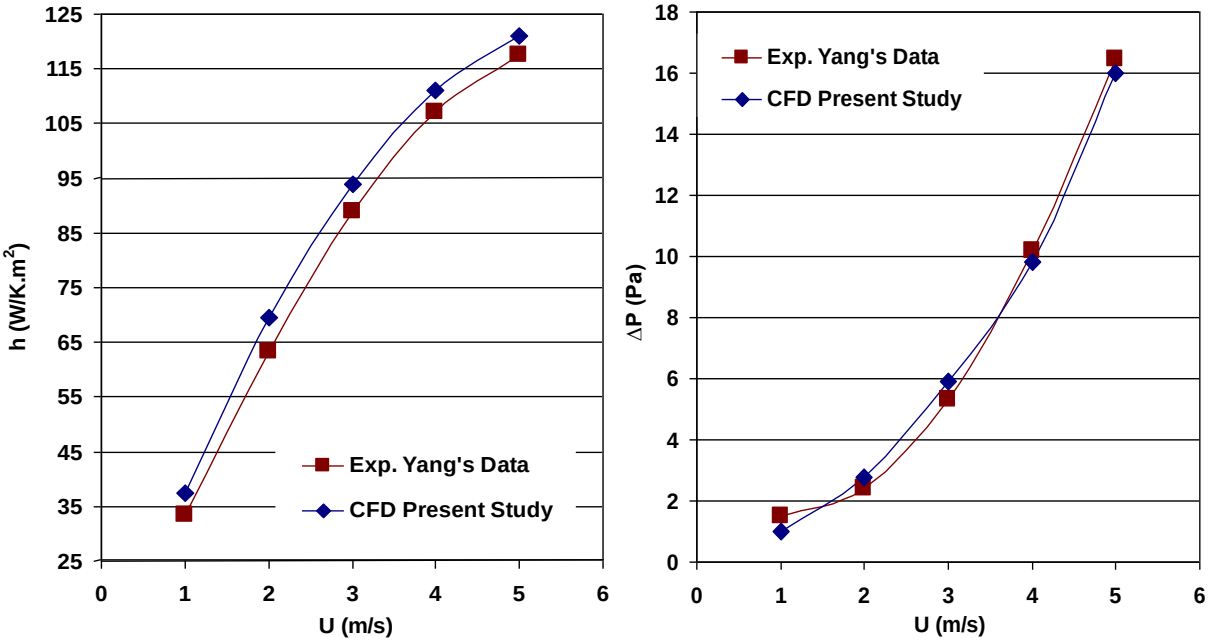

Figure 5.8: Validation between the experimental data of Yang et al. (2007) and CFD analysis of heat transfer coefficient and pressure drop

Perforated Pin Fin Heat Sinks

The predictions of the current CFD model are compared with the experimental data of Sahin & Demir (2008) for flow past a heat sink where the pin fins have a single perforation. Figure 5.9 compares CFD predictions of the ratio Nu/Nu_s with the previous experimental data, where $Nu_s=0.077Re^{0.716}\ Pr^{1/3}$ is Sahin & Demir's experimental correlation for heat transfer from a smooth surface without pins. Again, the agreement with the experimental data is generally good, with a maximum discrepancy of less than 7%.

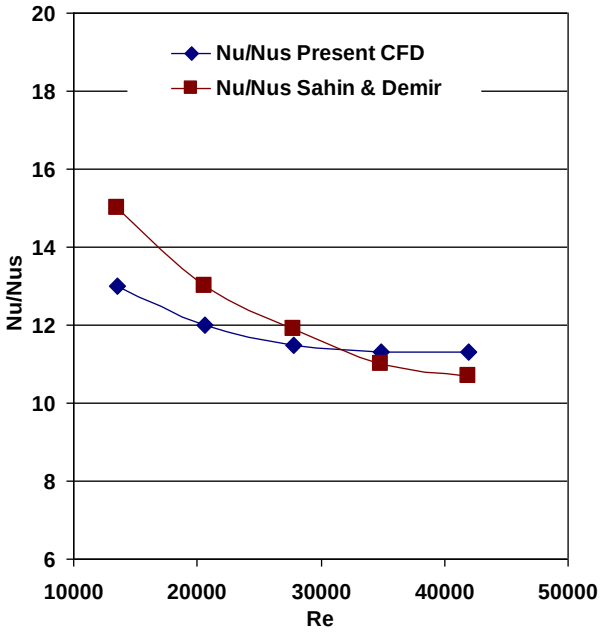

Figure 5.9: Comparison between CFD predictions of *Nu/Nus* with experimental data of Sahin & Demir (2008) for pin fins with a single perforation

Given the range of factors that affect experimental and numerical data for flow over heat sinks, the above validation cases confirm that the numerical approach agrees well with previous results. The errors between the predicted numerical study and those previous works are acceptable because of boundary conditions variances, numerical solutions (discretization error), the type of grid independence, and uncertainties in the experimental tests. Hence, the conjugate heat transfer approach in the present work can be used for analysis of this type of heat sink.

5.9 CFD Validation with Present Experimental Results

In this section, complementary experimental and numerical simulation validation models are used to investigate the main benefits of using the novel perforated pinned heat sink with multiple perforations. The numerical data is considered at constant and variable physical air properties (i.e. as a function of temperature as indicated previously) to highlight the effect of air properties on the hydraulic and heat transfer characteristics of pinned heat sinks when comparing with experimental results. The inlet velocities are varied from 6.5m/s to 12m/s for the range of Reynolds number 3500-6580 based on the mini-duct hydraulic diameter, with 8x8 in-line pins array at constant longitudinal and transverse distance 6.5mm.

5.9.1 Validation of Hydraulic Characteristics

The main hydraulic characteristics of airflow are pressure drop (ΔP), fan power (P_{fan}), and pressure drag coefficient (P_d) of 0P and 3P pinned heat sink design, Figure 3.1, that are validated with CFD commercial code as air properties are constant (Num.) and variable (Num. Variable).

Figures 5.10 compares experimental measurements with numerical predictions into the effect of perforations on the pressure drop, ΔP, across pinned heat sinks (PHSs) and the power required to overcome the pressure drop.

In the experimental data, the pressure drop with three perforations is typically around 7% smaller than that of solid pin fins, while for the numerical predictions this reduction is approximately 9%. For the solid and perforated pins, the average error in the pressure drop predicted using constant air properties are typically 9.2% and 10.5 % respectively, whereas for predictions using variable air properties the error has been reduced by two thirds to around 2.9% and 3.8% for the solid and perforated pins respectively. Part of this may be due to the practical difficulties of fabricating PHSs with several perforations, when slight misalignment of the perforations with the dominant airflow direction and finite roughness of perforation surface can increase the pressure drop considerably. However, the numerical predictions at variable air properties are closer to the experimental pressure drop and within 5% error percentage. Since, in practical ways, the viscosity of air will increase with increasing air temperature that required higher pressure drop to push the air through the heat sink. It is indicated that the behaviour of fan power is the same of pressure drop.

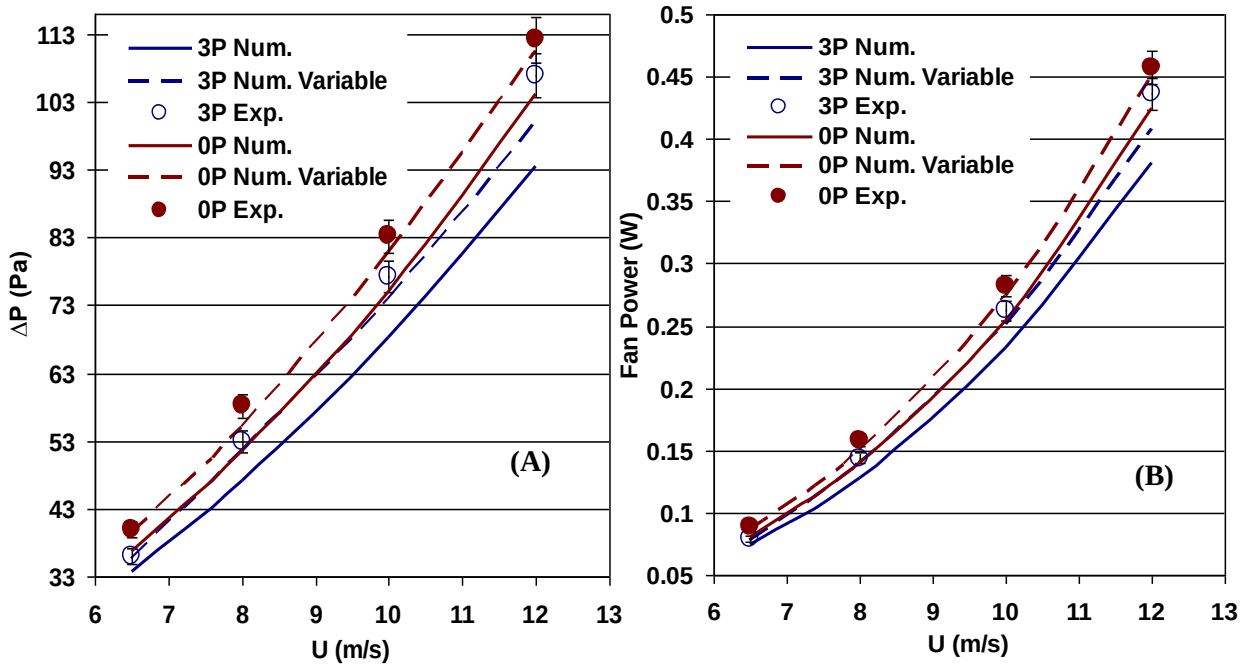

Figure 5.10: Effect of pin perforations on (A) pressure drop and (B) fan power as a function of airflow speed

Figure 5.11 shows the effect of the perforated pinned heat sinks model (3P) on the pressure drag coefficient for a range of inlet velocities from 6.5m/s to 12m/s at Re=3500-6580 and 8×8 in-line pins with longitudinal and transverse distance is 6.5mm. The numerical results indicated Num. is constant ρ, c_p, k, and μ; and Num. Variable is for ρ, c_p, k, and μ as a function of temperature

In line with the comparison between the pressure drag coefficient and air velocities, the pressure drag coefficient is larger within the experimental studies when compared with the numerical solution at constant air properties. Again, the numerical predictions at variable air properties are closer to the experimental pressure drag coefficient.

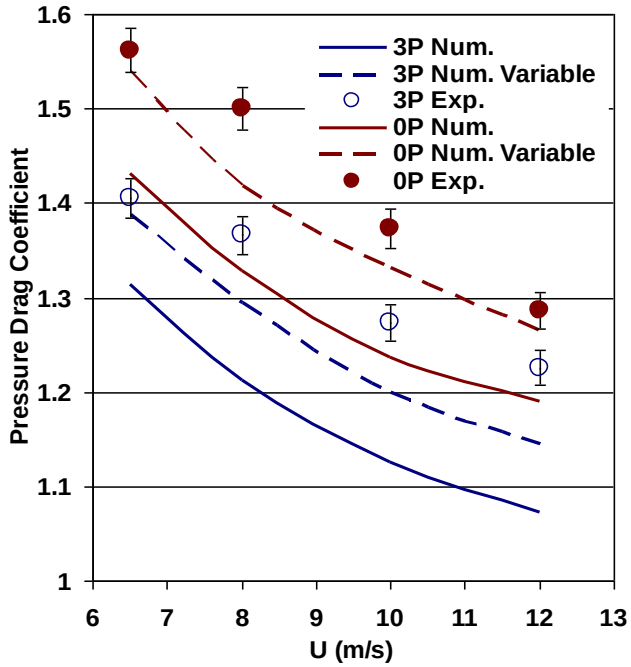

Figure 5.11: Effect of pin design and inlet air velocity on the pressure drag coefficient

5.9.2 Validation of Heat Transfer Characteristics

The experimental heat transfer characteristics such as the total and projected Nusselt number, Nu_T, Nu_P, respectively, the CPU temperature (T_{case}), and thermal resistance (R_{th}) of 0P and 3P pinned heat sink design are validated with numerical data again at constant (Num.) and variable (Num. Variable) air properties.

Average Nusselt Number

Figure 5.12 presents the corresponding experimental measurements and numerical predictions of Nusselt number, based on either the total PHS wetted surface area (Nu_T) or on the projected surface area (Nu_P) equivalent to the base surface area of HS.

The data shows that both Nu_T and Nu_P increase approximately linearly with the inlet air velocity and that the 3P pin fin design achieves a significant enhancement in heat transfer. The average error between the experimental and predicted values of Nu with constant air properties is 8.9% and 12.1% for 0P and 3P respectively, whereas for those with variable air properties, this discrepancy is reduced to 4.2% and 7.7% for 0P and 3P respectively. Since the viscosity of air increases with increasing air temperature this causes reducing heat transfer rate. In addition, the considerations mentioned above.

Thus, the Nu_T and Nu_P of numerical data at variable air properties are lower and closer to the experimental findings than that at constant air properties.

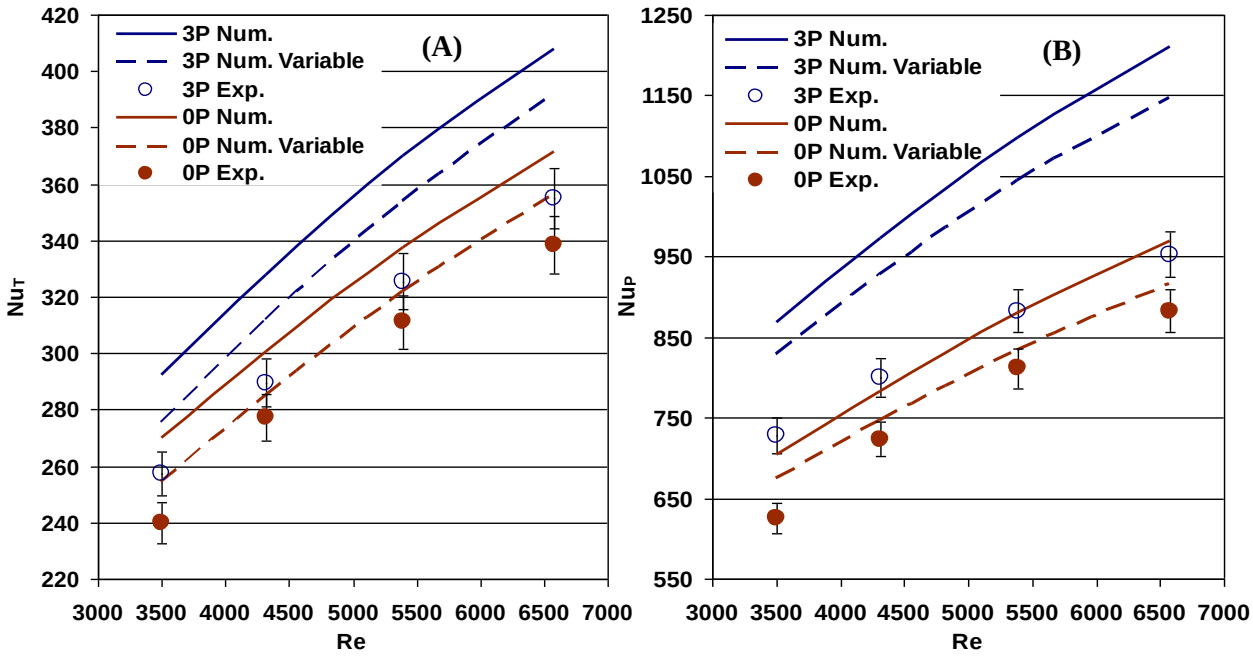

Figure 5.12: Effect of inlet velocity on Nusselt number based on (A) total and (B) projected surface area

Thermal Management

Figures 5.13 and 5.14 compare experimental measurements and numerical predictions from the conjugate heat transfer analysis for the average base plate temperature, T_{case} and thermal resistance, R_{th} with fan power for 6.5m/s≤U≤12m/s, through a system of 8x8 pins a pin pitch of 6.5mm.

As expected, the T_{case} and R_{th} of experimental results are the highest. The heat transfer coefficient measured experimentally is lower than the predicted values from computation. For instance, in the experimental data the T_{case} with three perforations is typically around 6% smaller than for solid pin fins, while for the numerical predictions at constant air properties this reduction is approximately 8%. The average error in the numerical predictions of T_{case} with constant thermo-physical properties is around 2.8% and 5.2% for 0P and 3P heat sink models respectively, while with variable thermo-physical properties these average errors are 2.5% and 5.1% for the 0P and 3P heat sink models, respectively. A further source of error is possibly around the additional thermal resistance as a result of the brazing process, where the brazing material does not completely fill the gap between the pin and the

base plate. Thus, some air gaps appear within soldering zones, as indicated previously in Figure 3.8, which causes greater thermal resistance for the experimental conditions. The predicted numerical data at variable air properties is slightly higher and closer to experimental results than for the constant air properties by approximately 1.5°C.

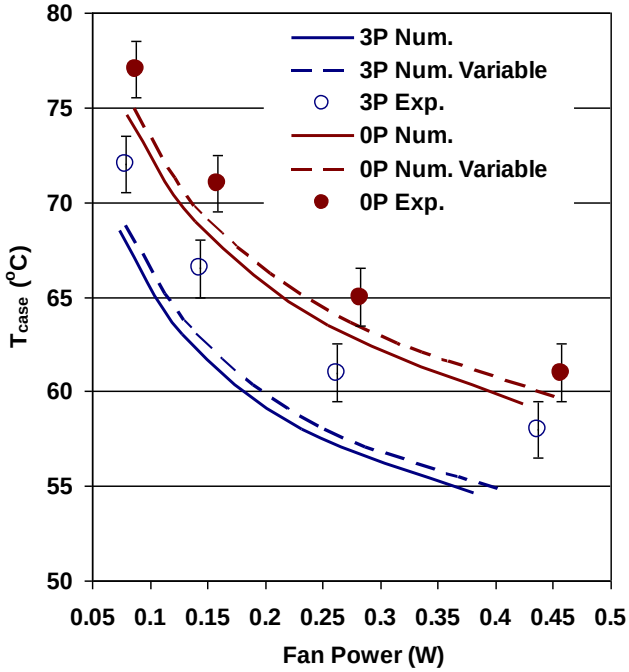

Figure 5.13: Comparison between experimental and numerical predictions of influence of fan power on T_{case}

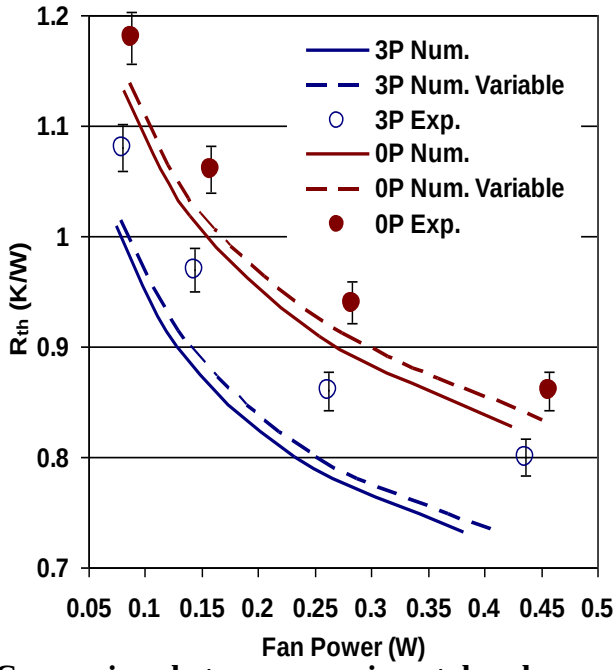

Figure 5.14: Comparison between experimental and numerical predictions of influence of fan power on R_{th}

This demonstrates the thermo-fluid benefits obtained from the perforated pinned heat sinks, in comparison to the solid PHS, since the two objectives designs of heat sinks are achieved. The heat transfer of perforated pin (3P) enhances at constant fan power when compared with the solid pin (0P) due to elimination the dead thermal-flow zones just downstream the solid pin fins. It means CPU temperature reduces at the minimum energy cost pin perforations.

5.10 Summary

The numerical approach for solving airflow over heat sinks has been described and validated against previous results. Computational Fluid Dynamics (CFD) has been used to simulate the conjugate heat transfer and turbulent airflow through PHSs designs using ANSYS FLUENT 14.5 as the commercial code. Furthermore, the key characteristics for airflow over PHSs are also understood and the grid independence test (GIT) and validations are described.

The numerical data of thermal and hydraulic characteristics is validated with the experimental results with the likely source of errors explained, Table 5.5, due to the practical difficulties of fabricating PHSs with several perforations, when slight misalignment of the perforations with the dominant airflow direction, and the effects of finite perforation surface roughness. A further source of error for the heat transfer measurements may be due to the additional thermal resistance because of the brazing process, where the brazing material did not completely fill the gap between the pins and the base plate. Thus, it may be that, in order to maximize the benefits from the perforations, care must be taken to ensure that they are aligned with the dominant flow direction and manufactured with a good-quality surface finish. Furthermore, the numerical data at variable air properties are closer to the experimental findings than that for constant air properties, Table 5.6.

Since there is good agreement between the experimental measurements and predicted numerical data with variable air properties, the CFD conjugate heat transfer model is now used to report further a parametric study of the influence of the number, positioning of circular perforations, and other perforations shapes in the next chapters.

Table 5.5: The experimental and numerical enhancement of Nusselt number (Nu), fan power (P_{fan}), and CPU temperature (T_{case}) of 3P heat sink design compared to solid pins (0P)

Parametric Studies / Heat Sink Designs	↑A_T	Nusselt Number		↓ P_{fan} (W)	↓ T_{case} (°C)
		↑ Nu_T	↑ Nu_P		
Numerical Perforated Pins with Three Perforations (3P)	15%	9%	24%	9%	8%
Experimental Perforated Pins with Three Perforations (3P)		5%	11%	7%	6%

Table 5.6: The errors percentage between the experimental and numerical data at constant and variable air properties

Parametric Studies / Heat Sink Designs	Nu_T		P_{fan} (W)		T_{case} (°C)	
	0P	3P	0P	3P	0P	3P
Constant air properties	8.9%	12.1%	9.2%	10.5%	2.8%	5.2%
Variable air properties	4.2%	7.7%	2.9%	3.8%	2.5%	5.1%

Chapter Six: Pinned Heat Sinks with Circular Perforation

6.1 Introduction

As the maximum discrepancy between the present experimental and simulation data is acceptable (Chapters 3 and 4), the validated CFD model procedure is utilised to perform parametric studies on perforated pinned heat sinks' (PPHSs) effect on the cooling performance in relation to the number, and positioning of circular perforations with the variable physical air properties.

In this chapter, solid pin fins (0P), and novel perforated pin fin HSs (1A, 1B, 1C, 2A, 2B, 2C, 3P, and 5P, Figure 6.1) have been simulated as a conjugate heat transfer and turbulent airflow problem for electronic cooling systems. CFD solutions are carried out to investigate the thermal airflow characteristics of these heat sinks to ascertain how these pin fins can reduce the hot spots inside them and enhance airflow through them. In addition, the effect of the pins in in-line and staggered arrays and the effect of the shapes of the perforations are considered as well.

6.2 Description of PHS Models

Eight types of perforated pinned heat sinks (PPHSs) are compared with solid pin fins (0P), as shown in Figure 6.1. These perforations are aligned in the direction of flow and their location (upper, lower, and centre of the pin) and their number (0, 1, 2, 3, and 5 perforations) vary, whilst their diameter is kept constant at 1mm. All these perforated pins have the same physical domain that consists of three parts: entrance section, test section (PHSs), and exit section. The pin fin heat sink symmetric section comprises eight rows in an in-line array perpendicular to the flow direction (cross flow) and each row has 8 pin fins.

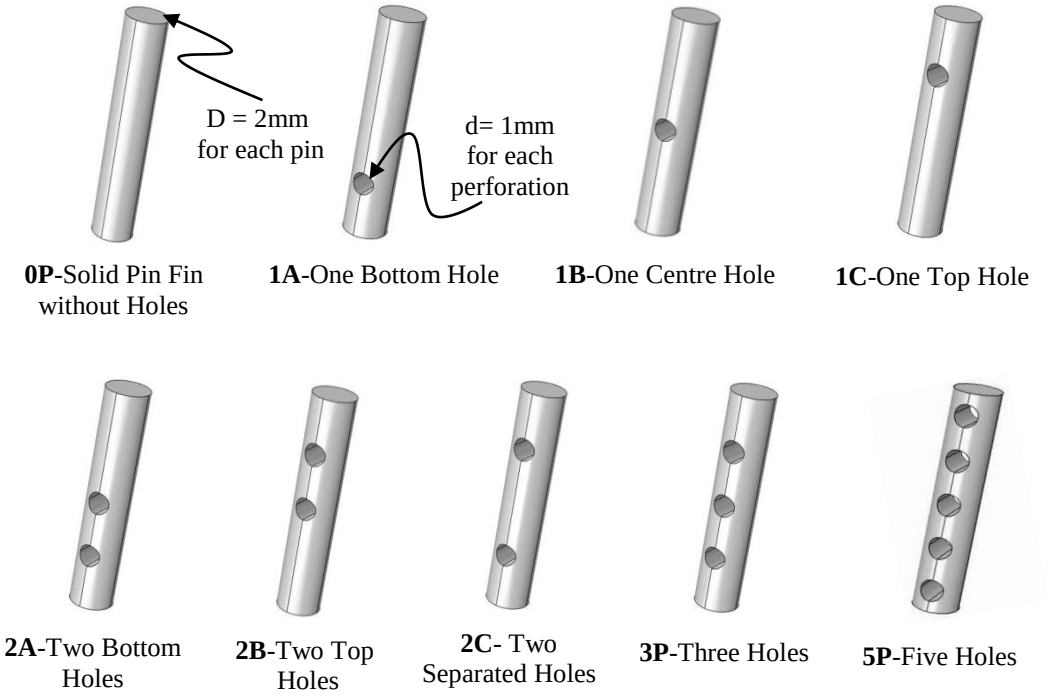

Figure 6.1: Solid and perforated pinned heat sink models

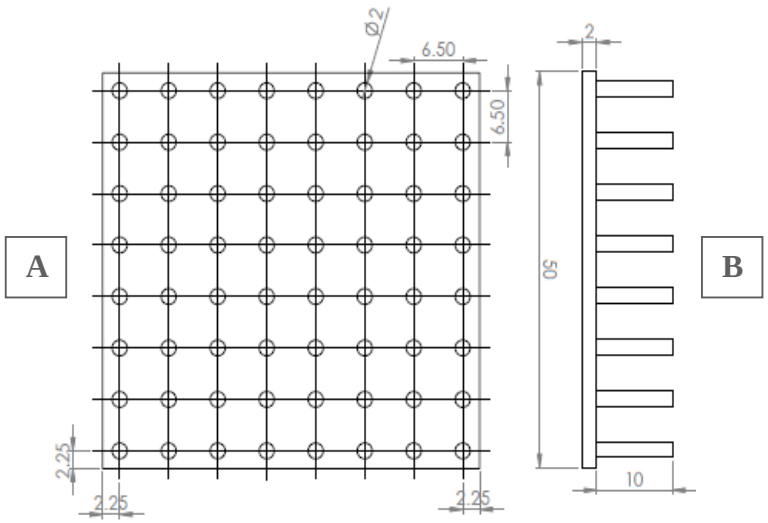

Figure 6.2: (A) Plan view and (B) Side view of the pin fin heat sink being analysed

The overall heat sink has a base of 50 mmx50mmx2mm with an 8x8 in-line array of 2mm diameter (D) and 10mm height pins (H) on a 6.5mm pitch in both directions (S_z, and S_x), Figure 6.2. The air flows past pin fins with 1mm diameter perforations. Different values of porosity are considered ($\phi = V_{hole}/V$) at 0, 0.05, 0.1, 0.15, and 0.25 for 0P, 1P, 2P, 3P, and 5P perforated pin heat sinks, where V_{hole}, and V are the perforation volume and solid pin volume, respectively. The entrance section is formed of a straight rectangular duct having 25mm (12.5D) as length, 10mm (5D) as height and 6.5mm (3.25D) as the width, where D is pin fin diameter. This section is located in front of the test section to ensure a hydrodynamically, fully developed turbulent flow.

The total surface area of these pinned heat sinks can be calculated as mentioned earlier in Chapter 2. Thus, the percentage of increase in this surface area regarding the solid pins (0P) is 5%, 10%, 15% and 25% for the perforated pins 1P, 2P, 3P and 5P models, respectively.

The thermal airflow through the perforated pinned heat sinks with thermal conductivity k=202W/m.K is analysed using CFD. The inlet air temperature is set to 25^{o}C and the inlet air velocity is varied between 6.5, 8, 10 and 12m/s, as per Yang & Peng (2009a), Yang & Peng (2009b), Kumar & Bartaria (2013), and Zhou & Catton (2011). This range of velocity leads to Reynolds numbers in the range 3500-6580 based on a length scale given by the hydraulic diameter of the duct $D_h = 2H.W/(H+W)$, where H and W are the height and width of the duct in which the heat sink is located.

6.3 Perforated Pins

The need to reduce our usage of the world's resources, combined with their actual reduction together with environmental considerations, makes it necessary to investigate ways of saving these resources and materials. Thus, there is clearly a need to develop heat sinks that use less energy, to achieve required rates of heat transfer (Sara et al., 2001).

Recently, many methods have been suggested to enhance the thermal characteristics of engineering devices. As mentioned in Chapter 1, one of those methods is the active cooling technique using traditional fins that cause heat transfer rate enhancement at the expense of increasing pressure drop (fan power). In other

words, the energy consumed will increase due to the extra friction of the fins. In addition to the frictional energy loss, the external fan power should be taken into account and this consumption of power should be reduced (Sara et al., 2001).

With respect to the literature review, the main problem of those traditional solid objects (fins, ribs, and blocks) is that dead thermal-flow zones (hot spot) will appear and develop in their wake, as shown in Figures 6.3A and 6.4A. In other words, airflow separation and low speed recirculating flow behind the solid objects are the main sources of poor cooling. This means that the heat transfer rates from their surfaces are not high enough, while the pressure drop is usually relatively high. Therefore, the thermo-flow characteristics of these solid objects are undesirable.

Many attempts have been proposed to overcome these adverse effects, depending on changing the pattern of fluid flow and geometric conditions. One of these attempts to enhance heat transfer rates and reduce fan power is to allow the airflow path to pass through these solid fins via perforations, as shown in Figures 6.3B, C and 6.4B, C. The perforated fins or the permeable fins will reduce the hot regions that usually appear behind solid fins by means of improving the fluid flow and demolishing vortexes zones, due to well-mixed fluid flow layers (Sara et al., 2001).

As a result, the main target of this study is to design and select the perforated pin fin heat sinks that will yield the maximum enhancement to the thermal characteristics with the minimum energy consumption.

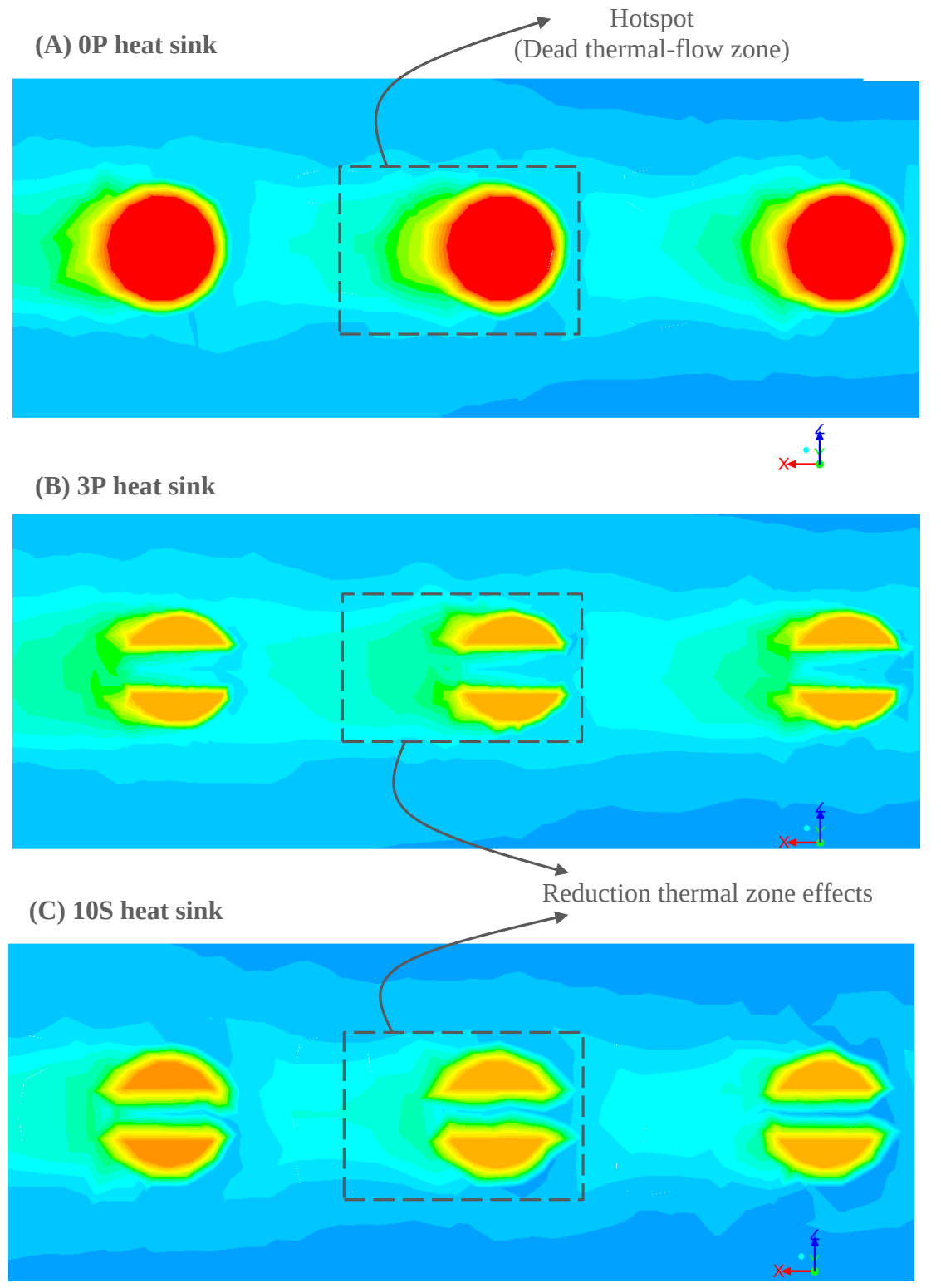

Figure 6.3: Plan views of hotspot zones through (A) solid 0P, (B) perforated 3P and (C) slotted 10S pinned heat sinks at *Re*=5393

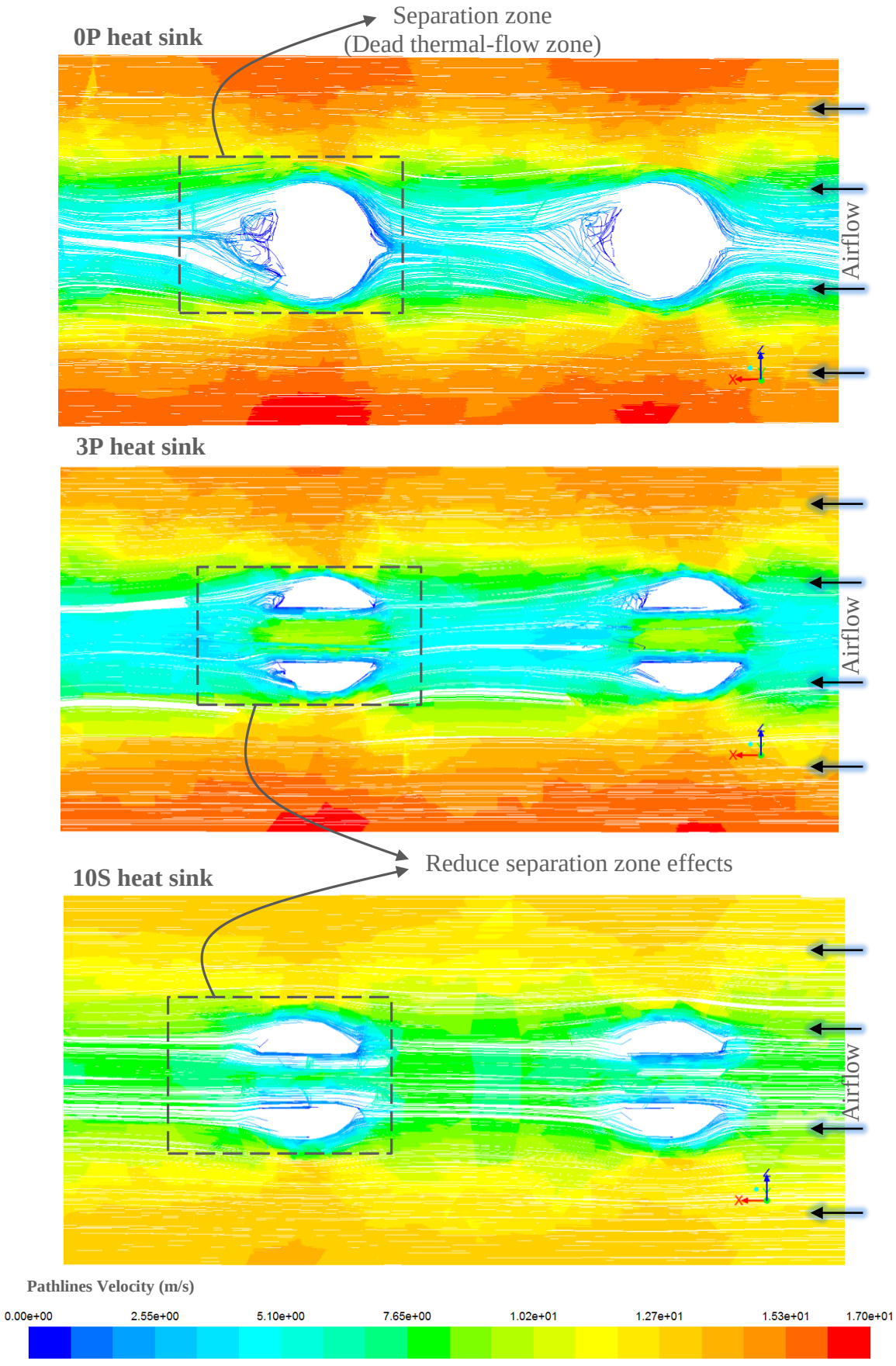

Figure 6.4: Plan views of airflow field through (A) solid 0P, (B) perforated 3P and (C) slotted 10S pinned heat sinks at *Re*=5393

6.4 Hydraulic Characteristics

Since the nature of the airflow passing through pin heat sinks is expected to enhance the thermal-hydraulic characteristics of these heat sinks, the airflow characteristics are explained first. The airflow behaviour, pressure drop (ΔP), fan power (P_{fan}), profit power factor (J), and pressure drag coefficient of perforated pinned (PPHSs) are explained and discussed in this section and compared with the solid PHS model.

6.4.1 Airflow Behaviour

The effects of heat sink models on airflow behaviour are presented in Figure 6.5 for the inlet air velocity 10m/s at Reynolds number = 5393 and 8x8 in-line array pins with streamwise and spanwise distances of 6.5mm.

The recirculation zones (vortices) behind the perforated pin fins will shrink compared with the solid pin fins due to effect of perforations. These vortices can be obvious behind the solid pin, while they are trivial in the case of perforated pin fins because the airflow passing through the perforations reduces the size of the vortices and the airflow path resembles a jet fluid flow. In addition, the size of the vortices will reduce more with increases in the number of perforations. Hence, the formed recirculation zones (wakes) are reduced in size in the case of perforated pin fin heat sinks. With regard to the solid pin fin heat sinks, however, the airflow separates from the frontal surface area of this pin.

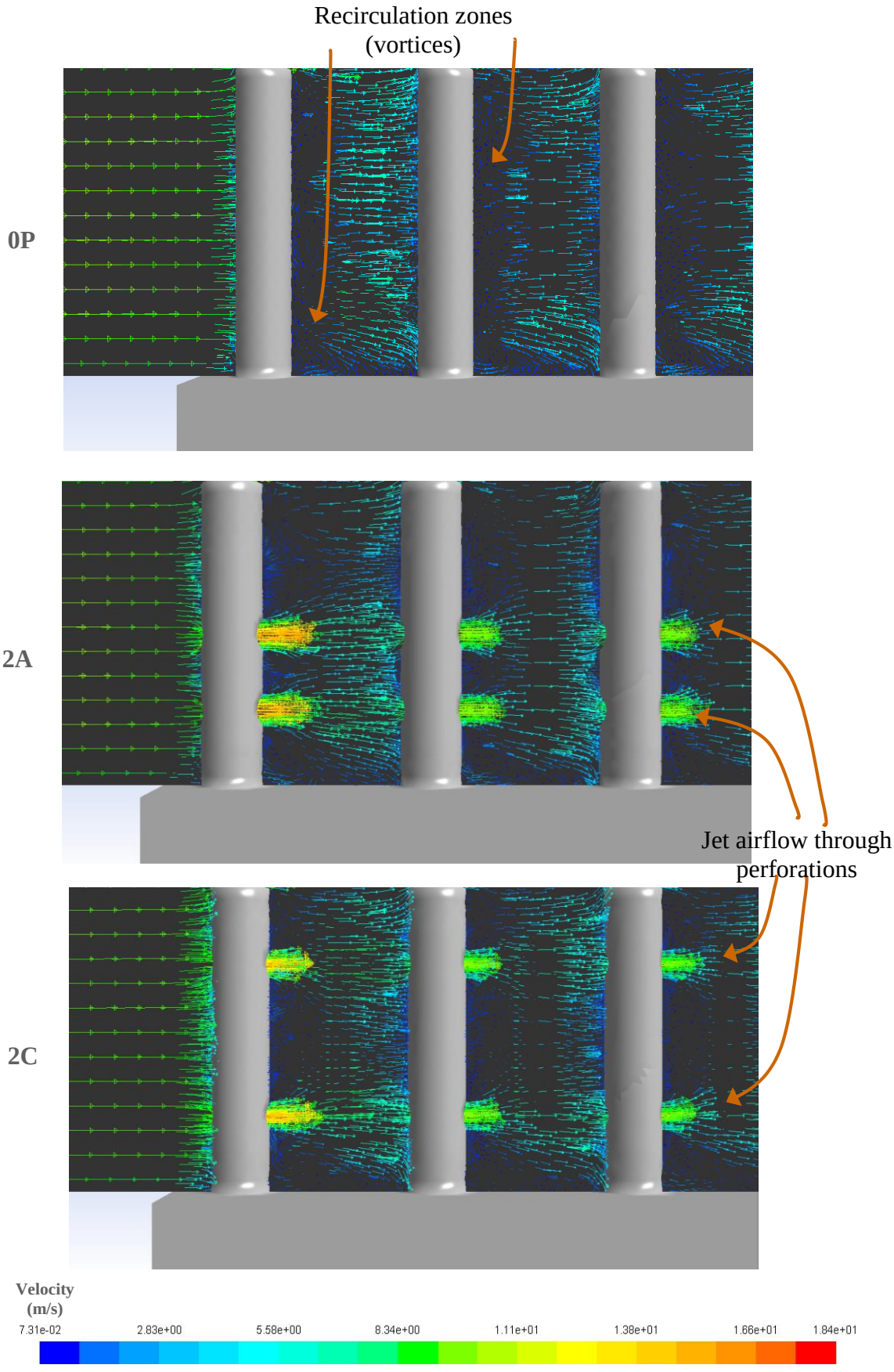

Figure 6.5: Comparison between predicted flow field in PFHSs with solid pin fins and for designs 2A and 2C with two perforations

6.4.2 Pressure Drop, Fan Power, Profit Power Factor, and Pressure Drag Coefficient

Figure 6.6 shows the effect of heat sink designs on the pressure drop (ΔP), fan power (P_{fan}), and profit power factor (J) for a range of Reynolds numbers from 3500 to 6580 relying on the inlet air velocities (6.5-12)m/s and 8x8 in-line array pins with longitudinal and transverse distances of 6.5mm.

The pressure drop over the perforated pins is lower compared with the solid pins (without perforations). The remarkable point here is that the solid pins' narrow airflow path is due to them being impermeable, which leads to more recirculation zones and airflow separation behind them. However, in the new designs, the airflow path will widen and will be a straighter flow leading to less separation behind the pins due to pin permeability. Therefore, the pressure drop and flow resistance of the perforated pins are less than for the solid pins, and that is in agreement with the findings of Yang et al. (2010).

For each of the pin designs (0P, 1A, 2A, 3P, and 5P) given, as shown in Figure 6.6, it is clear that the pressure drop reduces for pins that have more perforations since the amount of air passing through these perforations will be larger with increasing numbers of perforations. The pressure drop reductions of the 3P model with 3 perforations and 5P model with 5 perforations are approximately 9% and 14%, respectively, lower than that of the solid pin case.

The fan power pattern according to Figure 6.6 is similar to that for the pressure drop. This means that the amount of energy spent on a fan which is used to cool new heat sinks is lower than that for traditional solid pins at a given air velocity. However, the behaviour of the profit power factor is opposite to the pressure drop pattern, since this factor includes the amount of consumed fan power against the amount of heat applied at the heat sink base. The profit factor of perforated pins is the highest compared with the solid one. In addition, it increases as the number of perforations increases.

Commonly, as air velocity (Reynolds number) increases, the pressure drop and fan power increase as a result of the shear forces induced by increasing the Reynolds number, while the profit factor decreases.

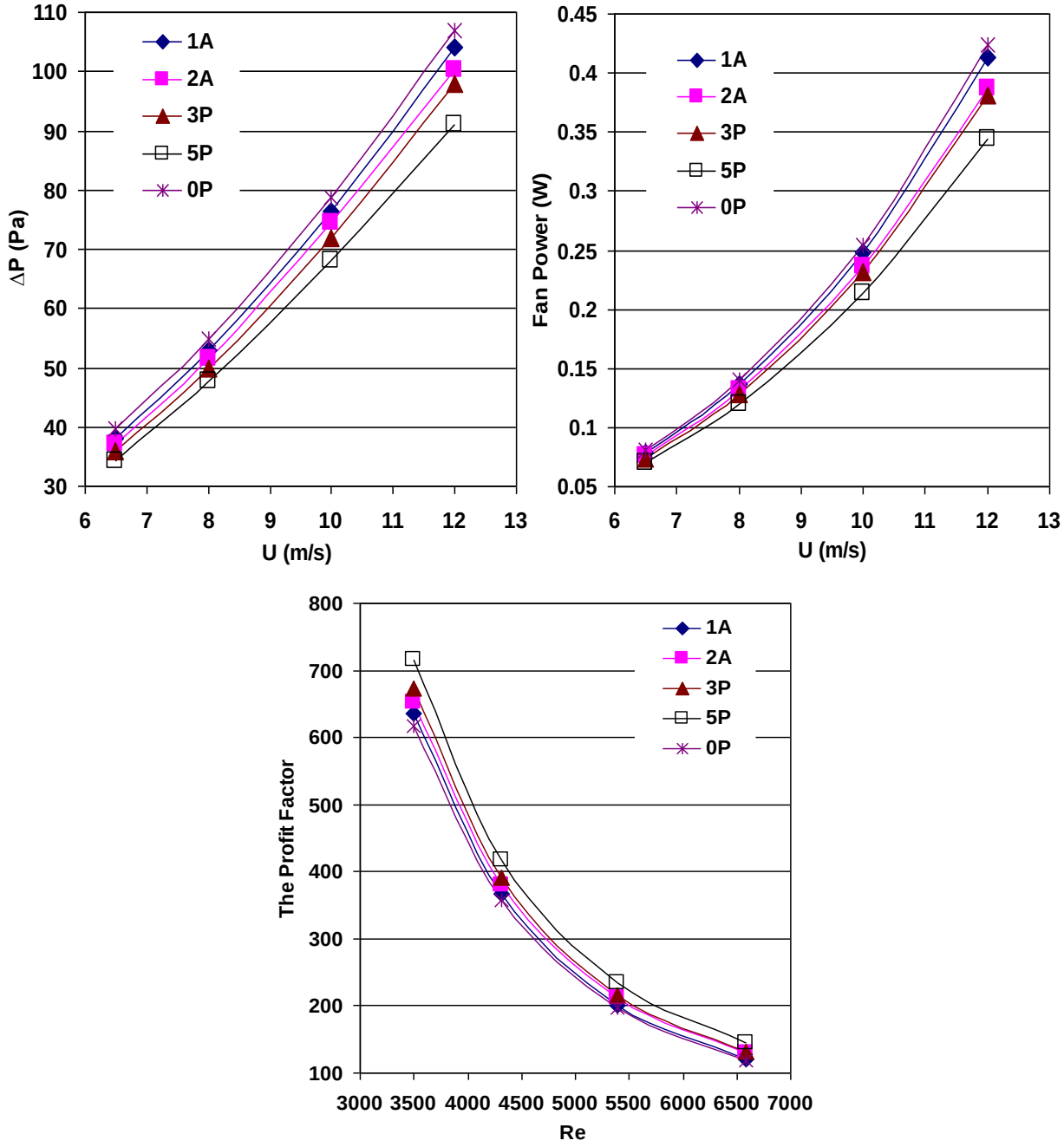

Figure 6.6: Effect of pin perforations and inlet velocity on pressure drop, fan power, and profit factor

The contour plots predict the variations in the local pressure through solid (0P), perforated (3P) and slotted (10S) pinned heat sinks within the airflow domain, as shown in Figure 6.7. The maximum local pressure is at the leading edge of heat sink and then it reduces gradually along the airflow direction in both cases to reach the minimum value at the end of heat sink due to the presence of pins (obstructions). The perforated 3P and slotted 10S pins show lower pressure penalty than the baseline case (0P) along the airflow direction due to perforations. These perforations allow a part of airflow to pass through them with less resistance to airflow compared to solid pins (0P). In the 0P case, local pressure varies between approximately 211Pa and –95.5Pa, whereas for the perforated pins 3P and 10S the corresponding local pressure varies from approximately 174Pa to –91Pa, and from 103Pa to –69Pa, respectively. The local pressure on the pins is also significantly lower, as indicated by the greater preponderance of blue regions on the perforated pins. Thus, the minimum local pressure is for slotted 10S pins due to its large perforations along pins.

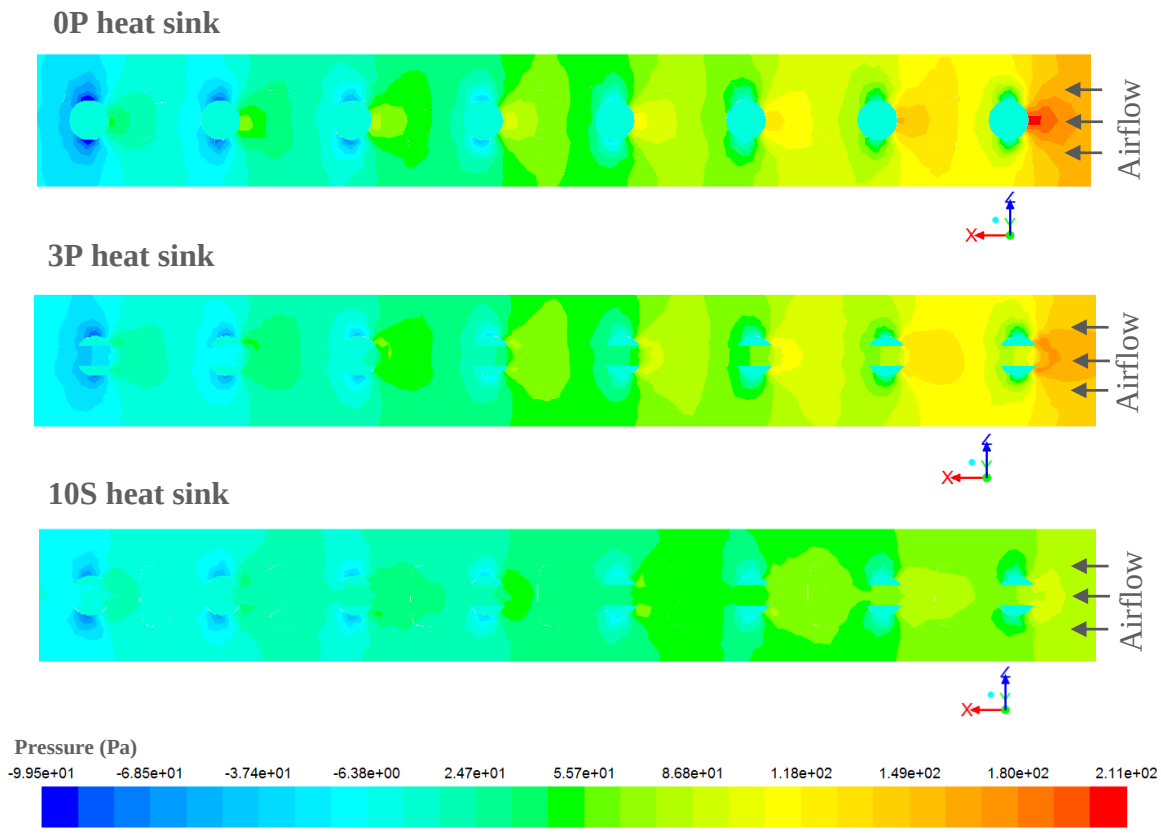

Figure 6.7: Plan views of pressure contour through solid 0P, perforated 3P and slotted 10S pinned heat sinks at *Re*=5393

Figure 6.8 shows the effect of the perforated pinned heat sink models on the pressure drag coefficient for a range of inlet velocities from 6.5m/s to 12m/s at Re=3500-6580.

The pattern of P_d shows the same behaviour for all perforated pin models. This coefficient is formed due to the resistance of pin fins to airflow path and is associated with a particular frontal surface area. With respect to the perforated pins, the pressure drag coefficient is the lowest and its value decreases with the addition of more perforations. The main reason for this is that the frontal surface area of the perforated pins is smaller than that of the solid pins (Ismail, 2013). In addition, the airflow passing through these perforations will be easier as there will be less resistance to airflow as the number of perforations increases. Accordingly, the pressure drag coefficient decreases as frontal area reduces with the presence of more perforations.

Overall, this factor decreases with increases in the inlet air velocity (Reynolds number) because the kinetic energy increases more than the pressure drop does.

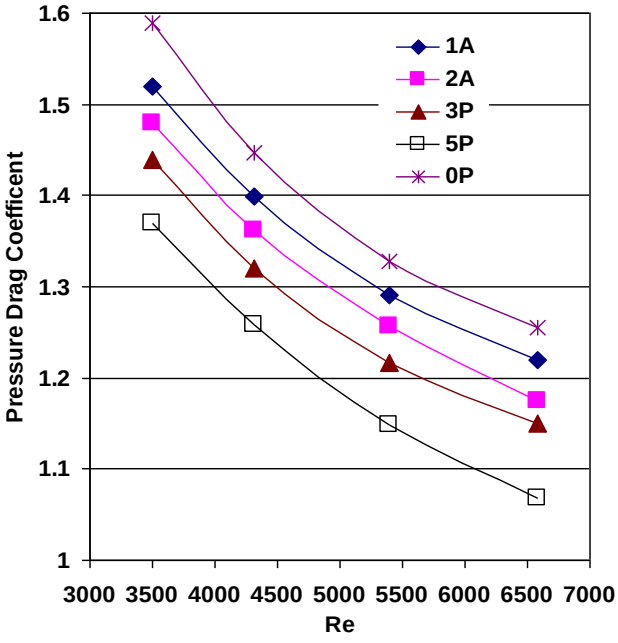

Figure 6.8: Variation of pressure drag coefficient with inlet air velocity for solid and different perforated pinned heat sink designs

6.4.3 Effect on Power Consumption

With regard to the fan power, energy that is consumed by the fan operation can be saved by reducing the pressure drop via the perforations. The reductions in fan power consumption are approximately 9% and 14% for the 3P model and 5P model PHSs, respectively, which is lower than that for the solid pin case. Thus, the profit factor of the 3P model and 5P model will increase by nearly 10% and 16%, respectively, compared to that for the solid pins. It is clear that these two factors, fan power and profit factor, have an opposite trend; in other words, as the fan power increases, the profit factor decreases. The solid pins require higher fan power consumption to overcome the pressure drop through the heat sinks compared with the perforated pins. This is because of the perforations, which enable air to easily pass through the perforated pin fins compared with the solid pin fins. In addition, when the number of perforations is increased, the fan power diminishes while the profit factor increases at a given air velocity.

Consequently, the first aim of this study, reducing the fan power (pressure drop) is achieved by using the perforated pinned heat sinks.

6.5 Heat Transfer Characteristics

The most important thermal characteristics of pinned heat sinks are illuminated and discussed in the following sections.

6.5.1 Average Nusselt Number

Figure 6.9 illustrates the effect of each of the given perforated pin designs on the Nusselt number for a range of Reynolds numbers from 3500 to 6580 relying on the inlet air velocities (6.5-12)m/s and 8×8 in-line pins with longitudinal distance of 6.5mm.

For the perforated pin fins, it is clear from Figure 6.9 that the highest percentage increase of Nu_T compared to the benchmark solid pin case is 11% when increasing the total surface area by 25% for pinned heat sink design 5P with 5 perforations.

Airflow separates from the surface of the solid pin heat sink and then dead-flow zones are generated behind these solid pins. Hence, the temperature is higher in

those zones and the Nu_T is lower for the solid pin fin compared with the perforated pins. In order to overcome the thermal dead zones, the perforations reduce the size of the high-temperature zones behind the solid pins. These perforations resemble a jet fluid flow, mixing fluid layers at the rear of the pin, and flow separation from the surface will be delayed because the airflow may not be strong enough to cause it. The improved heat transfer with perforations is due to the combined effects of increased surface area and localised enhancement near the perforations through the formation of localised air jets, as shown in Figure 6.5, and that is consistent with the finding of Sara et al. (2001), which attributed improved heat transfer with perforated rectangular blocks. As the number of perforations increases, the fluid mixing through the pin heat sink also increases, which leads to the pin temperature decreasing due to the multi-jet air and the Nu_T increases.

The results of the CFD simulation show that the Nu_T number is enhanced for higher air velocities (with increasing Reynolds number) for all pin fin heat sink designs due to the increases in the convective heat transfer.

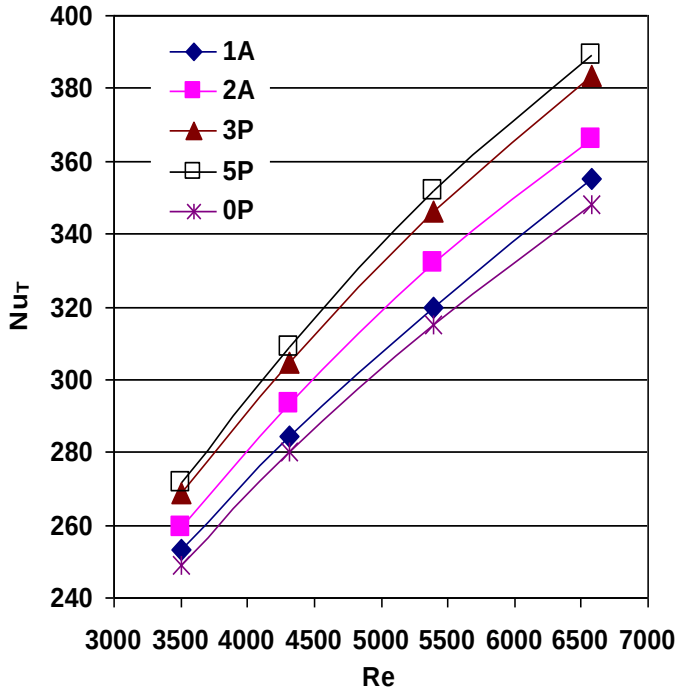

Figure 6.9: Effect of inlet velocity on Nu_T for the nine pin designs shown in Figure 6.1

Figure 6.10 shows the effect of the number of perforations and the total surface area (A_T) on the Nu_T number at U=10m/s, and shows clearly that the heat transfer rate increases monotonically with the number of perforations at a given air velocity.

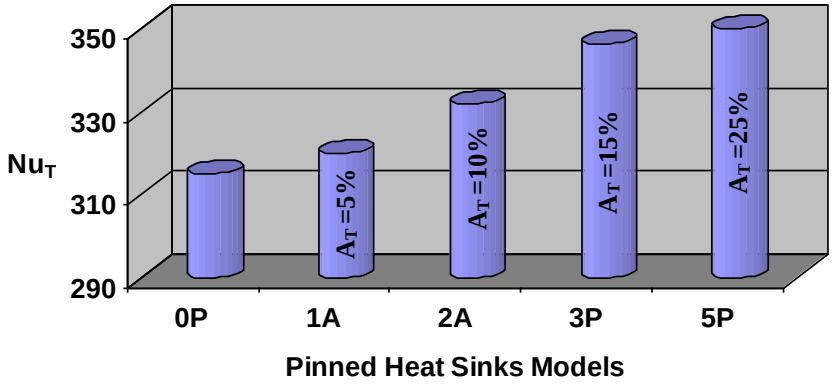

Figure 6.10: Effect of number of perforations on Nusselt number at 10m/s for the five pin designs

6.5.2 Thermal Management of PHSs

Figure 6.11 shows a more detailed investigation into the effect of pin fin perforations on the relationship between fan power and heat sink temperature (T_{case}) and the thermal resistance (R_{th}) through a system of 8×8 in-line pins separated longitudinally by a distance of 6.5mm for all perforated pin fin heat sink models.

For each of the pin designs (0P, 1A, 2A, 3P, and 5P) given, Figure 6.11 shows that the CPU temperature (T_{case}) and the thermal resistance (R_{th}) of the perforated pinned heat sinks are lower than those of the solid pin fins at a given fan power. In addition, these benefits increase as the number of perforations increases. For example, the enhancement in T_{case} for the 5P model is nearly 10% compared with the solid pins. In addition, the perforated pins exhibit more gradually reduced T_{case} with increasing inlet air velocity. It is from 73°C to 61°C for the 5P model with five perforations while from 81°C to 66°C for the solid pins. This confirms that the improved heat transfer rates of the perforated fins lead to the desirable effects of reducing both CPU temperature and thermal resistance of the heat sink. More generally, T_{case} and R_{th} reduce as the number of pin perforations increases at a constant pressure drop or fan power.

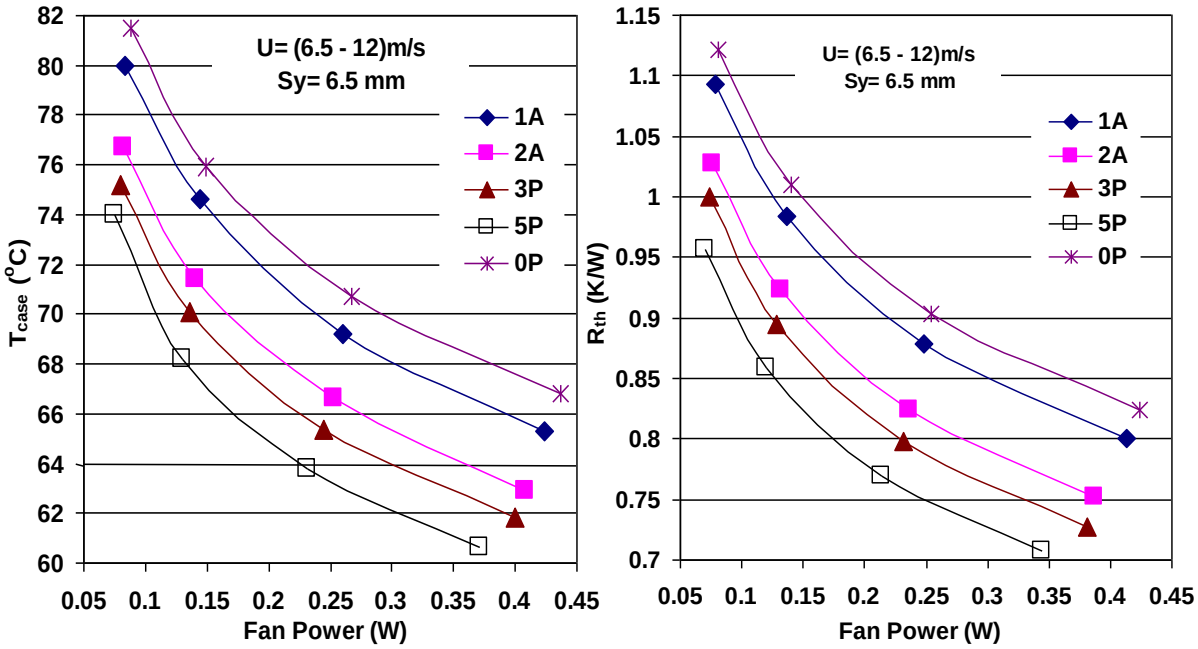

Figure 6.11: Effect of pin design and fan power on T_{case} and R_{th}

Figure 6.12 compares the surface temperature distribution of the solid pin heat sink (0P design) with those obtained on the pin fin with five perforations (5P) at Re=5393 (10m/s). In the former case, temperatures on the base plate vary between approximately 58.5°C and 71°C, whereas for the perforated pins the corresponding temperatures vary between approximately 49.5°C and 65.5°C. The temperatures on the pins are also significantly cooler, as indicated by the greater preponderance of blue regions on the perforated pins. This is because inlet airflow has more capacity to transfer heat along the heat sink due to its relative coolness, while the airflow temperature increases as it passes through the heat sink. Thus, the minimum temperature of the pins is at the tip of the first pin fins and the maximum temperature is at the bottom of the last pin fins.

Subsequently, the second aim of this study, reducing the CPU temperature by increasing the heat transfer rate, is achieved using the perforated pinned heat sinks (PPHSs). Since in an actual system, the two aims of the minimum T_{case} (maximum heat transfer rate) at the minimum fan power (less energy cost) are achieved for the 5P heat sink model in this study.

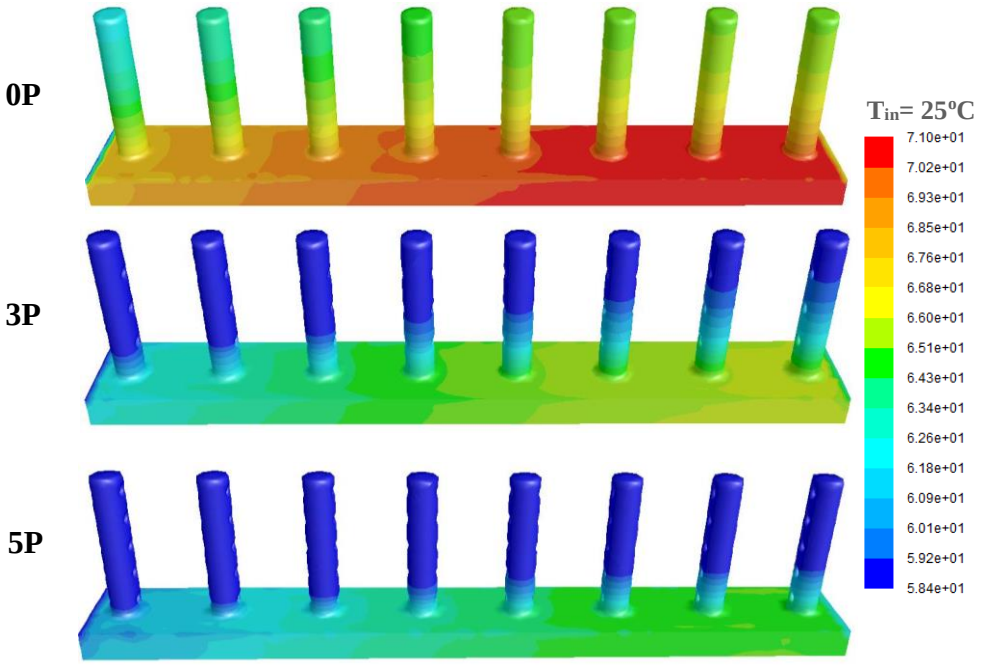

Figure 6.12: Temperature distribution through pinned heat sinks: 0P, 3P, and 5P models at *Re*=5393

6.6 Effect of Perforation Position

The effect of the position of the perforations is now investigated to obtain the optimum perforated pinned heat sink design based on pressure drop (ΔP), Nusselt number (Nu_T), and the CPU temperature (T_{case}).

For the cases with two perforations (2P) and three perforations (3P), the positions of the perforations do not have more influence on the pressure drop of the perforated pinned heat sink models. The 3P perforated pin models have the same lowest value of pressure drop, virtually 9% lower than that of the solid pin model (0P). Figure 6.13 shows the pressure drop variation over the pinned heat sinks when varying the perforations position in the 3P model at different inlet airflow values (6.5-12)m/s.

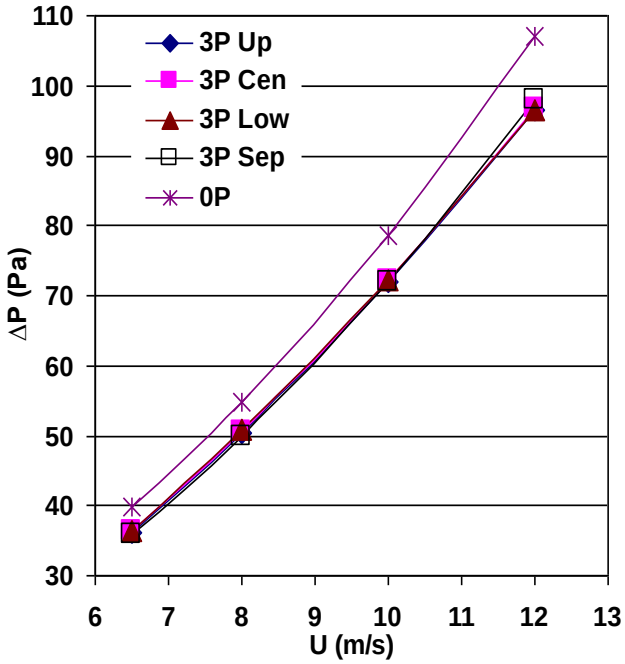

Figure 6.13: Effect of perforation positions on the pressure drop through heat sinks

The position of the perforations is far less influential on the Nu_T enhancement. The Nu_T of the perforated pin (2B) and (2C) models are slightly higher (typically up to 2% larger) than those for the perforated pin (2A) design, Figure 6.14. The CFD results indicate that this may be due to the larger air speeds through the perforations in cases 2B and 2C compared with case 2A, Figure 6.5. In addition, the conductive heat transfer of the 2A pin model may decreases, leading to reduction in the Nu_T due to removing part of the pin material from the bottom of these pins.

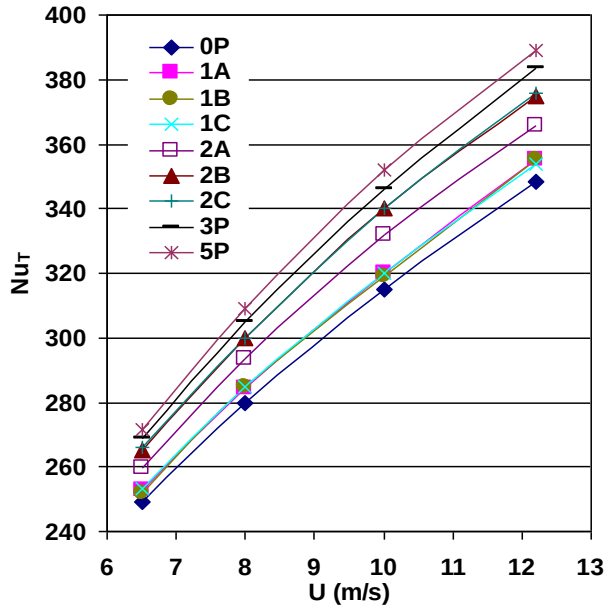

Figure 6.14: Effect of different perforation positions with inlet velocity on Nu_T for the nine pin designs shown in Figure 6.1

The vertical position of the three perforations model (3P) as shown in Figure 6.15, however, can enhance the overall characteristics to some extent. Figure 6.16 explains the effect of the position of the three perforations model (3P) on the Nusselt number with variation in the Reynolds number (3500-6580). The Nu_T of the perforated pin 3P-SEP model is nearly 2% larger than that of the other perforated pin designs. Since the distribution of perforations is uniform along the 3P-SEP pins model, the formation of localised air jets through the perforations is uniform along the pins, which enhances the convective heat transfer of the 3P-SEP pinned heat sinks. In the perforated pin 3P-LOW model that has perforations at the lower part of the pins, the Nu_T is lower compared to the other 3P models because of the decrease in vertical conductive heat transfer due to removing part of the material at the bottom of these pins.

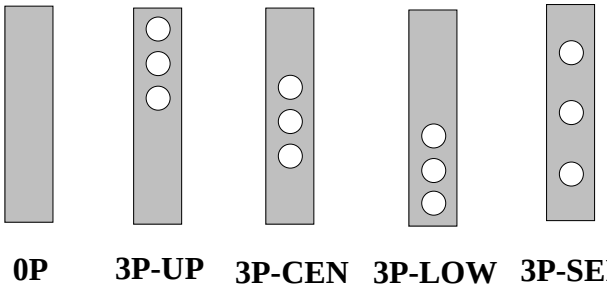

Figure 6.15: Different vertical positions of the three perforations model (3P)

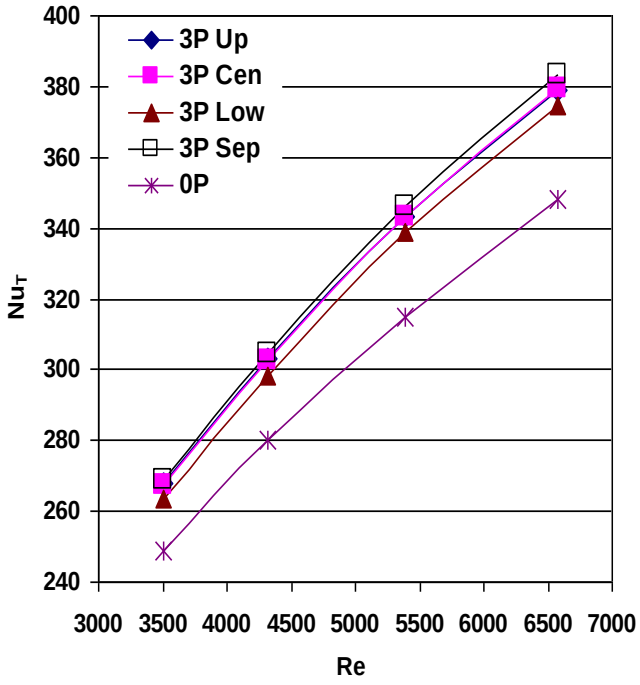

Figure 6.16: Variation of Nu_T with different perforation positions and *Re*

Figure 6.17 explains the effect of the position of the three perforations (3P) model on the CPU temperature with variation in the fan power. It is indicated that all 3P models have the lowest CPU temperature, except the 3P-LOW model. This is because, again, the conductive heat transfer is weak at the bottom of the 3P-LOW pin model due to the perforations.

It can be concluded that the pinned heat sink with the optimum overall performance is the perforated pin 3P-SEP (standard design), as shown in Figure 6.16, which was previously tested experimentally.

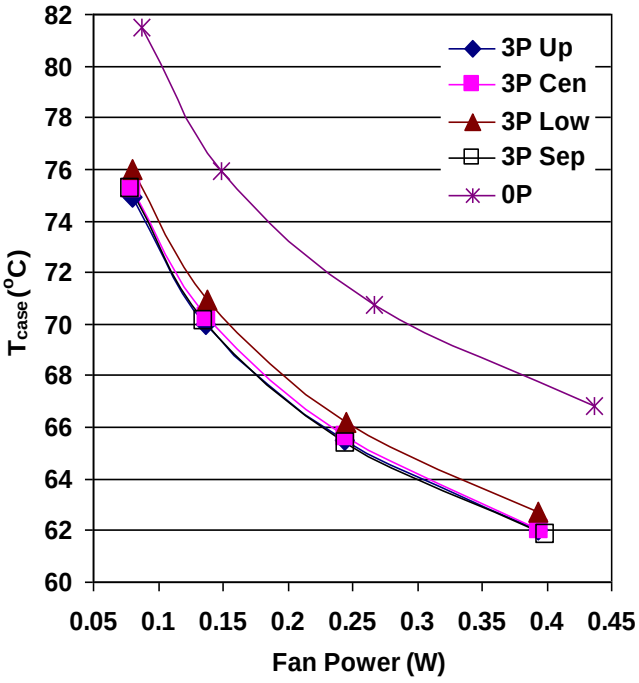

Figure 6.17: Comparisons of CPU temperature with the three perforations in different positions

From an existing heat sink, wire Electrical Discharge Machining can be used to directly cut into the circular perforations. This would also retain the high thermal conductivity between the pins and the base plate of a heat sink cast from a single block. The effect of the horizontal position of the three perforations models (3P) on the Nusselt number and pressure drop is considered in the current study. The positions of these perforations are shifted from the centre of the pin (0% moving percentage) to the outside of the pin (100% moving percentage) with respect to the centre solid pin (0P), as shown in Figure 6.18.

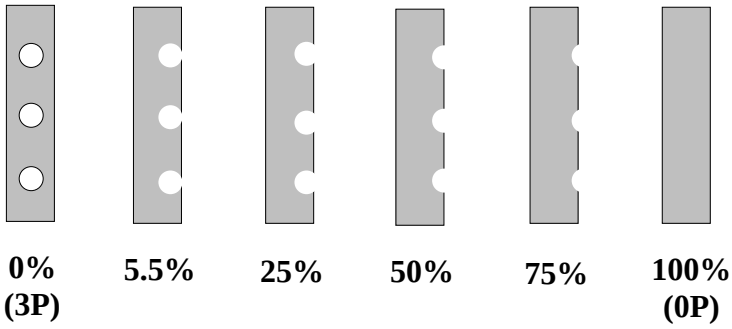

Figure 6.18: Horizontal movement percentage of perforations from the centre (0%) to the outside of the pins (100%)

Figures 6.19 and 6.20 show the variation of pressure drop and Nusselt number with different horizontal positions of the three perforations and inlet airflow at 10m/s. It is pointed out that, when the perforations are moved from the centre to the outside of the pin fin, the Nu_T diminishes while the pressure drop will increase. The pressure drop of those perforated pins will increase as the perforations are moved to the outside, owing to reducing the pins' porosity and increasing the airflow blockage passing over them. In addition, the maximum Nusselt number and minimum pressure drop are for perforations positioned at the centre of the pins in the 3P model. Although the moving percentage is 5.5%, 25%, 50%, and 75% caused an increase in surface area of the pins, the Nu_T of the pinned heat sink models reduces due to reduction of localised air jets near the perforations

This indicates that two important reasons resulted in enhancement of the overall characteristics' benefits. These benefits arise due to not only the increased surface area but also heat transfer enhancement near perforations through the formation of localised air jets.

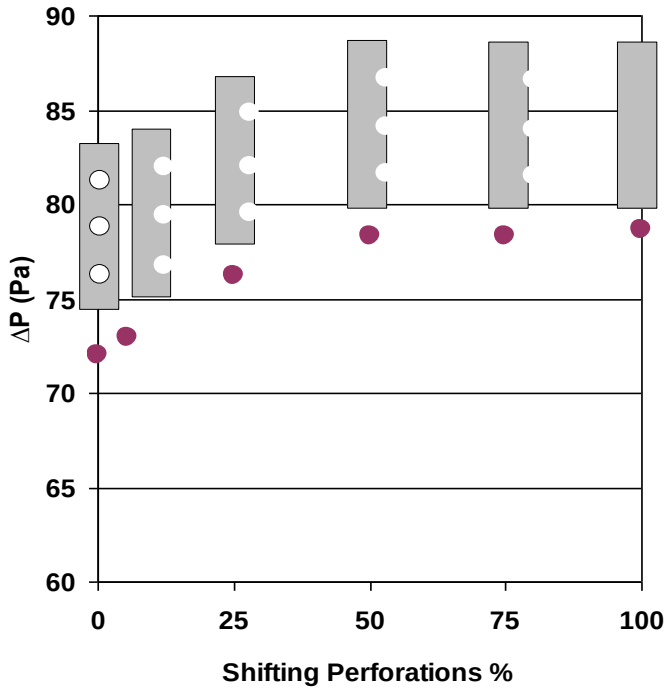

Figure 6.19: Pressure drop trend with different perforation positions of the 3P heat sink model

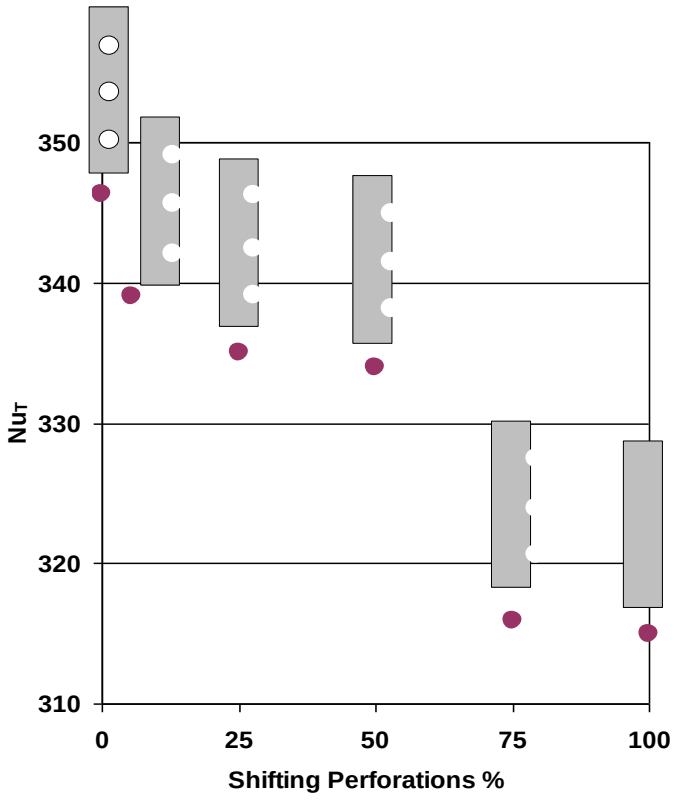

Figure 6.20: Comparisons of Nu_T with the three perforations in different positions

6.7 Effect of Pin Fins Arrangement

In this section, the effects of pin fins in in-line and staggered arrangement on fan power (P_{fan}) and CPU temperature (T_{case}) are described in detail for solid (0P) and perforated (3P) pinned heat sink designs. A total of 64 pin fins (8x8) separated longitudinally and transversely by a constant distance of 6.5mm in in-line and staggered arrays are tested for both models, heat sinks (0P) and (3P) models, with variation, whether to the inlet airflow (6.5-12)m/s or Reynolds number (3500-6580).

Figure 6.21 shows the pressure drop behaviour for both in-line and staggered arrays of the solid (0P) and perforated (3P) pinned heat sink models. It is found that the pressure drop of the staggered array is approximately 30% higher than the in-line array for both models. The main reason for this is that the staggered arrangement will increase the flow blockage in the airflow direction while the airflow relatively smoothly passes over the in-line array pinned heat sink.

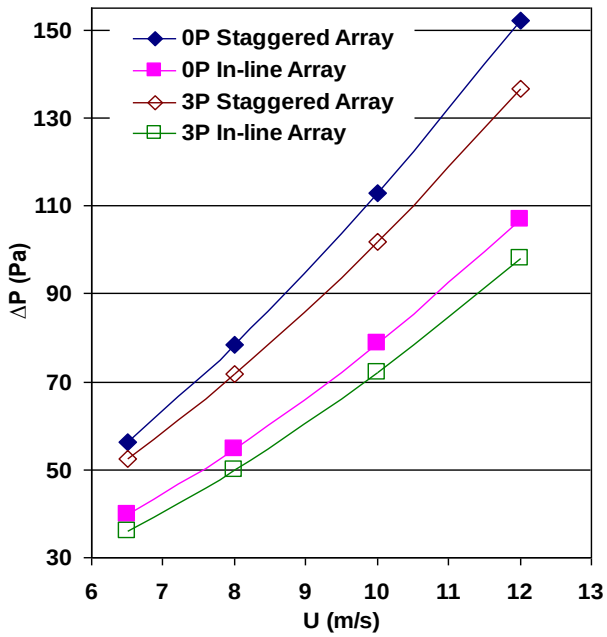

Figure 6.21: Effects of pin array on pressure drop with variation in Reynolds number for solid (0P) and perforated (3P) pinned HS models

With respect to thermal management, Figure 6.22 illustrates the effect of pin fins alignment on the CPU temperature of heat sinks with fan power for both solid and perforated pin fins. The staggered array for both solid (0P) and perforated (3P) models shows the lowest CPU temperature. The CPU temperature of the staggered array is approximately 10% and 12% lower with a high-fan power for both 0P and 3P heat sink designs, respectively, compared with the in-line pin array. This is because the staggered arrangement breaks down the thermal boundary layer and increases intermixing of airflow layers, with more surface heat transfer area in contact with the cooling air.

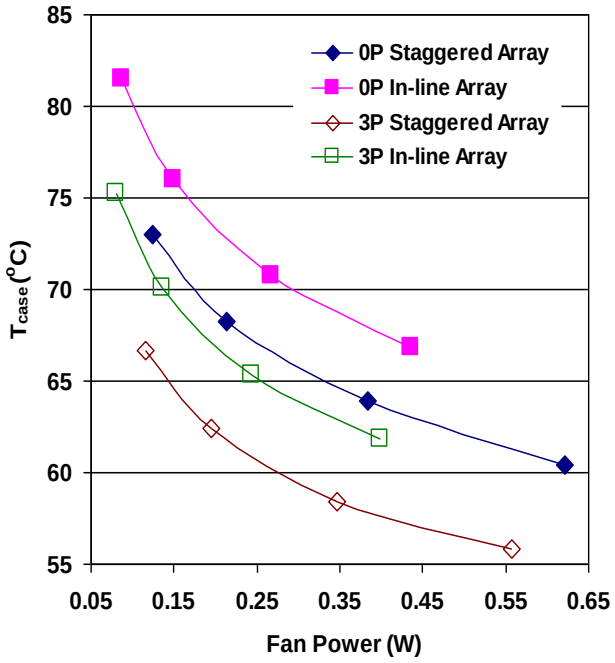

Figure 6.22: Effects of pin array on T_{case} and P_{fan} for solid (0P) and perforated (3P) pinned heat sink models

CFD predicts that the staggered pinned heat sinks for both solid and perforated pins provides lower T_{case} with higher fan power consumption than that of the in-line array under the same boundary conditions. These thermal and airflow characteristics findings are consistent with the recent conclusions of Yang et al. (2007), which considered improved heat transfer with different solid pin fin configurations at an in-line and staggered arrangement.

6.8 Effect of Square and Elliptic Perforation Shapes

Since perforated pin fins have been shown to enhance the thermofluid characteristics of heat sinks, the effect of perforation shape is now considered. The primary goal is to investigate the effect of square, elliptic and circular perforation configurations, as shown in Figure 6.23, on the cooling performance in electronic devices. Each pin has three perforations and the hydraulic diameter of each perforation is nearly 1mm, aligned in the direction of flow. Thus, the porosity is considered with different values ($\phi=V_{hole}/V$) at 0.15, 0.19, and 0.22 for circular, square, and elliptic perforations, respectively, where V_{hole} is the perforation volume and V is the solid pin volume. Hence, the percentage of increasing the total wetted surface area with respect to the solid pins (0P) is 15%, 18%, and 17% for the circular perforated (3CP), square perforated (3SP), and elliptic perforated (3EP) pinned heat sinks, respectively.

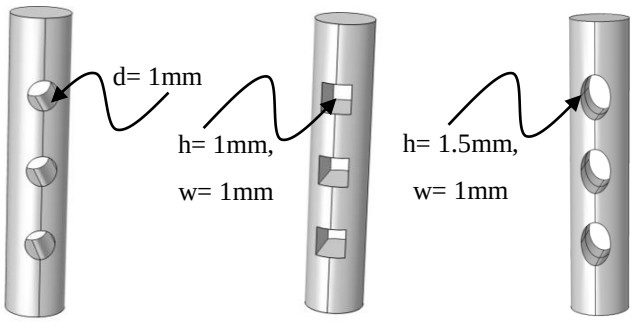

3PC- Circular Holes **3PS**- Square Holes **3PE**- Elliptic Holes

Figure 6.23: Circular, square, and elliptic perforated pinned heat sink models

The effects of perforation shape in a given PHS on thermal airflow characteristics as pressure drop (ΔP), Nusselt number (Nu_T), and CPU temperature (T_{case}) with various inlet air velocity (6.5-12)m/s are considered for 8×8 pins with a constant pin spacing of 6.5mm in either direction.

With respect to ΔP of these heat sinks, Figure 6.24, the elliptic perforated pins (3EP) have the lowest pressure drop and fan power, nearly 12%, compared with the equivalent solid pinned heat sink (0P) model, while the pressure drop reduction for square and circular perforations are 7% and 9%, respectively. This is because the void volume of the elliptic perforations is larger compared with the other perforation

configurations. This induces airflow to pass through the elliptic perforated pin fins, as it can do so easily and with less obstruction compared with the other perforated pin fins.

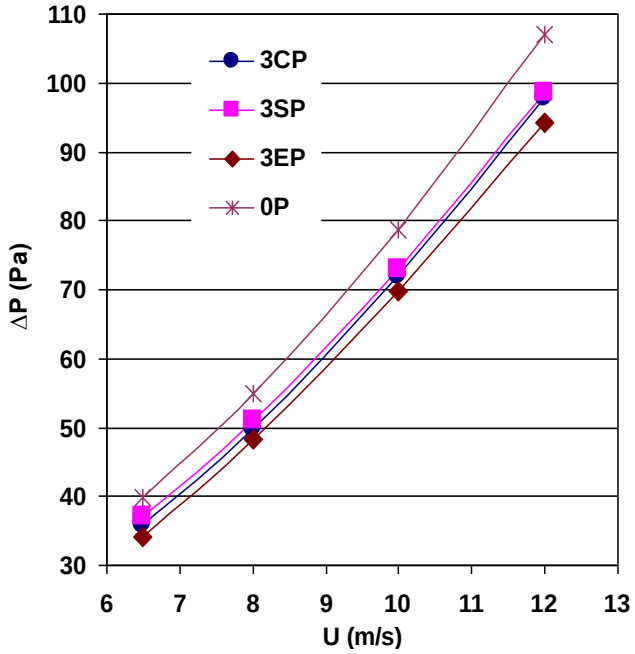

Figure 6.24: Effect of perforation shape on the pressure drop with various inlet air velocities

Figure 6.25 shows the effect of perforation shape on the Nusselt number (Nu_T) with various Reynolds numbers (3500-6580) and 8×8 pins at the constant longitudinal distance of 6.5mm.

The predicted data illustrates that the Nu_T of the perforated pin fins provides the maximum value. The Nu_T for the pins with circular perforations (3CP) is typically 9% superior to that of the other perforated pins. Furthermore, the square and elliptic perforation shapes have the same Nu_T enhancement percentage, approximately 4%, compared with the solid pins (0P) model. It may be that the major cause for this is that the circular perforations have the maximum mean jet-local air velocity through those perforations compared with other perforation shapes, as shown in Figure 6.27.

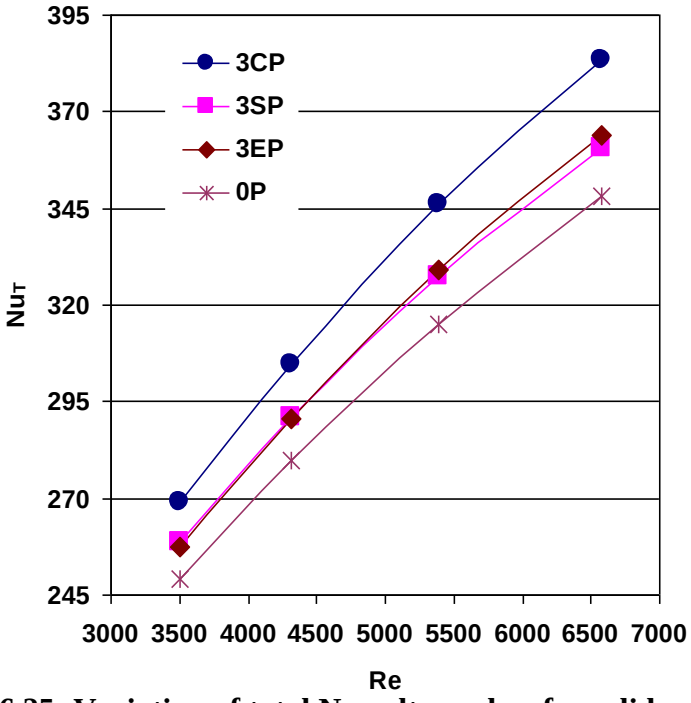

Figure 6.25: Variation of total Nusselt number for solid and different perforation shapes with various *Re*

Figure 6.26 shows that the T_{case} of the perforated pin fins are smaller than those of the solid pin fins at a given airflow. The data shows that the lowest T_{case} is typically 8% for the circular (3CP) model and 5% for both square (3SP) and elliptic (3EP) perforated pinned heat sinks compared to the solid pins system.

The principal cause for this relates to the effects of two parameters on the enhancement heat transfer rate: the mean jet-local air velocity through perforations (U_x) and total heat transfer surface area (A_T). Although the heat transfer surface area of the perforated pins increases for all pinned heat sink designs, jet-local air velocity through the perforations still plays an important role in enhancing the heat transfer rate. The maximum mean jet-local air velocity through the perforations of the perforated pins is for the circular perforations, as shown in Figure 6.27. In other words, cool air goes through circular perforations faster than through the other perforation shapes, so removing more heat created by CPU running. Thus, the circular perforated pins, 3CP model, have the lowest values of T_{case}.

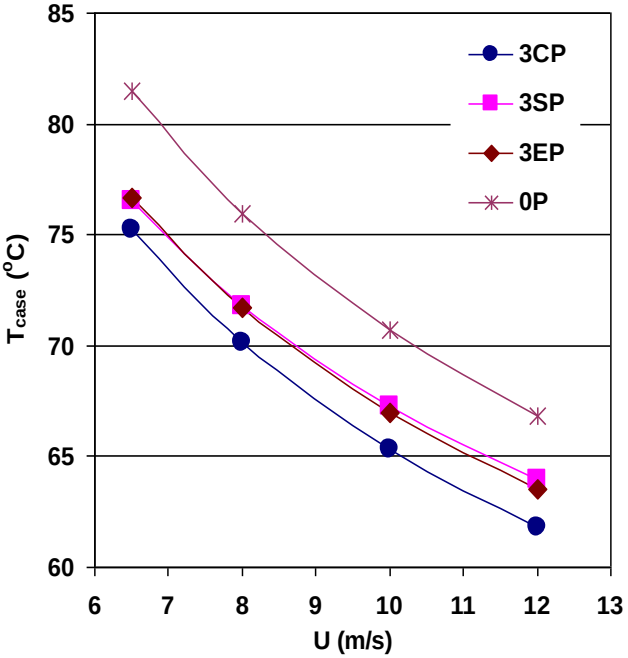

Figure 6.26: Variation of temperature with perforation shapes and various inlet air velocities

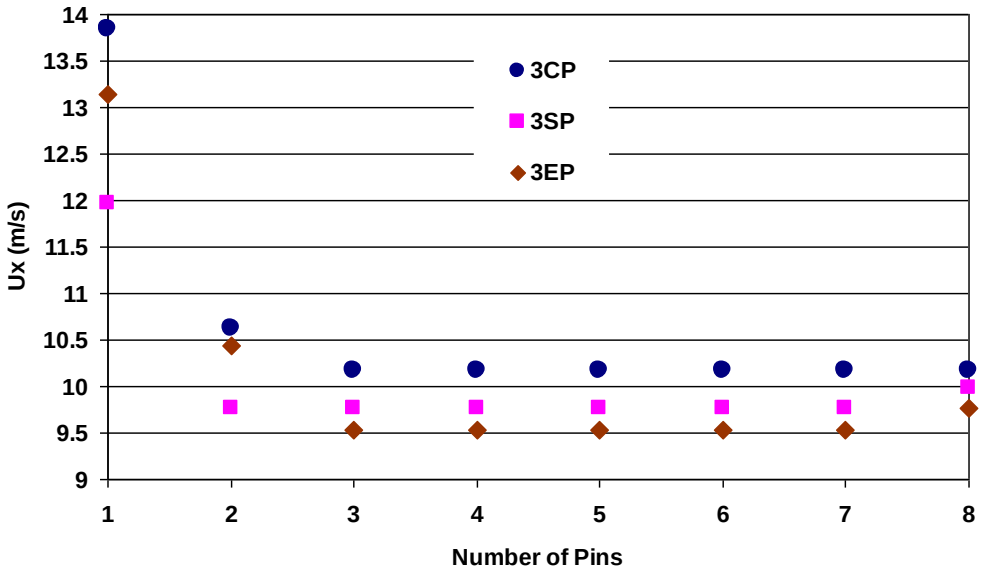

Figure 6.27: Variation in mean local air velocity through different perforation shapes of each pin

Figure 6.28 shows the comparison between the surface temperature distribution of the solid pin heat sink and those obtained on the circular (3CP), square (3SP), and elliptic (3EP) with inlet airflow at 10m/s (Re= 5393).

In the first model, 0P model, the temperatures variation on the base plate vary between approximately 58.5°C and 71°C, whereas for the perforated pins the corresponding lower temperatures vary between approximately 52°C and 66.5°C for

the circular perforations (3CP), 52.5ºC to 67ºC for the square perforations (3SP), and 53ºC to 67ºC for the elliptic perforations (3EP), as shown in Figure 6.28. This indicates that the heat transfer rate of the circular perforated pin fins (3CP) is the largest, as explained previously (Figure 6.27) that the maximum mean jet-local air velocity through the perforations of the perforated pins is for circular perforations. Thus, the temperatures on the pins are also significantly cooler: the lower temperature is at the tip of the first pin fins and the highest temperature is at the bottom of the last pin fins.

Consequently, the two aims of this study are achieved. The heat transfer rate is enhanced with less power consumption to drive air through the pin fins and that leads to the desirable benefits of reducing the CPU temperatures of the heat sink in the case of a fixed heat sink size.

Commonly, a compromise needs to be made between choosing either the elliptic perforated pins, 3EP, which provide the smallest pressure drop and fan power, or the circular perforated pins, 3CP, which have lowest CPU temperature and highest Nusselt number.

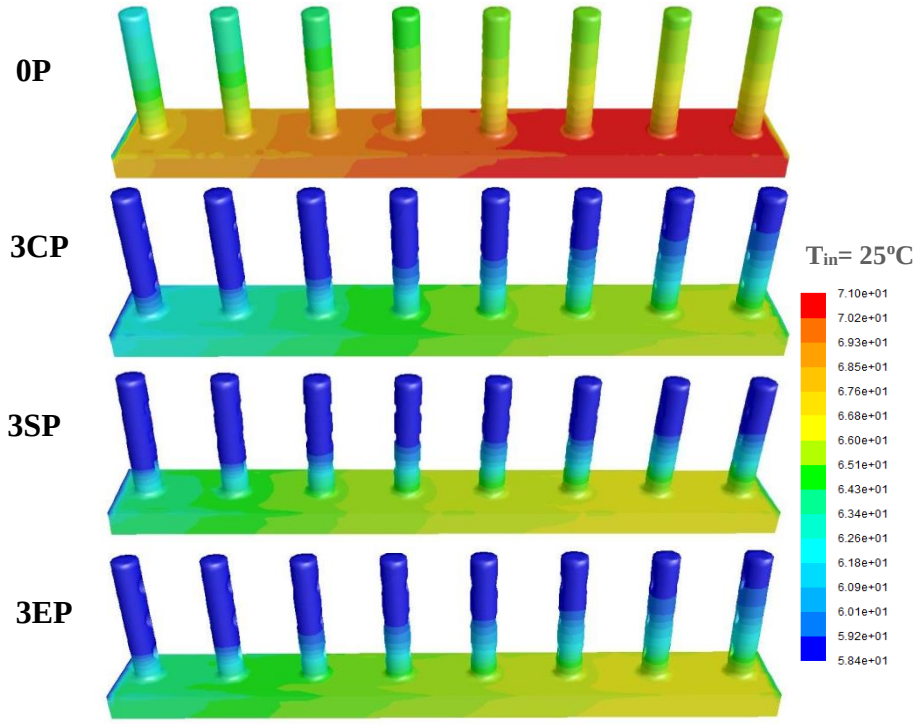

Figure 6.28: Temperature distribution through perforated pinned heat sinks: 0P, 3CP, 3SP, and 3EP models at *Re*=5393

6.9 Optimum Design of the Perforated Pinned Heat Sink (1P)

PHSs are designed to maintain the processors below critical temperatures for minimal fan power consumption input into the system. Recently, there have been a number of previous studies dealing with the optimum heat sink designs with solid plates and pins. For example, the multi-objective Genetic Algorithms was used to optimise plate fin geometries for total heat transfer and annual costs (Najafi et al., 2011). The pin density, pin size and air flow direction in PHSs were optimised by Shaukatullah et al. (1996), while Soodphakdee et al. (2001) optimised for the cross-sectional shape of solid pins heat sinks. This part deals with the optimisation of single perforated pins, 1P, as a function of perforation diameter, d, and perforation location, y, for PHSs with an 8x8 array of pins and a constant pin spacing of 6.5mm in either direction. The multi-objective optimisation problem studied here is to minimise T_{case} and P_{fan} for 0.5mm$\leq d \leq$1mm and 2mm$\leq y \leq$8mm for a constant air inlet velocity, U_{air}= 8m/s, since the above results may indicate that minimising T_{case} and minimising P_{fan} is in conflict with one another. Hence, the optimisation problem it can be defined as follows:

Objective function: minimise T_{case} & P_{fan}

Subject to: $0.5\text{mm} \leq d \leq 1\text{mm}$

$$2\text{ mm} \leq y \leq 8\text{mm}$$

Following a number of recent, successful optimisation studies, see e.g. Khatir et al. (2015), the response surface functions are built using the Moving Least Squares (MLS) method from a set of known values at specified Design of Experiments (DoE) points. The latter are obtained using an Optimal Latin Hypercube approach, that uses a permutation genetic algorithm to achieve a uniform points spread within the design space (Narayanan et al., 2007). In the present study, it is found that 30 DoE points are sufficient to provide accurate response surface functions for both T_{case} and P_{fan}. These 30 points are divided into 20 building points that are used to determine the response surface and 10 validation points that are utilised to validate the response surface, as shown in Figure 6.29. This approach distributes the two design variables in the spacing design uniformly within the lower and upper limits of each variable.

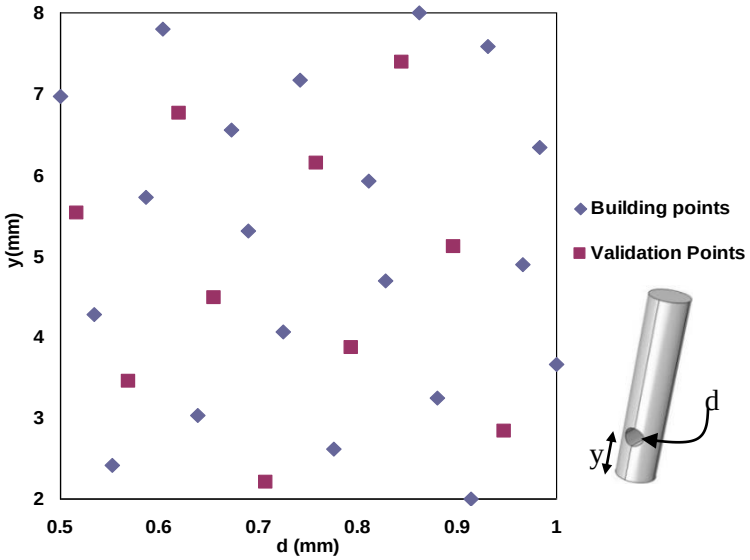

Figure 6.29: Distribution of design points in design variable space for the perforation diameter, *d* (mm) and the position of single perforations, *y* (mm)

The multi-objective function of CPU temperature and fan power of the pinned heat sink in terms of the design variables perforation diameter, *d* (mm) and the position of single perforations, *y* (mm) of the (1P) heat sink model are illuminated in Figures 6.30 and 6.31. The ten model validation points are used to optimise a closeness of fit parameter and the optimised MLS method has given very good agreement with merged DoE (R^2 value of 0.982 for DoE_m for T_{case} and P_{fan}). The optimum values of T_{case} and P_{fan} are on the design variable boundaries. This means that the design variables, perforation diameter (*d*) and the height of perforation (*y*) have an insignificant effect on the objective functions, T_{case} and P_{fan}; it is less than 1.5%. Therefore, a Pareto front does not required to find in this case, as will be explained in the next chapter, as a constrained optimisation design for the design variables of the single perforated pinned heat sink (1P) model. It is easy to find that a perforation diameter of 1mm for any perforation position is the optimum design for the single perforated pinned heat sink (1P) model to provide the lowest T_{case} and P_{fan} at 68.4°C and 0.2W, respectively, as inlet air velocity of 8m/s (Re=4315).

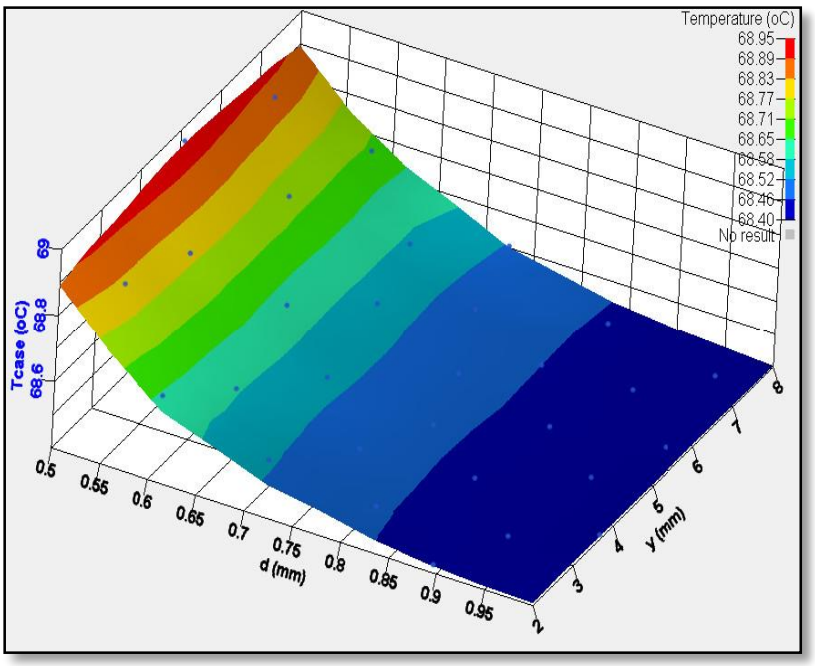

Figure 6.30: Response surface function of CPU temperature (T_{case}) of the single perforated pinned heat sink (1P) model

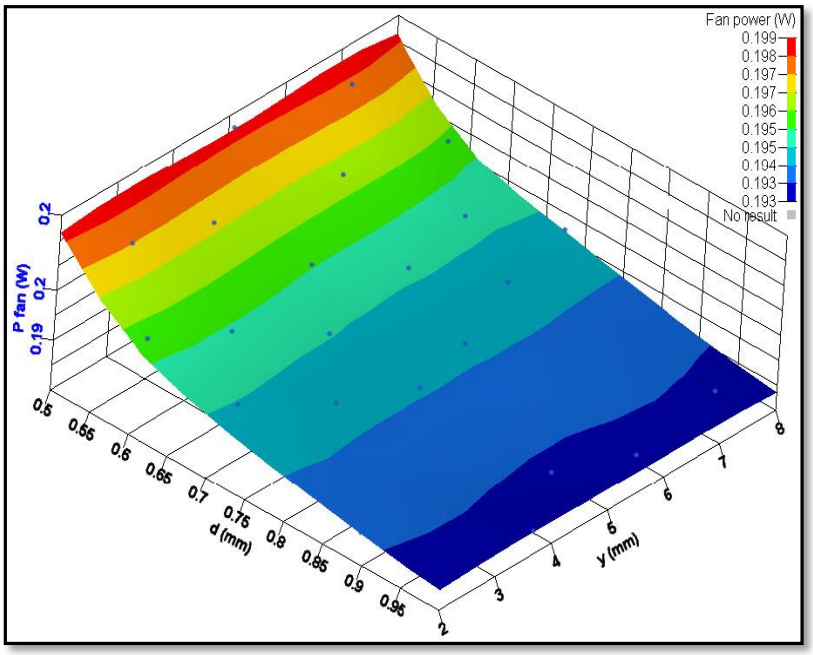

Figure 6.31: Response surface function of fan power (P_{fan}) of the single perforated pinned heat sink (1P) model

6.10 Conclusions

According to the predicted CFD data, perforated PHSs enhance thermal airflow characteristics compared to the equivalent solid PHSs. These benefits increase as the number of perforations increase. Evidently, pressure drop decreases monotonically and Nusselt number increases monotonically when increasing the number of perforations. For a given Reynolds number, the 5P pin fin design provides the peak heat transfer rate and the lowest pressure drop and fan power requirement. Thus, this cooling technique, using the perforated pins, can be regarded as an effective cooling method because it reduces processor temperatures and fan power, which is a key goal of the thermal management of electronics, as detailed in Table 6.1. CFD analysis indicates that the improvement in heat transfer is due to the combined effects of enhanced heat transfer near the perforations through the formation of localised air jets and increased total surface area (A_T).

Based on the pin arrangement, the staggered pinned heat sinks for both solid and perforated pins provide a lower CPU temperature than that of the in-line array, while more fan power is required to overcome the pressure drop through these pins compared with the in-line arrangement under the same boundary conditions, as shown in Table 6.2.

Regarding the perforation shape, it is shown that a compromise is needed between the choice of either the elliptic perforated pins, 3EP, which provide the smallest amount of pressure drop and fan power, or the circular perforated pins, 3CP, which have the lowest CPU temperature and the highest Nusselt number, Table 6.3.

The optimum design of the single perforated PHSs (1P) was investigated for two design variables: diameter of perforations (d, mm) and the locations of single perforations (y, mm). It was found that these design variables do not have a significant effect on the objective functions, T_{case} and P_{fan}; it is less than 1.5%.

Table 6.1: The enhancement of Nusselt number (*Nu*), and fan power (P_{fan}) of each 3P and 5P design compared with solid (0P) pins HSs

Heat Sink Designs \ Parametric Studies	↑ A_T	↑ Nu_T	↓ P_{fan} (W)	↓ T_{case} (°C)
Perforated Pins with Three Perforations (3P)	15%	9%	9%	8%
Perforated Pins with Five Perforations (5P)	25%	11%	14%	10%

Table 6.2: The reduction of CPU temperature (T_{case}), and the increasing fan power (P_{fan}) of staggered array compared with in-line array for solid (0P) and perforated (3P) pins HSs

Heat Sink Designs \ Parametric Studies	↑ P_{fan} (W)	↓ T_{case} (°C)
Staggered array of solid Pins (0P)	30%	10%
Staggered array of perforated Pins (3P)	30%	12%

Table 6.3: Enhancement of Nusselt number (*Nu*), fan power (P_{fan}), and CPU temperature (T_{case}) of different perforations shapes

Heat Sink Designs \ Parametric Studies	↑ A_T	↑ Nu_T	↓ P_{fan} (W)	↓ T_{case} (°C)
Circular Perforated Pins (3CP)	15%	9%	9%	8%
Square Perforated Pins (3SP)	18%	4%	7%	5%
Elliptic Perforated Pins (3EP)	17%	4%	12%	5%

Chapter Seven: The Benefits of Slotted and Notched PHSs

7.1 Introduction

This chapter further investigates the effects of different configurations of rectangular perforated pinned heat sinks on conjugate heat transfer and turbulent airflow. The two designs tested are slotted PHS (3S, 6S, 10S) designs with rectangular perforations removed from the centre of the pin (henceforth referred to as slotted pins, SPHSs) and notched PHS (2.5N, 5N, 7.5N) designs with rectangular notches removed from the top of the pin (notched pins, NPHSs), as shown in Figure 7.1. The CFD predictions of thermal airflows over those new heat sink designs are examined in detail in relation to heat transfer and airflow characteristics.

The main goal is to understand the airflow and thermal characteristics of these new heat sink designs to discover how these pin fin models can reduce the hot spots through the heat sink and enhance airflow along it compared with solid pin fins (0P). In addition, the optimum new PHSs design is considered to reduce the processor temperature for minimal fan power consumption input into the system.

7.2 Description of PHS Models

Six types of pinned heat sinks are examined for conjugate heat transfer and turbulent airflow, as shown in Figure 7.1. Three pin designs with rectangular perforations removed from the centre of the pin as slotted pins, SPHSs, and three with rectangular notches removed from the top of the pin as notched pins, NPHSs, are compared with baseline cases with solid pins and pins with circular perforations based on thermal airflows past PHSs as considered in previous chapters. Slotted and notched PHSs with 8×8 in-line arrangement of these pins are analysed comprehensively under the same computational domain and boundary conditions as previously mentioned. The pinned heat sink section comprises eight rows in the in-line array perpendicular to the flow direction (cross flow), as shown in Figure 7.2.

Generally, the heat sink layout has a base of 50mmx50mmx2mm with an 8x8 array of 2mm diameter (D) and 10mm height pins (H) on a 6.5mm pitch in both directions (S_x, S_z), as seen in Figure 7.2. Air flows past through the slots and notches of these pin fins. The slot height (h) is changed at 3mm (3S), 6mm (6S), and 10mm (10S) but the slot width (w) is kept constant at 1mm. The porosity is considered with different values ($\phi = V_{hole}/V$) where V_{hole} is the slot and the notch volume and V is solid pin volume, respectively. Hence, the porosity of these slotted pin fins is 0.185, 0.370, and 0.617 for the S3, S6, and S10 designs, respectively. With respect to the notched pin fins, the height of the notch (h) is varied at 2.5mm (2.5N), 5mm (5N), and 7.5mm (7.5N) whilst the notch width (w) is kept constant at 1mm. Thus, the porosity of these notched pins is 0.154, 0.308, 0.562, for N2.5, N5, N7.5 models, respectively.

Total wetted area (A_T) = Projected area + Total surface area contribution from the pin fins

For solid pin fins:

$$A_T = WL + N(\pi DH) \tag{7.1}$$

For slotted pin fins:

$$A_T = WL + N[(\pi DH) + (2hD) + (2wD) - (2hw)] \tag{7.2}$$

For notched pin fins:

$$A_T = WL + N[(\pi DH) + (2Dh) - (2wh)] \tag{7.3}$$

where *(W, L)* are the width and length of the base plate heat sink (50x50) mm, *(N)* the total number of fins (64 pins), *(H)* the height and *(D)* the diameter of the pins, which are 10mm and 2mm, respectively, *(h)* the height of the slot or notch, and *(w)* the width of the slot or notch (1mm). Therefore, the percentage of increase in the total surface area with respect to solid pins (0P) is 10%, 16%, and 20% for the slotted pins 3S, 6S, and 10S, respectively, while, for the notched pins 2.5N, 5N, and 7.5N, it is 5%, 10%, 15%, respectively.

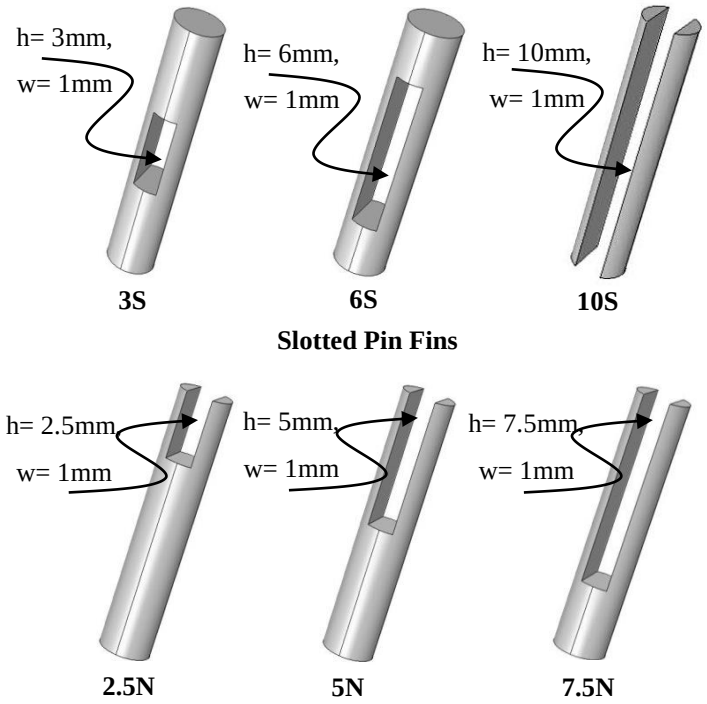

Figure 7.1: Slotted and notched pinned heat sink designs

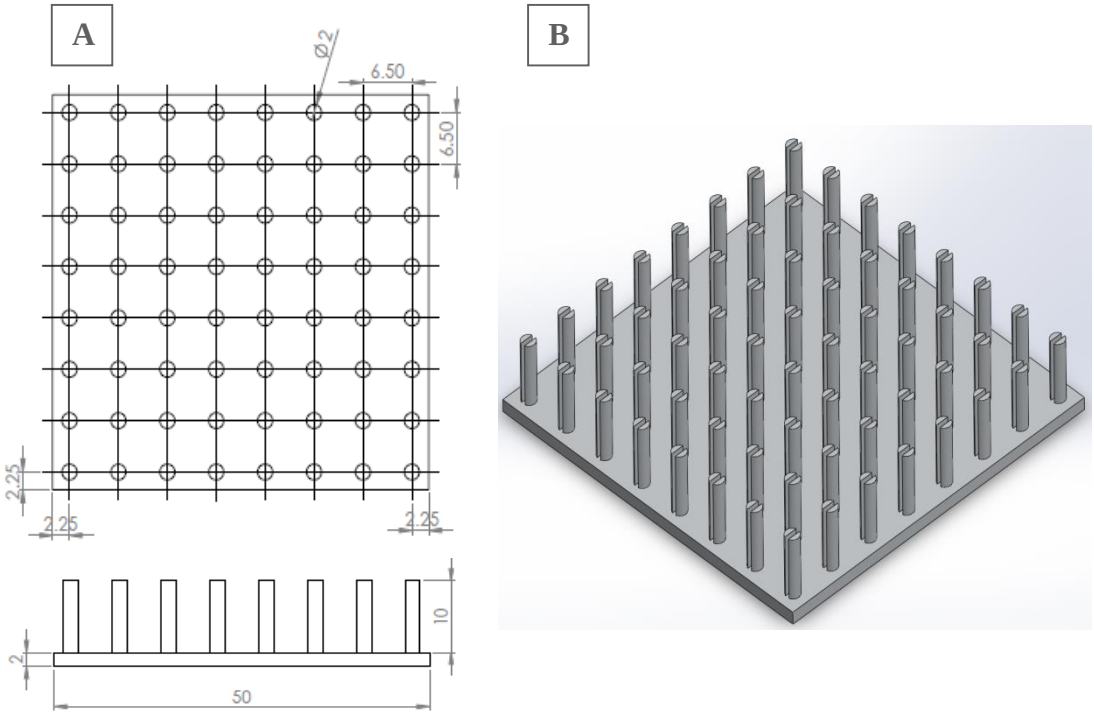

Figure 7.2: (A) Plan view and Side view (B) 3D of the notched pinned heat sink being analysed

7.3 Open Slotted and Notched Area

The behaviour of the airflow passing through the pin fin heat sinks is described firstly. The effects of the new heat sink models on airflow are presented in Figure 7.3 for inlet air velocity 10m/s at Reynolds number =5393 and 8 pins with a longitudinal distance of 6.5mm.

As mentioned earlier, in the perforated pins section (Chapter 6), the dead thermal-flow zones will appear and develop just in the wake of solid objects such as fins, ribs, and blocks. The airflow separates from the surface of these objects and the speed of recirculating flow behind solid objects is low, (see section 6.3, as shown in Figure 6.3A and Figure 6.4A). This causes the heat transfer rate from these zones to reduce and the pressure drop through these solid objects will usually be high. Thus, to avoid this adverse effect, many attempts have been proposed depending on changing the fluid flow pattern and geometric conditions (Sara et al., 2001). One of these attempts to enhance thermal and fluid flow characteristics is allowing the flow to pass through the solid fins by replacing them with slotted or notched fins. The slotted or notched pin fins will reduce the hot spots that typically occur behind solid fins by means of improving the airflow and vanishing vortexes zones, resulting in a well-mixed layer of fluid flow, (see section 6.3, as shown in Figure 6.3B, C and Figure 7.4B, C). Hence, the thermal characteristics and pressure drop characteristics are enhanced in this case (Sara et al., 2001).

Consequently, a detailed investigation of the thermal and hydraulic characteristics of slotted and notched PHSs is now presented.

7.4 Hydraulic Characteristics

The air fluid flow behaviour, pressure drop (ΔP), fan power (P_{fan}), profit power factor (J), and pressure drag coefficient of the slotted and notched pin fins HSs are discussed in this section.

7.4.1 Airflow Behaviour

Enhancement of thermal characteristics and reduction in the fan power of heat sinks are affected by airflow behaviour across pin fin heat sinks. Thus, it is important to discuss this parameter study in this work first (Sara et al., 2001). The effects of the new heat sink models on airflow behaviour are shown in Figure7.3 for the air inlet velocity 10m/s at Reynolds number (5393).

Similarly to the perforated pin fin heat sinks, the recirculation zones behind the slotted and notched pin fins will gradually reduce in size with the expansion of the open slotted and notched area (increase the height of the slot and notch), as shown in Figure 7.3. These vortices can be seen behind the solid pin heat sink (0P) model while they will be less significant in the slotted and notched pin fins cases. The main reason for this is that the airflow passing through the open slotted and notched area is straighter and so the vortex zones will be reduced. Hence, the recirculation zones (wakes) are eliminated for the slotted and notched pin fin heat sinks, while the airflow attacks and interacts with the frontal surface area of the solid pin and so air separation will occur.

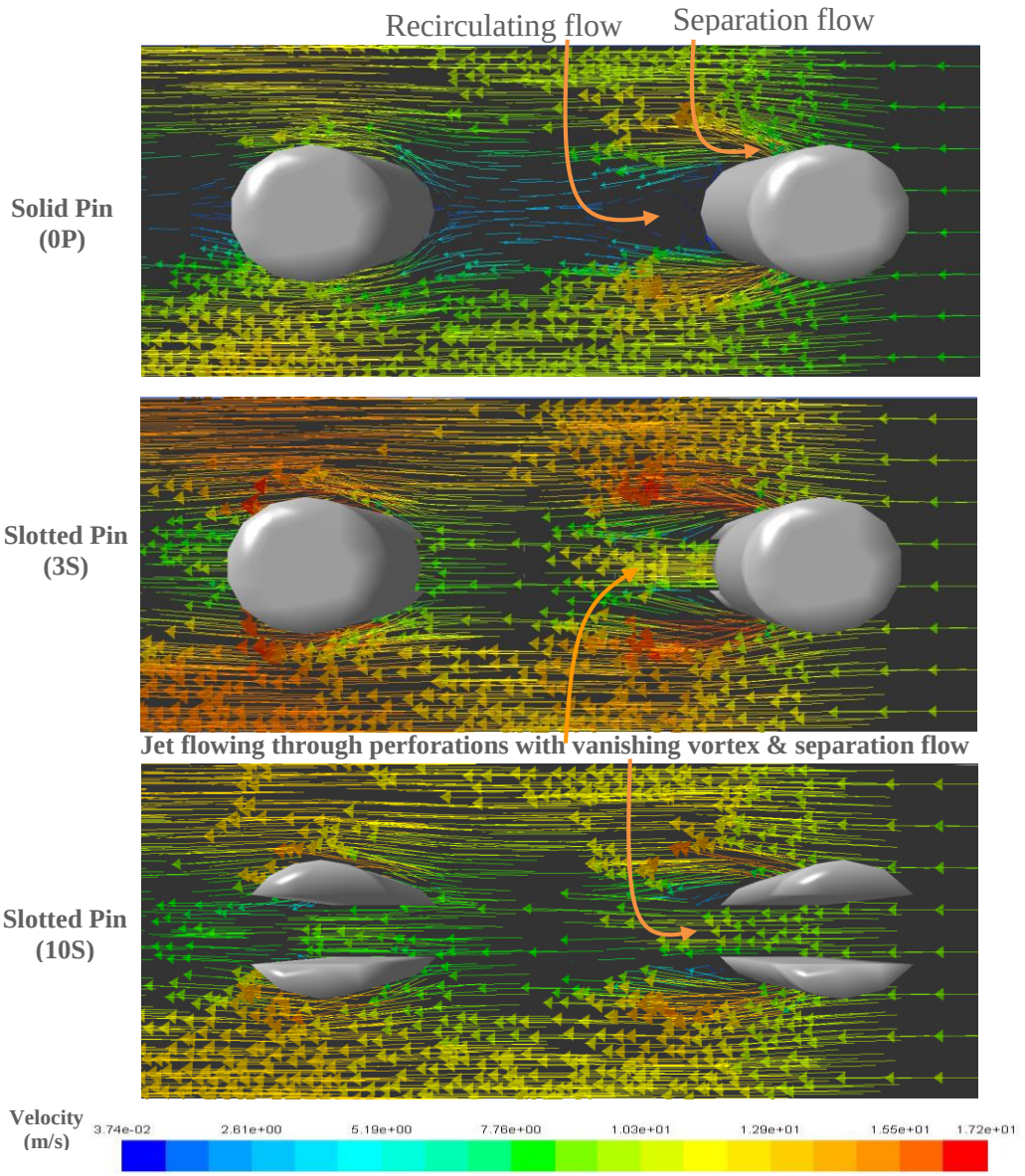

Figure 7.3 Comparison between predicted flow field in PFHSs with solid pin fins 0P and for designs 3S and 10S

7.4.2 Pressure Drop, Fan Power, Profit Power Factor, and Pressure Drag Coefficient

Figures 7.4, 7.5, and 7.6 illustrate the effects of the slotted and notched pin fin heat sink designs on the pressure drop, fan power, and profit power factor for a range of Reynolds numbers (3500-6580) with the inlet air velocities ranging from 6.5m/s to 12m/s.

It can be seen from these figures that the pressure drop of the slotted and notched pins is smaller than that of the benchmark PHS. The main cause of this is that the airflow path across the solid pins is narrow and wavy, which results in more recirculation zones and greater separation of airflow behind the solid pins, as indicated previously. In the case of the new designs, however, these rectangular perforations enhance the mixing of fluid at the rear of the pin, and flow separation from the surface will be delayed. Thus, there is less pressure drop and flow resistance for the slotted and notched pins than for the solid pins (Yang et al., 2010).

For slotted (3S, 6S, 10S) and notched (2.5N, 5N, 7.5N) pin heat sinks, Figures 7.4 and 7.5, the pressure drop and fan power reduction is monotonically higher when increasing the height of the slot or notch due to these rectangular perforations. The highest reduction is nearly 40% for the 10S slotted pin model and approximately 33% for the 7.5N notched pin in relation to the solid pin fin (0P) model.

Figure 7.5 shows that the reduction in fan power has the same pattern of pressure drop and they increase as the Reynolds number increases. This indicates that the slotted and notched pin fins will save more energy that is consumed via the fan than will the solid fins.

As indicated previously, the profit power factor compares the amount of consumed fan power against the applied amount of heat flux at the heat sink base. The profit factor of the slotted and notched pins is highest compared with the solid one, Figure 7.6.

For more information about local pressure drop along pinned heat sinks, see section 6.4.2.

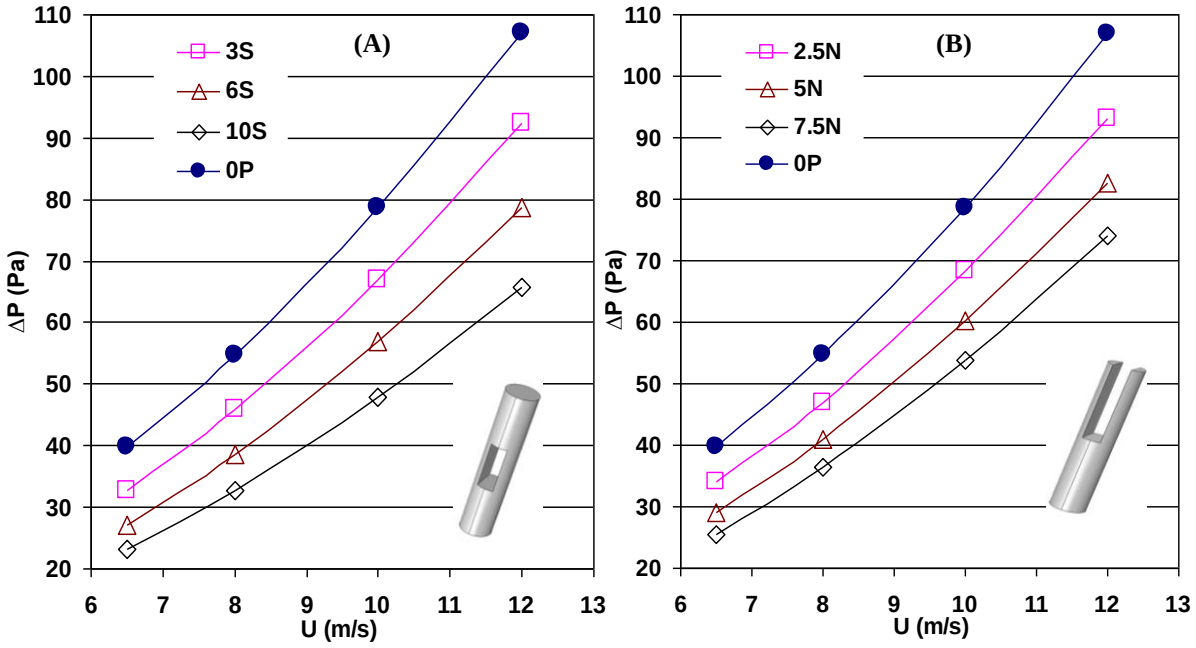

Figure 7.4 Effect of (A) slotted and (B) notched pins on pressure drop with variation in airflow speed

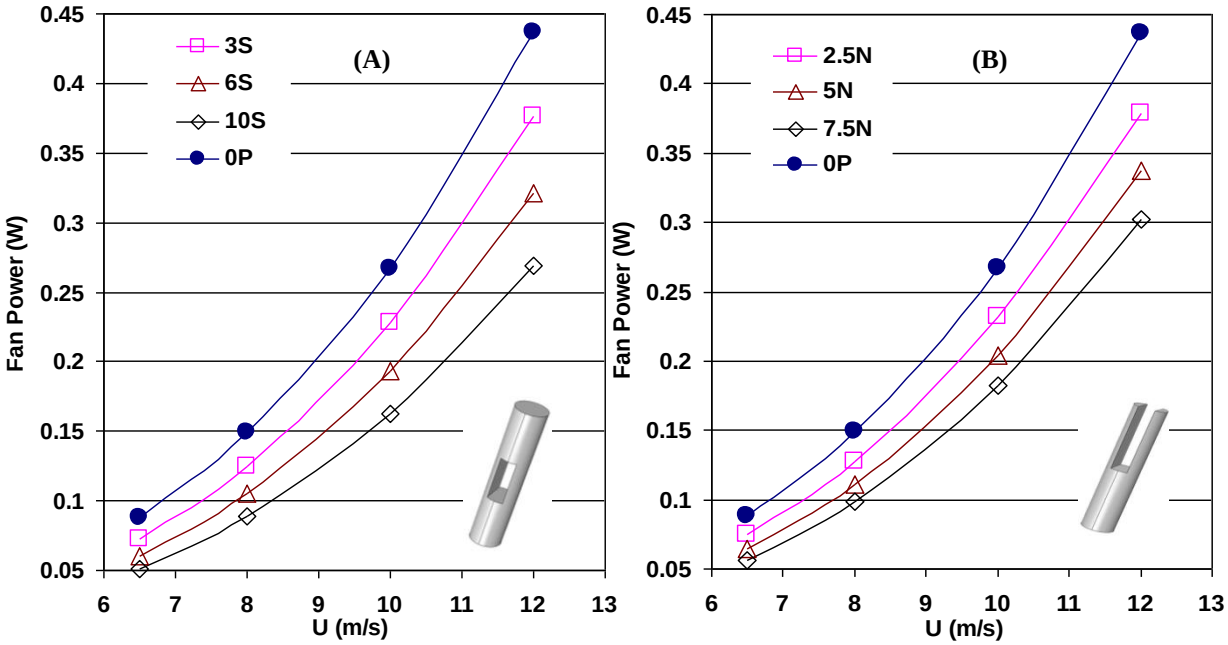

Figure 7.5: Effect of (A) slotted and (B) notched pins on fan power as a function of airflow speed

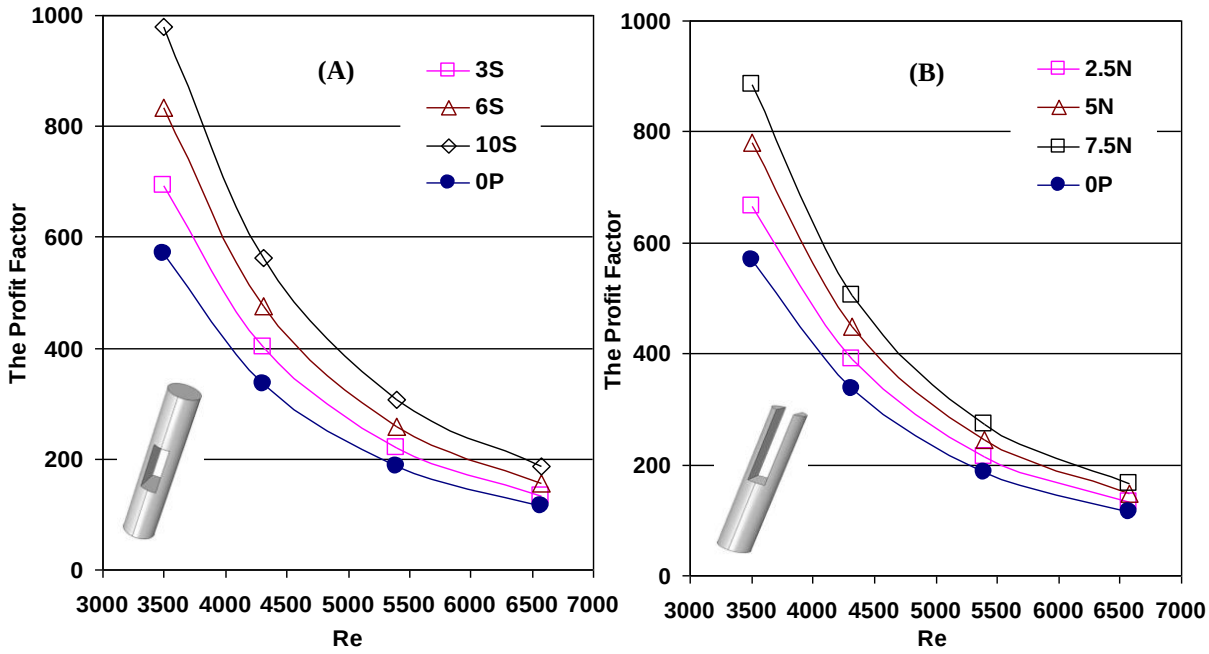

Figure 7.6: Comparisons of the profit factors with different heat sinks (A) slotted and (B) notched pins

The effects of the slotted and notched pin fin heat sink models on the pressure drag coefficient are shown in Figure 7.7 for a range of inlet velocities between 6.5m/s and 12m/s at Re=3500-6580 and 8 pins with a longitudinal distance of 6.5mm.

The pressure drag coefficient of these six pinned heat sink models is smaller than that of the solid pins as well as its value decreases as the open area expands (the height of the slot or notch increases). As mentioned earlier, the frontal area of the slotted and notched pins is smaller than that of the solid pins, which means that part of the airflow passes through this open area easily, as the open area is larger and so has less resistance to airflow, and that is in agreement with the findings of Ismail (2013). Therefore, the pressure drag coefficient decreases as the open area expands when the slot and notch height are increased.

Generally, the ratio of pressure drop and kinetic energy is defined as the pressure drag coefficient. This factor decreases when the inlet air velocity (Reynolds number) is increased due to increasing the kinetic energy more than increasing the pressure drop due to the open slotted and notched area.

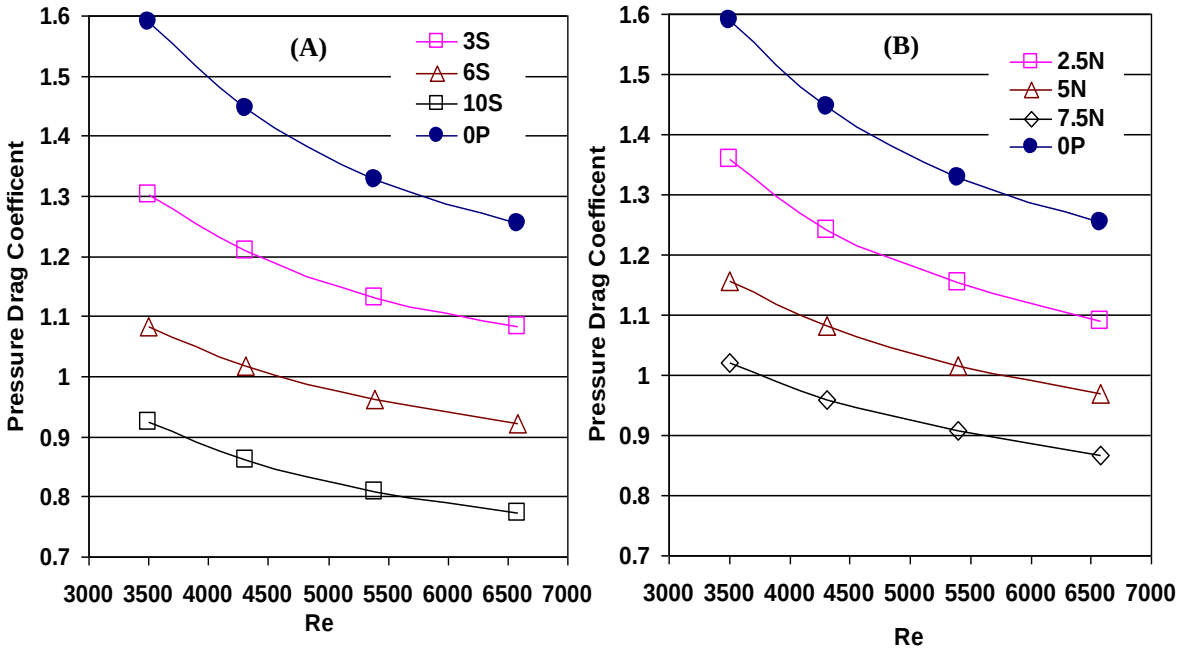

Figure 7.7: Variation in pressure drag coefficient of slotted (A) and notched (B) pins with different Re

7.4.3 Effect on Power Consumption

As mentioned previously, the fan power factor plays a vital role in minimising the power consumption, which increases the profit factor of PHSs. The reduction in power consumption of the slotted and notched pins is higher than that of the solid pins (0P), as shown in Figure 7.5. Additionally, the fan power consumption reduces with expansions in the slot and notch areas and leads to the profit factor increaseings at a given air velocity. For example, the reduction in power consumption is approximately 15.5%, 30% and 40% for slotted pins 3S, 6S, and 10S respectively, and nearly 13.5%, 24.5% and 33% for notched pins 2.5N, 5N, and 7.5N respectively. The profit factor increases by approximately 18.5%, 40.5% and 66.5% for slotted pins 3S, 6S, and 10S respectively, and by nearly 16%, 33% and 49.5% for notched pins 2.5N, 5N, and 7.5N respectively, as seen in Figure 7.6.

Subsequently, the first aim of the current study in reducing the fan power consumption (pressure drop) is achieved by using the slotted and notched PHSs.

7.5 Heat Transfer Characteristics

Some important thermal characteristics such as the Nusselt number and the base heat sink temperature (T_{case}) are explained and discussed in the following sub-sections.

7.5.1 Average Nusselt Number

Figures 7.8A and 7.8B indicate the effect of each of the given slotted and notched pin designs on the total Nu_T and projected Nu_P for a range of inlet velocities from 6.5m/s to 12m/s (Re = 3500-6580) and 8 pins with streamwise and spanwise distances of 6.5mm.

For the slotted and notched pin fin heat sinks, it can be observed from Figure 7.8A that the solid pin fin has a slightly higher Nu_T than those of slotted and notched pin fins. When the height of the slot or notch increases, increasing the open area, the Nu_T number decreases. The maximum percentage increase in Nu_T of the solid pin does not exceed 2% compared with the other pin fin designs. The main reason for this is that some of the airflow passes inside the open area and the local mean velocity through this open area decreases with increases to the height of the slot or notch, as shown in Figure 7.9 (local mean velocity). This local mean air velocity through the slots and notches may be not strong enough to accelerate the airflow over the slot or notch areas, which results in weakening the flow turbulence and flow mixing (Alam et al., 2014). Secondly, the Nu_T of the slotted and notched pinned heat sinks have decreased slightly, which means that the increase in heat transfer is proportionately slightly less than the increase in the total wetted surface area in the heat sink due to the perforations. These findings are consistent with the recent conclusions of Shaeri & Yaghoubi (2009a). In addition, for heat conduction along pin fins, the reduction in the cross-sectional area along the pins when increasing the height of the slot or notch results in reduction to the heat transfer conduction rate of these pins and to the Nusselt number (Nu_T).

However, as shown in Figure 7.8B, the projected Nusselt number (Nu_P) of each of the slotted and notched pinned heat sinks will increase compared with the solid pin (0P) model. For instance, the Nu_p enhancement reaches approximately 8%, 14.5%, and 17% for the 3S, 6S, and 10S slotted pins, respectively, while it is nearly 5%, 8%, and 12% for the 2.5N, 5N and 7.5N notched pins, respectively. Thereby,

Nu_P may be a more effective measure of a heat sink's cooling capacity for a given PHS size compared with Nu_T. It can be observed that the enhancement in the projected Nusselt number, Nu_P, of the slotted pinned heat sinks is twice that of the notched pins, except for the 10S and 7.5N models. This means that the amount of heat removed from the heat sinks increases with these new pin designs because Nu_P is based on a constant projected surface area, which demonstrates that perforations significantly improve the magnitude of the heat transfer.

Regarding to the above results, the Nusselt number might not represent the actual heat transfer rate from heat sink. The main reason for this is that the calculation of the Nusselt number depends on the heat transfer coefficient (h) and the characteristic length (X) and each of these parameters are found in different procedure. For example, the heat transfer coefficient (h) are found based on either the total wetted surface area (A_T) of heat sink or the projected surface area (A_P). In addition, the characteristic length (X) might represent either the length of heat sink in direction of flow (L), the pin diameter (d), or the duct hydraulic diameter (D_h). Thus, it is required another thermal parameter to evaluate the thermal performance of heat sinks that might be the CPU temperature, which is discussed in the next section.

Collectively, Figures 7.4, 6.5 and 6.8B show that the pressure drop and fan power decrease monotonically and Nu_P increases monotonically with increases to the slotted and notched perforation area (the height of slot and notch).

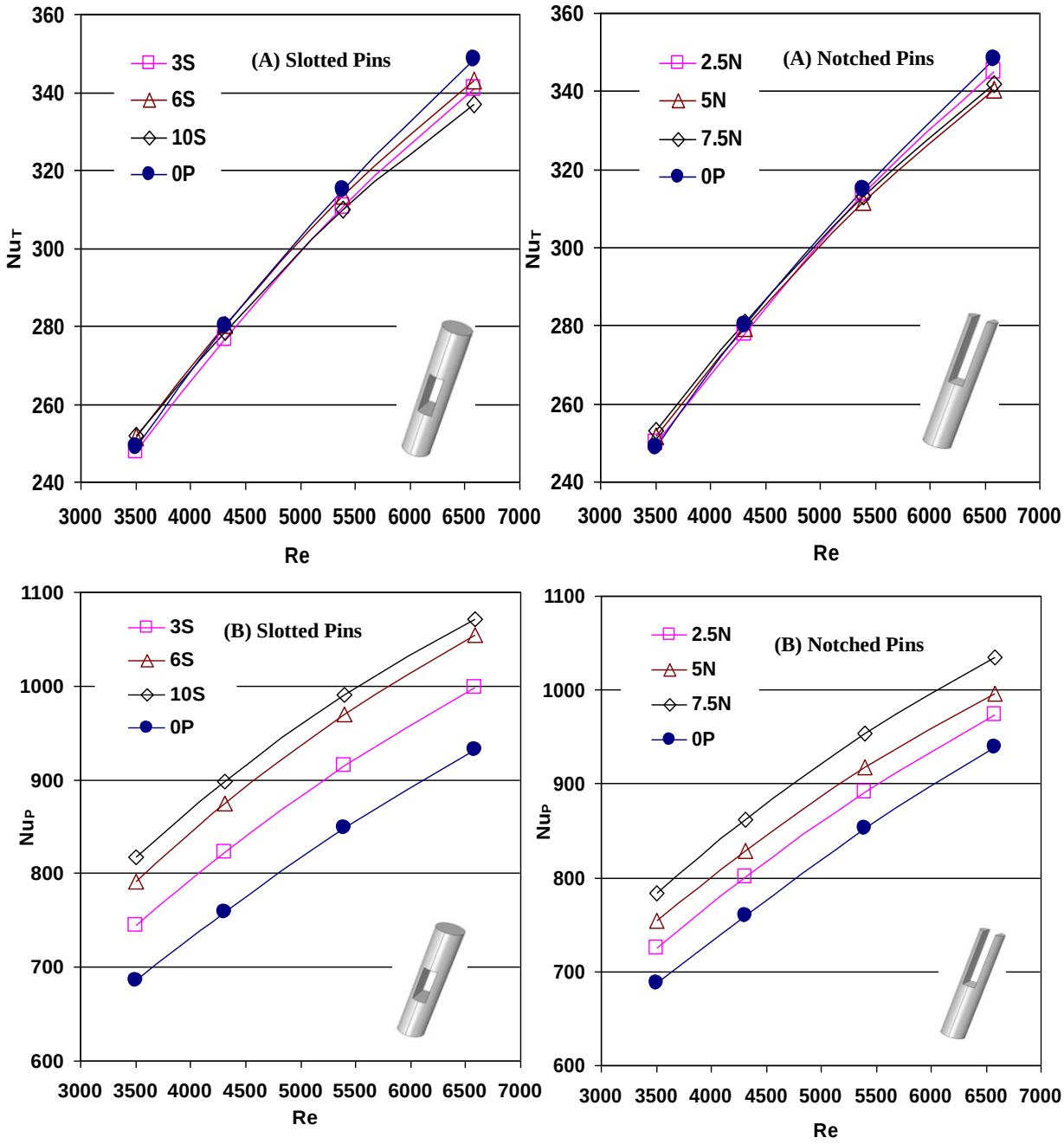

Figure 7.8: Effect of slotted and notched pinned heat sinks on Nusselt number based on (A) total (B) projected surface area

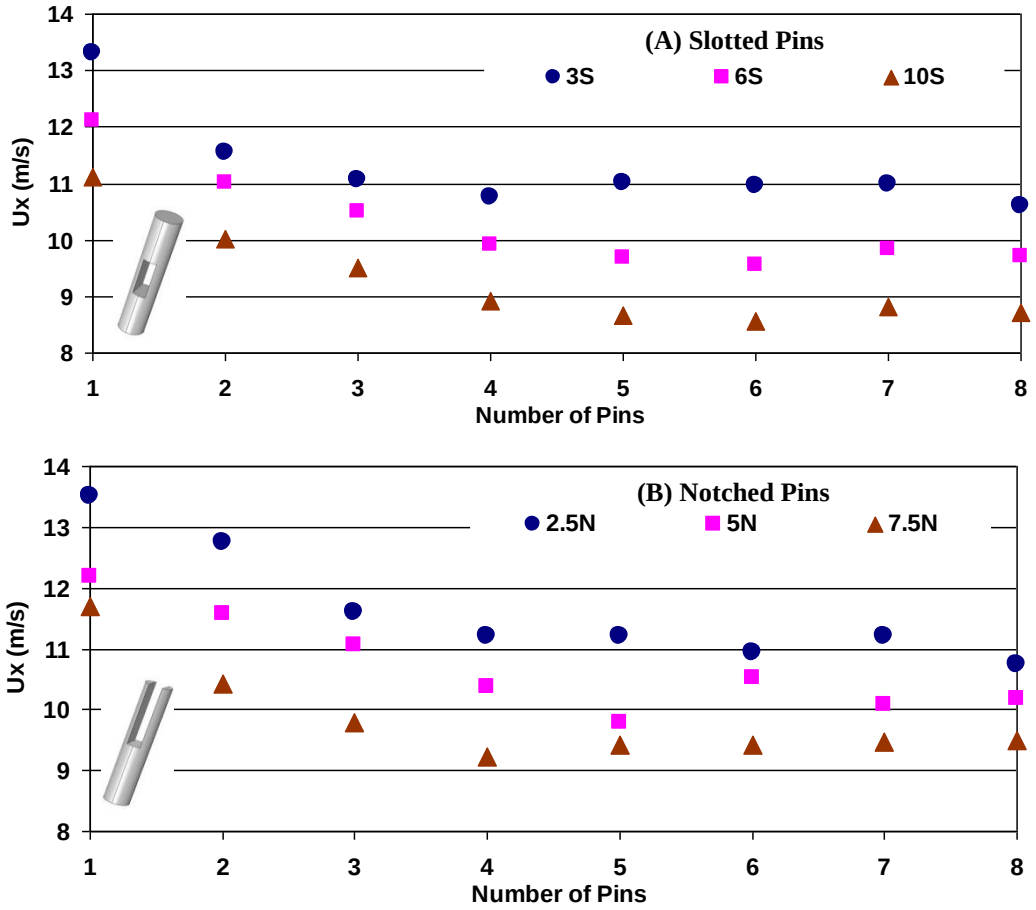

Figure 7.9: Variation in the mean local air velocity through (A) slotted and (B) notched pins

7.5.2 Thermal Management of PHSs

Figure 7.10 shows an example of a conjugate heat transfer analysis which predicts the average base plate temperature T_{case} with fan power as inlet air velocity is varied from 6.5m/s to 12m/s through a system of 8 pins separated longitudinally by a distance of 6.5mm for all new models – slotted (SPHSs) and notched (NPHSs) pinned heat sinks.

Figure 7.10 illustrates that the slotted and notched pin fins have smaller T_{case} and fan power than that of the solid pin fins (0P), except that the T_{case} of the 10S slotted pin model is slightly hotter than that of 0P solid pin model. This may be because the number of slotted pins (10S) has been doubled, from 64 to 128 pins, by making them thinner by reducing their diameter to half the diameter of the solid pin fins (0P), leading to reductions in the conductive heat transfer rate through them. Thereby, the 10S model requires more airflow to help to lower the CPU temperature

than does the solid pin (0P) model. It can be noticed that the lowest T_{case} are nearly 4°C for slotted the 6S pin fins with h=6mm and notched 7.5N pin fins with h=7.5mm both with notch and slot width w=1mm at a given fan power.

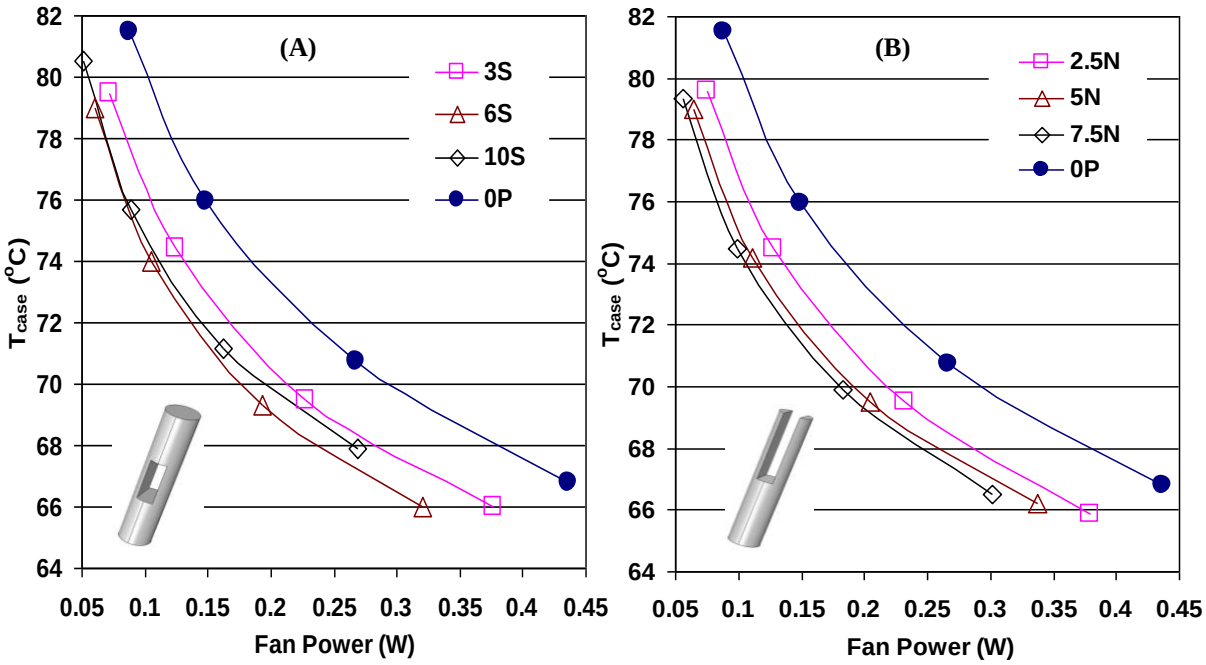

Figure 7.10: Effect of (A) slotted and (B) notched pins on T_{case} and fan power

Figure 7.11 compares the surface temperature distribution of the solid pin heat sink (0P design) with those obtained on the slotted and notched pin fins. The maximum temperature is at the fin base and it reduces to the fin tip. It can be observed that the drop in temperature of these new pin fin designs is less significant with changes to the height of the slot or notch. The maximum temperature drop from the fin base to the fin top increases by increasing the height of the notch from 2.5mm to 7.5mm and by increasing the slot height from 3mm to h=6mm.

The CPU temperatures of the solid pins vary between approximately 58.5°C and 71°C. In terms of the new heat sink designs, however, in the slotted pin 3S, 6S, and 10S models the corresponding temperatures change between roughly 57.5°C – 70°C, 54.5°C –70°C, and 54°C –72°C, respectively. In the notched pin 2.5N, 5N, and 7.5N designs the temperature distributions vary from nearly 58°C –70°C, 57.5°C – 70°C, and 55.5°C –70°C, respectively.

According to the predicted CFD data, the first and second aims of the current study, that is, slightly enhancing the CPU temperature (by nearly 2%) and producing valuable reductions in the fan power of the slotted and notched PHSs, are achieved. This means that the heat transfer rate increases at a given fan power (pressure drop) using these heat sinks, which is one of the usual active cooling techniques.

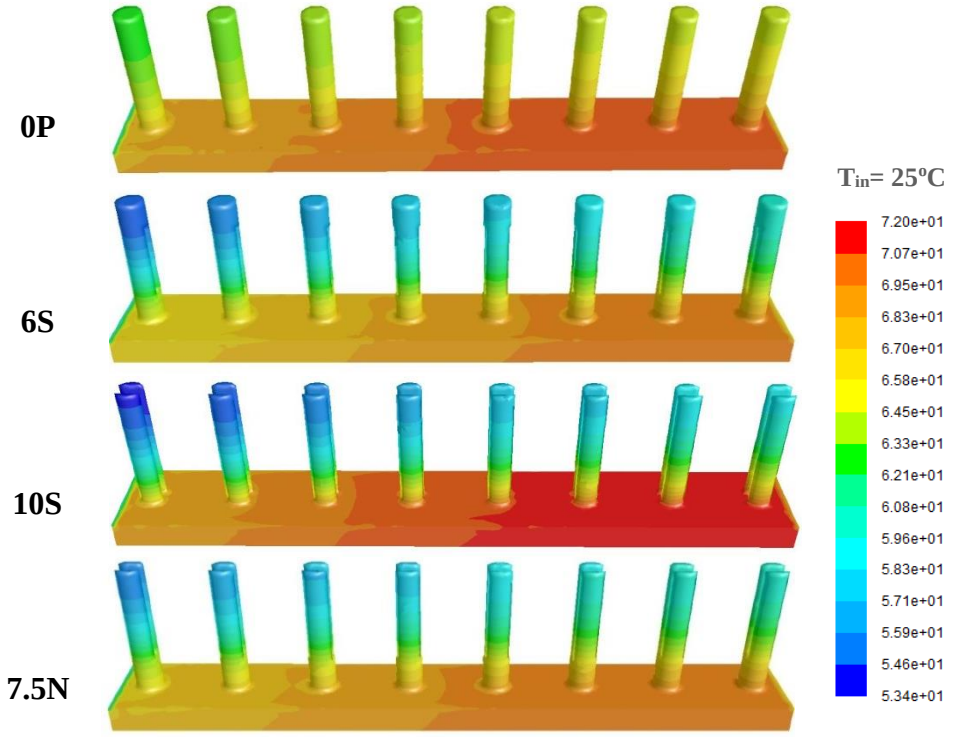

Figure 7.11: Temperature distribution through pinned heat sinks: 0P, 6S, 10S, and 7.5N models at *Re*=5393

7.6 Optimum Design of the Notched Pinned Heat Sink

As indicated previously, PHSs are designed to maintain the processors below critical temperatures for minimal energy input into the system. This section focuses on the optimisation of notched pins as a function of notch height, h, and width, w, for PHSs with an 8x8 array of pins with a constant pin spacing of 6.5mm in either direction. The multi-objective optimisation problem studied here is to minimise T_{case} and P_{fan} for 2.5mm$\leq h \leq$10mm and 0.5mm$\leq w \leq$1.5mm for a constant air inlet velocity, U_{air}= 8m/s (Re=4315). Since the above results have shown that minimising T_{case} and minimising P_{fan} leads to conflict between them, the goal is to construct a Pareto front of non-dominated solutions, from which an appropriate compromise design can be chosen.

Thus, the optimisation problem can be defined as follows:

Objective function: minimise T_{case} & P_{fan}

Subject to: 2.5 mm $\leq h \leq$ 10mm

0.5 mm $\leq w \leq$ 1.5mm

Again, an Optimal Latin Hypercube approach uses a permutation genetic algorithm to achieve a uniform spread of points within the design space (Narayanan et al., 2007). This approach distributes the two design variables in the spacing design uniformly within the lower and upper limits of each variable, as shown in Figure 7.12.

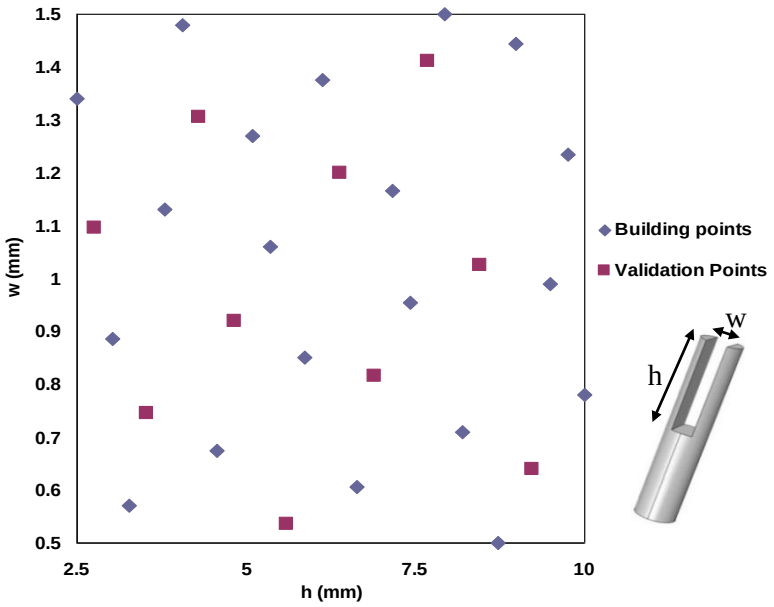

Figure 7.12: Distribution of design points in the design variable space for the height, *h* (mm) and the width, *w* (mm) of the notch

Figures 7.13 and 7.14 show the response surface function of CPU temperature and fan power of the notched PHS regarding the design variables height (h) and width (w) of the notch at inlet air velocity 8m/s. The optimised response surface function demonstrates that the T_{case} and P_{fan} minima occur on the domain boundaries. P_{fan} is reduced by increasing the notch area through increases to both h and w, whereas the T_{case} response surface function further highlights the importance of localised air jets through the perforation. T_{case} is reduced by increasing h and decreasing the notch width, w. The optimised MLS method has given very good agreement with merged DoE_m: R^2 =0.938 for T_{case} and P_{fan}.

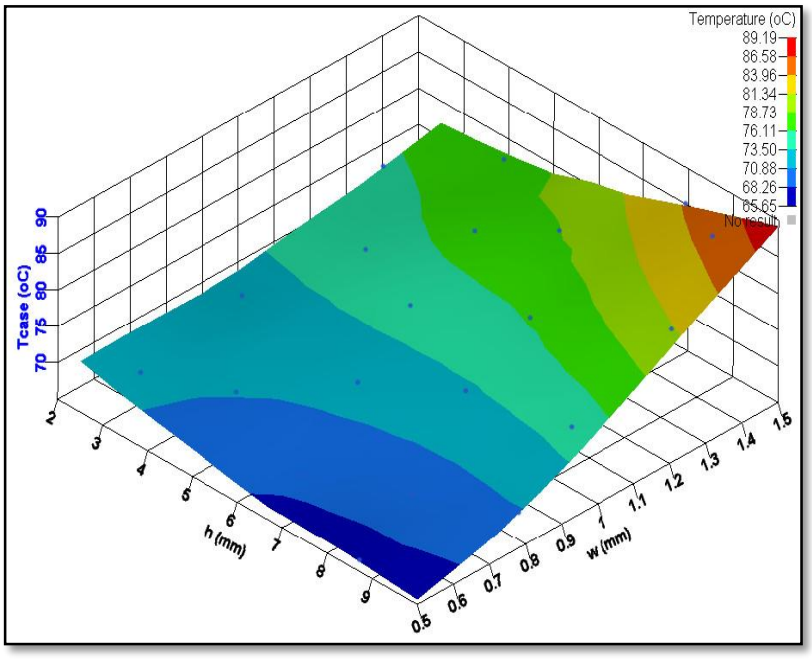

Figure 7.13: Response surface function of CPU temperature (T_{case}) of the notched pinned heat sink model

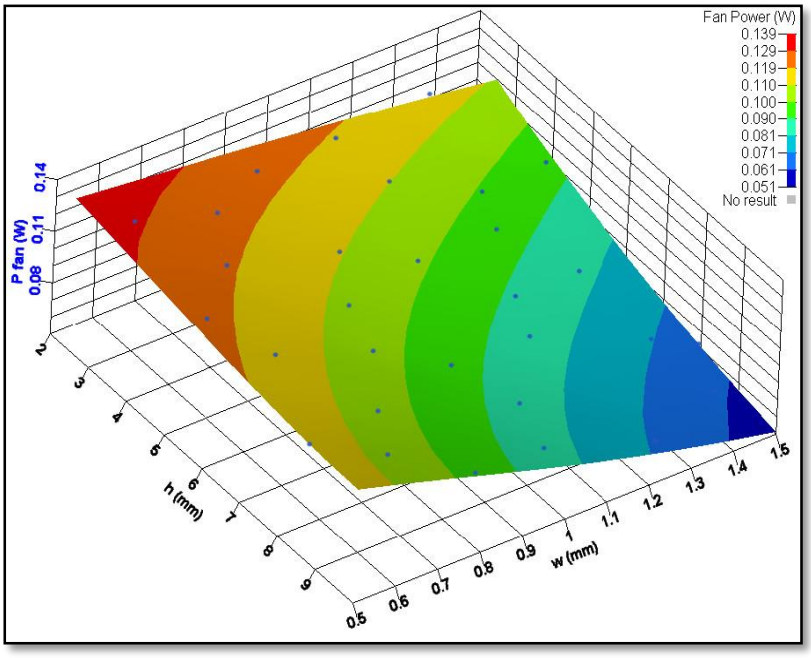

Figure 7.14: Response surface function of fan power (P_{fan}) of the notched pinned heat sink model

The Pareto front is obtained by using the T_{case} response surface function to determine the design points (h, w) at which T_{case} is a specified value and then using the P_{fan} response surface function to determine which of these design points has the smallest fan power. The resultant Pareto front is shown in Figure 7.15, where the brown triangles compare numerical predictions of T_{case} and P_{fan} against the Pareto front values obtained from the response surface function. These are generally in very good agreement, with typical discrepancies of less than 2%.

The Pareto curve shows the compromise options that are available between a low T_{case} and a low P_{fan}. In the cases considered, the minimum P_{fan} that can be experienced while ensuring T_{case} is below the reference critical temperature of 85°C is approximately 0.06W, and this has to be increased by 30% (to 0.078W) and 60% (to 0.096W) to ensure T_{case} remain below 75°C and 70°C, respectively.

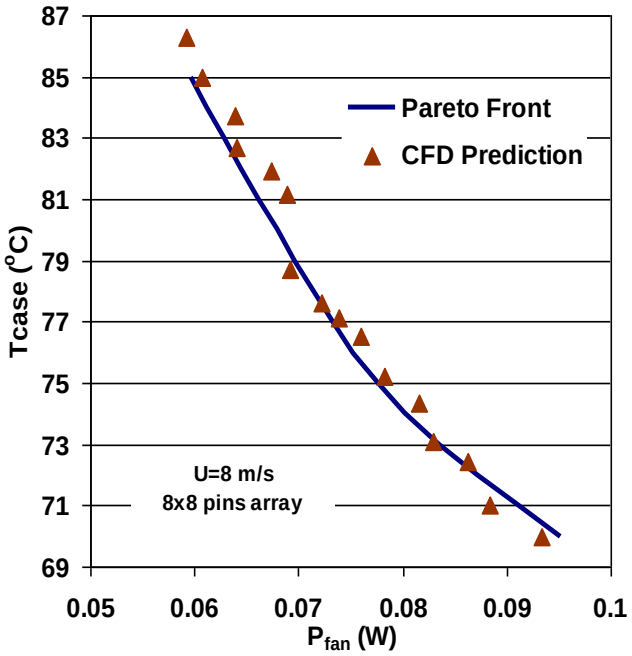

Figure 7.15: Pareto curve of T_{case} and P_{fan} for an 8x8 PHs with notched pins, with an inlet air speed of 8m/s

Figure 7.16 shows plan views of the flow fields for the points on the Pareto curve with T_{case}=86.3ºC and P_{fan}=0.0592W, with h=10mm and w=1.35mm as a wide notch pin model, and T_{case}=70ºC and P_{fan}=0.0934W, with h=10mm and w=0.8mm as a narrow notch pin model; airflow is from right to left in both cases. The former case corresponds to the low pressure drop case where air flows rapidly through the notch (with a maximum speed of approximately 12.0m/s compared to the inlet air speed of 8m/s) and with minimal separation around the pins. The latter case, with the smaller notch width w=0.8mm, causes a larger increase in air speed through the notch (up to a maximum of approximately 13.3m/s) which leads to more effective convective heat transfer at the cost of greater levels of separation and pressure drop across the pins.

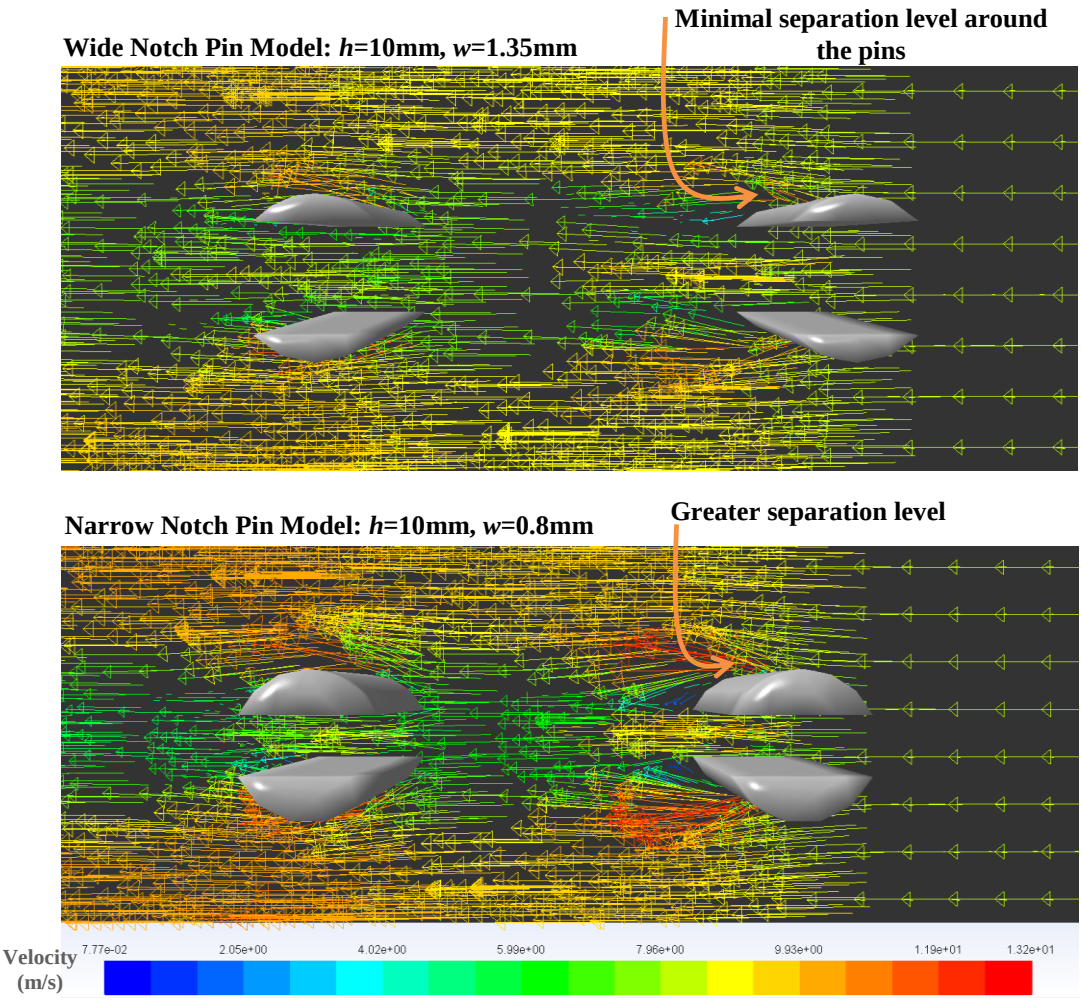

Figure 7.16 Plan views of flow field through notch perforations for a wide notch with T_{case}=86.3ºC and P_{fan}=0.0592W and a narrow notch with T_{case}=70ºC and P_{fan}=0.0934W

The surface temperature distribution for the wide and narrow notch pin models are shown in Figure 7.17. It is clear that the maximum temperature is for the wide notch pin model compared to the narrow notch pin model that has lowest temperature distribution. It can be observed that the drop in temperature of the notched PHS design is significant with changes to the width of notch. The CPU temperatures of the wide notch pin model vary between approximately 58°C and 88°C with low fan power consumption while the narrow notch pin model the corresponding temperatures change between roughly 54°C–71.5°C with high fan power consumption required. Table 7.1 shows the comparing between the predicted T_{case} and P_{fan} from MLS with simulated T_{case} and P_{fan} from CFD with very well agreement.

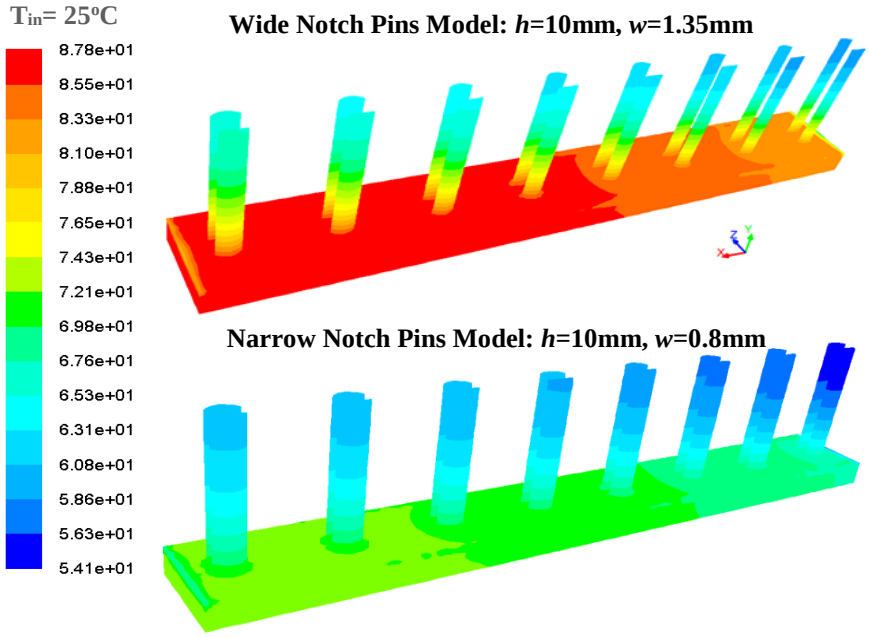

Figure 7.17 : The optimum temperature distribution of the wide and the narrow notch pin models with an inlet air speed of 8m/s

Table 7.1: Compare between T_{case} and P_{fan} of predicted MLS and simulated CFD

Design Variable		Multi-Objective Function					
h (mm)	w (mm)	Predicted MLS T_{case} (°C)	Simulated CFD T_{case} (°C)	Error %	Predicted MLS P_{fan} (W)	Simulated CFD P_{fan} (W)	Error %
10	1.35	86.3	85	1.5	0.0596	0.0592	0.67
Wide Notch Pin							
10	0.8	70	70	00.0	0.0934	0.0951	1.78
Narrow Notch Pin							

7.7 Comparison between Circular Perforated Pins, Rectangular Slotted, and Notched PHSs

Table 7.2 illustrates the comparison between the Nusselt number (Nu_T, Nu_P), fan power (P_{fan}), and CPU temperature (T_{case}) for the circular perforated, slotted, and notched PHSs compared to the equivalent solid pin HSs.

Despite increasing surface area of the slotted and notched pin designs, heat transfer rate (in terms of Nu_T and Nu_P) and CPU temperature of the multiple circular perforated PHS models show the greatest enhancement. This means that the benefits arise due to not only the increased surface area but also to the heat transfer enhancement near the perforations through the formation of localised air jets. However, the fan power consumption required for the slotted and notched pins is smaller than that for the multiple circular perforated PHSs because the porosity of the slotted and notched pins is larger compared with that of the circular perforated pins, which enables air to flow easily across the pins.

It can be concluded that a compromise has to be struck between the choice of perforations. Since the larger enhancements in heat transfer with multiple circular perforations come at the price of both significantly increased power consumption and, perhaps most importantly, a much more complex manufacturing process, while the slotted and notched PHSs are more practical and bring about a greater reduction in fan power consumption.

Table 7.2: Comparison of Nusselt number, fan power (P_{fan}), and CPU Temperature (T_{case}) between perforated, slotted, and notched PHSs

Heat Sink Designs \ Parametric Studies		$\uparrow A_T$	Nusselt Number		$\downarrow P_{fan}$ (W)	$\downarrow T_{case}$ (°C)
			$\uparrow Nu_T$	$\uparrow Nu_P$		
Circular PPHSs	Perforated Pins with One Perforation (1CP)	5%	1.7%	5%	2%	2%
	Perforated Pins with Two Perforations (2CP)	10%	5%	14.5%	6%	5%
	Perforated Pins with Three Perforations (3CP)	15%	9%	24%	9%	8%
	Perforated Pins with Five Perforations (5P)	25%	11%	36%	14%	10%
SPHSs	Slotted Pins (3S)	10%	-1%	8%	15.5%	2%
	Slotted Pins (6S)	16%	0%	14.5%	30%	2%
	Slotted Pins (10S)	20%	-1%	17%	40%	0%
NPHSs	Notched Pins (2.5N)	5%	0%	5%	13.5%	1%
	Notched Pins (5N)	10%	-1%	8%	24.5%	2%
	Notched Pins (7.5N)	15%	0%	12%	33%	2%

7.8 Weight Reduction of Heat Sinks

Figure 7.18 illustrates the percentage weight reduction of all pinned heat sink designs. The weight of these pins decreases with increases in the number of perforations or the open slotted and notched area, which leads to saving material in manufacturing the pin fins and lighter assembly as well. Furthermore, the cost and energy of the force required to drive the air by fan power will reduce significantly. According to Shaeri (2009b), the two optimal outcomes for pin fin design are to maximise the heat transfer rate for any given fin weight or minimise the weight for a required heat transfer rate. Another advantage of this weight reduction is associated with heat transfer enhancement for the perforated pinned heat sink designs according to the numerical data. However, the cost manufacturing process of perforated pinned heat sinks is higher compared to that solid pined heat sink.

The total weight reduction of the pins considered here has been calculated utilising the following equations and the values are shown in Figure 7.18:

$$V_T = V_{Base} + V_{Pins} \tag{6.4}$$

$$W_T = \rho_{Al} \times V_T \tag{6.5}$$

where V_T is the total volume of PHS, V_{Base} is the volume of base PHS, V_{Pins} is the total volume of pins, W_T is the total weight of PHS, and the density of aluminium $\rho_{Al} = 2700$ Kg/m^3.

In the case of the perforated, slotted, and notched pins, the highest percentage of reduction in pin weight is seen in the 5P model with 5 perforations, 10S at 10mm slot height, and 7.5N with 7.5mm notch height at 7%, 14%, and 18%, respectively.

In terms of different types of perforation shape, the percentage total weight reduction is approximately 5% for both square perforated pin fins (3SP) and elliptic perforated pin fins (3EP). Therefore, by using these types of pinned heat sink, both aims of pin fin optimisation are achieved, particularly by increasing the number of perforations.

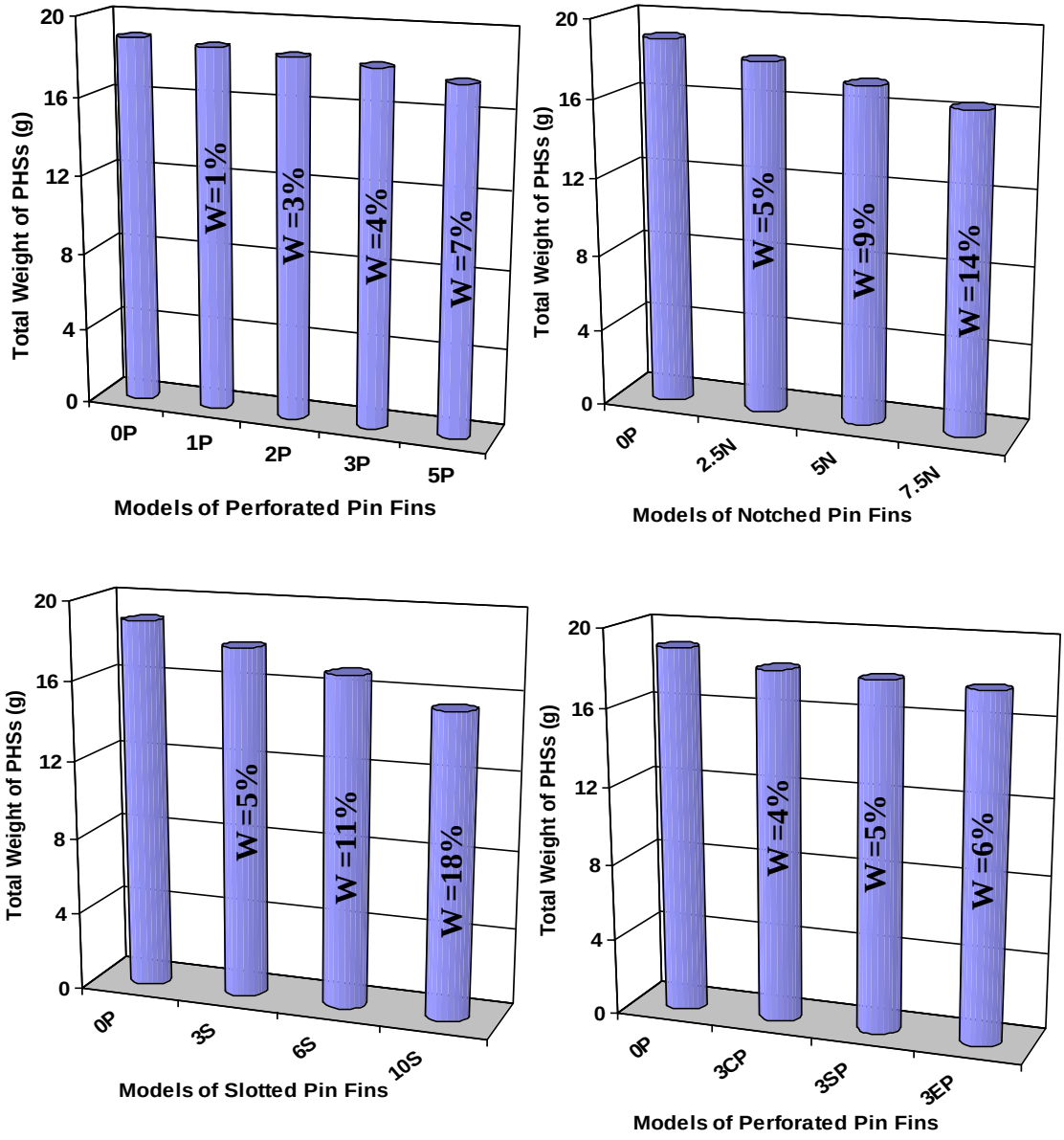

Figure 7.18: The percentage total weight reduction of PHSs

7.9 Conclusions

Airflow past a heat sink with arrays of slotted (SPHSs) and notched (NPHSs) pins has been solved numerically, and the solution method has explored the thermal and hydraulic characteristics of these heat sinks compared with the benchmark solid pin fin (0P) model. Slotted and notched pins may offer a more practical means of manufacturing perforated PHSs: either wire Electrical Discharge Machining could be used to directly cut into the slots/notches, or a series of thin cutting discs mounted on a common shaft could be used with support to the pins provided through a jig. This would also retain the high thermal conductivity between the pin and the base plate of a heat sink cast from a single block.

Generally, the CFD data shows that, in relation to the fan power (pressure drop) of the heat sinks, the new pinned heat sink designs require a smaller amount of fan power compared with the solid pins. The slotted (10S) pin model has the lowest fan power of 40%. The solid PHS has a Nu_T slightly higher than those of slotted and notched pins while the Nu_P of the new pinned heat sinks is the largest. The maximum percentage increase in Nu_P is nearly 17% for 10S model compared with the other pin designs. The T_{case} of the slotted and notched pins is slightly (2%) lower than that of the solid pin model, as detailed in Table 7.3. The perforations etched into the top of the pins, notched pins, may offer a more practical means of manufacturing perforated PHSs, as indicated previously.

The optimum design of the notched PHS has been investigated for two design variables: the height (h, mm) and width (w, mm) of the notch. The main goal of this study was to reduce both CPU temperature and fan power of the pinned heat sinks. The formal optimisation study has demonstrated the practical compromise that has to be struck between low processor temperatures (modelled in terms of the variable, T_{case}) and the fan power needed to achieve the required rate of cooling. Thus, the minimum P_{fan} that can be experienced while ensuring T_{case} is below the reference critical temperature of 85^{o}C is approximately 0.06W, and this has to be increased by 30% (to 0.078W) and 60% (to 0.096W) to ensure T_{case} remains below 75^{o}C and 70^{o}C, respectively.

The new pinned heat sink SPHS and NPHS models are superior to the solid PHS because they require less fan power to push air over the pin heat sinks and there is an acceptable reduction in thermal resistance while, as discussed earlier, they require more preparation in their manufacture.

Table 7.3: Enhancement of Nusselt number (*Nu*), fan power (P_{fan}), and CPU temperature (T_{case}) of slotted and notched pinned heat sinks

Heat Sink Designs \ Parametric Studies		$\uparrow A_T$	Nusselt Number		$\downarrow P_{fan}$ (W)	$\downarrow T_{case}$ (°C)
			$\uparrow Nu_T$	$\uparrow Nu_P$		
SPHSs	Slotted Pins (3S)	10%	10%	-1%	8%	15.5%
	Slotted Pins (6S)	16%	16%	0%	14.5%	30%
	Slotted Pins (10S)	20%	20%	-1%	17%	40%
NPHSs	Notched Pins (2.5N)	5%	5%	0%	5%	13.5%
	Notched Pins (5N)	10%	10%	-1%	8%	24.5%
	Notched Pins (7.5N)	15%	15%	0%	12%	33%

Chapter Eight: Effect of Pin Density and Applied Heat Flux

8.1 Introduction

After an indication that the new pinned heat sinks, perforated and notched PHSs, have a lower CPU temperature and fan power for active air-cooling of electronic systems, the reliable performance of high-power density electronics for PHSs is another important consideration for efficient cooling design strategies. Essentially, the thermal effects cause some failure of the mechanisms in devices containing electronic components, such as void formation, metal migration, and inter-metallic growth. For each 10^{o}C increase above the operating temperature of high-power electronics, the rate of these failures almost doubles (Gurrum et al., 2004). Thus, thermal management of electronics is of crucial significance to the industry market.

This chapter considers two key parameters for the performance of pinned heat sinks: density distribution of the pin fins and heating power applied at the sink base. This consideration specifically relates to the CPU temperature value in addition to the Nusselt number, Nu_T, Nu_P, and pressure drop (ΔP). The main purpose for this is to investigate the application reliability (capability) of these pinned heat sink designs in the desktop PC UPS for waste heat dissipation. In addition, the study also wishes to estimate the allowable level of applied heating power on these new pinned heat sink designs.

8.2 Effect of Pin Density Distribution

The effects of the distance between pins (S_x, pin columns) on the pressure drop (ΔP), heat transfer rate (Nu_T, Nu_P), and CPU temperature (T_{case}) are explained in detail in this section for the in-line array solid (0P), perforated (3P), and notched (7.5N) pinned heat sinks to obtain the optimum distribution of pin density on pinned heat sinks.

According to previous researchers such as Sahin & Demir (2008), the flow blockage increases as the distance between pins (S_y, pins rows) decreases, leading to increases in the pressure drop (fan power) along the heat sink as well. Thus, the pin spacing (S_x, pin columns) is only considered at 15mm, 9mm, 6.5mm, and 4.5mm while the pin spacing (S_y, pin rows) is not reported in this study and its value is constant at 6.5mm, Figure 8.1. In other words, there will be models with 4, 6, 8 and 11 pin columns in the stream flow direction and each transverse column that is perpendicular to the airflow direction has 8 pin fins only for solid (0P), perforated (3P), and notched (7.5N) pin heat sink models.

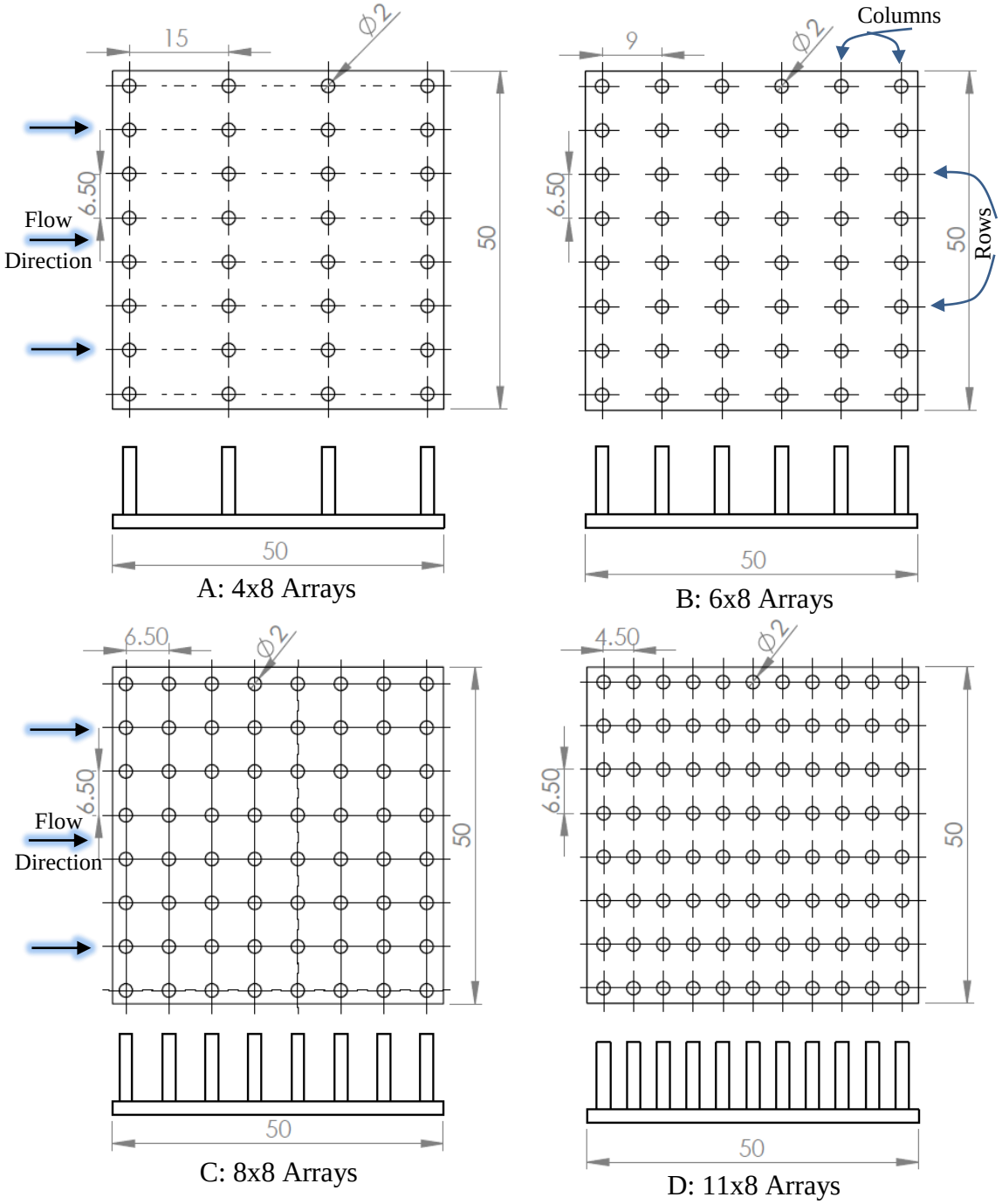

Figure 8.1: Schematic of different heat sink geometries in in-line arrangement for top and side views

The variations in pressure drop with the number of columns and different Reynolds numbers for solid (0P, left), perforated (3P, right), and notched (7.5N) pinned heat sink models are illustrated in Figure 8.2.

As expected, the pressure drop of the heat sink (ΔP) increases with increasing numbers of pins and Reynolds number as well. In all cases, halving the number of columns from 8 to 4 would reduce the pressure drop by approximately 35%. Commonly, the lowest pressure drop value is for the notched pins (7.5N) and then the perforated pins (3P), compared with that of solid pins (0P), due to the perforations. When increasing the Reynolds number from 3500 to 4315, the pressure drop gradually increases while, when the Reynolds number increases up to 6580, the pressure drop sharply increases. The pressure drop of the solid pins sharply increases when the columns are increased in number from 8 to 11 compared with the 3P and 7.5N pin models. This is because the presence of more solid pins (decreasing pin spacing) in addition to increasing air viscosity due to increasing air temperature through the heat sink, leads to increasing the blockage of the airflow passing over the solid pins.

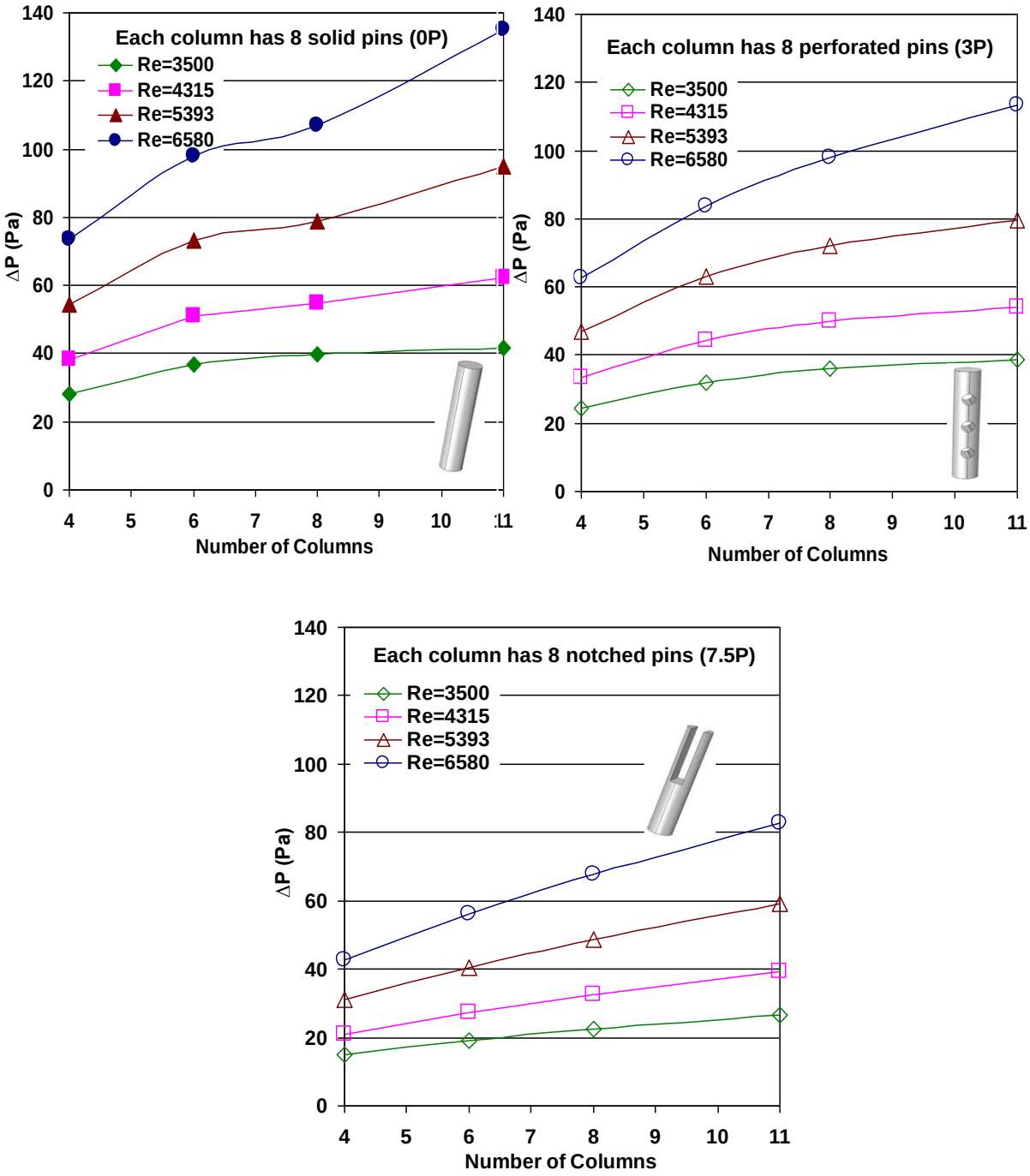

Figure 8.2: Variation of pressure drop with the number of columns and different Reynolds numbers for solid (0P), perforated (3P), and notched (7.5N) PHS designs

The dependence of total (Nu_T) and projected Nusselt number (Nu_P) on the number of columns and Reynolds number for both solid (0P), perforated (3P), and notched (7.5N) pinned heat sink models is shown in Figures 8.3 and 8.4.

The CFD data of the solid pinned heat sink (0P) indicates that the total Nusselt number (Nu_T) gradually increases when increasing the number of columns from 4 to 8 (nearly 11% larger), as shown in Figure 8.3. For additional pin columns from more than 8 columns up to 11 columns, however, the Nu_T increase remains almost constant because the total surface area will increase with the presence of more pin columns, leading to decreases the heat transfer coefficient as indicated previously. In terms of the notched pins (7.5N), the pattern of Nu_T with a different number of columns is similar to that of the solid pins (0P) and the Nu_T reaches a maximum value for the 8 pin columns nearly 10% higher than that of the 4 pin columns. However, the optimum total Nusselt number value of the 3P model is for the 6 pin columns, typically 4% higher than for the 4 pin columns. Conversely, it seems that the Nusselt number remarkably decreases when increasing the pin columns up to 11, as seen in Figure 8.3. This is because, with more perforated pin or notched pin columns, the total surface area will increase to higher than that of the solid pins, resulting in a remarkable decrease in the heat transfer coefficient.

On the other hand, the variations of projected Nusselt number (Nu_P) with the different number of columns and Reynolds number for solid (0P, left), perforated (3P, right), and notched (7.5N) pinned heat sink designs gave different results, as presented in Figure 8.4.

The projected Nusselt number, Nu_P, of the solid, perforated, and notched pinned heat sinks will enhance as the number of pin columns increases. The enhancement reaches approximately 50% as pin density doubles from 4 to 8 columns for all cases. It means that the amount of heat removed from the heat sinks will increase with the presence of more pin material due to moving the amount of heat through the base of the heat sink to the pins and then into the surrounding air.

Generally, the total and projected Nusselt number of the perforated pins (3P) is superior compared with the solid (0P) and notched (7.5N) pins, as well as this value increases when increasing the Reynolds number for the pinned heat sink designs.

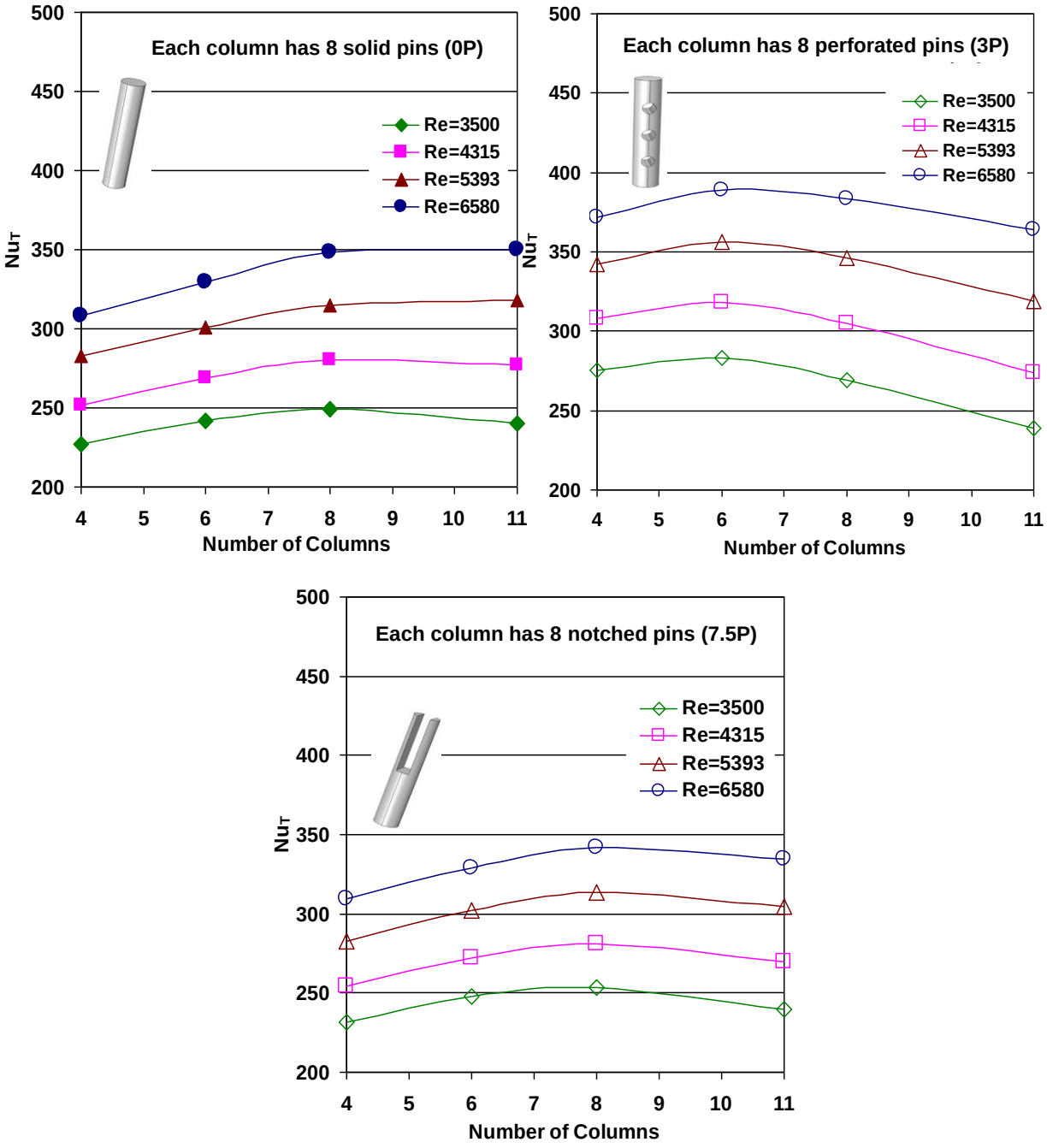

Figure 8.3: Effect of the number of columns on the Nusselt number and the Reynolds number for solid (0P), perforated (3P), and notched (7.5N) PHSs

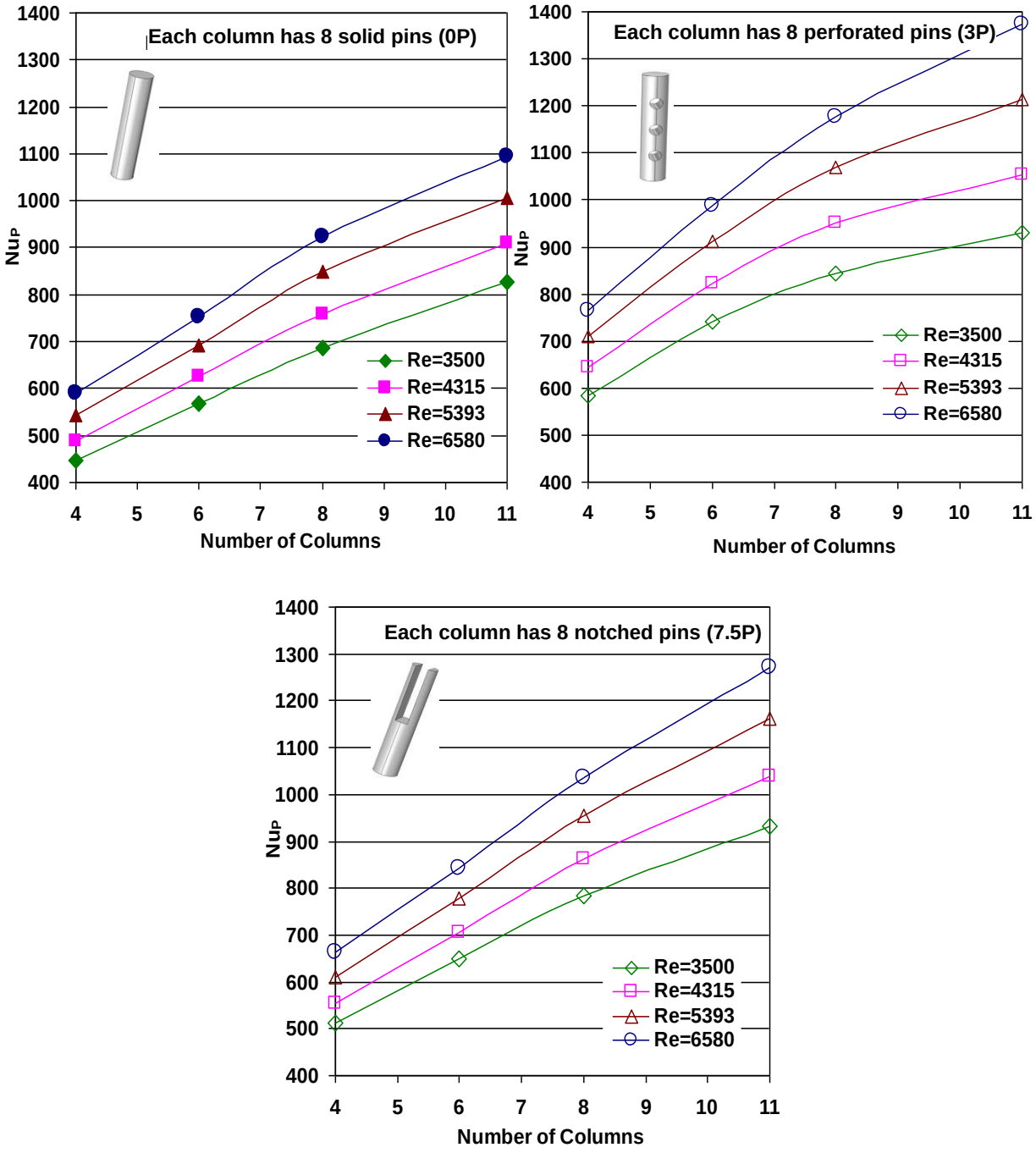

Figure 8.4: Variation in pressure drop with the number of columns and different Reynolds number for solid (0P), perforated (3P), and notched (7.5N) PHS designs

Figure 8.5 shows the effect of the number of pin columns on the CPU temperature with variations in the Reynolds number for solid (0P, left), perforated (3P, right), and notched (7.5N) pinned heat sink models. It is indicated that the CPU temperature of the perforated pins is lower than those of the other pin designs due to the perforations.

The reliability of these pin fin heat sink designs in a desktop PC CPU should be considered in relation to the minimum number of pin columns in order to obtain the cheapest cost and simplify fabrication of the heat sinks. Hence, the most important thermal parameter in practical applications of heat sinks is to keep the CPU temperature at less than the critical temperature (~85^{o}C). Figure 8.5 indicates that the maximum allowed temperature of a PC CPU is as a red line at 85^{o}C with different pin density (Yuan et al., 2012; Yu et al., 2005).

This temperature value drops as the Reynolds number increases and with the presence of more pin material resulting from the increased convection and conduction heat transfer via the amount of heat moving through the heat sink base to the pins and then being transferred to airflow passing over the pins, causing a drop in CPU temperature. At the lowest given Reynolds number (3500), it is recommended that the number of pin columns should be no lower than 8 columns for the solid (0P) and notched (7.5N) pins, while 6 pin columns is enough for the perforated pins (3P) to cool the PC CPU. With the highest given Reynolds number (6580), however, it is recommended to use the 4 pin columns for PC CPU cooling for the perforated pinned heat sink model (3P) while no fewer than 5 columns are required for both the solid (0P) and the notched (7.5N) pins to keep the CPU temperature lower than 85^{o}C.

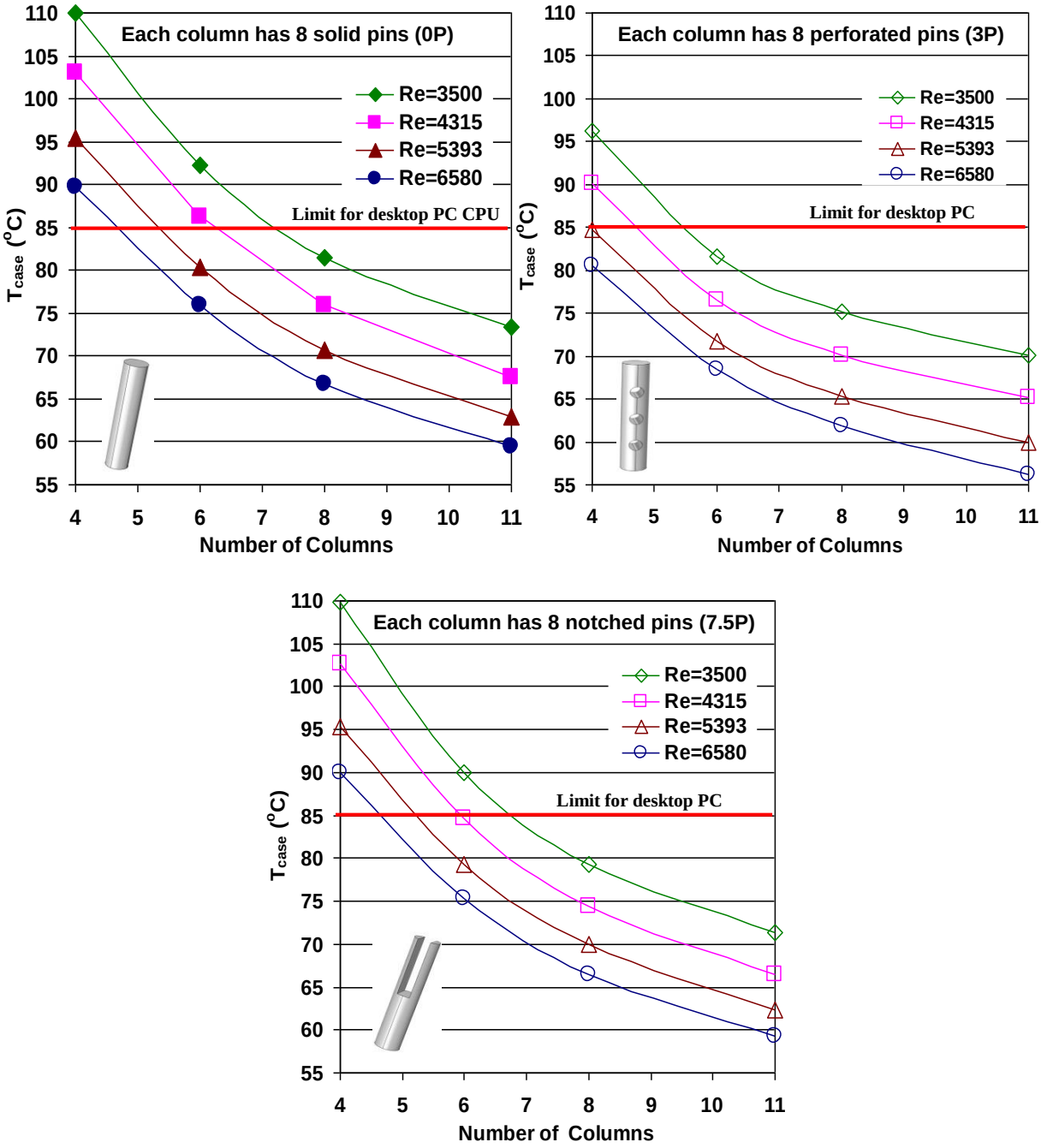

Figure 8.5: Effect of the number of columns on the CPU temperature and the Reynolds number for solid (0P), perforated (3P), and notched (7.5N) pinned heat sink models

Focussing on the practical outcomes of the cooling, reducing the heat sink temperature for a given fan power input with pin density is shown in Figure 8.6. Results are plotted with respect to a critical reference temperature of 85^{o}C as a red line. The results show that, as heat transfer rate from the CPU increases, convection and conduction heat transfer increases, resulting from the higher pin densities. It means that the CPU can be cooled below the critical temperature for a significantly lower fan power input with greater pin density. For example, the T_{case} reduces by approximately 30~35% as the number of pins increases from 4 to 11 pin columns.

At a given fan power, the lowest base plate temperature T_{case} is for the 11 pin columns compared with the other heat sinks. This is because the column with the smallest number of pins requires more airflow passing over the pins to remove a certain amount of heat, while less airflow is required to cool columns with a denser number of pins due to the increased conduction and convection heat transfer (presence of more pin material) for the CPU to be significantly cooler. The perforated pins (3P) exhibit smaller T_{case} than the solid and notched pins, while the notched pin (7.5N) model consumes less fan power than the solid and perforated pinned heat sinks due to the large notched area.

For the solid and notched pins, a fan power of 0.1W enables the CPU temperature to be maintained below 73^{o}C when 11 columns of pins are used whereas, for 4 columns, the CPU temperature of 100^{o}C is well above the critical CPU temperature. Using columns of the 3P perforated pin model reduces the CPU temperature yet further, for a given fan power input, and even makes the adoption of 4 columns of perforated pins viable for fan power inputs above 0.15W.

Generally, the CPU temperature reduces and the heat transfer rate enhances as pin density increases, while the pressure drop increases.

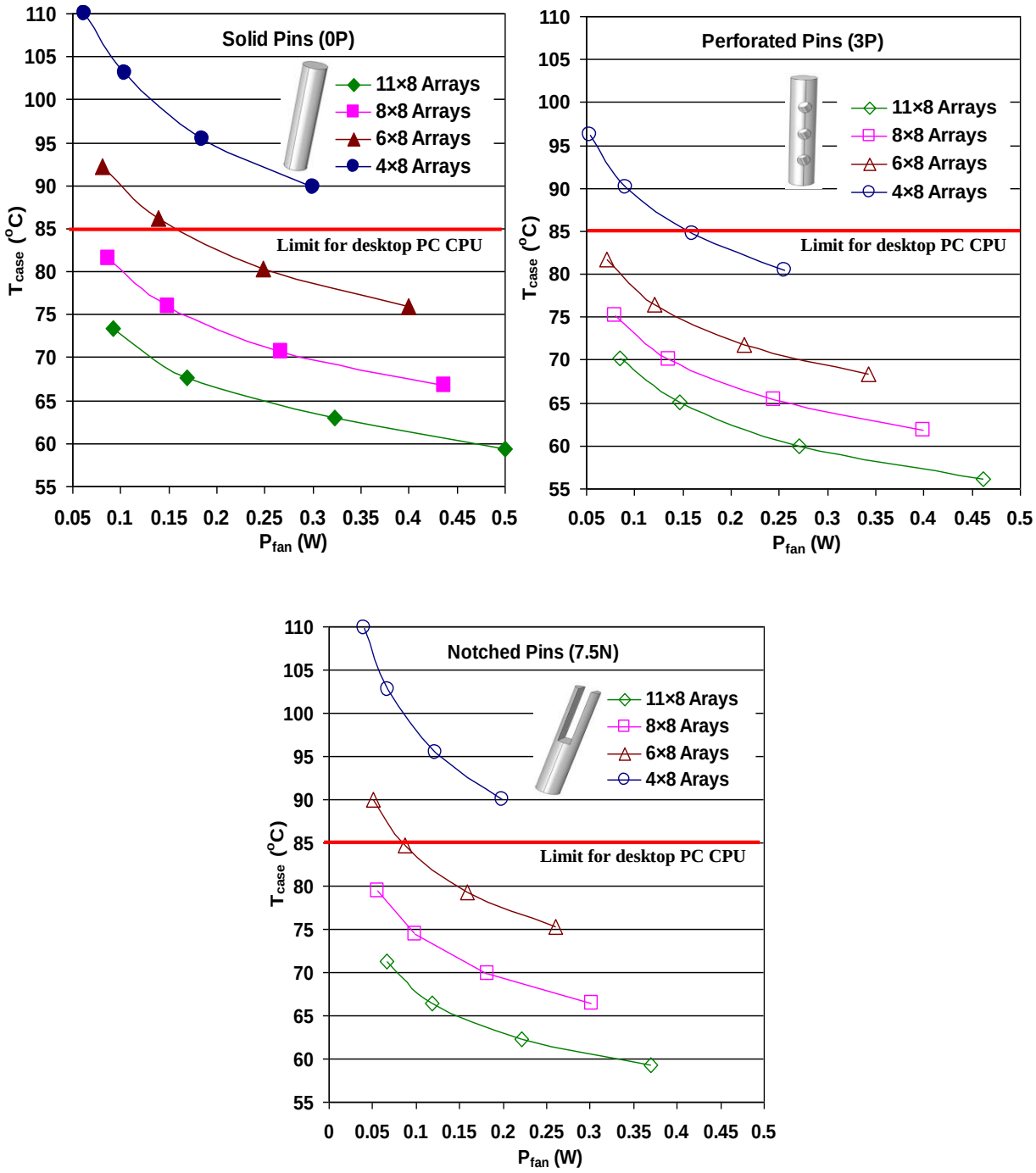

Figure 8.6: Effect of the number of columns on the CPU temperature and fan power of solid (0P), perforated (3P), and notched (7.5N) pinned heat sink models

8.3 Effect of Applied Heat Flux

Since modern CPUs have dynamically changing voltages, leading to variations in heating power $\dot{Q}$, at the base of a PHS. This section of the numerical investigation considers the supplied heating power that is selected based on the real working conditions of the PC CPU (Yuan et al., 2012), to estimate the allowable level of applied heating power on these new pinned heat sink models. Thus, the heating power applied at the base of the pin fin heat sinks is considered 10, 20, 40, 60, 70, 80, and 90W typical of heating generated by PCs (Yuan et al., 2012). In other words, the heat flux employed on the solid (0P), notched (7.5N) and perforated (3P) pin heat sink models is 0.4, 0.8, 2.4, 2.8, 3.2, 3.6W/cm^2, respectively. Figures 8.7, 8.8, 8.9 and 7.10 illustrate the variation of pressure drop (ΔP) and CPU temperature (T_{case}) with different applied heat flux on the pinned heat sink bases.

According to the heating power at 10W, the effect of air temperature inside the flow passage on the variation in air properties is small and can be ignored. The air properties, however, will be affected by this temperature inside a test section as the heat flux increases above 20W. Thermodynamic properties of air such as density, thermal conductivity and other properties vary with temperature through the heat sink. Thus, the air temperature variation inside the heat sink is significant to the analysis and it cannot be disregarded when increasing the applied heat flux (Yuan et al., 2012). It can be chosen among different methods to compute the corrected air properties. As indicated previously, ANSYS FLUENT-CFD code will calculate the property values by piecewise-linear interpolation method among the values defined at several air temperatures.

The variation of the pressure drop along heat sinks with different applied heat flux and inlet air velocities from 6.5 to 12 m/s is illustrated for the solid (0P), Figure 8.7, perforated (3P), Figure 8.8, and notched (7.5N), Figure 8.9, PHSs with (A) constant air properties and (B) variable air properties. Generally, the pressure drop of these heat sinks will increase as the supplied heating power increases from 10W to 90W, considering the variable air properties, while the change of pressure drop is unremarkable when the air properties are constant. The main reason for this is that the air viscosity will increase due to the increase in air temperature that results from increasing the supplied heating by 800% with variable air properties. Therefore,

higher air viscosity results in more fan power being required to push the air through the heat sink (test section). It can be seen that this pressure drop increases slightly – by nearly 4% for the solid (0P) design while it is approximately 6% and 8% for notched (7.5N) and perforated (3P) heat sinks, respectively – when the applied heat flux increases from 10W to 90W. This indicates that the heat transfer rate from the 3P model is higher than that of the 7.5N and solid (0P) designs, meaning that the temperature of the airflow passing through the 3P and 7.5N models is higher compared with that of the solid (0P) design. These findings are consistent with the recent conclusions of Yuan et al. (2012), which attributed improved heat transfer to plate-pin heat sinks to illustrate the effect of increasing applied heat flux on the pressure drop through a compact heat sink.

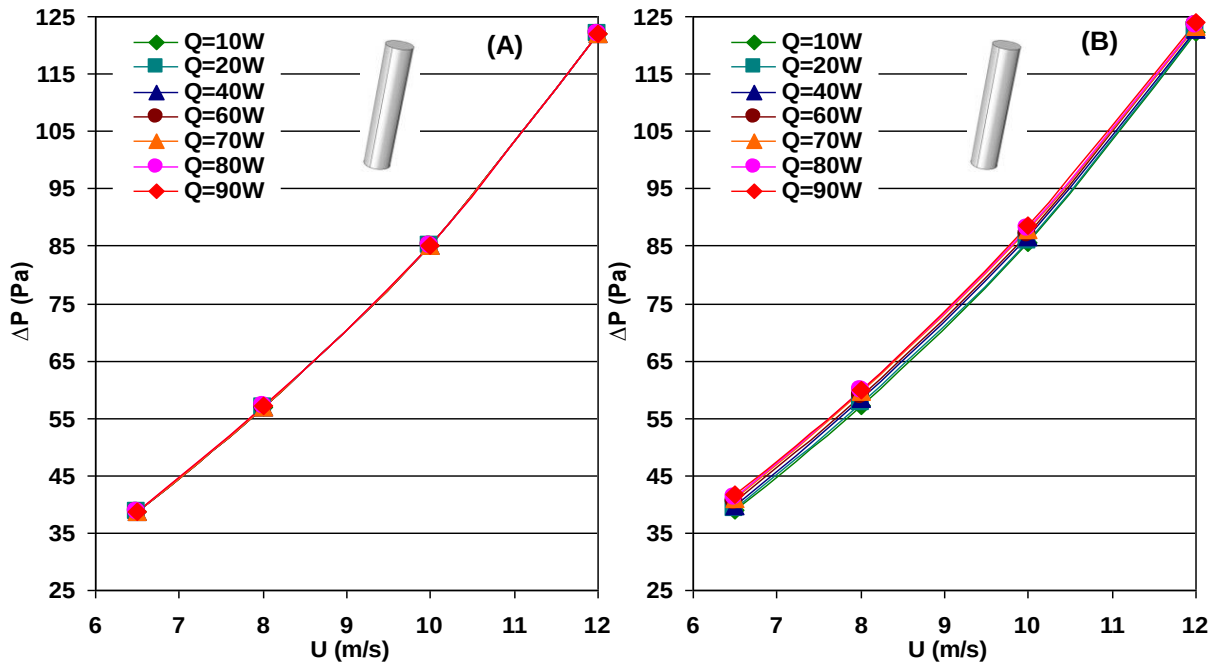

Figure 8.7: Variation in pressure drop through perforated pins (3P) with different applied heat flux and inlet air velocities (A) constant and (B) variable air properties

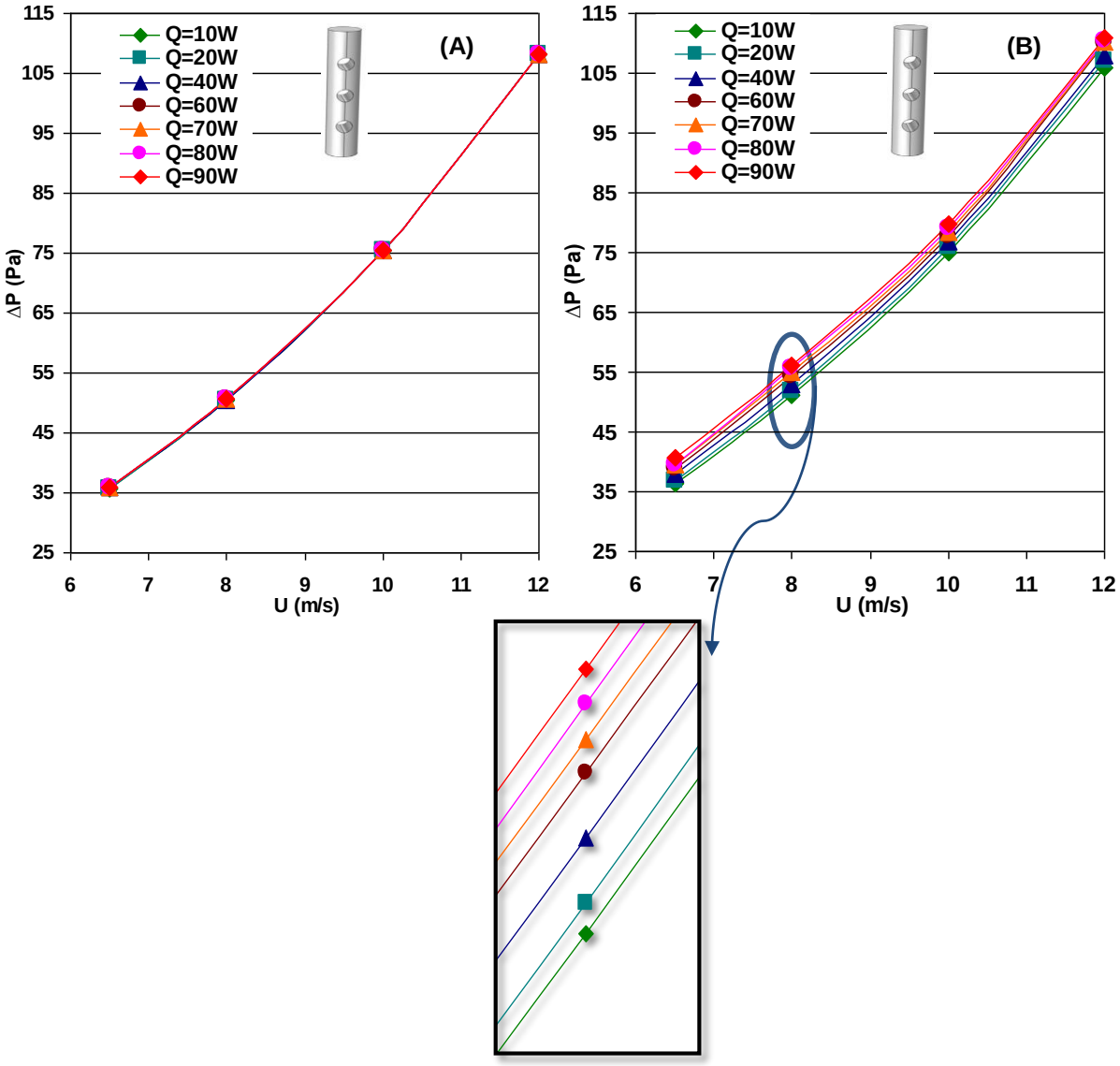

Figure 8.8: Variation in pressure drop through perforated pins (3P) with different applied heat flux and inlet air velocities (A) constant and (B) variable air properties

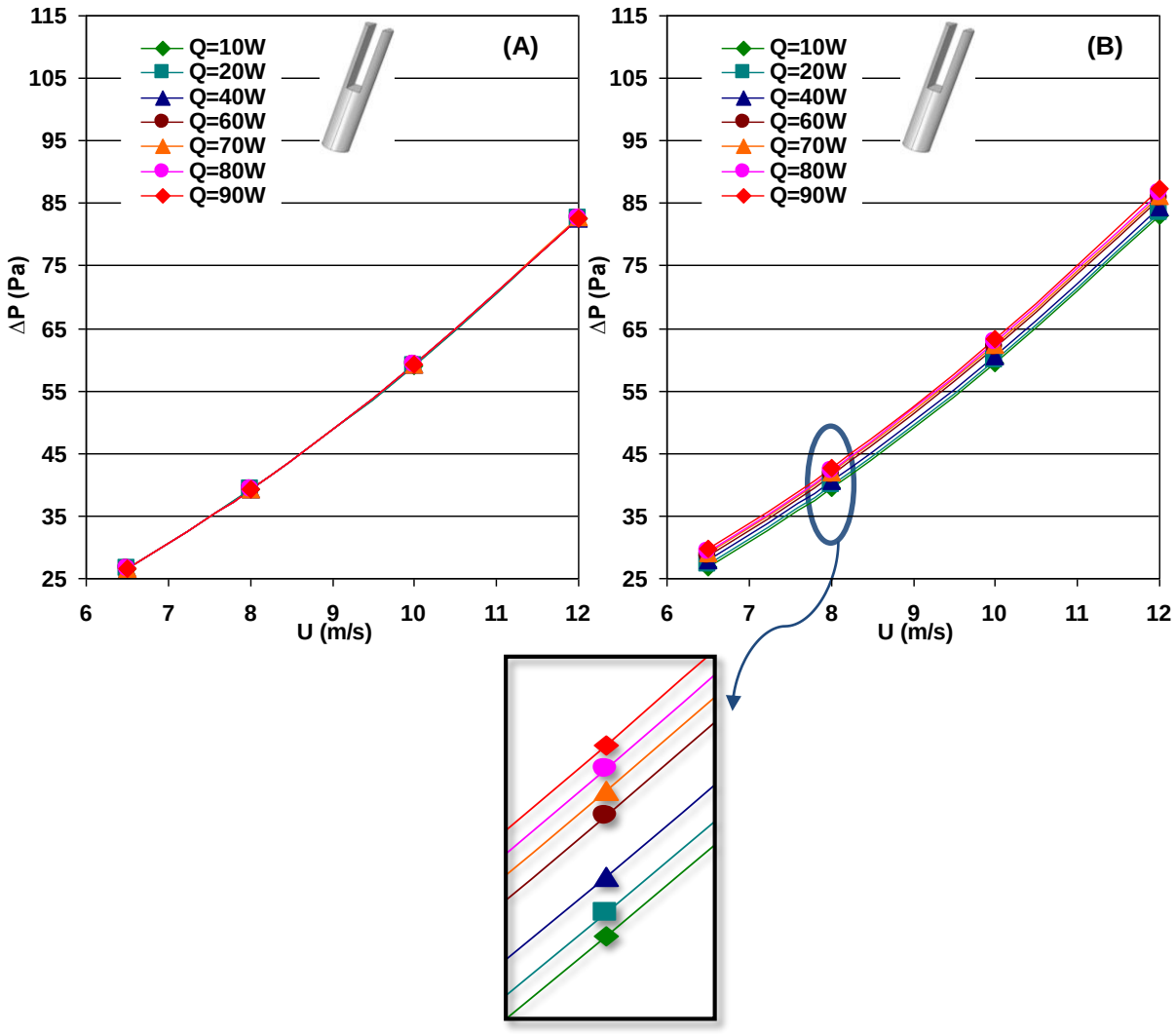

Figure 8.9: Variation in pressure drop through notched pins (7.5P) with different applied heat flux and inlet air velocities (A) constant and (B) variable air properties

Figure 8.10 indicates that the maximum allowed temperature of a PC CPU is as a red line at 85°C for solid (0P), perforated (3P), and notched (7.5N) PHSs with variable air properties. The CPU temperature increases as more heat flux is applied on the base of the heat sinks while it decreases as air velocity increases from 6.5m/s to 12m/s. At heat flux 70W, the critical temperature is exceeded for air speeds below 8m/s. However, the air speed must be above 10m/s for the perforated pin (3P) model and it must be above 12m/s for the solid pins (0P) and notched pins (7.5N) if the power is greater than 90W. Thus, the perforated (3P) model has T_{case} lower than the other pinned heat sink (PHS) models.

Commonly, an applied heat flux of 60W is recommended since the peak CPU temperature is still under the required maximum temperature at the lowest inlet air velocity for all pinned heat sink cases, as shown in Figure 8.10 and that is in agreement with the findings of Yaun et al. (2012).

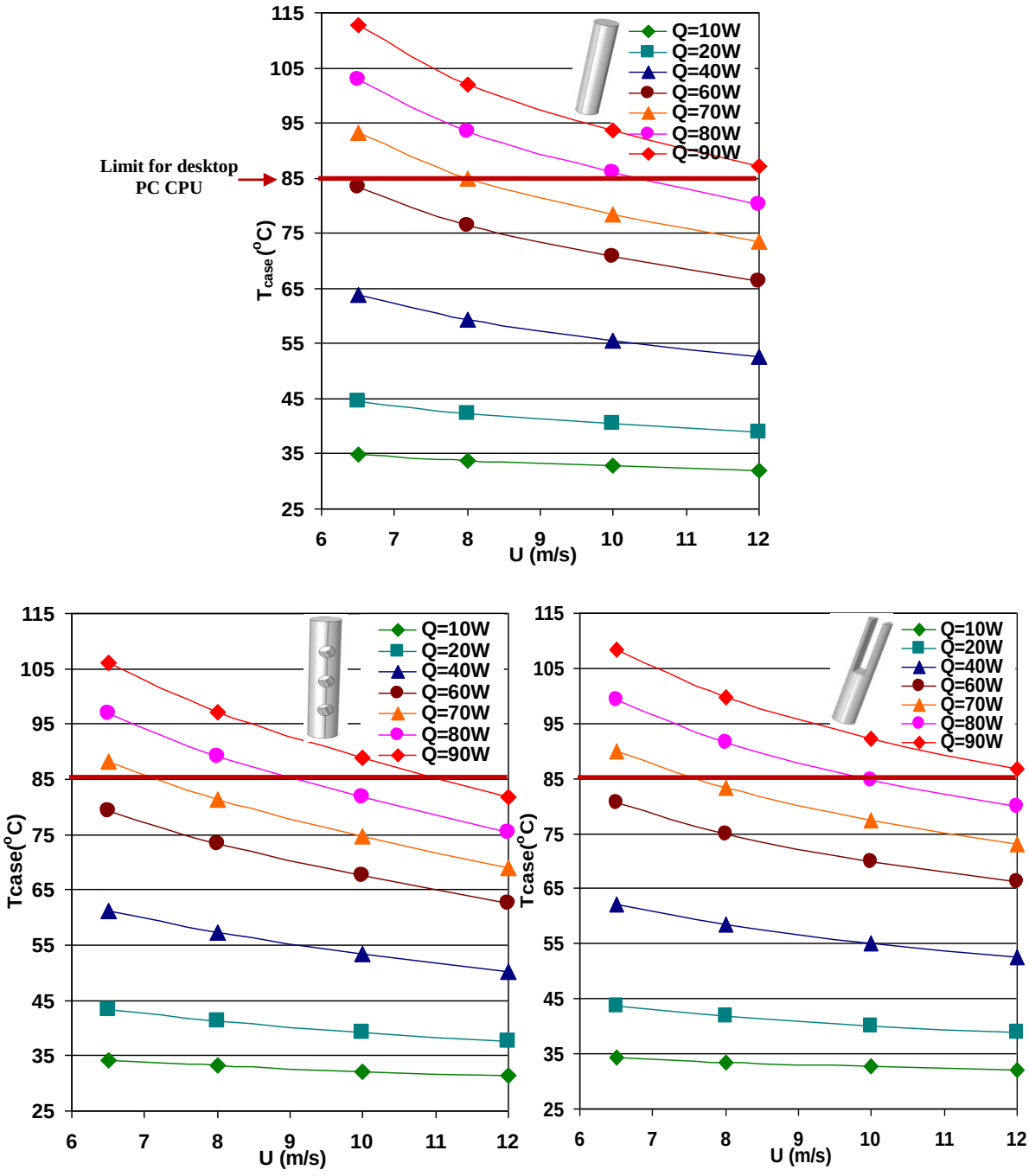

Figure 8.10: Variation in CPU temperature of 0P (top), perforated (3P, Left), and notched (7.5N, Right) pins with different applied heat flux and inlet air velocities

8.4 Conclusion

Results indicate that, with higher pin density, the CPU temperature of the pinned heat sinks reduces while the fan power (pressure drop) increases through the heat sinks. In all cases (0P, 7.5N, and 3P models), halving the pin density from 8 to 4 pins reduces the pressure drop by roughly 35%. The projected Nusselt number (Nu_P) increases up to 50% as the pin density doubles from 4 to 8 columns. However, the total Nusselt number (Nu_T) is slightly enhanced with greater pin density, from 4 to 8 columns for solid and notched pins and from 4 to 6 columns for perforated pins, whereas no further enhancement is seen when increasing the number of pins up to 11.

In terms of the possibility of heating power to the desktop PC CPU for waste heat dissipation, the CPU temperature and the fan power increase when increasing the supplied heating power from 10W to 90W. For example, the pressure drop of the solid (0P) increases by nearly 4% while it is almost 6% and 8% for the 7.5N and 3P pin models, respectively, when increasing supplied heat flux.

Generally, under the same conditions, the heat dissipation performance will be enhanced with more pin columns while the pressure drop will increase. Furthermore, the perforated PHS (3P) has the lowest CPU temperature and largest Nu_T, Nu_P while the notched PHS (7.5) has the lowest pressure drop to satisfy the electronic cooling applications at these conditions of pin density and applied heating power.

Chapter Nine: Conclusions and Recommendations

9.1 Main Conclusions

The main conclusions of this study can be divided into three parts: perforated pinned HSs, slotted and notched pinned HSs, and the practical limitations with optimised pinned heat sink design. Collectively, the PHSs with perforations provide an effective cooling technique to enhance the thermal hydraulic characteristics of heat sinks by improved airflow mixing and increasing of the surface heat transfer area with less fan power required.

9.1.1 Perforated PHSs

The following major conclusions for the perforated pinned HSs have been determined from the present study:

1. The thermal airflow characteristics experimental data of the perforated (3P) PHS model are improved compared with the solid (0P) PHS. The Nusselt number of 3P model is higher while the pressure drop, fan power and CPU temperature are lower than that of 0P model.
2. The maximum deviation between the experimental and numerical results with constant air properties is acceptable within 10-15% for solid (0P) and perforated (3P) models, given the practical difficulties of fabricating PHSs with several perforations, when slight misalignment of the perforations with the dominant airflow direction and finite perforation surface roughness may occur. A further source of error for the heat transfer measurements may be due to the additional thermal resistance because of the brazing process, where the brazing material did not completely fill the gap between the pins and the base plate.
3. Numerical results with variable air properties are closer to the experimental results, within 5-10% for the solid (0P) and perforated (3P) models. Since the air viscosity will increase with increasing air temperatures, more pressure drop is required to push the air through the heat sink.

4. The Nusselt number of the perforated PHSs increases with the presence of more perforations, up to the maximum Nu_T and Nu_P values for the 3P model with 3 perforations and the 5P model with 5 perforations, respectively, compared with the solid (0P) PHS.
5. The pressure drop and pressure drag coefficient reduce with increasing numbers of perforations. Thus, the fan power consumption is reduced for the perforated PHSs compared with the solid PHS design.
6. The average CPU temperature (T_{case}) of the perforated PHSs is lower than that of the solid PHS (0P) design.
7. To maximise the benefits from the perforations, care must be taken to ensure that they are aligned with the dominant flow direction and manufactured with a good-quality surface finish.
8. The change of perforations vertically for the 2P and 3P PHS models only has minor influence on the heat transfer enhancement. Since the perforations are uniformly distributed along the pins, the formation of localised air jets through perforations is also uniform along the pins. In addition, the conductive heat transfer for the perforations at the bottom of the pins may be not enough to augment the Nusselt number due to removing a part of the pin material at the bottom of these pins.
9. When the perforations are moved from the centre to the outside of the pin fin (horizontal perforations movement), the Nusselt number reduces while the pressure drop increases. This may be due to vanishing the localised air jets near the perforations and reducing the porosity of the pins and increasing the blockage to the airflow passing over them.
10. Staggered arrangements for both the solid and perforated PHSs have the lowest CPU temperature compared to the in-line arrangement under the same boundary conditions, while the staggered pin array has the largest pressure drop.
11. The different configurations of perforations shapes show a compromise between the choices of either the elliptic perforated pins, 3EP, which provide the smallest amount of pressure drop and fan power, or the circular perforated pins, 3CP, which have the lowest CPU temperature and highest Nusselt number.

12. The optimum design of the singular perforated PHS (1P), the perforation diameter (d) and the height of perforation (y) have an insignificant effect on the objective functions, T_{case} and P_{fan}.

9.1.2 Slotted and Notched PHSs

In the case of the rectangular perforations, slotted, SPHSs, and notched, NPHSs, the following conclusions can be drawn from this study:

1. The perforations etched into the top of the pins, slotted pins, may offer a more practical means of manufacturing perforated PHSs. For example, either wire Electrical Discharge Machining could be used to directly cut into the notches, or a series of thin cutting discs mounted on a common shaft could be used with support to the pins provided through a jig. This would also retain the high thermal conductivity between the pin and the plate of a heat sink cast from a single block.
2. The Nusselt number might not represent the actual heat transfer rate from heat sink. Because the calculation of the Nusselt number depends on the heat transfer coefficient (h) and the characteristic length (X) and each of these parameters are found in different procedure. Hence, it is required another thermal parameter to evaluate the thermal performance of heat sinks that might be the CPU temperature.
3. The solid PHS (0P) design has Nu_T slightly higher than those of the slotted and notched pins, while the Nu_P of the new SPHSs and NPHSs is the largest. The maximum percentage of increase is seen in Nu_P for the slotted (10S) model compared with the other pin fin designs.
4. Nusselt number based on the projected surface area of a PHS, Nu_P, may be a more effective measure of a heat sink's cooling capacity for a given PHS size compared with Nusselt number based on the total wetted surface area of a PHS, Nu_T.
5. The average CPU temperature (T_{case}) of the slotted and notched pins is slightly lower than for the solid pin model.
6. With respect to the fan power or pressure drop, the SPHS and NPHS designs use a smaller amount of fan power compared with the solid pins. The slotted (10S) pin model uses the lowest fan power. This results in the fan power

consumption of the SPHSs and NPHSs being smaller than that of the solid (0P) PHS model.

7. The optimum design of the notched perforations has demonstrated the practical compromise that has to be struck between a low processor temperature (T_{case}) and the fan power needed to achieve the required rate of cooling.
8. The Pareto curve shows the minimum P_{fan} that can be experienced while ensuring that T_{case} should be below the reference critical temperature of 85^{o}C.

9.1.3 Pin Density and Applied Heat Flux

General conclusions regarding the application limitations of PHSs have been discovered from the present study:

1. In terms of pin density, the projected Nusselt number (Nu_P) increases up to 50% as pin density doubles from 4 to 8 columns for all models. However, halving the pin number from 8 to 4 pins would reduce pressure drop by roughly 35%.
2. The CPU temperature reduces and the Nu_P enhances as pin density increases while the fan power increases.
3. With respect to the possibility of heating power applied on the desktop PC CPU for waste heat dissipation, the CPU temperature and the fan power increase when increasing the supplied heating power from 10W to 90W.
4. The comparison between the circular perforated pins, rectangular slotted and notched pins highlights that a compromise needs to be struck between the choice of perforations since the larger enhancements in heat transfer with multiple circular perforations come at the price of both a significantly increased power consumption and, perhaps most importantly, a much more complex manufacturing process.
5. The total weight of these pins decreases when increasing the number of perforations or the open slotted and notched area; this results in saving material when manufacturing the pin fins and lighter assembly as well. Furthermore, the cost and energy of the force required to drive the air fan (fan power) will reduce remarkably.

Generally, at the same conditions of pin density and applied heating power, the perforated pinned heat sink (3P, 5P) models have the largest Nu_T, Nu_P and lowest T_{case}. If the fan power and pressure drop are considered, however, the notched PHSs are superior to those of the perforated PHSs. That is because the porosity of the notched pins is larger when compared with the perforated pins, leading to increasing the airflow passing across the pins. In addition, the notched pins are much more practical.

Finally, this study provides a mechanism for designing the optimal perforations for specific heat transfer, fan power consumption and heat sink weight requirements.

9.2 Recommendations for Future Works

The following points are suggested for future studies:

1. The investigation of unsteady flow effects (e.g. vortex shedding) could be proposed as a future consideration.
2. Perforated heat sink models such as perforated pinned HS, perforated strip fins HS, perforated plate fin HS, perforated folded fin HS and on lateral perforation plate fins HS can be experimentally and numerically investigated using water, Nanofluids, and polymers liquid as a coolant for forced and natural convection heat transfer and fluid flow.
3. The thermal and airflow characteristics of perforated strip fins heat sink can be experimentally and numerically conducted for forced and natural convection heat transfer and fluid flow.
4. It is recommended that the experimental and numerical investigation of natural convection heat transfer and fluid flow should be studied for perforated pinned heat sink models.
5. The perforations can be employed for other types of fins, such as square pins, elliptic pins, and compact plate-pin heat sinks to study the thermo-fluid characteristics using air, water, Nanofluids, and polymer liquid as a coolant for forced and natural convection heat transfer and fluid flow.
6. The perforations might be employed for other applications that require remove amount of heat such as solar collectors, PV panels, turbine blades etc.
7. Investigate the effect of noise and vibration of high level of inlet fluid on thermal and hydraulic characteristics of solid and perforated heat sinks.

References

AIREDALE COMPANY in the UK, http://www.airedale.com/web/Home.htm.

ALAM, T., SAINI, R. P. and SAINI, J. S. (2014a). Heat and flow characteristics of air heater ducts provided with turbulators—A review. Renewable and Sustainable Energy Reviews, 31, 289-304.

ALAM, T., SAINI, R. P., and SAINI, J. S. (2014). Experimental investigation on heat transfer enhancement due to V-shaped perforated blocks in a rectangular duct of solar air heater. Energy Conversion and Management. 81, 374-383.

ALKASMOUL, FAHAD SALEH (2015) Characterisation of the Properties and Performance of Nanofluid Coolants with Analysis of Their Feasibility for Datacentre Cooling. PhD thesis, University of Leeds

ALMANEEA, ABDULMAJEED H (2014) Thermal analysis of liquid immersed electronics for data centres. PhD thesis, University of Leeds.

ALMOLI, A. M. (2013). Air flow management inside data centres. PhD thesis, University of Leeds.

ALUTRONIC.DE (2015) http://www.alutronic.de/POWERBLOCS-Stiftkuehlkoerper-Aluminium-pur_detail_804.html

AMOL B. D., FARKADE H. S. (2013). Heat Transfer Analysis of Cylindrical Perforated Fins in Staggered Arrangement. International Journal of Innovative Technology and Exploring Engineering (IJITEE), 28, 621-632.

ANANDAN, S. and RAMALINGAM, V. (2008). Thermal management of electronics: A review of literature. Thermal Science, 12, 5-26.

ANSYS FLUENT User's Guide (2013).

ARULARASAN R., VELRAJ R. (2008) CFD Analysis in a Heat Sink for Cooling of Electronic Devices. The Internet and Management, 16, 1-11.

BERGMAN, T.L., INCROPERA, F.P. and LAVINE, A.S., 2011. Fundamentals of heat and mass transfer. John Wiley & Sons.

BUSINESS COMMUNICATIONS COMPANY (BCC Research, 2011) http://www.bccresearch.com/market-research/semiconductor-manufacturing/thermal-management-technologies-market-smc024g.html.

CENGEL, YUNUS A., CIMBALA JOHN M. (2006) Fluid Mechanics, Fundamentals and Applications. McGraw-Hill.

CHAUBE, A., SAHOO, P., and SOLANKI, S. (2006). Analysis of heat transfer augmentation and flow characteristics due to rib roughness over absorber plate of a solar air heater. Renewable Energy. 31, 317-331.

CHI, Y.Q., SUMMERS, J., HOPTON, P., DEAKIN, K., REAL, A., KAPUR, N. and THOMPSON, H., 2014, March. Case study of a data centre using enclosed, immersed, direct liquid-cooled servers. In Semiconductor Thermal Measurement and Management Symposium (SEMI-THERM), 2014 30th Annual (pp. 164-173). IEEE.

CHIANG, K.T. (2005). Optimization of the design parameters of Parallel-Plain Fin heat sink module cooling phenomenon based on the Taguchi method. International Communications in Heat and Mass Transfer, 32, 1193-1201.

CHIANG, K.T., CHOU, C.C., and LIU, N.M. (2009). Application of response surface methodology in describing the thermal performances of a pin-fin heat sink. International Journal of Thermal Sciences. 48, 1196-1205.

DAI, J., OHADI, M. M., DAS, D., and PECHT, M. (2014). Optimum cooling of data centers: application of risk assessment and mitigation techniques.

DEWAN, A., MAHANTA, P., RAJU, K. S. and KUMAR, P. S. (2004). Review of passive heat transfer augmentation techniques. Proceedings of the Institution of Mechanical Engineers, Part A: Journal of Power and Energy, 218, 509-527.

DEWAN, A., PATRO, P., KHAN, I., and MAHANTA, P. (2010). The effect of fin spacing and material on the performance of a heat sink with circular pin fins. Proceedings of the Institution of Mechanical Engineers, Part A: Journal of Power and Energy. 224, 35-46.

DHANAWADE, K. H. and DHANAWADE H. S. (2010). Enhancement of Forced Convection Heat Transfer from Fin Arrays with Circular Perforation. IEEE, Frontiers in Automobile and Mechanical Engineering (FAME), 192-196.

DHANAWADE, K. H., SUNNAPWAR, V. K. and DHANAWADE, H. S. (2014). Optimization of Design Parameters for Lateral Circular Perforated Fin Arrays under Forced Convection. Heat Transfer-Asian Research.

DHANAWADE, K. H., SUNNAPWAR, V. K., and DHANAWADE, H. S. (2014). Thermal Analysis of Square and Circular Perforated Fin Arrays by Forced Convection. International Journal of Current Engineering and Technology, 2, 109-114.

DIANI, A., MANCIN, S., ZILIO, C. and ROSSETTO, L. (2013). An assessment on air forced convection on extended surfaces: Experimental results and numerical modeling. International Journal of Thermal Sciences, 67, 120-134.

Diit.cz (2013) http://diit.cz/clanek/prichazi-amd-opteron-x-hp-jej-nabidne-v-projektu-moonshot

GANORKAR, A.B. and KRIPLANI, V.M. (2012). Experimental Study of Heat Transfer Rate by Using Lateral Perforated Fins in a Rectangular Channel. MIT International Journal of Mechanical Engineering, 2, 91-96.

GREENBERG, S., MILLS, E., TSCHUDI, B., RUMSEY, P. and MYATT, B. (2006). Best practices for data centres: Lessons learned from benchmarking 22 data centres. Proceedings of the ACEEE Summer Study on Energy Efficiency in Buildings in Asilomar, CA. ACEEE, August, 3, pp.76-87.

GURRUM, S. P., SUMAN, S. K., JOSHI, Y. K., and FEDOROV, A. G. (2004). Thermal issues in next-generation integrated circuits. Device and Materials Reliability, IEEE Transactions on, 4, 709-714.

HOLMAN, J. P. (2011). Experimental Methods for Engineers, McGraw Hill Book Company, 10971, 8th edition.

INCROPRERA, F., DEWITT, P.D., BERGMAN, T.L., LAVINE, S. (2011). Fundamentals of Heat and Mass Transfer, 7th edition, John Wiley and Sons Inc.

ISMAIL M.F. (2013). Effects of perforations on the thermal and fluid dynamic performance of a heat exchanger. IEEE Transactions on Components, Packaging and Manufacturing Technology. 3, 1178-1185.

ISMAIL M.F., HASAN M.N., and ALI M. (2014). Numerical simulation of turbulent heat transfer from perforated plate-fin heat sinks. Heat and Mass Transfer/Waerme- Und Stoffuebertragung. 50, 509-519.

ISMAIL, M. F., HASAN, M. N. and ALI, M. (2013a). Numerical simulation of turbulent heat transfer from perforated plate-fin heat sinks. Heat and Mass Transfer, 50, 509-519.

ISMAIL, M. F., HASAN, M. N. and SAHA, S. C. (2014). Numerical study of turbulent fluid flow and heat transfer in lateral perforated extended surfaces. Energy, 64, 632-639.

ISMAIL, M. F., REZA, M. O., ZOBAER, M. A. and ALI, M. (2013b). Numerical Investigation of Turbulent Heat Convection from Solid and Longitudinally Perforated Rectangular Fins. Procedia Engineering, 56, 497-502.

JENG, T. M., and TZENG, S. C. (2007). Pressure drop and heat transfer of square pin-fin arrays in in-line and staggered arrangements. International Journal of Heat and Mass Transfer, 50, 2364-2375.

JIA, T. H., KIM, S. Y., and CHANG, K. S. (2004). Cooling performance of triangular folded fin heat sinks in a duct flow. Thermal and Thermomechanical Phenomena in Electronic Systems, ITHERM'04. The Ninth Intersociety Conference, 325-330. IEEE.

JIA, T. H., KIM, S. Y., and HYUN, J. M. (2007). Pressure Drop and Heat Transfer Correlations for Triangular Folded Fin Heat Sinks. IEEE TRANSACTIONS ON COMPONENTS AND PACKAGING TECHNOLOGIES. 30, 3-8.

JONSSON, H., and MOSHFEGH, B. (2001). Modeling of the thermal and hydraulic performance of plate fin, strip fin, and pin fin heat sinks-influence of flow bypass. Components and Packaging Technologies, IEEE Transactions on, 24, 142-149.

KHATIR, Z., TAHERKHANI, A., PATON, J., THOMPSON, H., KAPUR, N., and TOROPOV, V. (2015). Energy thermal management in commercial bread-baking using a multi-objective optimisation framework. Applied Thermal Engineering. 80, 141-149.

KHOSHNEVIS, A., TALATI, F., JALAAL, M. and ESMAEILZADEH, E (2009a). Analysis of Heat-Transfer Enhancement and Design Parameters of Heat-Sink with Perforated Rectangular Ribs. International Journal of Scientific & Engineering Research, 4, 1-8.

KHOSHNEVIS, A., TALATI, F., JALAAL, M. and ESMAEILZADEH, E (2009b). Heat Transfer Enhancement of Solt and Hole Shape Perforateions in Rectangular Ribs of a 3D Channel. 17th Annual (International) Conference on Mechanical Engineering, University of Tehran, 1-6.

KIM, D.K., KIM, S. J. and BAE, J.-K. (2009). Comparison of thermal performances of plate-fin and pin-fin heat sinks subject to an impinging flow. International Journal of Heat and Mass Transfer, 52, 3510-3517.

KIM, T. Y. and KIM, S. J. (2009). Fluid flow and heat transfer characteristics of cross-cut heat sinks. International Journal of Heat and Mass Transfer, 52, 5358-5370.

KRAUS, A.D., AZIZ, A. and WELTY, J., (2002). Extended surface heat transfer. John Wiley & Sons.

KUMAR, V., and BARTARIA, V. N. (2013). CFD Analysis of an Elliptic Pin Fin Heat Sink using ANSYS Fluent v12. International Journal of Modern Engineering Research (IJMER), 2, 1115-1122.

LEUNG, C. W., and PROBERT, S. D. (1989). Heat-exchanger performance: effect of orientation. Applied energy, 33(4), 235-252.

MCMILLIN, T. W. (2007). Thermal Management Solutions for Low Volume Complex Electronic Systems. M. Sc. Thesis, College Park, University of Maryland.

MOHAN, R. and GOVINDARAJAN, P. (2011). Experimental and CFD analysis of heat sinks with base plate for CPU cooling. Journal of Mechanical Science and Technology, 25, 2003-2012.

MOSTAFAVI, G. (2012). Natural convective heat transfer from interrupted rectangular fins. Master of Applied Sciences: School of Engineering Science, Simon Fraser University.

NABATI, H. (2008). Optimal pin fin heat exchanger surface. PhD Thesis, School of Sustainable Development of Society and Technology.

NAGARANI, N., MAYILSAMY, K., MURUGESAN, A. and KUMAR, G. S. (2014). Review of utilization of extended surfaces in heat transfer problems. Renewable and Sustainable Energy Reviews, 29, 604-613.

NAIDU, M. S., and KAMARAJU, V. (2013). High voltage engineering. New York, McGraw-Hill.

NAIK, S., PROBERT, S., and SHILSTON, M. (1987). Forced-convective steady-state heat transfers from shrouded vertical fin arrays, aligned parallel to an undisturbed air-stream. Applied Energy. 26, 137-158.

NAIK, S., PROBERT, S., and SHILSTON, M. (1987). Forced-convective steady-state heat transfers from shrouded vertical fin arrays, aligned parallel to an undisturbed air-stream. Applied Energy. 26, 137-158.

NAJAFI H., NAJAFI B., & HOSEINPOORI P. (2011). Energy and cost optimization of a plate and fin heat exchanger using genetic algorithm. Applied Thermal Engineering. 31, 1839-1847.

NAPHON, P. and KHONSEUR, O. (2009). Study on the convective heat transfer and pressure drop in the micro-channel heat sink. International Communications in Heat and Mass Transfer, 36, 39-44.

NAPHON, P. and KLANGCHART, S. (2011). Effects of outlet port positions on the jet impingement heat transfer characteristics in the mini-fin heat sink. International Communications in Heat and Mass Transfer, 38, 1400-1405.

NAPHON, P. and NAKHARINTR, L. (2013). Heat transfer of Nanofluids in the mini-rectangular fin heat sinks. International Communications in Heat and Mass Transfer, 40, 25-31.

NAPHON, P. and SOOKKASEM, A. (2007). Investigation on heat transfer characteristics of tapered cylinder pin fin heat sinks. Energy Conversion and Management, 48, 2671-2679.

NAPHON, P. and WONGWISES, S. (2010). Investigation on the jet liquid impingement heat transfer for the central processing unit of personal computers. International Communications in Heat and Mass Transfer, 37, 822-826.

NAPHON, P., and WONGWISES, S. (2011). Experimental Study of Jet Nanofluids Impingement System for Cooling Computer Processing Unit. Journal of Electronics Cooling and Thermal Control. 01, 38-44.

NAPHON, P., KLANGCHART, S. and WONGWISES, S. (2009). Numerical Investigation of Heat Transfer Enhancement for a Perforated Fin in Natural Convection. International Communications in Heat and Mass Transfer, 36, 834-840.

NAPHON, P., KLANGCHART, S. and WONGWISES, S. (2009). Numerical investigation on the heat transfer and flow in the mini-fin heat sink for CPU. International Communications in Heat and Mass Transfer, 36, 834-840.

NARAYANAN, A., TOROPOV, V. V., WOOD, A. S., and CAMPEAN, I. F. (2007). Simultaneous model building and validation with uniform designs of experiments. Engineering Optimization, 39(5), 497-512.

NDAO, S., PELES, Y. and JENSEN, M. K. (2009). Multi-objective thermal design optimization and comparative analysis of electronics cooling technologies. International Journal of Heat and Mass Transfer, 52, 4317-4326.

OH S.K., PUTRA A.B.K., and AHN S.W. (2009). Heat transfer and frictional characteristics in rectangular channel with inclined perforated baffles. Proceedings of World Academy of Science, Engineering and Technology. 37, 324-329.

PAN, Y., YIN, R., and HUANG, Z. (2008). Energy modeling of two office buildings with data center for green building design. Energy & Buildings. 40, 1145-1152.

PRASHANTA DUTTA, S. D. (1998). Effect of baffle size, perforation, and orientation on internal heat transfer enhancement. International Journal of Heat and Mass Transfer, 41, 3005-3013

PUTRA, A., AHN, S., and KANG, H. (2009). A numerical study on heat transfer and friction in rectangular channel with inclined perforated baffles. The Canadian Journal of Chemical Engineering. 87, 415-421.

RAMESHA .D .K, MADHUSUDAN M. (2012). Thermal Characterization of Heat Sinks in Electronics Cooling Applications. International Journal of Emerging trends in Engineering and Development, 2, 521-529.

SAHIN, B. and DEMIR, A. (2008a). Performance analysis of a heat exchanger having perforated square fins. Applied Thermal Engineering, 28, 621-632.

SAHIN, B. and DEMIR, A. (2008b). Thermal performance analysis and optimum design parameters of heat exchanger having perforated pin fins. Energy Conversion and Management, 49, 1684-1695.

SAHIN, B., YAKUT, K., KOTCIOGLU, I. and CELIK, C. (2005). Optimum design parameters of a heat exchanger. Applied Energy, 82, 90-106.

SARA, O. N, T. PEKDEMIR, S. YAPICI AND H. ERSAHAN (2000). Thermal Performance Analysis for Solid and Perforated Blocks Attached on a Flat Surface in Duct Flow. Energy Conversion & Management, 41, 1010-1028.

SARA, O. N, PEKDEMIR, S, S. YAPICI AND M. YILMAZ (2001). Heat Transfer Enhancement in a Channel Flow with Perforated Rectangular Blocks. International Journal of Heat and Fluid Flow, 22, 509-518.

SARA, O. N., (2003). Performance analysis of rectangular ducts with staggered square pin fins. Energy Conversion and Management. 44, 1787-1803.

SEYF, H. R. and LAYEGHI, M. (2010). Numerical Analysis of Convective Heat Transfer From an Elliptic Pin Fin Heat Sink With and Without Metal Foam Insert. Journal of Heat Transfer, 132, 071401.

SHAERI, M. R. and JEN, T.C. (2012). The effects of perforation sizes on laminar heat transfer characteristics of an array of perforated fins. Energy Conversion and Management, 64, 328-334.

SHAERI, M. R. and YAGHOUBI, M. (2009a). Numerical analysis of turbulent convection heat transfer from an array of perforated fins. International Journal of Heat and Fluid Flow, 30, 218-228.

SHAERI, M. R. and YAGHOUBI, M. (2009b). Thermal enhancement from heat sinks by using perforated fins. Energy Conversion and Management, 50, 1264-1270.

SHAERI, M. R., YAGHOUBI, M. and JAFARPUR, K. (2009). Heat transfer analysis of lateral perforated fin heat sinks. Applied Energy, 86, 2019-2029.

SHAH, A., PATEL, C., BASH, C., SHARMA, R., and SHIH, R. (2008). Impact of rack-level compaction on the data center cooling ensemble. In Thermal and Thermomechanical Phenomena in Electronic Systems, ITHERM. 11th Intersociety Conference on (pp. 1175-1182). IEEE.

SHAUKATULLAH, H., STORR, W. R., HANSEN, B. J., & GAYNES, M. A. (1996). Design and Optimization of Pin Fin Heat Sinks for Low Velocity Applications. IEEE TRANSACTIONS ON COMPONENTS PACKAGING AND MANUFACTURING TECHNOLOGY PART A. 19, 486-494.

SOODPHAKDEE DENPONG, M. B. A. D. W. C. (2001). A Comparison of Fin Geometries for Heat Sinks in Laminar Forced Convection Part I: Round Elliptic, and Plate Fins in Staggered and In-Line Configurations The International Journal of Microcircuits and Electronic Packaging, 24, 68-76.

SPARROW, E. M., RAMSEY, J. W., and ALTEMANI, C. A. C. (1980). Experiments on In-line Pin Fin Arrays and Performance Comparisons with Staggered Arrays. Journal of Heat Transfer. 102, 44.

TANDA, G. (2001). Heat Transfer and Pressure Drop in a Rectangular Channel with Diamond-Shaped Elements. International Journal of Heat and Mass Transfer, 44, 3529-3541.

THE RAYPAK COMPANY IN THE USA, http://www.raypak.com/.

Triplet (2012) Optimize Airflow Management in your Data Center. http://www.triplite.com/lp/direct/rackcooling/

TUMA P.E. (2010). The merits of open bath immersion cooling of datacom equipment. Annual IEEE Semiconductor Thermal Measurement and Management Symposium. 123-131.

VELAYATI, E. and YAGHOUBI, M. (2005). Numerical study of convective heat transfer from an array of parallel bluff plates. International Journal of Heat and Fluid Flow, 26, 80-91.

VENTOLA, L., CHIAVAZZO, E., CALIGNANO, F., MANFREDI, D., and ASINARI, P. (2014, April). Heat Transfer Enhancement by Finned Heat Sinks with Micro-structured Roughness. In Journal of Physics: Conference Series (Vol. 494, No. 1, p. 012009). IOP Publishing.

VERSTEEG, H. K., and MALALASEKERA, W. (2007). An introduction to computational fluid dynamics: the finite volume method. Pearson Education.

VILLA, H. (2006), Rittal liquid cooling series, White paper 04. http://www.rittal.de/downloads/rimatrix5/cooling/WP%20Liquid%20Cooling_Stand%20Jan%202006_englisch.pdf.

YAGHOUBI, M., SHAERI, M. R., and JAFARPUR, K. (2009). THREE-DIMENSIONAL NUMERICAL LAMINAR CONVECTION HEAT TRANSFER AROUND LATERAL PERFORATED FINS. Computational Thermal Sciences. 1, 323-340.

YAKUT, K., ALEMDAROGLU, N., KOTCIOGLU, I. and CELIK, C. (2006a). Experimental investigation of thermal resistance of a heat sink with hexagonal fins. Applied Thermal Engineering, 26, 2262-2271.

YAKUT, K., ALEMDAROGLU, N., SAHIN, B. and CELIK, C. (2006b). Optimum design-parameters of a heat exchanger having hexagonal fins. Applied Energy, 83, 82-98.

YANG, J., ZENG, M., WANG, Q. and NAKAYAMA, A. (2010). Forced Convection Heat Transfer Enhancement by Porous Pin Fins in Rectangular Channels. Journal of Heat Transfer, 132, 051702.

YANG, K. S., CHU, W. H., CHEN, I. Y. and WANG, C. C. (2007). A comparative study of the airside performance of heat sinks having pin fin configurations. International Journal of Heat and Mass Transfer, 50, 4661-4667.

YANG, Y. T. and PENG, H. S. (2009a). Investigation of planted pin fins for heat transfer enhancement in plate fin heat sink. Microelectronics Reliability, 49, 163-169.

YANG, Y. T. and PENG, H. S. (2009b). Numerical Study of Thermal and Hydraulic Performance of Compound Heat Sink. Numerical Heat Transfer, Part A: Applications, 55, 432-447.

YU X.L., FENG Q.K. LIU Q. (2003). Research on the heat transfer and flow performance of a composite heat sink, Journal of Xi'an Jiaotong University. 37(7): p. 670-673.

YU X.L., FENG Q.K., FENG J.M. (2004). Research on thermal performance of plate-pin fin heat sink, Journal of Xi'an Jiaotong University, 38(11):p. 1114-1118.

YU, X., FENG, J., FENG, Q. and WANG, Q. (2005). Development of a plate-pin fin heat sink and its performance comparisons with a plate fin heat sink. Applied Thermal Engineering, 25, 173-182.

YUAN, W., ZHAO, J., TSO, C. P., WU, T., LIU, W. and MING, T. (2012). Numerical simulation of the thermal hydraulic performance of a plate pin fin heat sink. Applied Thermal Engineering, 48, 81-88.

ZEADALLY, S., KHAN, S. U., and CHILAMKURTI, N. (2012). Energy-efficient networking: past, present, and future. The Journal of Supercomputing: An International Journal of High-Performance Computer Design, Analysis, and Use. 62, 1093-1118.

ZHANG, H. Y., PINJALA, D., WONG, T. N., TOH, K. C. and JOSHI, Y. K. (2005). Single-phase liquid cooled microchannel heat sink for electronic packages. Applied Thermal Engineering, 25, 1472-1487.

ZHOU, F. and CATTON, I. (2011). Numerical Evaluation of Flow and Heat Transfer in Plate-Pin Fin Heat Sinks with Various Pin Cross-Sections. Numerical Heat Transfer, Part A: Applications, 60, 107-128.

Appendix A: Drawing of Experimental Rig Design

The parts of experimental rig design such duct and test sections are illustrated as drawing figures in this appendix. All dimensions in mm.

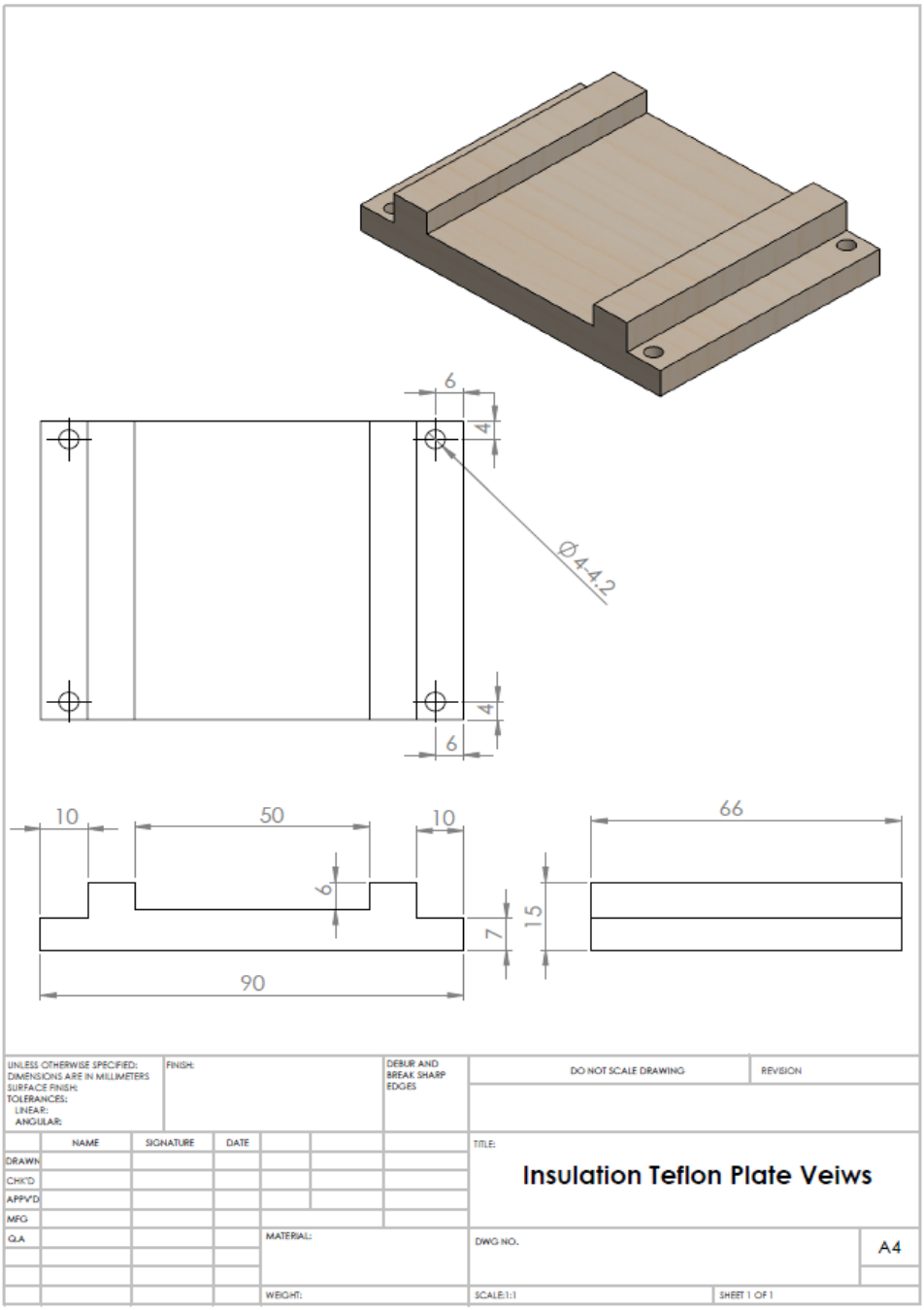

Figure A 1: Insulation Teflon plate views

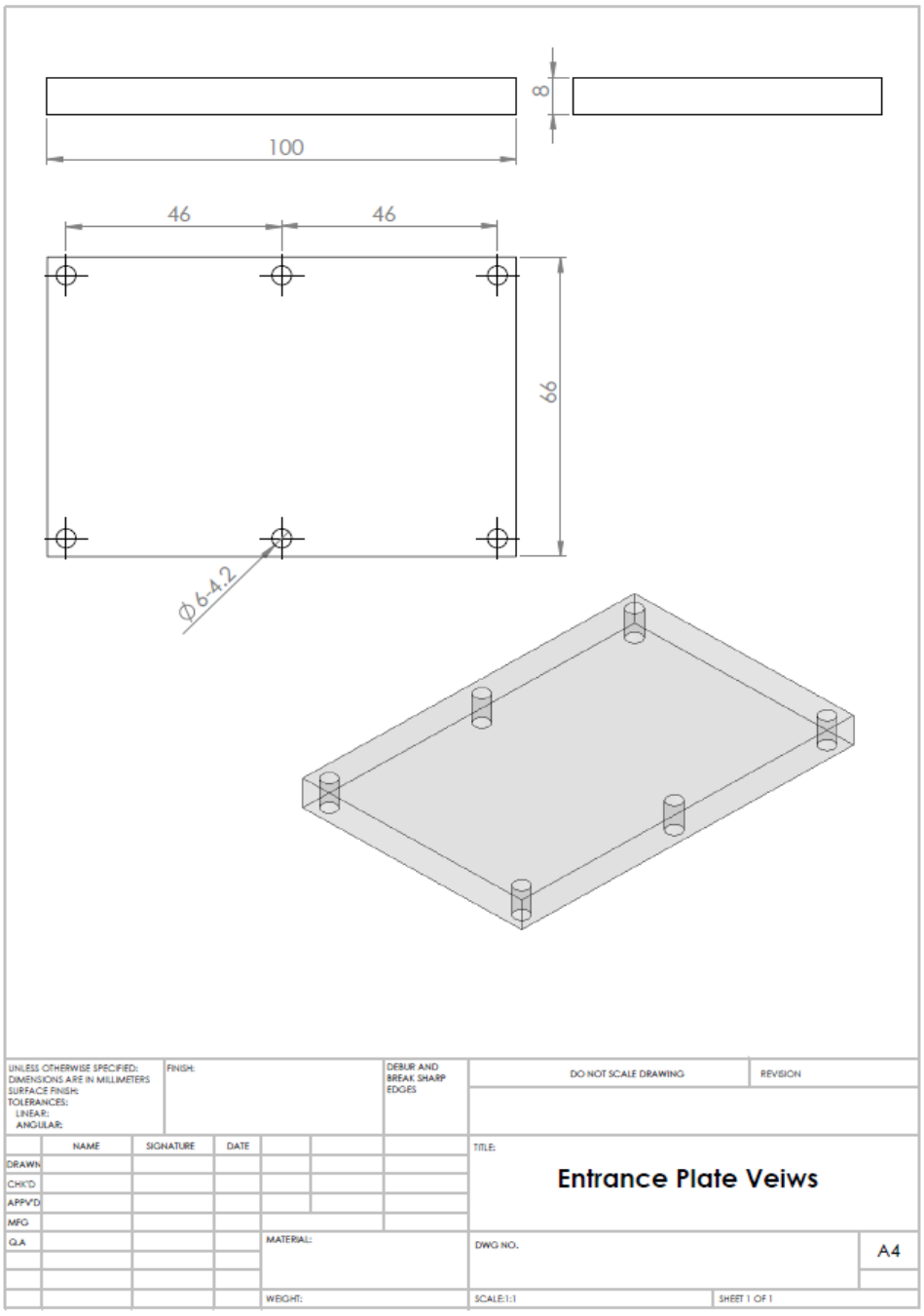

Figure A 2: Other plate of duct views

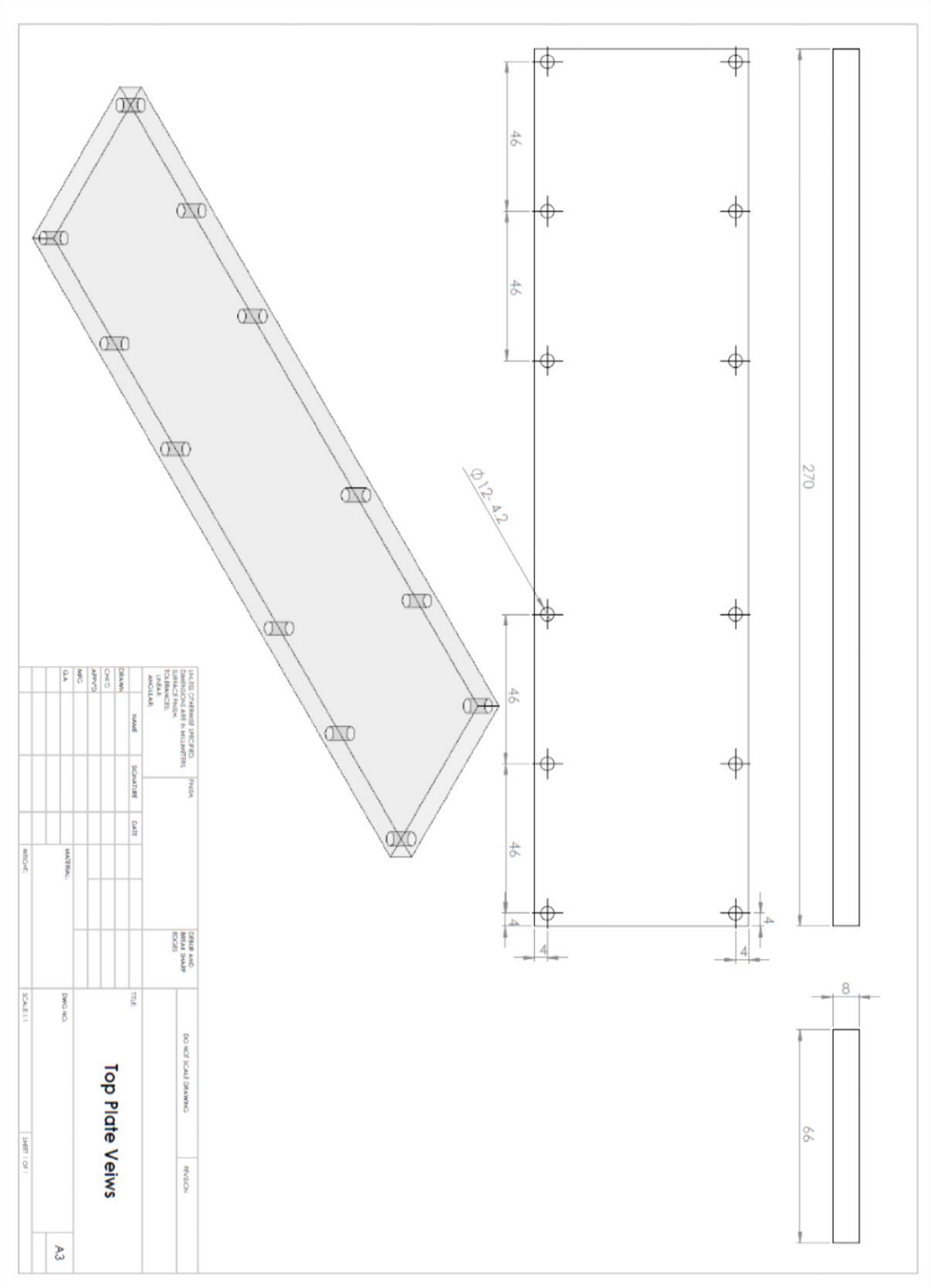

Figure A 3: Top Plate of duct views

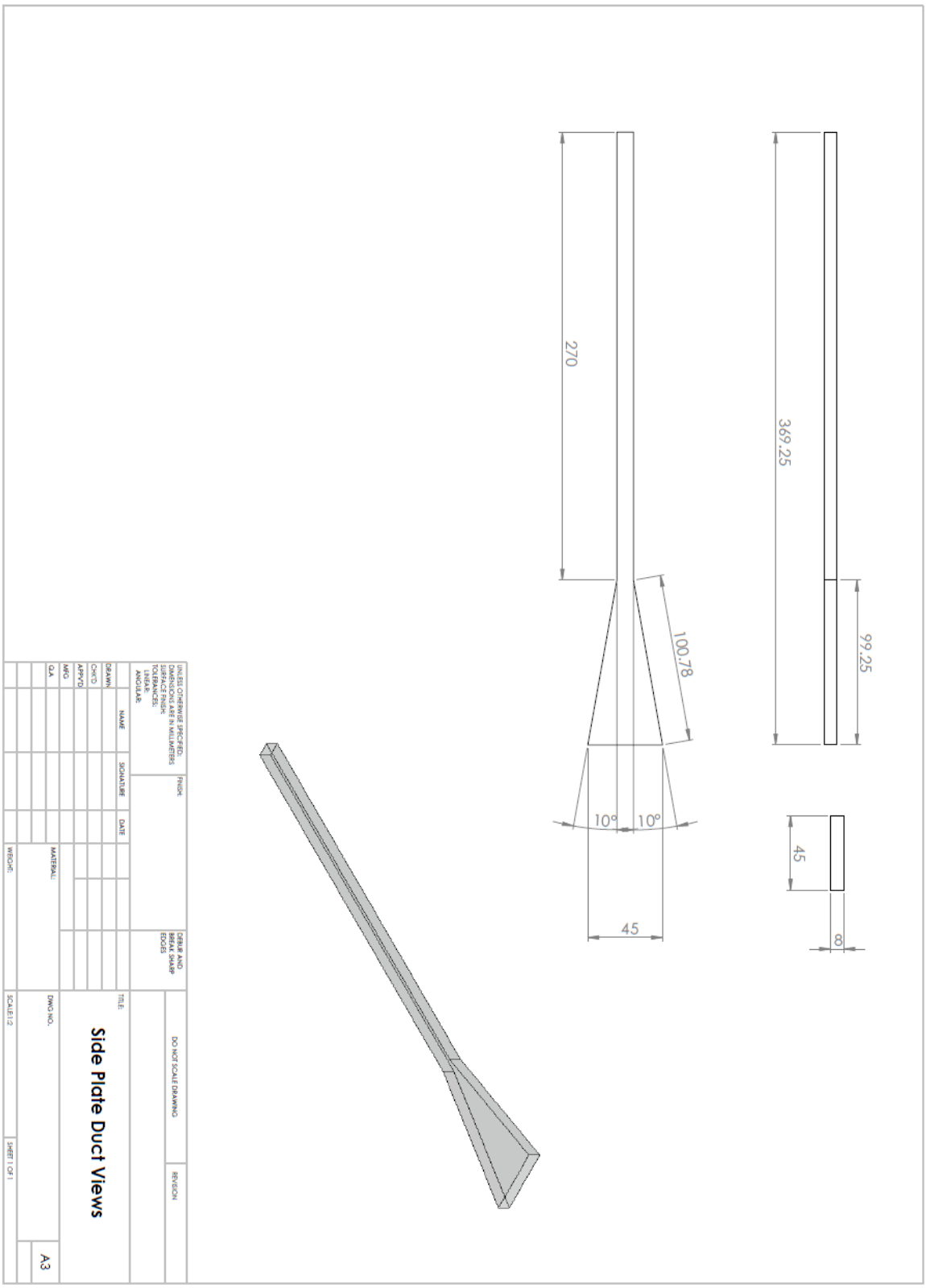

Figure A 4: Side plate of duct views

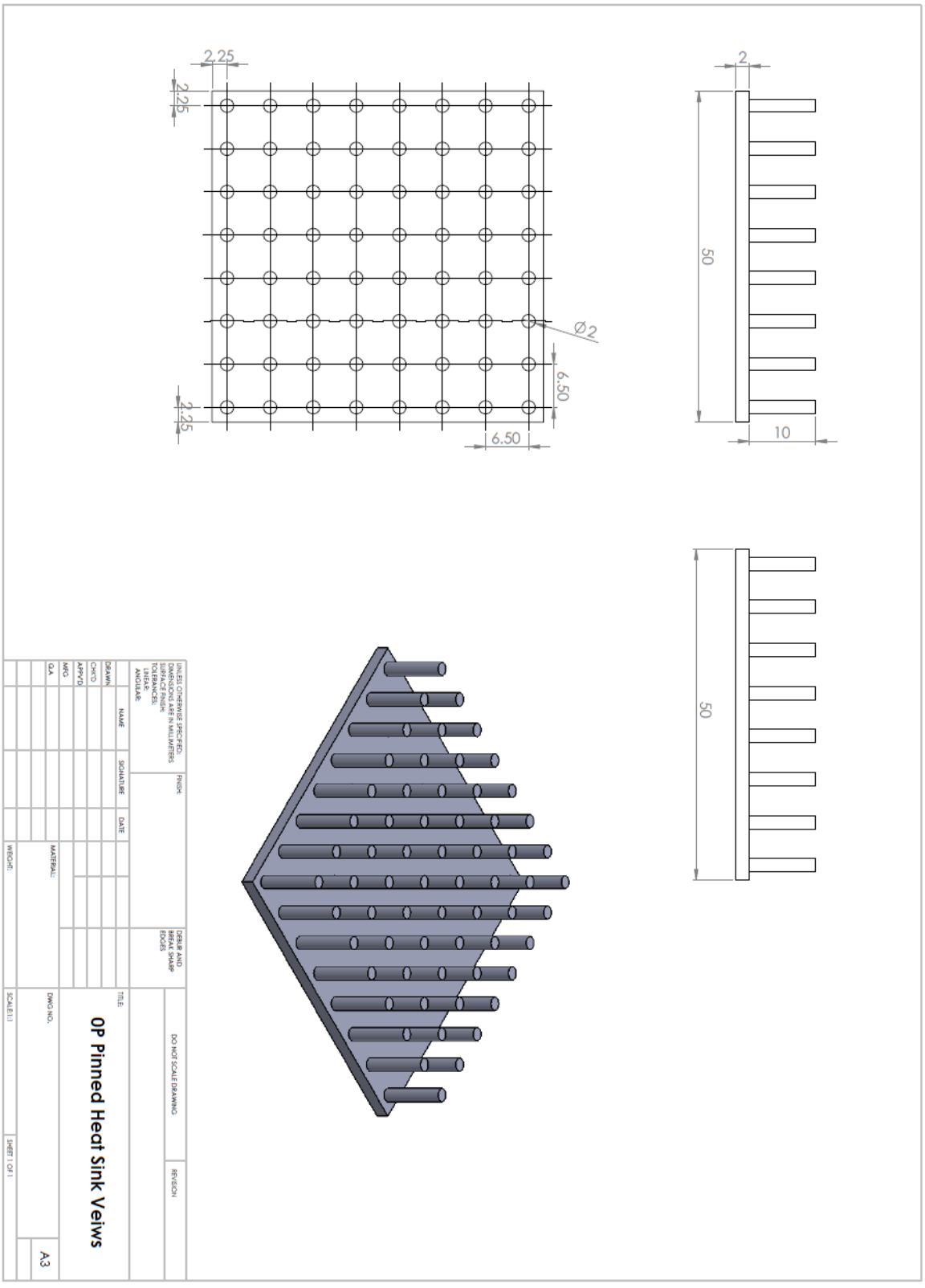

Figure A 5: Solid pinned heat sinks (0P) model views

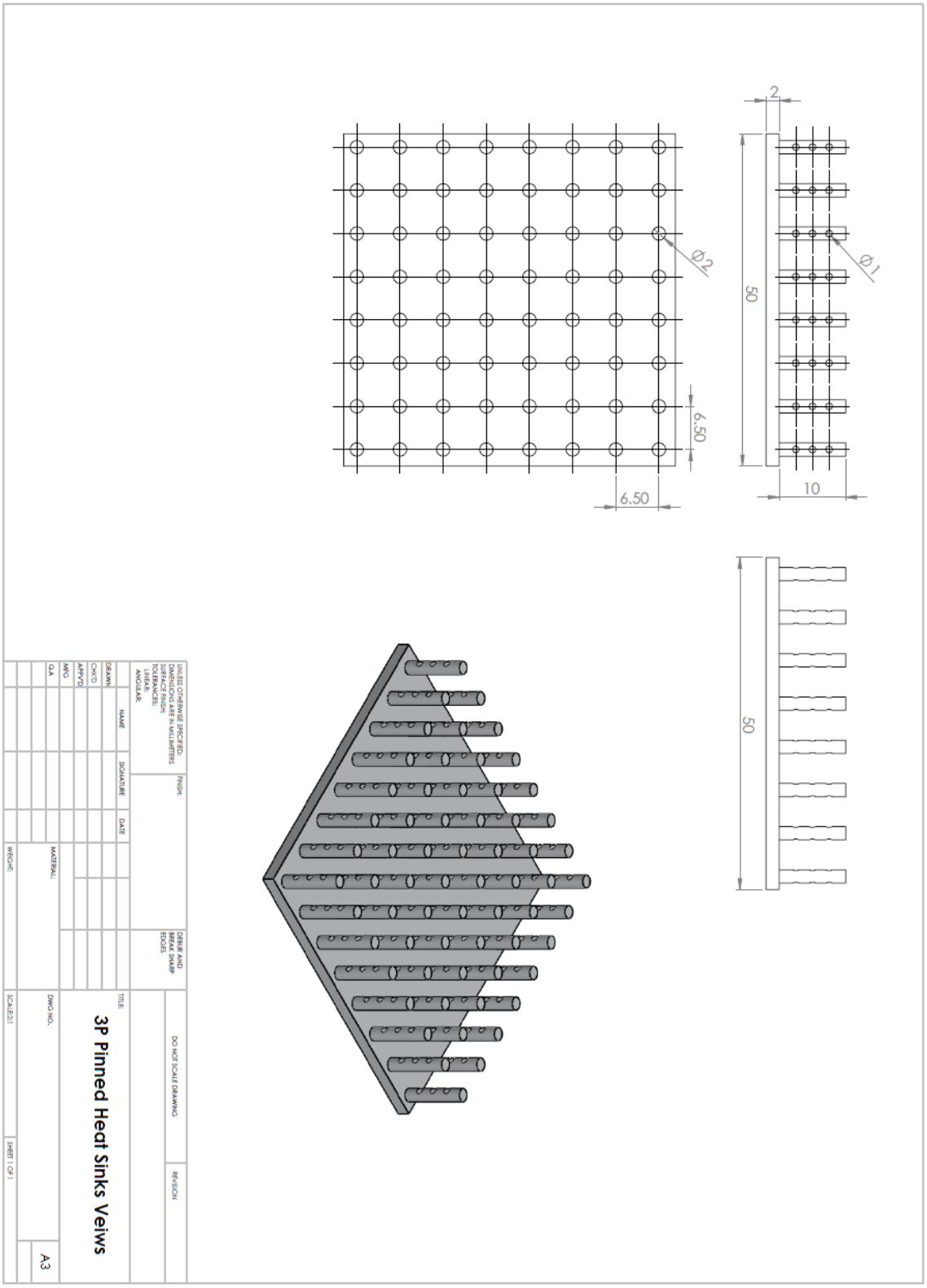

Figure A 6: Perforated pinned heat sinks (3P) model views

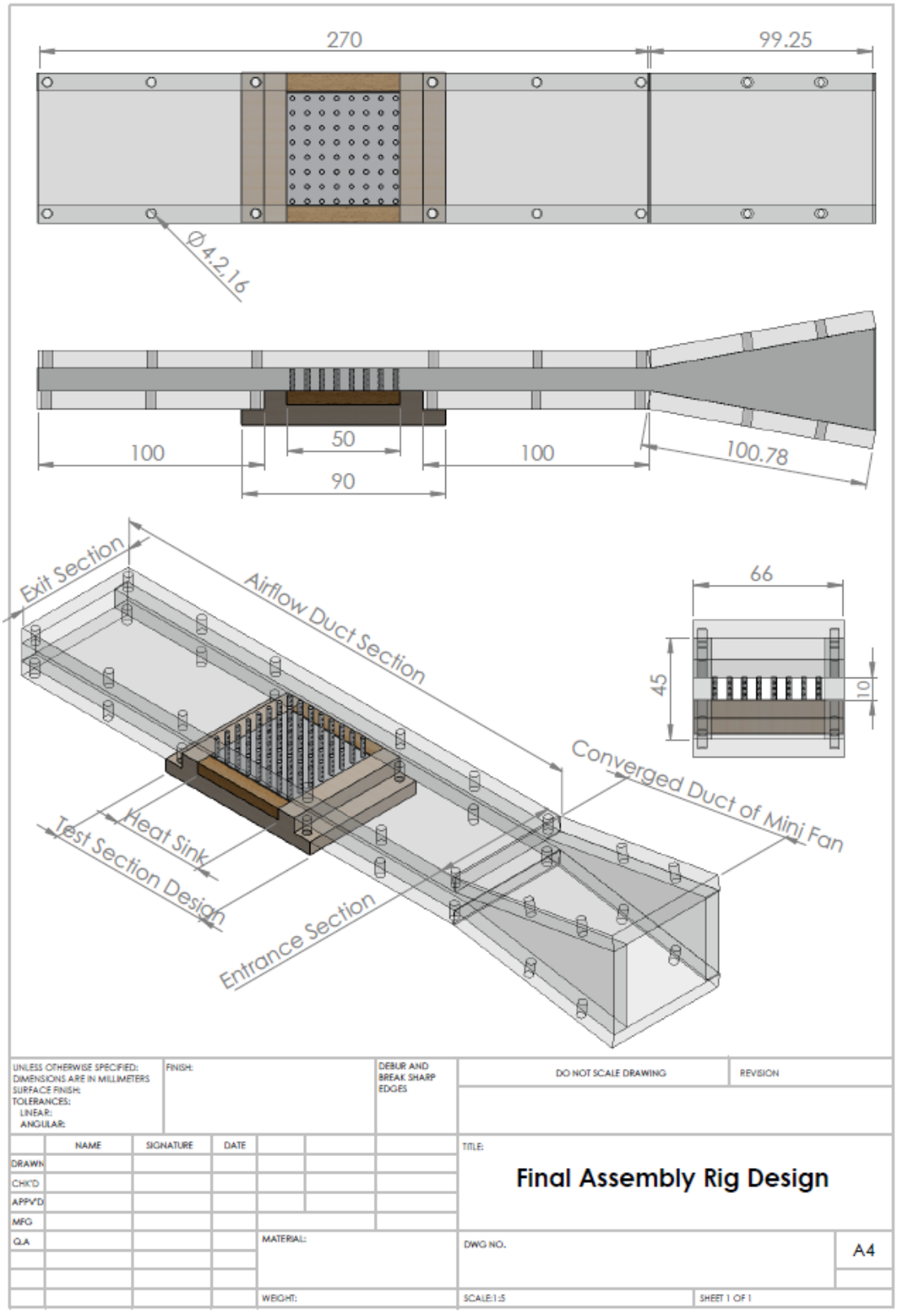

Figure A 7: Final rig design assembly with three views

Appendix B: Experimental Uncertainty Analysis

By following Holman J. P. (2011) and McClinctock, (1988), errors in experimental testing can be generally classified into two groups: precision errors (random errors) and bias errors. Precision errors are discovered via a lack of repeatability in the experimental measurement output and can be reduced by generating multiple results and averaging them. Main sources of the bias errors are calibration errors, an accuracy of measurements devices. Thus, it is often difficult to detect these errors to the experimenter and reduce them. The experimental errors can be given within a certain range of uncertainty. The uncertainty range of experimental test (*Un*) that is associated with experimental parameters results (ψ) as a function of other measured variables (*A, B, C,….., Z*) are found in this section with utilised accepted errors analysis,

$$\Psi = f(A^n, B^m, C^p, ..., Z^i)$$

$$\frac{Un\Psi}{\Psi} = \sqrt{\left(n \times \frac{UnA}{A}\right)^2 + \left(m \times \frac{UnB}{B}\right)^2 + \left(p \times \frac{UnC}{C}\right)^2 + ... + \left(i \times \frac{UnZ}{Z}\right)^2} \qquad \text{(B.1)}$$

The uncertainties of each of the sensors and instruments in the experiment are evaluated. The effect of these uncertainties on the values of convective heat transfer coefficient, Nusselt number, thermal resistance, pressure drop, fan power, and pressure drag coefficient is then.

Therefore, the uncertainty of heat transfer characteristics can be expressed as:

Heat transfer rate;

$$h_{ave} = \frac{Q_{conv}}{A_s[T_s - T_m]}$$

$$\frac{Unh_{ave}}{h_{ave}} = \sqrt{\left(\frac{UnQ_{conv}}{Q}\right)^2 + \left(\frac{UnAs}{As}\right)^2 + \left(\frac{UnT_s}{T_s}\right)^2 + \left(\frac{UnT_m}{T_m}\right)^2} \qquad \text{(B.2)}$$

$$Q_{conv} = Q_{\text{electrical}} = V.I$$

$$\frac{UnQ_{conv}}{Q_{conv}} = \sqrt{\left(\frac{UnV}{V}\right)^2 + \left(\frac{UnI}{I}\right)^2} \qquad \text{(B.3)}$$

$$A_s = A_{base} + A_{fins}$$

$$\frac{UnA_s}{A_s} = \sqrt{\left(\frac{UnA_{base}}{A_{base}}\right)^2 + \left(\frac{UnA_{fins}}{A_{fins}}\right)^2} \quad \text{(B.4)}$$

$$A_{base} = W.L$$

$$\frac{UnA_{base}}{A_{base}} = \sqrt{\left(\frac{UnW}{W}\right)^2 + \left(\frac{UnL}{L}\right)^2} \quad \text{(B.5)}$$

For solid pin fins

$$A_{fins} = N.(\pi.D.H)$$

$$\frac{UnA_{fin}}{A_{fin}} = \sqrt{\left(\frac{UnD}{D}\right)^2 + \left(\frac{UnH}{H}\right)^2} \quad \text{(B.6)}$$

For perforated pin fins

$$A_{fins} = \pi.N[(H.D) - (\frac{1}{2}n.d) + (n.d.D)]$$

$$\frac{UnA_{fin}}{A_{fin}} = \sqrt{\left(\frac{UnD}{D}\right)^2 + \left(\frac{UnH}{H}\right)^2 + \left(\frac{Und}{d}\right)^2} \quad \text{(B.7)}$$

$$T_m = \frac{(T_{in} + T_{out})}{2}$$

$$UnT_m = \sqrt{\left(\frac{1}{2}\times 0.5\right)^2 + \left(\frac{1}{2}\times 0.5\right)^2} = \pm 0.353^o C$$

Where, the uncertainty of thermocouples (*UnT*), voltage (*UnV*) and current (*UnI*) of power supplied (Aim-TTi EX354RD, EX-R Series) are ±0.5ºC, ±0.003V, and ±0.006Amps, respectively. The number of pin fins (*N*) is 64.

The uncertainty of Nusselt number;

$$Nu = \frac{h.L}{k_{air}}$$

$$\frac{UnNu}{Nu} = \sqrt{\left(\frac{Unh}{h}\right)^2 + \left(\frac{UnL}{L}\right)^2 + \left(\frac{Unk_{air}}{k_{air}}\right)^2} \quad \text{(B.8)}$$

$$\frac{Unk_{air}}{k_{air}} = 0$$

$$\frac{UnL}{L} = \pm 0.0002$$

Thermal resistance uncertainty;

$$R_{th} = \frac{\Delta T}{Q_{electrical}} = \frac{T_{case} - T_{in}}{Q_{electrical}}$$

$$\frac{UnR_{th}}{R_{th}} = \sqrt{\left(\frac{Un\Delta T}{\Delta T}\right)^2 + \left(\frac{UnQ_{electrical}}{Q_{electrical}}\right)^2} \quad \text{(B.9)}$$

$$Un\Delta T = \sqrt{(0.5)^2 + (0.5)^2} = \pm 0.707^o C$$

The uncertainty of airflow characteristics such as; pressure drop, fan power, and pressure drag coefficient can be expressed as:

Pressure drop;

$$\Delta P = P_{outlet} - P_{inlet}$$

$$\frac{Un\Delta P}{\Delta P} = \sqrt{\left(\frac{UnP_{out}}{P_{out}}\right)^2 + \left(\frac{UnP_{in}}{P_{in}}\right)^2} \quad \text{(B.10)}$$

The uncertainty of fan power;

$$P_{fan} = U.A_c.\Delta P$$

$$\frac{UnP}{P} = \sqrt{\left(\frac{UnU}{U}\right)^2 + \left(\frac{UnA_c}{A_c}\right)^2 + \left(\frac{Un\Delta P}{\Delta P}\right)^2} \quad \text{(B.11)}$$

$$Ac = H.S_z.(n-1)$$

where, (n) is number of pins rows and the uncertainty of air velocity (UnU) is ±0.1

$$\frac{UnAc}{Ac} = \sqrt{\left(\frac{UnH}{H}\right)^2 + \left(\frac{UnS_z}{S_z}\right)^2} \quad \text{(B.12)}$$

The uncertainty of pressure drag coefficient

$P_d = \Delta P/0.5\rho.U^2$

$$\frac{UnP_d}{P_d} = \sqrt{\left(\frac{Un\Delta P}{\Delta P}\right)^2 + \left(\frac{Un\rho}{\rho}\right)^2 + \left(2 \times \frac{UnU}{U}\right)^2} \quad \text{(B.13)}$$

As a result of that, the minimum and maximum uncertainties of the thermal and the airflow relevant parameters such: heat transfer coefficient, Nusselt number, thermal resistance, fan power, and pressure drop coefficient are illustrated in Table B.1.

Table B.0.1: Uncertainties of Experimental Parameters Studies

Parameters	Uncertainty	Parameters	Uncertainty	Parameters	Uncertainty
h_{ave}	± 2.5%	R_{th}	± 2%	P_d	± 2%
Nu	± 2.5%	ΔP	± 2%	T	± 0.5°C